Universitat Politècnica de Catalunya (UPC)

Institut de Bioenginyeria de Catalunya (IBEC)

Doctoral program: Biomedical Engineering

Doctoral thesis

BREATHING PATTERN CHARACTERIZATION IN PATIENTS WITH RESPIRATORY AND CARDIAC FAILURE

by

Ainara Garde Martinez

Thesis advisor: Dr. Beatriz F. Giraldo Giraldo

Biomedical Signals and Systems (SISBIO) group, UPC
Biomedical Signal Processing and Interpretation (BIOSPIN) group, IBEC
Departament d'Enginyeria de Sistemes, Automàtica i
Informàtica Industrial (ESAII)

Barcelona, June 2010

Ama, ahizpa eta
Fernandorentzat...

Ez diren gauzak ere badira
Bizitza, ez diren gauzez ere osatzen delako.
Joseba Sarrionandia

ABSTRACT

BREATHING PATTERN CHARACTERIZATION IN PATIENTS WITH RESPIRATORY AND CARDIAC FAILURE

Ainara Garde Martinez

Departament d'Enginyeria de Sistemes, Automàtica i Informàtica Industrial (ESAII)

Doctoral thesis

The main objective of this thesis is to study and characterize breathing patterns through the respiratory flow signal applied to patients on weaning trials from mechanical ventilation and patients with chronic heart failure. The aim is to contribute to the understanding of the underlying physiological processes and to help in the diagnosis of these patients. Acute respiratory, cardiac and neurological failures lead to intubation and mechanical ventilation support. One of the most challenging problems in intensive care units is still the process of discontinuing mechanical ventilation, as over 10% of patients who undergo successful T-tube trials have to be reintubated in less than 48 hours. Withdrawal of mechanical ventilation should be performed as soon as spontaneous respiration can be sustained. It is undesirable to unnecessarily delay the

discontinuation process or to take weaning trials too early. A failed weaning trial is discomforting for patients, since it may induce cardiopulmonary distress and carries a higher mortality rate. Our purpose is to obtain indices that provide enhanced information about the respiratory pattern and the dynamic interaction between heart rate and breathing rate. This is achieved through a comparison of patients with successful trials, patients who fail to maintain spontaneous breathing in the weaning procedure and are reconnected, and patients who successfully maintain spontaneous breathing and are extubated, but require the reinstitution of mechanical ventilation in less than 48 hours because they are unable to breathe spontaneously. Since electrocardiographic (ECG) and respiratory flow signals can be measured noninvasively, this analysis could facilitate future automatic diagnoses of patients during weaning trials.

This study was carried out using the weaning dataset, which contains 30-minute ECG and respiratory flow signals acquired during T-tube tests. Three groups of patients are considered: GS, 94 patients with successful weaning; GF, 39 patients who failed to maintain spontaneous breathing; and GR, 21 patients with successful weaning trials, who needed to be reintubated in less than 48 hours. The ECG and the respiratory flow signals used in this study were acquired during T-tube tests and last 30 minute.

In a first study, the respiratory pattern was characterized by means of a number of respiratory time series. Clustering and validation techniques enabled the selection of the best subset of input features. Histogram equalization mapped the distribution of the selected features back to the distribution of the feature that gave the best classification result. After a search for the most suit-

able features and the application of the histogram equalization method, a total accuracy of 80% was obtained in the classification of GS versus GF through support vector machines (SVM), using only 8 of the 35 features.

In a second study, the cardiorespiratory interactions of the patients on weaning trials were studied by a nonlinear procedure. Joint symbolic dynamics applied to time series of heart rate and respiratory frequency can be used to describe the cardiorespiratory interactions of patients during the weaning trial process. The values of cardiac interbeat and breath duration series were synchronized and interpolated.

An optimized feature selection algorithm based on SVM was used to obtain good predictive performance for a set of unbalanced data. We proposed a new optimization metric for unbalanced classification problems, and established a new SVM feature selection method, based on the balance index B. The proposed B-based SVM feature selection provided a better balance between sensitivity and specificity in all classifications. The best classification result was obtained with this new feature selection based on both accuracy and the balance index, which classified GS and GF with an accuracy of 80%, considering only 6 features. The advantage of this approach is that the classification is based on 6 features instead of 8. Moreover, good results and a balance between sensitivity and specificity were obtained using this algorithm with 4 features or more. In the classification of GS patients versus the rest of the patients, the best result was obtained with 9 features, with an accuracy of 81%. In the classification of GR versus GS, 83% of patients were correctly classified with 9 features. Finally, in the classification of GR versus the rest of the patients, 10 features were chosen from the SVM, which gave an accuracy of

81%. Therefore, the SVM-based method accurately classified different groups of patients and maintained a good balance between sensitivity and specificity, even for unbalanced datasets.

The results show good performance of the proposed SVM-based feature selection, since it selects the most relevant features and maintains a balance between sensitivity and specificity for unbalanced groups of data. It might be a useful tool for enhancing the analysis of patients on weaning trials because it adds objective information to the doctor's expertise. Nevertheless, additional features and clinical information about patient condition before the weaning trial, should be considered to further increase the discrimination among these three groups, and to identify the reintubated patients in particular.

Chronic heart failure (CHF) is an increasingly widespread, costly and deadly disease that is frequently called an epidemic of the twenty-first century. Despite advances in modern treatment, the mortality rate in CHF patients remains high. Risk stratification in these patients is still one of the major challenges of contemporary cardiology. CHF patients often develop breathing abnormalities, including various forms of periodic breathing patterns, such as Cheyne-Stokes respiration (CSR) and periodic breathing without apnea. Periodic breathing in CHF patients is associated with increased mortality, especially in CSR patients. Under the hypothesis that an in-depth study of the respiratory pattern could improve identification of the risk level of a CHF patient, our purpose is to obtain objective indices that can provide enhanced information about the pathophysiological condition of these patients.

This study was carried out using a CHF dataset and a healthy dataset, which contain 15-minute and 30-minute long respiratory flow signals of CHF

patients and healthy subjects, respectively. Subjects included 26 CHF patients with periodic breathing (PB) and nonperiodic breathing (nPB) patterns and 35 healthy volunteers.

In a first study, we assumed the stationarity of the signals and developed an envelope-based respiratory pattern characterization for CHF patients and healthy subjects. The aim was to study respiratory pattern periodicity as a risk index by characterizing the respiratory flow signal envelope. The objective was to identify and characterize respiratory patterns from healthy subjects or CHF patients with periodic or nonperiodic breathing. In a second study, the nonstationarity of the signals was considered through time-varying AR modelling applied to the respiratory envelope signal, to characterize the temporal evolution of breathing patterns. Power-related parameters achieved the best results in all of the classifications involving healthy subjects and CHF patients with CSR, PB and nPB. The main pole magnitude produced good results in the classification of PB and nPB patterns. The ROC curves validated the results obtained for the identification of different respiratory patterns.

These results indicate that power-related parameters of the respiratory envelope signal are powerful indices to detect periodic breathing. Additionally, time-varying modulation of the respiratory envelope signal provided accurate results that characterized the temporal evolution of respiratory patterns.

In a third study, we investigated the use of correntropy for the spectral characterization of respiratory patterns in CHF patients. In contrast to the conventional second-order correlation function, the correntropy function accounts for higher-order moments and is robust to outliers. Due to the former property, the respiratory and modulation frequencies appear at their actual

locations along the frequency axis in the correntropy spectral density (CSD).

When correntropy was used to classify PB and nPB patients, the accuracy (88.9%) was higher than that obtained with parameters derived from envelope's time–frequency representation. The importance of this results lies in the fact that the present classification is based on only one parameter.

The main goal of this research was to identify CHF patients' condition noninvasively by characterizing and classifying respiratory flow patterns from patients with PB and nPB. In general, the best results were achieved with CSD-related parameters that characterized the power in the modulation and respiration discriminant bands, which is defined as a frequency interval centred on the modulation and respiration frequency peaks, respectively. These parameters achieved the best results in all the classifications performed with CHF patients, including CSR patients, PB patients without apnea, and nPB patients. All patients, i.e. both PB and nPB, exhibit various degrees of periodicity depending on their condition, whereas healthy subjects have no pronounced periodicity. The correntropy mean and the correntropy spectral density mean provide excellent results in the classification of CHF and healthy subjects, as well as that of nPB patients and healthy subjects (CHF versus healthy 95.2%, and nPB versus healthy 94.4%).

The information extracted from the respiratory pattern appears to be useful to identify periodic breathing patterns in CHF patients and can therefore improve prognosis and serve as indicators of patient condition. The small size of the dataset is a limitation of this research. Therefore, although the results are promising, their significance needs to be further established using a larger set.

ACKNOWLEDGMENTS

This thesis has been developed in the research groups SISBIO at the Universitat Politècnica de Catalunya (UPC) and BIOSPIN (Recognized Research Group [GRC], 2009 SGR 722) at the Institute for Bioengineering of Catalonia (IBEC), led by Drs. Pere Caminal and Raimon Jané. I am sincerely grateful to them for helping me during my doctoral research.

First, I would like to express my gratitude to my supervisor, Dr. Beatriz F. Giraldo, whose encouragement and guidance from start to finish enabled me to write this thesis. Her support and advice, particularly in the search for funding, was critical to the success of the entire thesis. I would also like to thank the people from the Department of Automatic Control (ESAII) of the UPC.

I would like to acknowledge Drs. S. Benito and A. Bayés-Genis and their colleagues at Santa Creu i Sant Pau Hospital, Barcelona, Spain, for their fruitful collaboration in the signal database acquisition and their help in the interpretation of clinical aspects of this thesis.

I am grateful to Prof. Andreas Voss and the people from the Department of Medical Engineering at the University of Applied Sciences Jena for their warm welcome, help and support during my stay. The research stay in Germany was partly supported under HA2005-0085 grant (Acción integrada MEC).

Thank you also to Prof. Leif Sörmno for support, advice and valuable

corrections. It is always a stimulating and rewarding experience working with you. Thanks also to the signal processing group at the Department of Electrical and Information Technology and Centre of Integrative Electrocardiology at Lund University. Thank you for being so kind during my stay. The research stay in Sweden was partly supported by the Centro de Investigación Biomédica en Red en Bioingeniería, Biomateriales y Nanomedicina (CIBER-BBN).

Thank you to Dr. Javier Hernando and the TALP Research Center in the Department of Signal Theory and Communications at the Universitat Politècnica de Catalunya (UPC) for introducing me to machine learning techniques.

I would also like to thank all of my colleagues at the UPC, IBEC and CIBER-BBN, for their companionship.

A big thank you to all my friends in Jena and Lund, for being my family during my stay and for making my time there so incredible.

Thanks to all of my friends at the UPC for your constant support, the entertaining conversation during meals, the incredible experiences at different congresses and all the good times we have had together. It has been a real pleasure to work with you.

I am very grateful to all my close friends who have been always there with and for me during the good and the bad times. Thank you for your support, advice, love and presence in my life. I am really lucky to have such good friends.

I would like to thank the entire Lopez family for their constant support, exceptional advice and goodwill.

I owe my deepest gratitude to my family: to my Mum, my sister and Fernando for their unlimited patience, love and support. There have been

difficult times in this period and I have been a bundle of nerves, so thank you for supporting me and not giving up on me.

Thanks to all of you: this thesis would not have been possible without your support and trust.

The thesis was partly supported by the Spanish Ministry of Science and Innovation under grants TEC2007-68076-C02-01 and TEC2007-63637.

Contents

List of Tables

List of Figures

Chapter 1

Introduction

1.1 Thesis introduction

In order to help clinical doctors in the diagnosis of patients, in this research we analyse the respiratory system of patients with different pathologies in depth. Specifically, we study patients on weaning trials and patients with chronic heart failure.

The process of discontinuing mechanical ventilation that is referred to as weaning is still one of the most challenging problems in intensive care units. Although a lot of research has been done on this topic, a high percentage of patients who undergo successful T-tube trials have to be reintubated in less than 48 hours. Reintubation percentages that range from 6% to 47% have been reported for different populations. Withdrawal of mechanical ventilation should be performed as soon as spontaneous respiration can be sustained. Critical care clinicians must carefully assess the benefits of prompt liberation from mechanical ventilation against the risks of premature tests of spontaneous breathing and extubation. Both delayed and failed extubation have detrimental consequences. A failed weaning trial is discomforting for patients, since

it may induce cardiopulmonary distress and carries a higher mortality rate.

Chronic heart failure (CHF) is an increasingly widespread, costly and deadly major health problem that is frequently called an epidemic of the twenty-first century. Despite advances in modern treatment, the mortality rate in CHF patients remains high. Risk stratification in these patients is still one of the major challenges of contemporary cardiology. Patients with CHF often develop breathing abnormalities, including various forms of periodic breathing (PB) patterns. Cheyne–Stokes respiration (CSR) is characterized by repetitive gradual increases and subsequent gradual decreases in ventilation, followed by periods of apnea. PB in CHF patients has a similar increase and decrease in ventilation, but there are no periods of apnea. Both ventilatory patterns may have the same mechanistic explanations, as PB is a less severe form of CSR. The prevalence of PB in CHF patients is as high as 70%, and is associated with increased mortality, especially in patients with CSR. The most relevant accepted clinical predictors of the outcome of heart failure patients perform well in the prediction of mortality due to disease progression, but the prediction of sudden cardiac death appears more problematic. In ambulatory patients with less severe CHF, symptoms may be less obvious and death is more often sudden in nature. The importance of being able to identify mildly symptomatic CHF patients at risk from sudden cardiac death is of paramount importance.

1.2 Thesis objective

The main objective of this thesis is to study and characterize breathing patterns through the respiratory flow signal applied to patients on weaning trials from mechanical ventilation and patients with chronic heart failure. The aim is to provide

information that could increase understanding of the underlying physiological processes and help in the diagnosis of these patients.

One goal of this thesis is to obtain objective indices that provide relevant information about the respiratory pattern and the dynamic interaction between heart rate and breathing rate. This could help to improve the weaning outcome in patients on weaning trials and reduce the number of patients who successfully maintain spontaneous breathing and are extubated, but require the reinstitution of mechanical ventilation in less than 48 hours, because they are unable to breathe spontaneously.

Under the hypothesis that an in-depth study of the respiratory pattern could improve identification of the risk level of a CHF patient, another goal of this thesis is to obtain objective indices that can provide enhanced information about the pathophysiological condition of these patients, which could help in the prognosis and subsequent risk stratification of these patients.

A final study should be carried out for each problem, including all the relevant clinical information and all the significant indices. This would increase our knowledge of these patients and contribute to clinical practice.

1.3 Thesis outline

The thesis is organized as follows:

Chapter 2: ***Weaning and chronic heart failure.*** An overview is given of the respiratory system. Acute respiratory failure and chronic heart failure are described briefly, and the state-of-the-art in weaning readiness assessment and periodic breathing in chronic heart failure is discussed.

Chapter 3: ***Pattern recognition techniques.*** The main issues in pattern

recognition techniques are reviewed. Support vector machines, and a number of metrics employed to evaluate the performance of respiratory pattern recognition, are described.

Chapter 4: ***Support vector machines applied to weaning.*** SVM is used to study the differences between patients with successful weaning trials, patients with unsuccessful trials and patients who successfully pass the trial, but cannot maintain spontaneous breathing and require the reinstitution of mechanical ventilation. The respiratory flow signal and the ECG of the patients are used to characterize the respiratory pattern and cardiorespiratory interactions.

Chapter 5: ***Time-frequency analysis of the respiratory pattern.*** This chapter describes a number of time-frequency techniques that are applied to the respiratory flow signal to characterize the respiratory pattern in patients with CHF. We review pre-processing for artefact reduction, various envelope extraction techniques, and a number of parametric and nonparametric methods for power spectral analysis that are applied in all cases to the respiratory flow signal.

Chapter 6: ***Respiratory pattern analysis applied to chronic heart failure.*** This chapter analyses the breathing pattern through the respiratory flow signal in CHF patients and healthy subjects using the envelope of the respiratory flow signal. On the basis of autoregressive power spectral analysis of the envelope, the relevant discriminant band is characterized by a number of spectral parameters.

Chapter 7: ***Correntropy-based respiratory pattern analysis.*** We introduce the correntropy measure and a number of functions that are derived from it, such as centred correntropy and correntropy spectral density. We use centred correntropy to study the respiratory flow signal in CHF patients with periodic breathing and nonperiodic breathing patterns, to define parameters that can improve prognosis

and serve as indicators of patient condition.

Chapter 8: *Conclusions.* The outcome and contributions of this thesis are summarized in this chapter. Some possible future extensions are briefly presented for further work on this topic.

Publications derived from this thesis.

The publications that have resulted from this doctoral thesis are listed at the end of the document.

Chapter 2

Weaning and chronic heart failure

Breathing is essential to life and must occur in the conscious or unconscious state, awake or asleep. The voluntary and involuntary control of the respiratory system is unparalleled and a highly complex process. It constantly adapts to environmental changes, from small environmental variations that are nearly imperceptible to the senses to changes that provoke an explicit response, such as a cough or sneeze. In spite of its relevance to our daily life, some aspects of the mechanics and physiology of the respiratory system are still unknown. Thus, the study of the respiratory system's complexity has became a promising area, in which scientific progress can be made.

Respiratory failure is a dysfunction of one or more essential components of the respiratory system and represents a medical emergency. Health care professionals treat respiratory failure by restoring normal function, and by using devices such as mechanical ventilators to maintain gas exchange until the respiratory system heals. When mechanical ventilation is discontinued, problems may arise. Extubation failure occurs in 6% to 47% [5] of cases in different populations.

An alteration in respiratory pattern provides a sensitive, consistent sign of res-

piratory failure. Respiratory pattern is closely linked with the circulatory system, therefore its abnormalities could reveal a loss of stability in the closed-loop chemical control of ventilation. For instance, it has been reported in the literature that patients with chronic heart failure develop specific breathing abnormalities.

To enhance the available information in the diagnosis of patients, we have studied in depth the respiratory pattern of patients with different pathologies, specifically patients on weaning trials and patients with chronic heart failure.

2.1 Respiratory system

The primary role of the respiratory system is to provide oxygen to the tissues and to remove carbon dioxide (Fig. 2.1). To achieve these goals, respiration can be divided into four major functions: (1) pulmonary ventilation, which means the inflow and outflow of air between the atmosphere and the alveoli in the lungs; (2) diffusion of oxygen and carbon dioxide between the alveoli and the blood; (3) transport of oxygen and carbon dioxide in the blood and body fluids to and from the body's tissue cells; and (4) regulation of ventilation and other aspects of respiration [2].

2.1.1 Pulmonary ventilation

Breathing is the result of periodic contractions and expansions of the thoracic cavity, which are produced by the intermittent contraction of respiratory muscles. Respiratory muscle movement forces the thoracic cavity to modify its volume, which creates positive and negative pressures that bring air in and out of the lungs. The lungs are expanded and contracted by the downward and upward movement of the diaphragm to lengthen or shorten the thoracic cavity. Thoracic cavity expansion moves air into

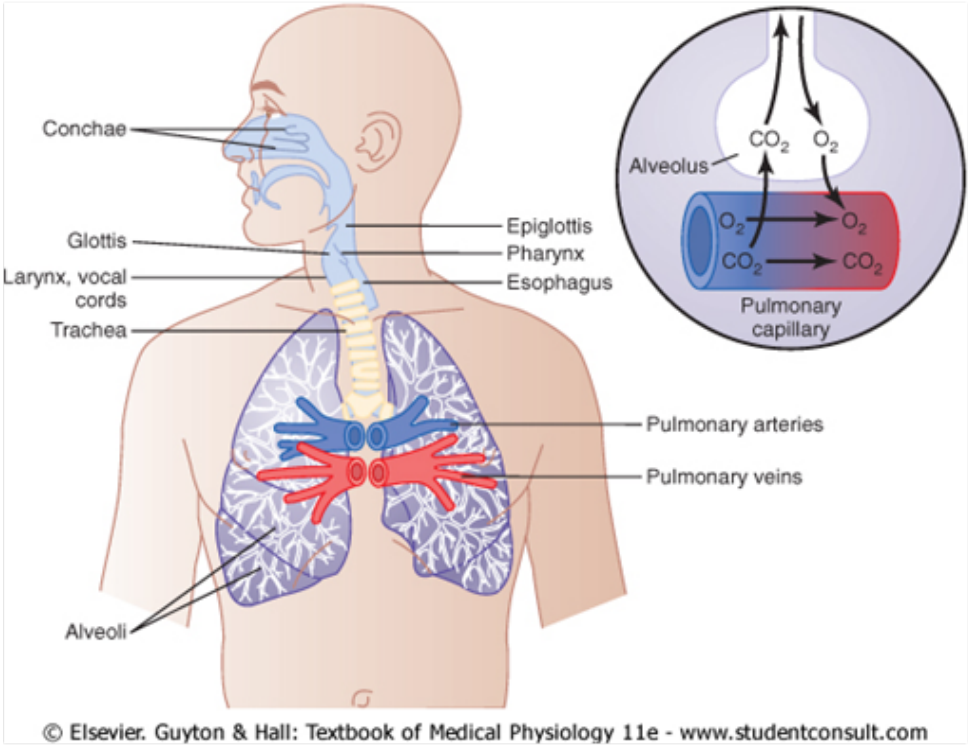

Figure 2.1 The respiratory system. The air is distributed to the lungs by way of the trachea, bronchi and bronchioles (authorized by [2]).

the lungs and a return to the initial volume moves the air out. During inspiration, contraction of the diaphragm pulls the lower surfaces of the lungs downward. Then, during expiration, the diaphragm simply relaxes, and the elastic recoil of the lungs, thoracic wall, and abdominal structures compresses the lungs and expels the air (Fig. 2.2). Inspiration is an active process and expiration is generally a passive process, due to the natural elasticity of the lungs.

Lung capacity for inspiration and expiration depends on the components of the airways, thoracic cavity, respiratory muscles, and the features of the muscles. In practice, different measures are used to evaluate these factors separately, although

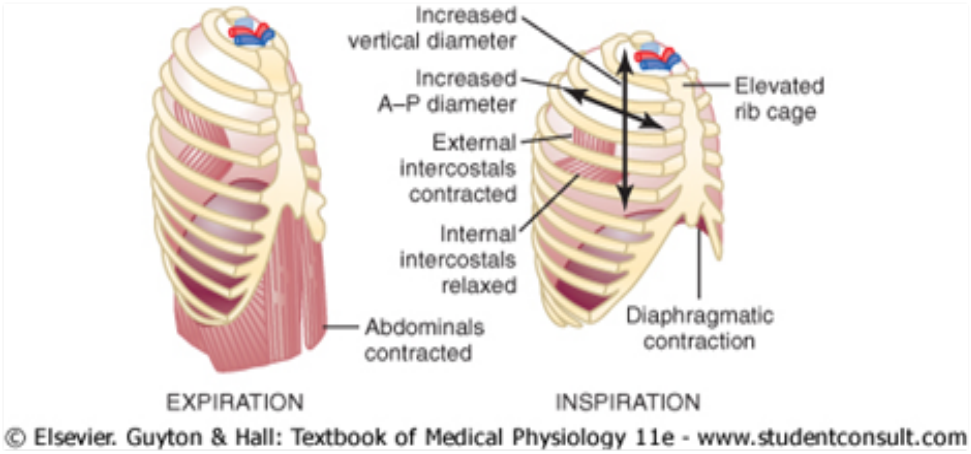

Figure 2.2 The process of inspiration and expiration (authorized by [2]).

there is no reliable method for properly evaluating pulmonary ventilation. Thus, respiration is clinically studied through measurements of static and dynamic volume, pressure and pulmonary capacity [6]

2.1.2 Pulmonary volumes and capacities

Pulmonary volume and capacity measurements can be used to investigate pulmonary disorders, to characterize severity and to control responses to therapy. Measurements are typically reported as absolute volumes, pulmonary capacities and percentages of predicted values, using data derived from large populations of people who are presumed to have normal lung function. The variables that are used to predict normal values include age, sex, weight and height.

Some static and dynamic measurements are made through spirometry, which consists of registering on a spirometer the whole inspiration and expiration cycle, either under normal volumes or by forcing maximum inspiration and expiration. Static

volume measurements are obtained by simple spirometry and dynamic measurements are made by forced spirometry. Measurements are influenced by the state of each subject's breathing mechanism and also by his/her characteristics. Table 2.1 describes some of the static respiratory volume and pulmonary capacity measurements and includes their normal ranges for a healthy subject (Fig. 2.3).

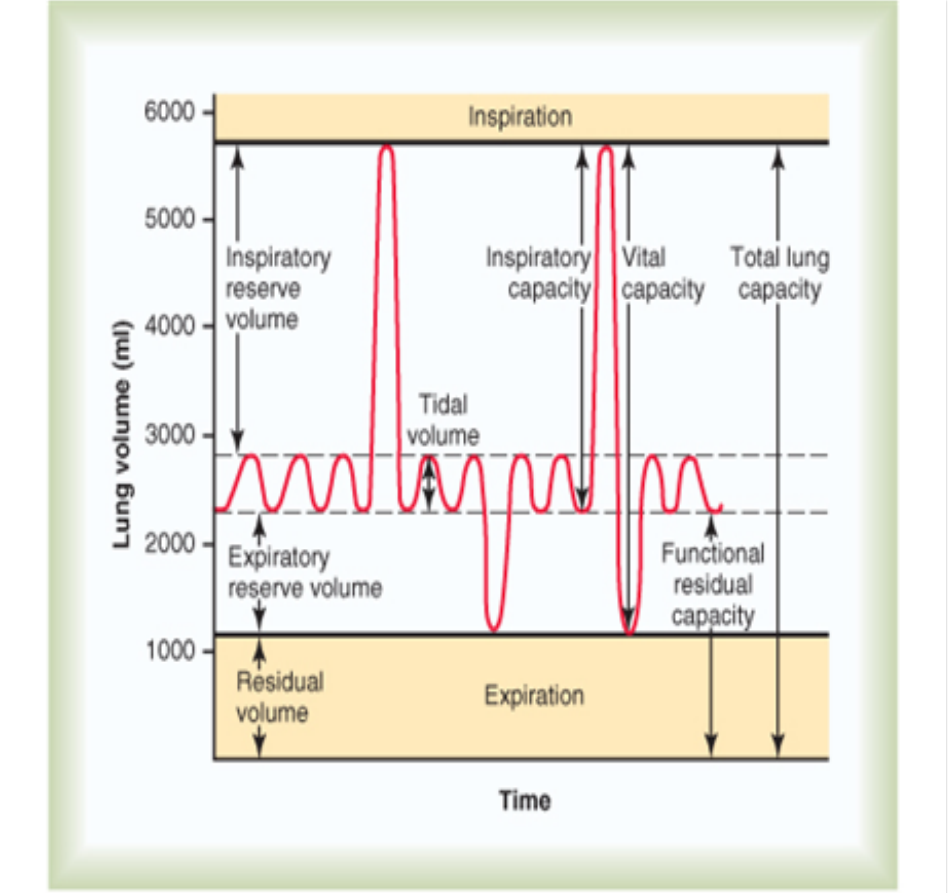

Figure 2.3 Spirogram with lung volume changes under different breathing conditions. The air in the lungs has been subdivided into four volumes and four capacities, which are the average for a young adult man (authorized by [2]).

Table 2.1 Static volume measures

Measurement	Description	Normal value
Tidal Volume (V_T)	The amount of air moved into and out of the lungs during a normal breath at rest.	500 ml
Residual Volume (RV)	The amount of air left in the lungs following a maximal exhalation. There is always some air remaining to prevent the lungs from collapsing.	1200 ml
Inspiratory Reserve Volume (IRV)	The amount of extra air inspired (above the tidal volume) during a deep breath.	3000 ml
Expiratory Reserve Volume (ERV)	The amount of extra air exhaled (above the tidal volume) during a forceful breath out.	1200 ml
Vital Capacity (VC)	The most air you can exhale after taking the deepest breath you can. It can be up to ten times more than you would normally exhale.	4500-5500 ml
Total Lung Capacity (TLC)	This is the total amount of air the lungs can hold, which is the vital lung capacity plus the residual volume.	4400-6400 ml
Inspiratory Capacity (IC)	The volume of gas that can be taken into the lungs in a full inspiration, starting from the resting inspiratory position. It is equal to the tidal volume plus the inspiratory reserve volume.	3600 ml
Functional Residual Capacity (FRC)	The volume of gas in the lungs at the end of a normal tidal volume expiration. It is equal to the residual volume plus the expiratory reserve volume.	2400 ml

The dynamic measurements resulting from spirometry can be used to evaluate the existence of respiratory pathologies in the subject. Numerous parameters have been proposed by different researchers, but spirometry can be fully interpreted with just three of them. Some general considerations for appropriate lung function testing are presented in [7] and some spirometric reference values are given in [8].

Forced Vital Capacity (FVC)

FVC is the maximum volume of air that a subject can forcibly exhale after taking a maximal inspiration. It is a capacity measurement that quantifies pulmonary capacity. It is expressed in litres, as is the percentage of the theoretical reference value. Values greater than or equal to 80% of the theoretical value are considered normal FVC measurements. The Spanish Society of Pulmonology and Thoracic Surgery (SEPAR) has accepted a theoretical value for Barcelona's population that is calculated by the following expressions [9]

$$FVC\ (Male) = 0.0678 \cdot Height - 0.0147 \cdot Age - 6.0548 \tag{2.1}$$

$$FVC\ (Female) = 0.0454 \cdot Height - 0.0211 \cdot Age - 2.8253 \tag{2.2}$$

Forced Expiratory Volume in 1 second (FEV_1)

FVE_1 is the maximum volume of air that a subject can forcibly exhale in the first second after taking a maximal inspiration. Like FVC, it is expressed in litres and as a percentage of the theoretical reference value. Within Barcelona's population, the reference value for a healthy subject is given by

$$FVE_1\ (Male) = 0.0499 \cdot Height - 0.0211 \cdot Age - 3.8370 \tag{2.3}$$

$$FVE_1\ (Female) = 0.0317 \cdot Height - 0.0250 \cdot Age - 1.2324 \tag{2.4}$$

In general, FVE_1 increases from childhood and reaches a maximum value at around 25 years old. It has been proved to be a discriminating factor in the prediction of obstructive disorders characterized by a reduction in airflow [9].

FEV_1/FVC ratio

Represented as FEV_1 / FVC or $FEV_1\%$, this is the percentage of FVC exhaled during a forced expiration. A drop in this index implies the existence of respiratory obstruction. The FEV_1 / FVC value varies with age and is higher in healthy young people than in older people. A percentage of 75% is considered normal in young people and 70% in elderly people [9].

2.1.3 Respiratory flow and volume signals

The volume signal represents the circulating air volume in a subject's airway. The volume signal of healthy subjects generally has an oscillation waveform with an amplitude and frequency that varies for each subject. The average amplitude and frequency values are 500 ml and 12 breaths per minute, respectively. When deep breaths occur, these average values can vary remarkably. Inspiratory volumes can reach up to 3500 ml and expiratory volumes can reach 1000 ml during a deep breath. In addition, respiratory frequency can decrease unconsciously up to 5 breaths per minute during sleep or during apnea events, and increase automatically to 70 breaths per minute during intense effort. Therefore, a respiratory volume signal contains a large number of breathing cycles that can vary in frequency and amplitude even when they are consecutive.

Respiratory flow occurs by convection, as a result of the pressure difference between the chest and the atmosphere. It is a measure of the circulating air volume over time. Consequently, it can be estimated through a time derivative of the volume signal. During inspiration, the air volume increases and the airflow is positive. In contrast, during expiration the volume decreases, which generates negative flow values. Usually, the flow signal's sign changes position to indicate the beginning and the end of breathing cycles. Forced expiratory vital capacity and forced expiratory volume are exceedingly useful as simple clinical pulmonary tests to study respiratory abnormalities (Fig. 2.4).

2.1.3.1 Respiratory signal acquisition

The most common methods to acquire the respiratory flow signal are: plethysmography, which is based on quantifying abdominal and thoracic respiratory movements, and pneumotachography, which is based on quantifying the air that moves into and out of the patient. Respiratory inductive plethysmography is a widely accepted method for quantitative and qualitative noninvasive respiratory measurements. When correctly calibrated, respiratory inductive plethysmography allows the measurement of volume and time components of the breathing cycle, as well as the relative participation of thorax and abdomen in this cycle [10].

A study by Strömberg [11] investigates the reliability of respiratory inductive plethysmography compared to pneumotachography. In an analysis of the respiratory phase that was chosen for the calibration, the authors observed that respiratory inductive plethysmography underestimated lung volume at the start of inspiration and overestimated lung volume at the end of inspiration. They found a similar tendency during expiration.

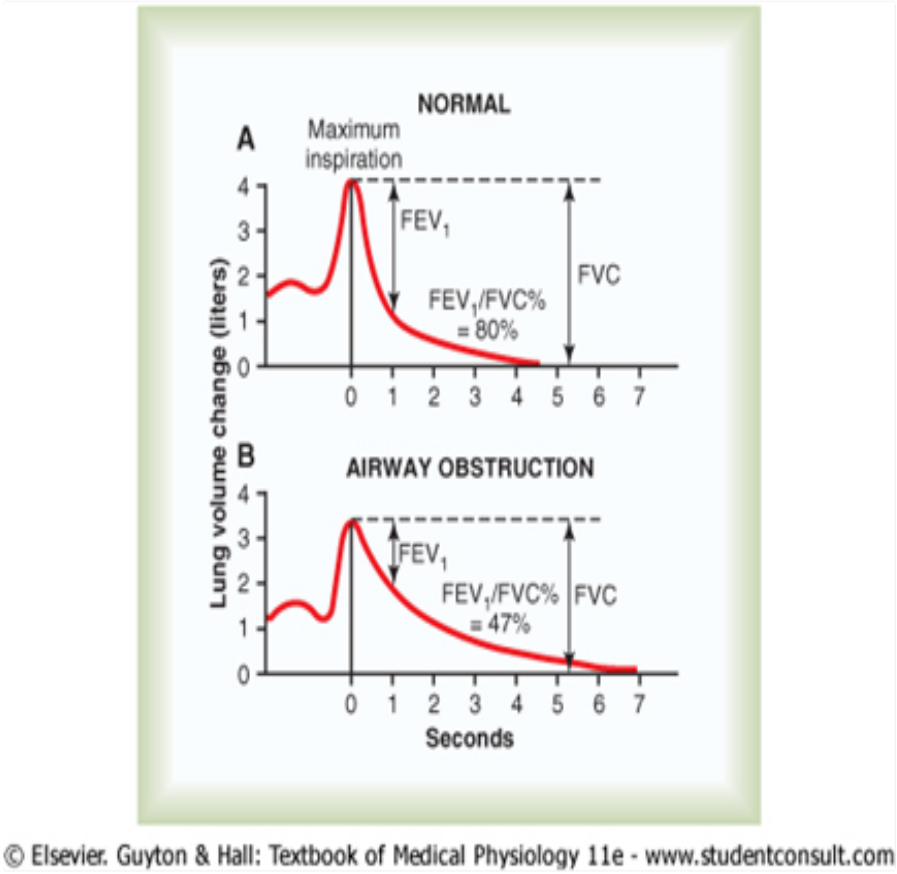

Figure 2.4 Forced vital capacity measurements in a healthy and with partial airway obstruction subject (The " zero" on the volume scale is the residual volume), (authorized by [2]).

The most commonly used device to measure respiratory flow is the pneumotachograph. In this device, the flow signal is derived from the pressure difference over a fixed resistance. A linear relationship between pressure drop and flow is assumed to exist, and thus Poiseuille's law is valid in pneumotachograph measurements. Carry et al. [12] assessed the accuracy of the respiratory inductive plethysmography waveform by comparing it with the volume waveform obtained from the whole body plethys-

mograph. The same comparison was carried out with the pneumotachograph as it is currently used for breathing pattern analysis.

2.1.4 Respiratory failure or insufficiency

Respiratory failure is a syndrome of inadequate gas exchange due to the dysfunction of one or more essential components of the respiratory system. The diagnosis and treatment of most respiratory disorders depend heavily on understanding the basic physiological principles of respiration and gas exchange. Some respiratory diseases result from inadequate ventilation. Others result from abnormalities of diffusion through the pulmonary membrane or abnormal blood transport of gases between the lungs and the tissues. The therapy is often entirely different for these diseases, so it is no longer satisfactory simply to diagnose "respiratory insufficiency". Respiratory failure can be classified into:

- Type I or hypoxemic respiratory failure: failure of oxygen exchange, the blood oxygen saturation may fall critically.
- Type II or hypercapnic respiratory failure: failure to exchange or remove carbon dioxide, which manifests as abnormally high carbon dioxide.
- Type III or perioperative respiratory failure: increased atelectasis due to low functional residual capacity linked to abnormal abdominal wall mechanics. Atelectasis is defined as the lack of gas exchange within alveoli, due to alveolar collapse or fluid consolidation.
- Type IV or respiratory failure in shock, which describes patients who are intubated and ventilated in the process of resuscitation for shock. The goal of

ventilation is to stabilize gas exchange and to unload the respiratory muscles, thus lowering their oxygen consumption.

Respiratory failure represents a medical emergency. Health care professionals treat respiratory failure by restoring normal function, assisting crippled function or using devices such as mechanical ventilators to sustain gas exchange until the respiratory system heals [2].

2.1.5 Mechanical Ventilation

Mechanical ventilation is a method to assist or replace spontaneous breathing. It is the principal medical treatment for acute respiratory failure, and one of the most commonly used techniques in intensive care. Although mechanical ventilation provides assistance for breathing when the patient's spontaneous ventilation is not sufficient to maintain life, it does not cure a disease. Hence, the patient's underlying condition should be resolved over time.

Mechanical ventilation is initiated in situations of apnea, oxygen deficiency, acute ventilatory failure, imminent ventilatory failure, resuscitation from cardiorespiratory arrest, under anaesthetics, in cases of drug overdose, muscular paralysis, central nervous system malfunction, peripheral neuropathy, intoxications, loss of mechanical integrity of the thorax, hydroelectrolytic imbalance, pulmonary contusion, correction of mitral stenosis with severe pulmonary hypertension, acid aspiration and so on.

Invasive mechanical ventilation is associated with risks and complications that prolong the duration of the procedure and increase the risk of death. Therefore, discontinuation of mechanical ventilation should be performed as soon as possible.

The most commonly used ventilatory modes for mechanical ventilation are: con-

trolled ventilation, assisted ventilation, assisted controlled ventilation, intermittent mandatory ventilation, synchronized intermittent mandatory ventilation, pressure support ventilation, high-frequency oscillatory ventilation and so on.

2.1.6 Modes of mechanical ventilation

Ventilation modes are generally classified into controlled or assisted ventilation. In controlled ventilation, the ventilator initiates the breaths and does all the work of breathing. In assisted ventilation, the patient initiates and terminates some or all the breaths and the ventilator provides varying amounts of support throughout the respiratory cycle [13]. In order to meet the specific needs of each patient, mechanical support can be supplied by a number of ventilation modes, such as:

- *Controlled ventilation (CV)* is indicated primarily for patients who are unable or not required to generate a voluntary respiratory effort. It is a time-cycling process. The timing mechanism generates the inspiratory tidal volume breath, independent of the patient's respiratory effort. During this ventilation mode, the ventilator does not allow the patient to self-generate a tidal volume breath and assumes all the work.

- *Assisted ventilation (AV)* allows the patient to contribute to the ventilation, unlike CV. It offers several advantages over controlled ventilation, since it can reduce the need for sedation and paralysis, decrease the risk of barotrauma, improve intrapulmonary gas distribution and prevent muscle atrophy. During AV, ventilation is dependent on both the ventilator settings and the patient's ventilatory demand.

- *Assisted controlled ventilation (ACV)* is a combination of the previous modes (CV and AV). During assisted controlled ventilation, the patient receives a predetermined mechanical respiratory rate and tidal volume, as with CV, but is able to self-generate additional tidal volume breaths. The self-generated breaths occur due to the negative pressure created by the patient within the ventilator circuit.

- *Intermittent mandatory ventilation (IMV)* is similar to ACV, but it allows the patient to breathe spontaneously between predetermined ventilator breaths. The ventilator delivers a predetermined tidal volume at specific time intervals. Moreover, patients can determine their own tidal volume and respiratory rate during spontaneous breathing. This allows patients to slowly increase the work of breathing and provides more independence from full ventilator support. IMV can be used as full ventilator support with a high respiratory rate or as partial ventilator support.

- *Synchronized intermittent mandatory ventilation (SIMV)* is similar to IMV. The only difference is that the patient's own spontaneous breathing pattern is synchronous with the SIMV rate. During SIMV, the patient receives a predetermined number of mechanical ventilation breaths plus any additional self-generated breaths. The system prevents the accumulation of breaths between the mechanical breath and the patient's spontaneous inspiratory tidal volume.

- *Pressure support ventilation (PSV)* provides pressure assistance during each spontaneous breath. It can be used as full ventilator support or partial ventilator support. To decrease the patient's work of breathing, the PSV is used primarily to overcome the airway resistance of the endotracheal tube and the dead space in

the ventilator circuit. In addition, PSV is used as a tool for ventilator weaning, since it requires full spontaneous respiratory effort by the patient.

- *Continuous positive airway pressure (CPAP)* consists of a continuous level of elevated pressure that is provided through the patient circuit to maintain adequate oxygenation and decrease the work of breathing. There is no cycle of ventilator pressure, and the patient must initiate all breaths. Moreover, no additional pressure above the CPAP pressure is provided during breaths. CPAP may be used invasively through an endotracheal tube or non-invasively with a face mask or nasal prongs.

2.2 Discontinuation of mechanical ventilation or weaning

Weaning is usually carried out by gradually removing the mechanical support as spontaneous breathing is resumed. It involves the entire process of liberating the patient from mechanical support and from the endotracheal tube, including relevant aspects of terminal care.

Weaning procedures are usually started only after the underlying disease process that required mechanical ventilation has significantly improved or been resolved. The patient should also have adequate gas exchange, appropriate neurological and muscle status and stable cardiovascular function. There is still uncertainty about the best methods for this process. The most notable methods are the T-tube trial and pressure support ventilation.

2.2.1 Weaning methods

Different modes of mechanical ventilation have been used in weaning. Indeed, some modes, such as intermittent mandatory ventilation (IMV), were introduced specifically for weaning, and were then subsequently used for mechanical ventilatory support. Specifically, the ventilatory modes used for weaning include T-tube test, intermittent mandatory ventilation, synchronized intermittent mandatory ventilation, pressure support ventilation, and so on [14] and [15].

T-tube test forces the patient to breathe spontaneously through a T-tube system before the final disconnection from the ventilator. The T-tube system does not introduce additional breathing work. Periods of spontaneous ventilation are gradually lengthened, according to patient capability and endurance, until the patient becomes free from mechanical ventilation day and night. Extubation is postponed until successful weaning has been demonstrated. T-tube test is the simplest and most commonly used weaning mode. Psychological preparation is essential for patients to be weaned by this method. It is generally used in patients who have been ventilated for short periods, since some patients poorly tolerate the change from ventilator support to complete spontaneous breathing.

Intermittent mandatory ventilation is the first alternative to a T-tube trial to wean patients off the ventilator. It allows spontaneous breathing between the mandatory ventilator-delivered breaths, which enables the respiratory muscles to exercise. It involves a gradual reduction in the amount of support provided by the ventilator and a progressive increase in the amount of respiratory work performed by the patient. There is no disconnection from the ventilator and all the monitoring and alarm functions of the ventilator are retained. This method avoids the drastic change

from continuous mechanical ventilation to spontaneous breathing. Ventilator delivered breathing is progressively reduced as the patient's respiratory function improves. The patient is then weaned to spontaneous breathing by a T-tube or a CPAP circuit when the IMV ventilator's breath rate is as low as 2-4 breaths/min. In synchronized intermittent mandatory ventilation, the mechanical breaths are provided by assisted ventilation. If no breath is generated within a predetermined time period, a mandatory ventilator breath is automatically delivered.

Pressure support ventilation is the most commonly used weaning method. It provides constant, preset airway pressure at the start of inspiration. Pressure support stops after a given fraction of inspiratory time or when inspiratory flow falls below a predetermined fraction of the initial inspiratory flow. Expiration is passive. The pressure support level is gradually decreased as the patient improves, but the volume is not controlled. This method also allows a gradual transition from mechanical to spontaneous ventilation. Low levels of PSV (e.g. 5-10 cm H_2O) increase spontaneous tidal volumes and help to reduce inspiratory work from circuit impedance. High levels of PSV (e.g. 20 cm H_2O) are analogous to using the assisted ventilation mode in a pressure cycled ventilator, and will result in variable tidal volumes in a patient with unstable respiratory mechanics. When the required PSV is less than 2-3 cm H_2O, the patient is usually changed to spontaneous breathing by a T-tube system.

2.2.2 Weaning indices

In the assessment of extubation readiness, a number of indices have been defined to determine whether a patient is able to come off the ventilator. Some of the objective indices include: (a) ratio between arterial oxygen saturation and inspiratory oxygen fraction (PaO_2/FiO_2) >150-200 mmHg; (b) level of positive end expiratory pressure

($PEEP$) between 5-8 cm H_2O; (c) FiO_2 <50%; (d) pH >7.25; and (e) ability to initiate spontaneous breaths. Some of the subjective indices include: (a) hemodynamic stability; (b) absence of active myocardial ischemia; (c) absence of clinically significant, vasopressor-requiring hypotension; (d) appropriate neurological examination; (e) improving or normal chest radiogram; and (f) adequate muscle strength that enables the patient to initiate and sustain respiratory effort [16].

To determine which weaning parameters are clinically useful for evaluating a patient's ability to breathe without mechanical ventilation, some studies have generated a set of evidence-based clinical practice guidelines on managing the ventilator weaning process and extubation [17]. Meade et al. [18] analysed the performance of various clinical measurements as predictors of successful extubation. They then drew up a list of several useful weaning and extubation indices that are widely used today (Table 2.2). Despite the high sensitivity (78% to 100%) of these indices, the specificity is very low (11% to 36%). This low specificity contributes to preventing weaning and extubation in a certain percentage of patients who are otherwise able to breathec independently.

Table 2.2 Commonly used clinical parameters that predict successful weaning from mechanical ventilation

Parameter	Desired value
Respiratory rate (f)	Less than 30-38 breaths/min
Tidal volume (V_T)	4-6 ml/kg
Minute ventilation ($\dot{V}_E$)	10-15 l/min
Negative inspiratory force (NIF)	-20 to -30 cm H_2O
Maximal inspiratory pressure (P_{max})	-15 to -30 cm H_2O
Mouth occlusion pressure 100 ms after the onset of inspiratory effort ($P_{0.1}$) divided by P_{max}	0.3
Rapid shallow breathing index ($RSBI$) (respiratory rate divided by tidal volume, f/V_T)	60-105 breaths/min $\cdot$ l
Rapid shallow breathing index rate $[(RSBI_2 - RSBI_1)/RSBI_1] \cdot 100$	Less than 20%
$CROP$ score (index including compliance, rate, oxygenation and pressure)	13

2.2.3 Weaning versus extubation risks

Weaning procedures are usually started only after the underlying disease process that necessitated mechanical ventilation has significantly improved or is resolved. During the weaning process, mechanically ventilated patients are liberated from the ventilator. Weaning and extubation are two separate processes. Extubation failure is defined as the inability to sustain spontaneous breathing after removal of the artificial airway, which may be an endotracheal tube or a tracheostomy tube, and the need for

reintubation within a specified time period of 24-72 hours or up to 7 days. Weaning predictors and outcomes have been extensively described in the literature. However, most of them do not accurately predict extubation results. Intensive care units (ICU) aim to predict extubation failure, since both delayed and failed extubation have detrimental consequences, including prolonged mechanical ventilation, a longer ICU stay, a need for tracheostomy, higher treatment costs and greater mortality [19] and [20].

According to a study carried out by Kulkarni [5], the incidence of extubation failure varies between 6 and 47%. Patients who needed reintubation required mechanical ventilation for significantly longer, had longer ICU and hospital stays and greater mortality. The reported [19] and [21] mortality rates in patients with extubation failure vary between 30 and 40%.

As stated by Kulkarni [5], deconditioned muscles, poor nutrition, upper airway edema due to prolonged translaryngeal intubation, an inability to clear secretions, a decreased level of consciousness due to the persistent effects of sedative and analgesics and critical illness polyneuropathy can all lead to extubation failure.

Several hypotheses attempt to explain the increased mortality associated with failed extubation. The first hypothesis is that increased mortality after extubation failure may reflect a sicker group of patients, in which failed extubation acts as an additional marker of severity of illness. A second hypothesis is that reintubation itself might increase mortality, as it is an invasive procedure. This may be due to life-threatening events during reintubation, such as cardiac arrest, esophageal intubation, endobronchial intubation, aspiration of gastric contents and cardiac arrhythmias. In addition, patients who required reintubation were found to be more likely to develop nosocomial pneumonia (47% vs. 10%) with increased mortality. However, if reintubation itself causes mortality, then mortality should not vary for different causes of

extubation failure.

Esteban and colleagues [22] found lower mortality for patients who were reintubated for upper airway obstruction than those reintubated for respiratory failure (7% vs. 30%). This is because reintubation for upper airway obstruction rapidly corrects respiratory dysfunction; whereas organ dysfunction that is related to other causes of extubation failure may not be readily reversible.

The third hypothesis is that clinical deterioration occurs during spontaneous breathing with the development of new organ dysfunction, thereby increasing mortality. This may partly explain the relationship between the cause of extubation failure and the outcome. This hypothesis is further supported by the increase in mortality with increasing time between extubation and reintubation, independent of the etiology of the extubation failure. Mortality due to respiratory failure increased four times when reintubation occurred >12 h after extubation.

Another similar hypothesis assumes that there is a relationship between delay in reintubation and increased mortality. This delay allows progressive clinical deterioration in the patient's condition, which leads to organ dysfunction/failure.

2.2.4 Recommended weaning

2.2.4.1 Weaning process

Tobin proposed [23] six stages in the process of care, from intubation and initiation of mechanical ventilation through to the initiation of the weaning effort and the final liberation from mechanical ventilation and successful extubation. These stages consist in:

- The treatment of acute respiratory failure.

- The clinician suspects that weaning may be possible.
- The clinician actually initiates a process of daily tests of readiness to wean so as to confirm this suspicion.
- The spontaneous breathing trial (SBT) is performed when the results of the daily test confirm a high enough probability of passing the SBT , which is defined as a T-tube test or low-level pressure support ($\leq$8 cm H_2O).
- Extubation or removal of the endotracheal tube, if the SBT is successful.
- Reintubation with an endotracheal tube if the patient is unable to maintain spontaneous breathing.

2.2.4.2 Spontaneous breathing trial, SBT

Some reports claim that the best method to assess whether a patient is able to breathe on his/her own is to perform a trial of spontaneous ventilation. Numerous studies [15], [22], [24] and [25] have shown that 60-80% of mechanically ventilated patients can be successfully extubated after passing a spontaneous breathing trial (SBT). The best technique for such trials is not yet clear.

SBT that compared the use of continuous positive airway pressure of 5 cm H_2O with a T-tube test for one hour revealed no difference in the percentage of patients who failed extubation. In a study carried out by the Spanish Lung Failure Collaborative Group, no differences were observed in the percentage of patients who remained extubated 48 hours after trials of spontaneous breathing with either T-tube test or pressure support ventilation of 7 cm H_2O. In the case of the T-tube, 63% of patients were successfully extubated, compared to 70% in the pressure support group. In

addition, when SBT trials of 30 minutes were compared with those of 120 minutes, no differences were found in the rate of successful extubation (84% vs. 89%) between the members of the two study groups [22] who tolerated the SBT.

2.2.4.3 SBT readiness

According to the above information, the weaning process should start with an assessment of readiness for weaning, which should be followed by SBT as a diagnostic test to determine the probability of successful extubation. However, a literature review indicates that the criteria for assessing readiness to wean a patient are not clearly defined. According to the Consensus Conference on Intensive Care Medicine [1], a patient who is ready to be weaned should meet the requirements reported in Table 2.3.

Table 2.3 Considerations for assessing readiness to wean [1]

Clinical assessment
Adequate cough
Absence of excessive tracheobronchial secretion
Resolution of acute disease phase for which the patient was intubated
Objective measurements
Clinical stability
Stable cardiovascular status (i.e. $f_C \leq 140$ beats/min, systolic BP $90-160$ mmHg, no or minimal vasopressors)
Stable metabolic status
Adequate oxygenation
SaO_2 >90% on $\leq FIO_2$ 0.4 (or PaO_2/FIO_2 ≥150 mmHg)
$PEEP$ ≤8 cm H_2O
Adequate pulmonary function
f_R ≤35 breaths/min
P_{max} ≤-20 to -25 cm H_2O
V_T >5 ml/kg
VC >10 ml/kg
f/V_T <105 breaths/min · l
No significant respiratory acidosis
Adequate mental state
No sedation or adequate mental state under sedation (or stable neurologic patient)

f_C: cardiac frequency; BP: blood pressure; SaO_2: arterial oxygen saturation; FIO_2: inspiratory oxygen fraction; PaO_2: arterial oxygen tension; $PEEP$: positive end expiratory pressure; f: respiratory frequency; P_{max}: maximal inspiratory pressure; V_T: tidal volume; VC: vital capacity.

1 mmHg = 0.133 kPa

2.2.4.4 SBT failure

Weaning success is defined as extubation and the absence of ventilatory support 48 hours after extubation. Weaning failure is defined as a failed SBT or reintubation of the endotracheal tube for reinstitution of ventilatory support after a successful extubation or death within 48 hours after extubation.

Numerous studies [15], [26], [22], [24] and [27] have demonstrated that approximately 13% to 25% of patients who successfully pass the SBT and are extubated require reintubation. In patients who do not receive an SBT and are extubated, the failure rate is 40%. The criteria used to pass SBT include respiratory pattern, adequate gas exchange, hemodynamic stability and subject comfort.

As recommended by consensus [1], when patients fail an initial SBT, the clinician should repeat the SBT frequently (daily) to determine the earliest time at which the patient can be successfully extubated. The criteria for SBT failure are defined in Table 2.4.

2.2.4.5 Extubation

Extubation failure can occur for reasons that are not directly related to weaning failure. In addition to a successful SBT, several important factors have to be carefully considered prior to extubation, including the presence of a patent airway, the patient's ability to consistently protect the airway, the patient's ability to clear secretions, mental status compatible with maintenance of the airway, secretion clearance and absence of any other reasons for potential extubation failure (e.g. severe pain that prevents adequate respiratory function, presence of apnea, poorly controlled seizures, risk of massive upper gastrointestinal bleeding, etc.) [16].

Table 2.4 Failure parameters of spontaneous breathing trials [1]

Clinical assessment and subjective indices
Agitation and anxiety
Depressed mental status
Diaphoresis
Cyanosis
Evidence of increasing effort
Increased accessory muscle activity
Facial signs of distress
Dyspnoea
Objective measurements
PaO_2 ≤50-60 mmHg on FIO_2 ≥0.5 or SaO_2<90%
$PaCO_2$ >50 mmHg or an increase in $PaCO_2$ >8 mmHg
pH <7.32 or a decrease in pH ≥0.07 pH units
f/V_T >105 breaths/min
f >35 breaths/min or increased by ≥50%
f_C >140 beats/min or increased by ≥20%
Systolic BP >180 mmHg or increased by ≥20%
Systolic BP <90 mmHg
Cardiac arrhythmias

PaO_2: arterial oxygen tension; FIO_2: inspiratory oxygen fraction; SaO_2: arterial oxygen saturation; $PaCO_2$: arterial carbon dioxide tension; f: respiratory frequency; V_T: tidal volume; f_C: cardiac frequency; BP: blood pressure. 1 mmHg = 0.133 kPa.

Extubation failure is defined mainly by the clinical criteria shown in Table 2.5.

Table 2.5 Criteria for extubation failure [1]

f >25 breaths/min for 2 hours
f_C >140 beats/min or sustained increase or decrease of >20%
Clinical signs of respiratory muscle fatigue or increased work of breathing
SaO_2 <90%; PaO_2 <80 mmHg on FIO_2 ≥0.50
Hypercapnia ($PaCO_2$ >45 mmHg or 20% from pre-extubation), pH <7.33

f: respiratory frequency; f_C: cardiac frequency; SaO_2: arterial oxygen saturation; PaO_2: arterial oxygen tension; FIO_2: inspiratory oxygen fraction; $PaCO_2$: arterial carbon dioxide tension. 1 mmHg = 0.133 kPa.

2.3 Weaning readiness prediction by means of signal processing

The number of patients who perform a successful SBT but have to be reintubated in less than 48 hours is still below 25% for different populations. The management of these patients is particularly difficult, largely because of our limited understanding of the pathophysiological mechanisms that are responsible for weaning failure [17]. The maintenance of unnecessary ventilator support carries its own burden of risk of infection and other complications and increases hospital costs. Therefore, critical-care clinicians must carefully assess the benefits of prompt liberation from mechanical ventilation, against the risks of a premature test of spontaneous breathing and extubation [28].

Since weaning indicator selection and threshold setting for these descriptors may vary according to clinicians' perceptions, we studied objective indices that were extracted from temporal data by signal processing. These indices might help clinicians in their decisions to increase or decrease the level of respiratory support [25]. They may minimize incorrect decisions and inter/intra expert variability.

Numerous studies have been carried out to detect which physiological variables can identify readiness to undertake a weaning trial. The accuracy of a number of variables has been assessed by statistical tests that determine whether significant differences exist between a group of patients who underwent a successful weaning trial, those who failed such a trial, and those who successfully passed a weaning trial and the extubation process, but had to be reconnected because they were not able to maintain spontaneous breathing. Most of the information collected in the studies [29], [30], [14], [15], [31] and [26] establishes different guidelines for weaning criteria and protocols.

Multiple signal processing methods have been used to assess weaning and the extubation outcome. These techniques include tasks concerning the reduction of artefacts in noisy temporal signals, the treatment of missing data, feature extraction from temporal data, trend detection and processing techniques for multiple channel data merging. Some of the signal processing methods that are used in the weaning problem and their accuracy in weaning prediction are discussed in [29].

The extraction of weaning indices from a set of potentially informative temporal data is the first step in distinguishing between patients who can maintain spontaneous breathing, those unable to do so, and those who can maintain spontaneous breathing for 30 minutes, but not for more than 48 hours. We link weaning indices to physiological parameters that appear to be potential candidates for predicting whether a

weaning process will be successful or a failure.

A number of factors may influence weaning prediction, such as weaning indices, extubation criteria, days of mechanical ventilation before weaning, different clinical procedures, differences between patient populations and even the etiology of the respiratory failure [26], [32], [33] and [34]. Although some weaning indices appear to be useful in many studies, there is no one criterion available for all population groups [29]. Thus, indicators for accurate prediction are still under research.

2.3.1 Linear methods

One simple way of analysing the data is by applying descriptive statistics (means and dispersion measures) to the dataset. From a physiological perspective, these methods are easy to interpret, but they do not yield information on the system dynamics.

Analyses of respiratory function are commonly performed in terms of inspiration and expiration time series, which are often referred to as breathing pattern variables [35]. Inspiratory time (T_I), expiratory time (T_E), breath duration (T_{Tot}), tidal volume (V_T), fractional inspiratory time (T_I/T_{Tot}), mean inspiratory flow (V_T/T_I) and frequency-tidal volume ratio (f/V_T), where f is the respiratory frequency, are some of the time series that are studied [36] and [37].

Traditional linear analysis time series methods measure the strength of oscillations within a specific frequency range. A number of time-frequency methods are used to extract useful information from the temporal data. The Fourier transform is generally used to study the frequency components of the signal. The signals can be represented by autoregressive models which permit better frequency resolution of the spectrum [38] and [39]. Complex mixed models have been developed to model the respiratory system [40]. Short-time Fourier transform, wavelet analysis and adaptive

parametric models have been analysed, which permit the study of signals simultaneously in the time and frequency domain, with limited resolution [41] and [42]. Although quadratic energy distributions might improve both the time and frequency resolution, they are computationally very expensive and sensitive to artefacts. One review examines the time-frequency methods used in biomedical engineering. It provides objective criteria that might help to choose the correct analysis technique for a particular type of signal [43].

2.3.2 Nonlinear methods

Respiratory signal variations have traditionally been treated as uncorrelated noise superimposed on the output of the respiratory signal. Descriptive statistics have been used to quantify the effect of this type of noise. Averaging over many breathing cycles is carried out prior to the estimation of these parameters. However, it has been reported that variability in the breathing pattern is not only an artefact of biological noise, but also an integral component of respiratory control mechanisms [44]. Therefore, several analyses of weaning outcome assessment are based on the study of respiratory pattern variability [34], [40] and [45] and its influence on weaning outcome [33] and [32].

It is difficult to determine whether respiratory variability is random or deterministic, since random types create significant obstacles in the analysis of deterministic ones and vice versa. Certain physiological failures are represented by a specific type of variability. Thus, it may be useful to separate each of these types. As it is not easy to isolate each type of variability, integrated measurements that reflect the total complexity of a biological signal have been proposed [44] and [29].

Numerous nonlinear complexity assessment techniques have been used in the liter-

ature as weaning descriptors or for breathing pattern variability analysis. Some complexity metrics, including approximate entropy ($ApEn$) sample entropy ($SampEn$) and cross-entropies derived from $ApEn$ and $SampEn$, have been studied for the weaning readiness decision in [33], [46] and [47]. Kolmogorov entropy was used in [48] to conclude that the spontaneous breathing pattern during minimal mechanical ventilatory support is more chaotic in patients who fail extubation trials than in patients who pass such trials. Poincaré and phase plots with some automatic parameter extraction were used for weaning prediction in [48] and [32]. A huge number of data samples is needed for other nonlinear methods, such as correlation dimension and fractals. Symbolic dynamics and Lempel-Ziv entropy evaluate the complexity of the data from codified versions of the signal [49].

The aim of these nonlinear signal processing techniques is to extract variability information from certain measured variables and to assess the potential usefulness of this variability in predictions of the weaning outcome.

2.3.3 Multidimensional

Although most of the studies on postoperative patients showed that those who failed an extubation trial had more irregular patterns than those who passed the trial [33], [29] and [50], Bien et al. [32] found the opposite behaviour for postoperative patients recovering from systemic inflammatory response syndrome. The performance obtained with a one-dimensional variability based feature may be controversial in real clinical practice. However, when pattern variability is the only predictor, inconsistency arises between different patient groups. This inconsistency suggests that pattern variability should be combined with other potential predictors to improve the results of decisions in heterogeneous intensive care unit environments. Recent studies have demonstrated

that breathing pattern variability is a useful extubation readiness indicator, and that performance improves when multiple respiratory signals are processed together [50].

Hsu et al. [51] combined several classical predictors with categorical variables that took into account clinical issues. Twenty-seven variables in total were recorded. However, only 8 variables that reached a significant level were used for the support vector machine (SVM) classification after logistic regression analysis. The result showed that the successful prediction rate was as high as 81.5%. Hence, this method outperformed a recently published predictor (78.6%) that used a combination of sample entropy of three variables: inspiratory tidal volume, expiratory tidal volume, and respiration rate.

The multidimensional classification scheme proposed in [52] was constructed using sample entropy as the best performing extraction method. It was calculated over tidal volume signals, with mean respiratory rates as additional input patterns, to generate a two-dimensional Bayesian classifier with principal component analysis selection. The classification rate (78.6%) and misclassification probability (21.4%) is acceptable if compared with the performance of single feature classifiers.

Giraldo et al. [36] and [37] presented two proposals to predict readiness for extubation. Both studies were based on eight features of seven time series that were extracted from respiratory signals (T_I, T_E, T_{Tot}, V_T, T_I/T_{Tot}, V_T/T_I and f/V_T) and selected from an initial set of 35 features. Feature extraction was performed by moving a running window of several breathing cycles for each of the seven time series. Five statistics (mean, standard deviation, skewness, kurtosis, and interquartile range) were calculated for each window, which yielded 35 new time series. To obtain the most representative values of the time series, a clustering method based on k-means was applied. The time-varying statistics of the breathing pattern were clustered to

represent the most general trend for each patient. Therefore, each patient was represented by a 35-component feature vector (the centroid of the main cluster), whose final dimension was reduced to 8 after selection. The final classification was performed by either a multilayer perceptron [37] (84.25% of correctly classified patients) or an SVM classifier together with histogram equalization [36] (80%). The results are slightly better than previously reported, and the proposed feature extraction allows for nonstationary signal processing.

2.4 Cardiovascular system

As stated by Guyton [2], the function of the cardiovascular system is, in general, to maintain an appropriate environment in all the tissue fluids of the body for optimal cell function and survival. This is achieved by transporting nutrients to the body tissues and waste products away, and by conducting hormones from one part of the body to another. The rate of blood flow through most tissues is controlled, in response to the tissue's need for nutrients. In turn, the heart and circulation are controlled to provide the cardiac output and arterial pressure required to ensure the tissue blood flow. The heart, one of the main organs of the cardiovascular system, (Fig. 2.5) is actually two separate pumps: a right heart that pumps blood through the lungs, and a left heart that pumps blood through the peripheral organs. Each of these pumps is composed of an atrium and a ventricle. Each atrium is a weak primer pump that helps to move blood into the ventricle. The ventricles then supply the main pumping force that propels the blood either through the pulmonary circulation by the right ventricle or through the peripheral circulation by the left ventricle [2].

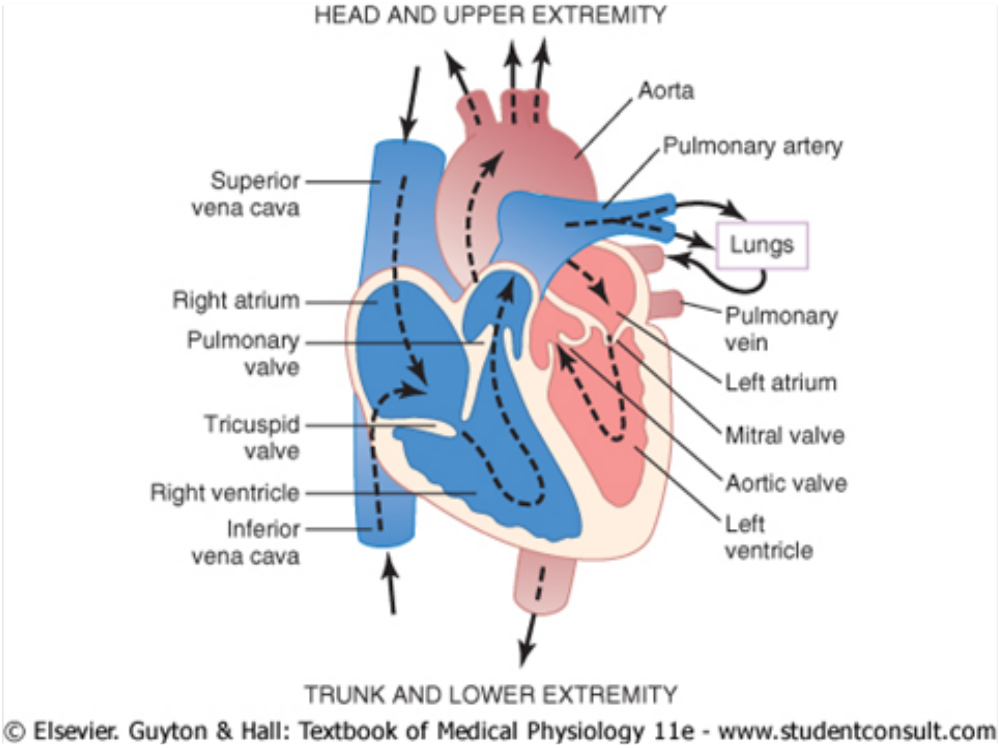

Figure 2.5 Heart muscle (authorized by [2]).

2.4.1 Cardiac function: electrocardiogram

The electrocardiogram represents the electrical activity of the heart. As shown in Fig. 2.6, a normal electrocardiogram is composed of a P wave, a QRS complex and a T wave. The QRS complex is usually formed by three separate waves: the Q wave, the R wave and the S wave.

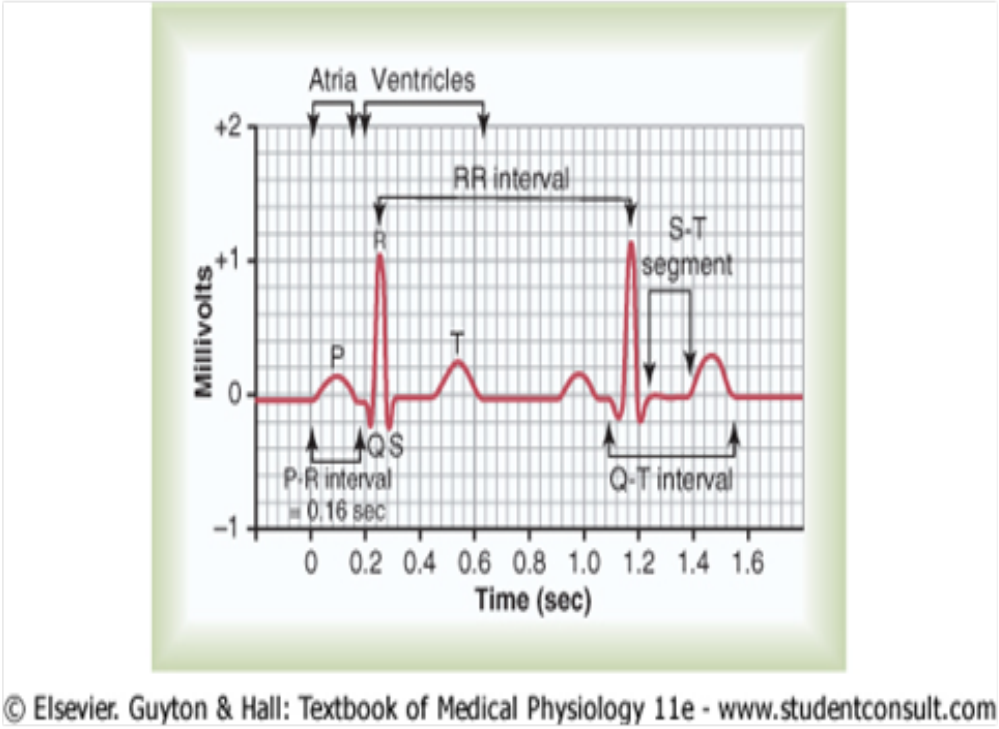

Figure 2.6 A normal electrocardiogram composed of a P wave, a QRS complex and a T wave (authorized by [2]).

Normal electrocardiogram

The electrocardiogram is composed of depolarization and repolarization waves. Both the P wave and the components of the QRS complex are depolarization waves. The P wave is caused by electrical potentials generated during normal atrial depolarization, before atrial contraction begins. The QRS complex is caused by potentials generated when the ventricles depolarize before contraction. The T wave is known as a repolarization wave and is caused by potentials generated as the ventricles recover from the state of depolarization. This process normally occurs in ventricular muscle from

0.25 to 0.35 seconds after depolarization. The time between the beginning of the P wave and the beginning of the QRS complex, which is referred to as the P-Q interval, normally lasts 0.16 second. The Q-T interval is the contraction of the ventricle from the beginning of the Q wave to the end of the T wave and normally lasts 0.35 second. The normal heart rate is 60 beats per minute.

2.4.2 Heart failure

The term heart failure simply means failure of the heart to pump enough blood to satisfy the needs of the body. Heart failure is one of the main ailments that must be treated by physicians. Any heart condition that reduces the ability of the heart to pump blood produces heart failure. The most usual cause of heart failure is decreased contractility of the myocardium, resulting from diminished coronary blood flow. However, it can also be caused by damaged heart valves, external pressure around the heart, vitamin B deficiency, primary heart muscle disease or any other abnormality that makes the heart an ineffective pump. If a heart suddenly becomes severely damaged, its pumping ability is immediately depressed, which reduces cardiac output and increases venous pressure.

When cardiac output falls precariously low, the sympathetic nerve signals become strongly stimulated within a few seconds, and the parasympathetic nerve signals to the heart become reciprocally inhibited at the same time. The sympathetic reflexes become maximally developed in about 30 seconds. Sympathetic stimulation has two major effects on circulation: on the heart, by strengthening the damaged musculature; and on the peripheral vasculature, by increasing venous return, which increases the tone of most of the blood vessels.

The dynamics of circulatory changes after acute heart failure are divided into

three stages: the instantaneous effect of the heart damage, compensation by the sympathetic nervous system, and chronic compensation resulting from partial heart recovery and renal retention of fluid.

The cardiac reserve is reduced in people with compensated heart failure. Hence, any attempt to perform heavy exercise usually causes immediate return of the symptoms of acute failure, because the heart is not able to increase its pumping capacity to the levels required for the exercise.

When the heart becomes severely damaged, either by sympathetic reflexes or by fluid retention, the weakened heart pump cannot achieve normal cardiac output. We refer to this as decompensated heart failure. In this situation, the cardiac output is not sufficient to excrete normal quantities of fluid and it is retained. This state of events eventually leads to death.

2.4.3 Chronic heart failure

Chronic heart failure (CHF) is an increasingly widespread, costly and deadly disease that is frequently called a twenty-first century epidemic. Despite advances in modern treatment, the mortality rate in CHF patients remains high. Risk stratification in patients with CHF remains one of the major challenges of contemporary cardiology [53].

The prevalence of CHF in the US population is 2%. Almost 5 million people are affected in total, and 30–40% of all patients die within one year of diagnosis [54]and [55]. Patients with chronic heart failure (CHF) often develop breathing abnormalities, including various forms of oscillatory breathing patterns that are characterized by rises and falls in ventilation [56] and [57]. Periodic breathing (PB) in CHF is attributed to many factors, including: low cardiac output, which increases the time it takes pul-

monary venous blood to reach central and peripheral chemoreceptors; low lung volume; lung congestion; increased chemoreceptor sensitivity; and the narrow difference between eupneic carbon dioxide tension and the apneic hypoventilatory threshold [58].

Periodic breathing patterns can be classified into Cheyne–Stokes respiration (CSR), and ventilation without apnea [59] and [60]. CSR is characterized by repetitive gradual increases and subsequent gradual decreases in ventilation, followed by periods of apnea. It occurs in patients with a variety of diseases and conditions. PB in CHF patients has a similar increase and decrease in ventilation, but there are no periods of apnea. Both ventilatory patterns may have the same mechanistic explanations, as PB is a less severe form of CSR [58].

The prevalence of periodic breathing is as high as 70% in CHF patients [61] and is associated with increased mortality [62], especially in CSR patients [63] and [64]. Accurate risk stratification is crucial to establish the prognosis and to appropriately allocate limited resources for advanced but expensive treatments, including heart transplantation [65]. Breathing patterns are also influenced by wakefulness or sleep, posture, physiological activity and mental activity [66]. Physiological parameters for the characterization and detection of different breathing patterns have been suggested in a number of clinical studies [67] and [68].

The most relevant clinical predictors of the outcome of heart failure patients are the New York Heart Association (NYHA) class, the left ventricular ejection fraction, systolic arterial pressure, and the peak VO_2 at cardiopulmonary exercise testing. Other risk factors include low exercise tolerance, arrhythmias, the cardiothoracic ratio and disturbances in the autonomic nervous system. These accepted risk indices perform well in the prediction of mortality due to disease progression, but the prediction of sudden cardiac death (SCD) appears more problematic. In hospitalized,

symptomatic CHF patients at high risk of all-cause mortality, death is often due to progressive pump failure. However, in ambulatory patients with less severe CHF, symptoms may be less obvious and death is more often sudden in nature. The importance of being able to identify mildly symptomatic CHF patients at risk from SCD is of paramount importance [69].

Normal breathing cycles range from 3 to 5 s (i.e. 0.20–0.33 Hz). PB patterns have cycles of 25 to 100 s (i.e. 0.01–0.04 Hz) [66]. The origin of the PB pattern is still a matter of debate among researchers. Respiratory modulation frequency appears to be essential for understanding periodic and nonperiodic breathing patterns in CHF patients.

Some of the clinical parameters that are used to estimate the severity of CHF have limitations, due to the heterogeneity and complexity of the syndrome. For example, exertional oscillatory ventilation, which is evaluated during exercise, is associated with a more advanced clinical status, cardiac functional impairment and reduced exercise capacity, and may reflect a more severe alteration of the ventilatory control system [65].

CHF has been related to alterations in breathing pattern [70]. For example, sleep-disordered breathing is associated with an accelerated decline in cardiac function and increased morbidity and mortality [71] in up to 50% of patients with CHF [72]. Several studies suggest that central sleep apnea is highly prevalent among patients with CHF, and the treatment of this sleep-disordered breathing by continuous positive airway pressure could be an important nonpharmacological complement to conventional drug therapy [73] and [74]. In patients with mild to severe CHF, the power of cardiovascular oscillations in the very low frequency band has been reported to be considerably increased by the presence of periodic breathing, which may alter prognosis [75].

Evidence that links exercise capacity to outcome in CHF patients has led to the use of peak oxygen consumption, which is derived from maximal cardiopulmonary exercise testing, and exertional oscillatory ventilation in prognostic assessment. However, these two indices have certain limitations, due to the heterogeneity and complexity of the syndrome [76].

Although CSR is a known sleep-related phenomenon, according to Poletti et al. [63], central apnea and hypopnea also occur in a high percentage of CHF patients during the daytime. Among all the risk factors for daytime CSR, the concentration of plasma NT-proBNP is the best independent predictor of breathing abnormalities.

Daytime CSR is significantly associated with more severe clinical impairment, left ventricular ejection fraction and functional capacity, and lower levels of resting. The latter finding suggests that there is a common pathogenesis for daytime and nocturnal CSR. The absence of obstructive apneas in awake patients during the daytime confirms that in awake states there is adequate stimulation of the dilator muscles to maintain upper airway patency.

In a recent study, Brack et al. [77] proposed that CSR during 10% of the daytime is an independent predictor of death, after adjusting for B-type Natriuretic Peptide (BNP), age, and NYHA class. However, the authors only enrolled 60 patients and employed a long-term recording device, without taking into account patient-to-patient variations in postural changes, speech and physical daily activity.

Maestri et al. [78] studied all the main families of nonlinear methods and found that several nonlinear indices of heart rate variability contained correlated information, whilst others were strongly correlated with classical linear indices. Only two nonlinear indices proved to have a prognostic value that was independent of major clinical and functional predictors, such as symptom severity, left ventricular ejection

fraction, peak VO_2 at cardiopulmonary exercise testing, and systolic arterial pressure. Therefore, the quantification of nonlinear properties of heart rate variability provides important information for the risk stratification of CHF patients.

ECG parameters based on ambulatory Holter monitoring have been documented to be independent risk predictors of total mortality and progression of heart failure. Modern Holter monitoring serves as a valuable tool for investigating factors that may contribute to the mechanism of sudden death. It provides complementary information on myocardial vulnerability and the autonomic nervous system. Nevertheless, data regarding its prognostic value in the prediction of sudden cardiac death remains controversial and the positive predictive value of most Holter-based risk stratifiers is low [53].

It is unlikely that one specific ECG risk predictor could be found to predict the risk level or sudden death in a heterogeneous population of patients with chronic heart failure. Therefore, it seems that the combination of various risk markers that cover different information should be considered a better approach. Thus, in view of the breathing abnormalities presented by CHF patients, we focused on extracting information from the respiratory system.

We investigated the hypothesis that an in-depth study of the respiratory pattern could improve the identification of the risk level of a particular pathological disturbance and the compensatory response of the organism under pathophysiological conditions. Our previous studies [38] and [39] were focused on characterizing the frequency band that was determined by the peak of the power spectral density (PSD) associated with the envelope of the respiratory flow signal. In [79], we expanded considerably on the initial results obtained with this approach. We characterized the respiratory flow signal in CHF patients and healthy subjects using the envelope. On

the basis of autoregressive (AR) power spectral analysis of the envelope, the relevant discrimination band (DB) was determined from the location of the modulation frequency peak, and characterized by a number of spectral parameters.

It has been reported that the same patient might often present a mixture of breathing patterns, ranging from nonperiodic breathing (without cyclic modulation of ventilation) through to mild PB and CSR patterns [66]. Conventional spectral analysis assumes stationarity in the signal and is therefore unable to identify pattern changes. An approach which better accounts for such changes is the time-varying autoregressive (TVAR) model [80].

A study of the time-varying envelope was carried out to characterize and study dynamic changes in the respiratory flow signal in CHF patients and healthy subjects. The characterization involved both spectral and temporal parameters, which were extracted from the power spectrum of the respiratory flow envelope. The statistical distributions of these parameters accounted for the temporal evolution of the breathing pattern [41].

To develop new quantitative parameters, our initial studies were focused on the periodicity of the respiratory pattern through the modulation of the respiratory flow signal. We characterized the relevant frequency band, which was determined by the frequency peak of the power spectral density (PSD) and related to the envelope of the respiratory flow signal [38] and [39]. Both respiratory modulation frequency and respiratory frequency are essential to the study of periodic and nonperiodic breathing patterns (PB and nPB, respectively).

The correlation function is probably the most widely used function in signal processing for quantifying the similarity of two random variables. The success of this measure depends on the assumption of Gaussian random variables, since it only con-

siders second-order statistics. Santamaria et al. recently introduced a generalization of the correlation function for stochastic processes, which was called correntropy [81] [82]. In [83] and [84], the respiratory flow signal in CHF patients with a PB and nPB pattern is studied through correntropy to define parameters that can improve prognosis and serve as indicators of a patient's condition. Correntropy involves information on higher-order statistics, which can be expected to facilitate the detection of respiratory nonlinearities that conventional second-order statistical techniques are unable to identify.

2.5 Datasets

A weaning dataset is used in this research to extract indices that may help to predict patients' readiness to wean. Considering the breathing abnormalities presented by chronic heart failure (CHF) patients, we analysed a dataset that includes the respiration of a number of CHF patients. A dataset containing healthy subjects was used to find differences between normal and pathological breathing patterns. These datasets are described below.

2.5.1 Weaning dataset

Electrocardiographic (ECG) and respiratory flow signals were measured in 154 patients on weaning trials from mechanical ventilation (WEANDB database). These patients were recorded in the Departments of Intensive Care Medicine at Santa Creu i Sant Pau Hospital, Barcelona, Spain, and Getafe Hospital, Getafe, Spain, according to protocols approved by local ethics committees. The patients gave their informed consent to participate.

Using clinical criteria based on the T-tube trial, the patients were included in this study according to standard indices that initially determine the spontaneous breathing test: resolution of the etiology of respiratory failure (with inspired oxygen fraction $[FiO_2] \leq 0.4$, oxygen saturation $[SO_2] \geq 90\%$ and the need for positive end-expiratory pressure [PEEP ≤ 5 cm to H_2O]), hemodynamic stability (absence of myocardium ischemia and/or heart failure, cardiac frequency ≤ 140 bpm, and stable arterial tension with tolerance of a reduction in inotropic support), and adequate respiratory muscle function (acceptable respiratory rate).

The patients underwent a test of spontaneous breathing, in which they were disconnected from the ventilator and maintained spontaneous breathing through an endotracheal tube for 30 minutes. Patients who were able to maintain spontaneous breathing were extubated, whereas patients who were not able to breathe spontaneously were reconnected. When the patients were still able to maintain spontaneous breathing after 48 hours, the weaning trial process was considered successful. If not, the patients were reintubated (Fig. 2.7).

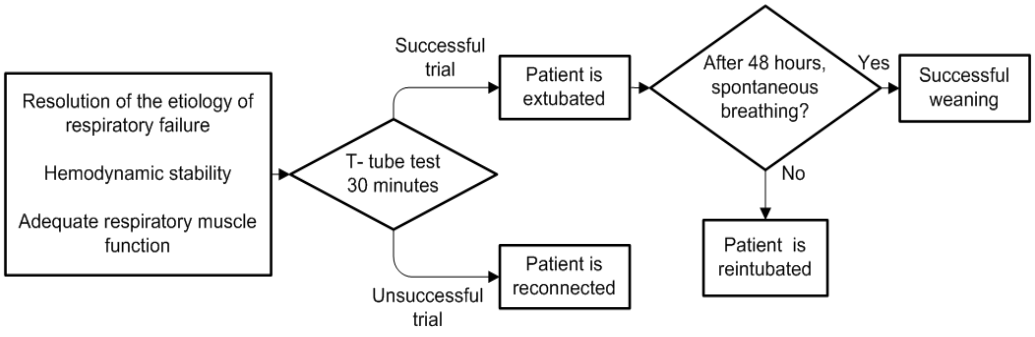

Figure 2.7 Weaning trial process.

Patients included in the study were classified into three groups according to spontaneous breathing test outcome: GS, 94 patients (61 male, 33 female, 65 $\pm$17 years)

with successful trials who could maintain spontaneous breathing after 48 hours; GF, 39 patients (24 male, 15 female, 67 $\pm$ 15 years) who failed to maintain spontaneous breathing and were reconnected after 30 minutes of weaning trials; GR, 21 patients (11 male, 10 female, 68 $\pm$ 14 years) who successfully passed the weaning trials but had to be reintubated in less than 48 hours.

The ECG signal was obtained using a SpaceLabs Medical monitor. The respiratory flow signal was recorded using a pneumotachograph connected to an endotracheal tube. The pneumotachograph consists of a Datex-Ohmeda monitor with a variable-reluctance transducer (Validyne Model MP45-1-871). Both signals were recorded synchronously with a sampling frequency of 250 Hz for 30 minutes. The time series of the cardiac interbeat interval, $RR(k_1)$, were extracted automatically from the ECG signal using an algorithm based on wavelet analysis [42]. Ectopic beats were determined, removed and interpolated using an algorithm based on local variance estimation. The time series of the breath duration, $T_{Tot}(k_2)$, were extracted automatically using an algorithm based on the zero-crossing of the respiratory flow signal. Thereafter, they were visually inspected and edited, if necessary.

2.5.2 Chronic heart failure dataset

Respiratory flow signals were recorded from 26 CHF patients (7 female, 65$\pm$9 years, 19.6$\pm$3.4 breaths/min) at Santa Creu i Sant Pau Hospital, Barcelona, Spain. All patients were studied according to a protocol approved by the local ethics committee. The respiratory flow signals were acquired using a pneumotachograph, consisting of a Datex-Ohmeda monitor with a Validyne Model MP45-1-871 variable-reluctance transducer. The pneumotachograph was connected to a mask. The signals were recorded at 250-Hz sampling rate and 12-bit resolution.

The same patient might present a mixture of breathing patterns, ranging from nonperiodic breathing (without cyclic modulation of ventilation) through to mild PB and CSR patterns. The respiratory flow signals of CHF patients were acquired during a check-up. Prior to data acquisition, a few minutes of adaptation were allowed, to enable the subjects to feel comfortable with the mask. The respiratory flow signals were acquired for 15 minutes. All patients were seated and remained awake throughout the data acquisition.

The classification of the CHF patients (PB, nPB and CSR) was undertaken by medical doctors at the Santa Creu i Sant Pau Hospital, Barcelona, Spain. The CHF patients were classified into two groups: 8 patients with PB patterns (1 female, 71±7 years, 18.4±2.2 breaths/min), and 18 patients with nonperiodic breathing (nPB) pattern (5 female, 62±9 years, 22.5±4.3 breaths/min). Within the PB group, 3 patients were classified as CSR (1 female, 68±6 years, 21.7±4.2 breaths/min) and 5 patients as PB without apnea (no females, 73±8 years, 23.0±4.7 breaths/min).

For the 26 subjects, the respiratory frequency was found to range from 0.2 to 0.4 Hz, and the modulation frequency from 0.01 to 0.04 Hz. These frequency ranges are in good agreement with those reported by Pinna et al. [66].

The flow signals were decimated from 250 to 2 Hz, using null-phase antialiasing filtering to account for the fact that the frequencies of interest only range up to about 0.5 Hz. It is particularly important to avoid oversampling when the AR spectral analysis is carried out [85].

CHF patients presented 19.6±3.4 breaths/min respiratory frequency and 0.95±0.26 l tidal volume in the nPB group, 19.42±3.16 breaths/min respiratory frequency and 1.66±0.48 l tidal volume in the PB group, and within the PB group, 18.11±1.86 breaths/min respiratory frequency and 1.76±0.59 l tidal volume in the periodic breath-

ing without apnea group, and 21.60±4.07 breaths/min respiratory frequency and 1.49±0.20 l tidal volume in the CSR group.

2.5.3 Healthy dataset

Respiratory flow signals were recorded from 35 healthy volunteers (23 female, 27±7 years, respiratory frequency 15.5±3.7 breaths/min) at Santa Creu i Sant Pau Hospital, Barcelona, Spain. All subjects were studied according to a protocol approved by the local ethics committee. The respiratory flow signals were acquired using a pneumotachograph, consisting of a Datex-Ohmeda monitor with a Validyne Model MP45-1-871 variable-reluctance transducer. The pneumotachograph was connected to a mask. The signals were recorded at 250-Hz sampling rate and 12-bit resolution.

Prior to data acquisition, a few minutes of adaptation were allowed to ensure that the subjects felt comfortable with the mask. Respiratory flow signals were acquired for 30 minutes. All subjects were seated and remained awake throughout the data acquisition.

For the 35 subjects, the respiratory frequency was found to range from 0.2 to 0.4 Hz, and the modulation frequency from 0.01 to 0.04 Hz. These frequency ranges are in good agreement with those reported by Pinna et al. [66].

The flow signals were decimated from 250 to 2 Hz, using null-phase antialiasing filtering to account for the fact that the frequencies of interest only range up to about 0.5 Hz. It is particularly important to avoid oversampling when AR spectral analysis is performed [85].

Healthy patients presented 15.5±3.7 breaths/min respiratory frequency and 0.49± 0.26 l tidal volume.

Fig. 2.8 illustrates the different flow patterns observed in CSR, PB and nPB patients, and a healthy subject.

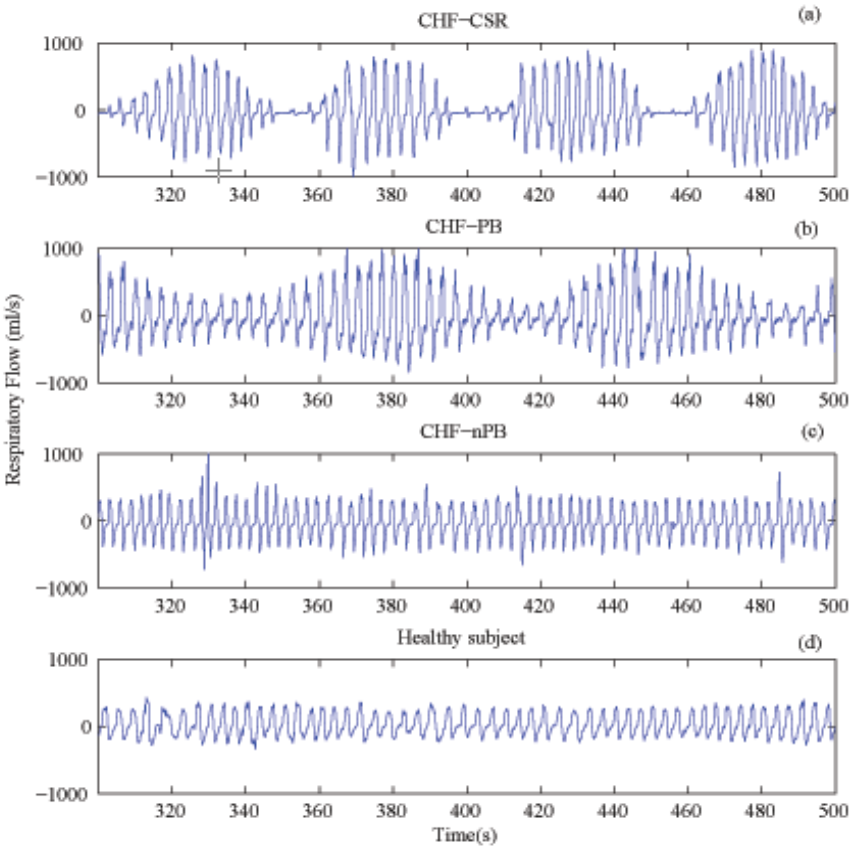

Figure 2.8 The respiratory flow signal exemplified for (a) a Cheyne-Stokes respiration patient, (b) a periodic breathing patient, (c) a nonperiodic breathing patient, and (d) a healthy subject.

2.6 Summary

The respiratory system is one of the vital systems for sustaining life. Its function is to allow gas exchange through all parts of the body.

Breathing is the result of periodic contractions and expansions of the thoracic cavity, which creates inspiration and expiration. Static and dynamic pulmonary volume and capacity measurements are described, which can be used to control the correct performance of the respiratory system. Both respiratory volume and flow signal represent the circulating air volume in a subject' airway. The most commonly used device for measuring respiratory flow is the pneumotachograph.

Respiratory failure is a dysfunction of the respiratory system and represents a medical emergency. Mechanical ventilation is the main medical treatment for acute respiratory failure, and one of the most commonly used techniques in intensive care.

Weaning involves the entire process of liberating the patient from mechanical support and from the endotracheal tube, including relevant aspects of terminal care. Weaning procedures are started only after the underlying disease process that required mechanical ventilation has significantly improved or is resolved. A number of indices have been defined to determine whether a patient can come off a ventilator.

Although much has been written about weaning predictors and outcomes, most of the techniques do not accurately predict extubation results. Critical-care clinicians must carefully assess the benefits of prompt liberation from mechanical ventilation against the risks of premature tests of spontaneous breathing and extubation. Both delayed and failed extubation have detrimental consequences. Patients who need reintubation require mechanical ventilation for significantly longer, remain in the intensive care unit and hospital for longer periods and have higher mortality.

A lot of research have been done on this topic, but the reintubation percentage remains between 6% and 47% [5] for different populations. Here, we review some of the more relevant studies that are based on predicting readiness for extubation through signal processing.

Chronic heart failure (CHF) is a major health problem. Despite advances in modern treatment, the mortality rate of CHF patients remains high. Risk stratification in patients with CHF remains one of the major challenges of contemporary cardiology.

Patients with CHF often develop breathing abnormalities, including various forms of oscillatory breathing patterns that are characterized by rises and falls in ventilation. The prevalence of periodic breathing in CHF patients is as high as 70%, and is associated with increased mortality, especially in patients with Cheyne-Stokes respiration.

A number of indices have been proposed in the literature to predict the condition of CHF patients, but many of them are correlated with clinical indices (no information is added), and tend to have low sensitivities.

To help clinical doctors in the diagnosis of patients, in this research we analyse the respiratory system of patients with different pathologies in depth. Specifically, we study patients on weaning trials and patients with chronic heart failure. For this purpose, we have used datasets that include patients on weaning trials, CHF patients and healthy subjects.

Chapter 3

Pattern recognition techniques

The objective of this chapter is to summarize and compare some of the well-known techniques that are used in a pattern recognition system. The design of a recognition system requires careful attention to the following issues: pattern class definition, the sensing environment, pattern representation, feature extraction and selection, cluster analysis, classifier design and learning, selection of training and test samples, and performance evaluation. Among the various frameworks in which pattern recognition has traditionally been formulated, the statistical approach has been the most intensively studied and used in practice. More recently, methods imported from statistical learning theory, such as support vector machines, have been receiving increasing attention. This chapter describes support vector machines and a number of metrics that are employed to evaluate the performance of respiratory pattern recognition.

3.1 Introduction

Pattern recognition or classification is concerned with predicting the class membership of an observation. There are a number of definitions of this topic in the literature . For instance, according to [3], pattern recognition is the study of how machines can observe the environment, learn to distinguish patterns of interest from their background, and make sound and reasonable decisions about the categories of the patterns. Duda and Hart [86] defined this as the assignment of a physical object or event to one of several pre-specified categories. According to Ripley [87], given some examples of complex signals and the correct decisions for them, pattern recognition consists of making decisions automatically for a stream of future samples. Schalkoff [88] defined it as a science that is concerned with the description or classification (recognition) of measurements.

The characterization, automatic recognition, classification and grouping of patterns are important problems in a variety of engineering and scientific disciplines, including biology, psychology, medicine, marketing, computer vision, artificial intelligence and remote sensing. A pattern can be defined as the opposite of chaos. Examples of patterns include a fingerprint image, a handwritten cursive word, a human face and a speech signal [3] and [89].

A pattern recognition system involves data acquisition and preprocessing, data representation, and decision-making. The real challenge lies in selecting the acquisition system, finding the most convenient preprocessing and characterization technique, and choosing the most suitable classifier.

The four best-known approaches for pattern recognition are based on template matching, statistical classification, syntactic or structural matching, and neural net-

works [3]. However, in this research we focus on statistical methods for pattern recognition.

3.2 Statistical pattern recognition

Statistical pattern recognition has been successfully applied to a number of pattern recognition problems. A pattern is represented by a set of L features that can be viewed as an L-dimensional feature vector. The decision boundaries between the different classes are established using concepts from statistical decision theory. Fig. 3.1 shows a statistical pattern recognition model that consists of two main processes: training or learning, and testing or classifying.

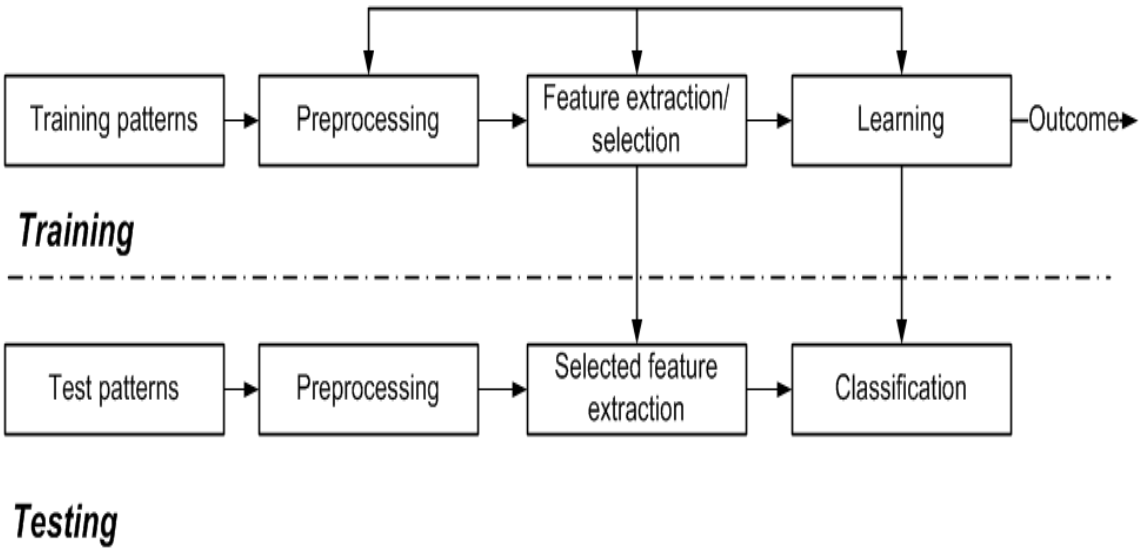

Figure 3.1 Proposed model for statistical pattern recognition (slightly modified from the model proposed by [3]).

In the preprocessing stage, the training data are prepared for accurate feature extraction by any operation that contributes to the compact characterization of the

pattern. In the training process, the feature extraction and feature selection stages calculate and find the appropriate features for representing the input patterns, and the classifier is trained to divide the feature space. The training feedback permits optimization of the preprocessing, feature extraction and selection stages. In the testing process, the trained classifier assigns the input pattern to one of the pattern classes under consideration, on the basis of the selected features.

3.3 Supervised and unsupervised learning

In statistical pattern recognition, there are two modes of training: supervised learning based on labelled training data samples; and unsupervised learning based on unlabelled training data samples.

In supervised training, the class to be recognized is known for each sample in the training data and a decision function is deduced from the labelled training data. The training data consist of pairs of input vectors and target outputs. When the output of the decision function is a continuous value, the process is known as regression. When the output predicts a class label, the process is called classification.

The aim of supervised learning is to predict the value of the decision function for any unlabelled input, after the study of a number of training examples that consist of pairs of input vector and target output. To achieve this, the training data must be generalized to unlabelled data.

Unsupervised learning is closely related to the problem of density estimation in statistics. However, it includes many other techniques that seek to determine how the data are organized. In contrast to supervised learning, there are no explicit target outputs associated with each input. Instead, unsupervised learning brings to bear

prior biases as to what aspects of the structure of the input should be captured in the output.

One form of unsupervised learning is clustering. This is a common technique for statistical data analysis that is used in many fields, including machine learning, data mining, pattern recognition, image analysis and bioinformatics. Cluster analysis or clustering is the assignment of a set of observations into subsets called clusters. It reveals the inner structure of the data, and recovers the natural grouping of the samples in the feature space. These methods are usually employed in data visualization procedures, data distribution structure understanding or as a support algorithms for the initialization of other more complex algorithms based on radial basis function or fuzzy approaches.

3.4 Generalization error

The goal of designing a recognition system is to classify future test samples that are likely to be different from the training samples. The performance of a classifier depends on the number of available training samples and the specific values of the samples. The optimization of a classifier to maximize its performance on the training set may not always result in the desired performance on a test set. The generalization ability of a classifier refers to its performance in classifying test patterns that were not used during the training stage. Poor generalization ability can be attributed to any one of the following factors: 1) the number of features is too large relative to the number of training samples, 2) the number of unknown parameters associated with the classifier is large (e.g. polynomial classifiers or a large neural network), and 3) a classifier is too intensively optimized on the training set (overtrained); this is

analogous to the phenomenon of overfitting in regression, which occurs when there are too many free parameters.

3.5 Classification techniques

3.5.1 K-means clustering

K-means clustering is a non-hierarchical method for cluster analysis. It fixes the number of partitions or clusters into which the data has to be split. First, the dataset is divided into K clusters. In the initialization, data points are randomly assigned to the clusters in such a way that each partition has approximately the same number of data samples. After initialization, the distance to each cluster is computed iteratively for each data sample, and each sample is assigned to the cluster at a minimum distance. This process is repeated until convergence. The choice of the initial partition is essential for cluster analysis, since it can dramatically affect the final convergence solution.

3.5.2 Discriminant analysis

Discriminant analysis is a common supervised machine learning method. The features of discriminant functions of the predictor are estimated in the training process. These are then used to separate the classes in the testing process. This method is useful for determining the accuracy of a set of features at predicting class membership. The results can be employed to reduce the complexity and/or dimensionality of a classification problem or as a classifier itself. Of the various discriminant analysis techniques, linear discriminant analysis (LDA) is the most frequently used classifier,

due to its simplicity and low computational cost.

The linear discrimination function is estimated by means of a set of data samples that are labelled into predefined classes. It is based on a set of features and is given by

$$f(x) = \sum_{i=1}^{L} b_i \cdot x_i + c \tag{3.1}$$

where b_i and x_i represent the discriminant coefficients and the input features, respectively and c is a constant. This discriminant function is used to predict the class of a new observation that has an unknown class.

In addition to linear discriminant analysis, there are a number of different discriminant functions, which are defined as:

- Diagonal linear discriminant analysis (DLDA): this is similar to 'LDA', but has a diagonal covariance matrix estimate (naive Bayes classifiers). It is the maximum likelihood discriminant rule for multivariate normal class densities when they have the same diagonal variance-covariance matrix.

- Quadratic discriminant analysis (QDA): this fits multivariate normal densities with covariance estimates that are stratified by class (unlike LDA, there is no assumption that the covariance of each of the classes is identical).

- Diagonal quadratic discriminant analysis (DQDA): this is similar to QDA, but has a diagonal covariance matrix estimate (naive Bayes classifiers).

- Mahalanobis discriminant analysis (MDA): this employs Mahalanobis distances with stratified covariance estimates.

3.5.3 Support vector machines (SVM)

3.5.3.1 Introduction

Support vector machines (SVM) are based on the theory of statistical learning that was introduced by Vapnik [90] in the late seventies. This theory is the basis of many applications and important theoretical results. In fact, the main area in which statistical learning techniques have been used is the field of pattern recognition. SVM have been used successfully in numerous applications, for example, as medical decision support systems that have led to significant improvements [38], [91] and [92]. This pattern recognition technique is successful, robust, efficient and versatile. In most cases, its generalization performance is significantly better than that of competing methods.

Support vector machines find a decision surface, formed by a hyperplane in the feature space, which separates the data into two classes. They are mainly based on two assumptions. Firstly, the transformation of data into a high-dimensional space called the feature space converts a complex classification problem into a simpler one, which can be solved by a linear discriminant function known as a hyperplane. Secondly, SVM are based on the training data that are close to the decision surface, as it is assumed that these data provide all the most useful information for classification. Therefore, SVM are mainly based on mapping the data to a predetermined high dimensional feature space via a kernel function and finding the hyperplane that maximizes the margin between the two classes. If data are not separable, the SVM find the hyperplane that maximizes the margin and minimizes misclassifications. This is achieved by allowing errors in what is known as a soft separation [93], [94].

3.5.3.2 Technique description

Separable case

Given a set of binary labelled training data vectors $X = \{x_1, \cdots, x_L\}$, where $x_i \in \Re^n$, and their corresponding labels $Y = \{y_1, \cdots, y_L\}$, where $y_i \in \{1, -1\}$, and assuming that the data are linearly separable, a hyperplane H_0 separates the positive examples ($y_i = 1$) from the negative ones ($y_i = -1$). If x_i is an arbitrary vector, we define the function as

$$f(x) = x \cdot w + b \tag{3.2}$$

where $w \in \Re^n$ is the normal vector to the hyperplane and $|b| / \|w\|$ is the perpendicular distance from the hyperplane to the origin. The vectors x_i that lie on the hyperplane H_0 satisfy $f(x) = 0$. H_1 and H_{-1} are the two hyperplanes parallel to H_0, which are defined by $f(x) = 1$ and $f(x) = -1$, respectively. The distance between the hyperplanes H_1 and H_{-1} is referred to as the margin and is therefore $|2| / \|w\|$. For the linearly separable case, the support vector algorithm simply looks for the separating hyperplane with the largest margin.

Thus, the goal is to find the optimal linear classifier (a hyperplane), such that it classifies every training example correctly and maximizes the classification margin. The above description can be formulated in the following way:

$$x_i \cdot w + b \geq +1, \qquad \text{when} \qquad y_i = +1 \quad \text{and} \tag{3.3}$$

$$x_i \cdot w + b \leq -1, \qquad \text{when} \qquad y_i = -1 \tag{3.4}$$

These can be combined into one set of inequalities

$$y_i \cdot (x_i \cdot w + b) \geq +1, \qquad \forall i. \tag{3.5}$$

Thus, the maximum-margin separating hyperplane H_0 is obtained by minimizing

$$\frac{1}{2}\|w\|^2 \qquad \text{subject to} \qquad y_i \cdot (x_i \cdot w + b) \geq +1, \qquad \forall i. \tag{3.6}$$

This minimization problem is convex, therefore there is a unique global minimum value. Only one value of w and b provides the minimum, as long as the data are linearly separable [93] and [95]. The technique of Lagrange Multipliers is applied to solve this problem. By replacing the constraints with constraints on the Lagrange multipliers themselves, the data will only appear in the form of a dot product between vectors, which is a crucial property that will allow generalization of the procedure to the nonlinear case. The primal optimization problem is therefore expressed by

$$L_P = \frac{1}{2}\|w\|^2 - \sum_{i=1}^{L} \alpha_i \left[y_i \cdot f(x_i) - 1 \right] \tag{3.7}$$

where the Lagrange Multipliers verify $\alpha_i \geq 0 \ \forall i$.

The Lagrangian L_P must be minimized with respect to w, b, which implies that its gradient must vanish.

$$\frac{\partial}{\partial w} L_P = 0, \qquad \frac{\partial}{\partial b} L_P = 0, \tag{3.8}$$

requiring that the gradient of L_P with respect to w and b vanish to give the conditions

$$\sum_{i=1}^{L} \alpha_i y_i = 0, \tag{3.9}$$

$$\text{and} \quad w = \sum_{i=1}^{L} \alpha_i y_i x_i. \tag{3.10}$$

We arrive to the dual optimization problem L_D by substituting these constraints into Eq. (3.7)

$$L_D = \sum_{i=1}^{L} \alpha_i - \frac{1}{2} \sum_{i=1}^{L} \sum_{j=1}^{L} \alpha_i \alpha_j y_i y_j x_i x_j. \tag{3.11}$$

Note that we have now given the Lagrangian different labels (P for primal, D for dual) to emphasize that the two formulations are different: L_P and L_D arise from the same objective function but with different constraints. The solution is found by minimizing L_P or by maximizing L_D.

Support vector training for the separable case maximizes L_D with respect to the Lagrange multiplier α_i, subject to the restriction Eq. (3.9) and the condition of $\alpha_i \geq 0$ with the solution given by Eq. (3.10). There is an α_i for every training point. In the solution, the data for which

- $\alpha_i \geq 0$ are called "support vectors" and lie on one of the hyperplanes H_1 and H_{-1}.
- $\alpha_i = 0$ are all the other training points and lie on the side of H_1 or H_{-1}.

Therefore, the support vectors are the critical data of the training set. They lie closest to the decision boundary. If all other training points were removed and the training was repeated, the same separating hyperplane would be found (Fig. 3.2).

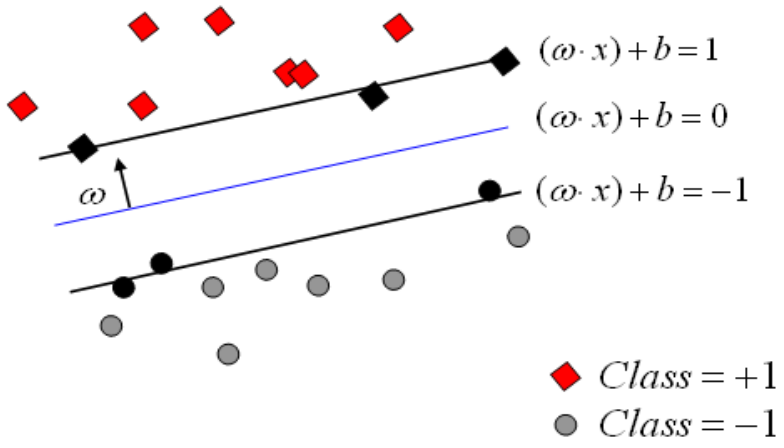

Figure 3.2 Two-class linear classification. The support vectors (coloured in black) provide the useful information for classification.

Non-separable case

The samples that exceed a number of standard deviations of the signal's data are usually considered as outliers. Some of the acquired respiratory flow signals are affected by outliers. If we take into account the outliers in the solution, the margin of separation decreases in such a way that the solution does not generalize as well and the data patterns may no longer be linearly separable. To account for the presence of outliers, we can relax the constraints and soften the decision boundaries. This can be achieved by introducing positive slack variables ξ_i for each training vector [96]. The slack variables allow violations of the margin constraints and modify the equations in the following way

$$x_i \cdot w + b \geq +1 - \xi_i, \qquad \text{when} \quad y_i = +1 \qquad \text{and} \tag{3.12}$$

$$x_i \cdot w + b \leq -1 + \xi_i, \qquad \text{when} \quad y_i = -1. \tag{3.13}$$

Thus, whenever an error occurs, the corresponding ξ_i must exceed unity, so $\sum_i \xi_i$ is an upper bound on the number of training errors. Hence, a natural way to assign an extra cost for errors is to change the primal optimization function, so that it is minimized to

$$\begin{aligned} &\tfrac{1}{2}\|w\|^2 + C \cdot \textstyle\sum_{i=1}^{L} \xi_i \qquad \text{subject to} \\ &y_i \cdot (x_i \cdot w + b) \geq +1, \qquad \forall i. \end{aligned} \tag{3.14}$$

where C is referred to as the penalty parameter and is a positive regularization constant that controls the degree of penalization of the slack variables ξ_i. When C increases, fewer training errors are permitted, although the generalization capacity may decrease. This convex quadratic programming problem can be solved by the dual formulation, maximizing

$$\begin{aligned} &L_D = \textstyle\sum_{i=1}^{L} \alpha_i - \frac{1}{2} \sum_{i=1}^{L} \alpha_i \alpha_j y_i y_j x_i x_j \qquad \text{subject to} \\ &0 \leq \alpha_i \leq C \qquad \text{and} \qquad \textstyle\sum_{i=1}^{L} \alpha_i y_i = 0. \end{aligned} \tag{3.15}$$

The resulting classifier is usually called a soft margin classifier. If $C = \infty$, no value for ξ_i except 0 is allowed. This is referred to as a hard margin SVM case. The penalty parameter has to be chosen by the user.

The optimal α_i of the data that lie outside the margin area is zero. The support vectors are training data x_i, which lie on the margin boundary or inside the margin area and have non-zero α_i. The SVM uses only the support vectors to create the hyperplane. It is assumed that these vectors provide all the relevant information for the classification. The classification problem consists of assigning to each input vector x one of two classes according to the following decision function:

$$f(x) = sign(\sum_{i=1}^{M} \alpha_i \cdot y_i \cdot (x_i \cdot x) + b) \tag{3.16}$$

where M is the number of support vectors. Since the support vectors are a small part of the training dataset, the SVM implementation is more practical for large data sets.

Nonlinear case

In some cases, the data requires a more complex, nonlinear separation. The same techniques as those used for linear machines are applied to generalize the above ideas to the nonlinear case. Since it is not possible to find a linear machine in the original space of the training set, we first map the training set to a Euclidean space with a higher dimension (or even an infinite dimension). This higher dimensional space is called the feature space, as opposed to the input space, which is occupied by the training set. With an appropriately chosen feature space of sufficient dimensionality, any consistent training set can be made separable (Fig. 3.3). However, the translation of the training set into a higher dimensional space implies both computational and learning-theoretic costs.

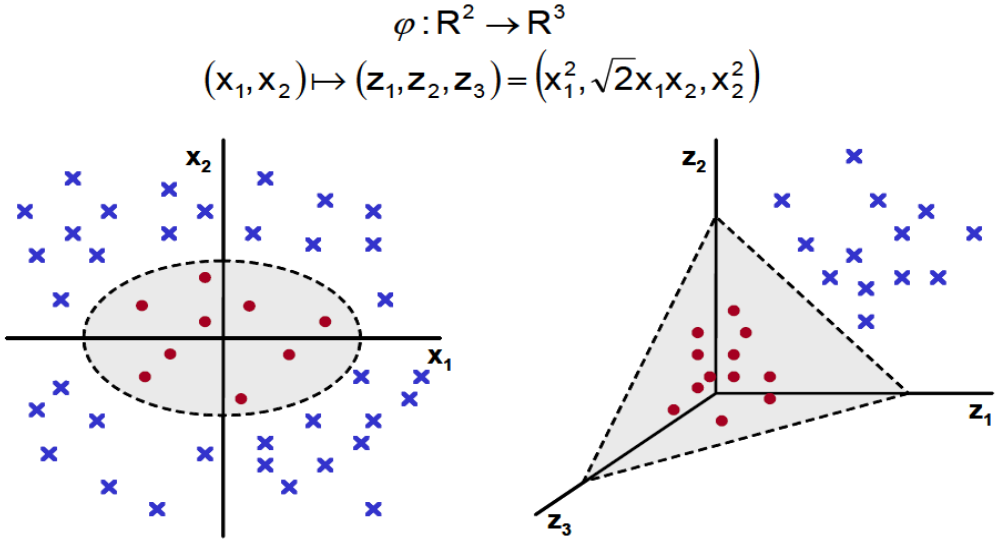

Figure 3.3 Example of transformation from a two-dimensional space to a three-dimensional space.

The decision function Eq. (3.16) depends only on the inner product between observations, which permits the generalization of the SVM to the nonlinear case by means of different kernel functions. The kernel function κ, maps input data into a higher-dimensional space called the feature space, by means of a nonlinear transformation $\phi : \Re^n \rightarrow \Re^l$ with $l > n$. If the kernel function is properly chosen, the inner product in the feature space accomplishes $\kappa(x_i, x_j) = \phi(x_i) \cdot \phi(x_j)$ and there is no need to know the mapping function ϕ explicitly [97]. The kernel used in the study is a radial basis kernel (the radial basis function, RBF), which is given by

$$\kappa(x_i, x_j) = exp\left[-\frac{1}{2}\left(\frac{\|x_i - x_j\|}{\sigma}\right)^2\right]. \tag{3.17}$$

The support vectors are the centre of the RBF, and σ determines their area of influence over the input space. The optimal hyperplane is then constructed in the feature space, which creates nonlinear boundaries in the input space. The nonlinear decision function has the form:

$$f(x) = sign\left(\sum_{i=1}^{L} \alpha_i \cdot y_i \cdot \kappa(x_i, x) + b\right). \tag{3.18}$$

Different cost functions for positively and negatively labelled data are applied to ensure that there are asymmetric soft margins [92]. According to the class populations (N_+ and N_-), the relation between the penalty parameters (C_+ and C_-) is fixed by

$$C_+ = C_- \cdot \frac{N_-}{N_+} \tag{3.19}$$

The choice of the appropriate penalty parameters (C_+, C_-) and the kernel characteristic parameter (σ) is essential to obtain a well tuned SVM.

Advantages and disadvantages of support vector machines

As stated in [98], the main advantages of SVM are:

- There are no local minimums, because the solution is a quadratic optimization problem.
- The optimal solution can be found in polynomial time.
- There are few model parameters to select: the penalty term C, the kernel function and parameters (e.g. in the case of RBF kernels).
- The final results are stable and repeatable (e.g. no random initial weights).
- The SVM solution is sparse; it only involves the support vectors.
- SVM represent a general method for many pattern recognition problems: classification, regression, feature extraction, clustering, etc.
- SVM rely on principled learning methods.
- SVM provide a method for controlling complexity independently of dimensionality.
- SVM have been shown to have excellent generalization capabilities theoretically and empirically.

The main disadvantages are:

- The choice of the kernel is crucial to the success of the SVM, since it constitutes prior knowledge that is available about a task.
- The kernel function parameters and parameter C controls slack variables.

- High algorithmic complexity and extensive memory requirements for quadratic programming in large-scale tasks.
- The disability of SVM to deal with non-static data (dynamic data, sequences).
- A lack of optimal design for multiclass SVM classifiers.

3.6 Performance evaluation measures

Performance evaluation is an important and challenging part of biomedical signal processing required before any algorithm can be implemented in a clinical context. There are several ways to evaluate the performance of supervised classification techniques. Measures of the quality of classification are based on correctly and incorrectly recognized data for each class. These measures are built from a confusion matrix (Table 3.1), which shows a binary classification where tp are true positive, fp false positive, tn true negative and fn false negative [99].

Table 3.1 Confusion matrix for binary classification

Class	**Recognized as positive**	**Recognized as negative**
Positive	tp	fn
Negative	fp	tn

3.6.1 Accuracy

The accuracy assesses the overall effectiveness of the algorithm through

$$Acc = \frac{tp + tn}{tp + fp + tn + fn} \tag{3.20}$$

Although this is the most commonly used empirical measure, it does not distinguish between the number of correct labels of different classes.

3.6.2 Sensitivity / specificity

To develop an algorithm that accurately discriminates information obtained from healthy subjects and patients with different condition, the performance may be evaluated in terms of its ability to correctly discriminate between the classes of healthy and different condition diseased subjects. The most commonly used performance evaluation measures for describing such discriminations are sensitivity and specificity, which separately estimate a classifier's performance on different classes [85].

$$Sensitivity = \frac{tp}{tp+fn} \tag{3.21}$$

$$Specificity = \frac{tn}{fp+tn} \tag{3.22}$$

3.6.3 Precision/Recall/F-measure

The following measures focus on one of the classes. They are applied mainly when the number of data samples belonging to one class is substantially lower than the overall number of data samples.

$$Precision = \frac{tp}{tp+fp} \tag{3.23}$$

This estimates the predictive value of a label, which may be positive or negative,

depending on the class for which it is calculated.

$$Recall = \frac{tp}{tp + fn} \tag{3.24}$$

Recall is the same as the sensitivity given in Eq. (3.21).

$$F - measure = \frac{(\beta^2 + 1) \cdot Precision \cdot Recall}{\beta^2 \cdot Precision + Recall} \tag{3.25}$$

This is a composite measure that favours algorithms with higher sensitivity and challenges those with higher specificity. The F-score is evenly balanced when $\beta = 1$. The measure favours precision when $\beta > 1$, otherwise it favours recall.

The measures of Youden's index γ and discriminant power DP combine sensitivity and specificity and their complements. In addition, they have been used in medical diagnoses to analyse tests [99].

3.6.4 Youden's index and discriminant power

The avoidance of failure increases accuracy or the ability to correctly label examples. Youden's index evaluates the algorithm's ability to avoid failure and gives equal weight to its performance on positive and negative data samples.

$$\gamma = sensitivity - (1 - specificity). \tag{3.26}$$

Discriminant power also summarizes sensitivity and specificity, by means of

$$DP = \frac{\sqrt{3}}{\pi}(logX + logY) \tag{3.27}$$

where X = sensitivity /(1-sensitivity) and Y= specificity / (1-specificity). DP evaluates how accurately an algorithm distinguishes between both classes. The algorithm is a poor discriminator if $DP < 1$, limited if $DP < 2$, fair if $DP < 3$, and good in all other cases.

3.7 Validation methods

Some of the usual validation methods found in statistical pattern recognition are leave-one-out cross-validation and n-fold cross-validation. Cross-validation is a technique used to assess the performance of a learning algorithm by estimating the capacity of a classifier to generalize for an independent data set. Mainly used in prediction, it estimates how accurately a predictive model performs in practice. The classifier is built only on data that are not used for evaluation (training data). The rest of the data are employed to test the classifier (testing data). Cross-validation trades off bias for variance, which means that it provides a better estimate in terms of bias, but with a higher variance estimate.

In leave-one-out cross-validation, each data sample is retained in turn and the classifier is built on the remaining samples. The class of the retained sample is then predicted using the classifier. The classification accuracy is estimated by repeating this process for the entire original dataset.

In n-fold cross-validation, the original dataset is randomly divided into n subsets. A subset is retained as the validation data for testing the model, and the remaining $n-1$ subsets are employed as training data. The cross-validation process is then repeated n times (the folds), with each of the n subsets used exactly once as the validation data. The n results from the folds are averaged to produce a single accuracy estimation.

3.8 Feature selection

Proper feature selection is crucial for fast and accurate performance of a pattern recognition system, since performance deteriorates in high dimensional spaces in which many features are irrelevant. Thus, the dimensionality of the pattern representation (i.e. the number of features) should be kept as small as possible. The accuracy is often improved by reducing dimensionality and both cost and complexity are also reduced. A small feature set simplifies both the pattern representation and the classifiers that are built on the selected representation. Consequently, the resulting classifier will be faster, simpler and will use less memory. However, a high reduction in the number of features may lead to a loss in the discrimination power and thereby reduce the accuracy of the resulting recognition system.

A number of well-known feature selection methods have been proposed in the literature [100]. Although it might still be useful as a first step to select some individually good features to reduce the size of very large feature sets, the simple method of selecting just the best individual features may fail dramatically. Further selection has to be performed by more advanced methods that take feature dependencies into account. These methods operate either by evaluating growing feature sets (forward selection) or by evaluating shrinking feature sets (backward selection). Sequential forward selection selects the best single feature and then adds one feature at a time. In combination with the selected features, this maximizes the criterion function. In contrast, sequential backward selection starts with all the features and successively deletes one feature at a time. The feature that is deleted is the one that contains the least information, according to the criterion function.

3.9 Unbalanced database: new balance metric

Despite progress in classification, problems may still occur when the training sample or population is unbalanced. In the literature, a lot of work has been carried out to address unbalanced classification by adjusting the class proportions [101], [102], [103] and [104]. Efficient and effective classification is a core problem in biomedical data mining. Most learning systems tend to assume that the training sets used for learning are balanced. When learning is performed with unbalanced datasets, machine learning algorithms tend to produce high predictive accuracy over the majority class, but poor predictive accuracy over the minority class [105].

Support vector machines have been used successfully in numerous applications as a medical decision support system [38], [91] and [92]. However, their classification results significantly deteriorate when they have to deal with unbalanced data, in which the number of positive and negative data items differs significantly [106]. This problem is also reflected in the SVM-based feature selection process [107].

To measure the classification balance at each iteration, a new metric is defined as the balance index (B), given by

$$B = \frac{|fpr - fnr|}{fpr + fnr} \tag{3.28}$$

where fpr and fnr are defined as the false positive rate and the false negative rate, respectively [85] and [108] given by

$$fpr = \frac{1}{N_-} \sum_{i \in I_+} f(x_i) = 1 - Sp, \quad \text{where} \quad I_+ = \{i \mid y_i = -1 \ \& \ f(x_i) = 1\} \tag{3.29}$$

$$fnr = \frac{1}{N_+} \sum_{i \in I_-} f(x_i) = 1 - Sn, \quad \text{where} \quad I_- = \{i \mid y_i = 1 \ \& \ f(x_i) = -1\} \tag{3.30}$$

being Sp and Sn are the specificity and sensitivity, respectively. Therefore, B is based on the difference in misclassified data within each class. To maintain a balanced classification outcome, a B threshold is fixed. The use of this threshold in optimization processes like feature selection not only provides good classification but also enables the maintenance of a minimum balanced classification error. However, as long as the feature selection process improves the accuracy and there is a commitment to balance, the balance index decreases.

3.10 Summary

A number of techniques have been developed in the literature for pattern recognition. The characterization, automatic recognition, classification, and clustering of patterns are important problems in engineering and scientific disciplines.

Statistical pattern recognition has been successfully applied to pattern recognition and classification problems in which a pattern is represented by a set of L features and the decision boundaries between the classes are established using concepts from statistical decision theory. There are two modes for training in statistical pattern recognition: supervised learning based on labelled training data samples; and unsupervised learning based on unlabelled training data samples.

The accuracy of a pattern recognition systems depends directly on its generalization ability, which refers to its performance in classifying test patterns that were not used during the training stage. A classifier that is too intensively optimized on the training set usually has poor generalization ability and leads to a phenomenon known as overfitting.

A number of classification techniques are based on statistical pattern recognition.

In this research, we focus on support vector machines, since we have used this pattern recognition technique to distinguish between different pathological respiratory patterns. The SVM are robust, efficient, versatile and, in most cases, their generalization performance is significantly better than that of competing methods. They have shown remarkable results in numerous applications, but their classification results significantly deteriorate when they have to deal with unbalanced data. This problem is also reflected in the feature selection process. Most biomedical data mining, and particularly the clinical information acquired to help in medical diagnoses, is provided by unbalanced structures, as in our case.

Suitable training and proper feature selection is essential for fast and accurate performance of the SVM. To avoid the imbalance problem in both optimization processes, a new metric called the balance index B is proposed in this chapter. A B threshold is fixed to maintain a balanced classification outcome. The use of B leads to good classification and the maintenance of a minimum balanced classification error.

Chapter 4

Support vector machines applied to weaning

The objective of this chapter is to study one of the most challenging problems in intensive care (ICU): the process of discontinuing mechanical ventilation. Extubation failure and the need for reintubation within 48 hours of extubation can cause increased morbidity, higher costs, longer ICU and hospital stays and higher mortality. Thus, critical-care clinicians must carefully assess the benefits of rapid liberation from mechanical ventilation against the risks of premature trials of spontaneous breathing and extubation. The percentage of extubation failure varies depending on the study (25% according to Tobin [28], from 4% to 23% according to MacIntyre [17], 47% according to Esteban et al. [109], etc). In their study, Kulkarni et al. [5] gathered all the extubation failure percentages and stated that the incidence of failure varies between 6 and 47%. The need for accurate prediction covers all phases of weaning: from the initial reduction in mechanical support as patients are increasingly able to support their own breathing, through the trials of unassisted breathing that often

precede extubation, and finally ending with extubation [18].

Various studies have been carried out to detect which physiological variables can identify readiness to undertake a weaning trial. As a result, guidelines have been established for weaning criteria and protocols [29], [30], [14], [15], [31] and [26]. Although some weaning indices appear to be useful in many studies, there is no one set of criteria available for all population groups [29]. Thus, research is still being undertaken on objective indicators to predict extubation failure accurately.

The aim of the present chapter is to use support vector machines (SVM) to analyse the differences between patients with successful weaning trials, patients with unsuccessful trials, and patients who successfully pass the trial but cannot maintain spontaneous breathing and require the reinstitution of mechanical ventilation in less than 48 hours. For this purpose, we analyse the weaning database described in Chapter 1. The respiratory flow signal and the ECG of the patients are used to characterize the respiratory pattern and cardiorespiratory interactions. By the application of methods from the field of signal processing, we aim to add objective information to the doctor's expertise, to reach a high enough level of reliability for the method to act as a decision support system in respiratory treatments. This research effort aims to exploit the capabilities of the SVM to improve prediction of the weaning outcome.

4.1 Medical application: weaning dataset

The American College of Chest Physicians, the American Association for Respiratory Care, and the American College of Critical Care Medicine have created evidence-based guidelines for weaning and discontinuing ventilatory support [17]. The need for reintubation carries an 8-fold higher odds ratio for nosocomial pneumonia and a 6-fold

to 12-fold increased mortality risk [17]. The reason for the higher mortality is still unknown; it is not clearly related to the development of new problems after extubation or to the complications of reinserting the tube [110]. However, the maintenance of unnecessary ventilator support carries its own burden of patient risk for infection and other complications. Moreover, it increases hospital costs. Nevertheless, it is important to balance the advantages and disadvantages of removing the ventilator, since mechanical ventilation discontinued prematurely carries its own set of problems, including difficulty in reestablishing artificial airways and compromised gas exchange. The duration of weaning from mechanical ventilation represents a large proportion of the overall ventilation period. It has been estimated that as much as 42% of the time that a medical patient spends on a mechanical ventilator is during the discontinuation process [17].

Clinical tolerance to spontaneous breathing trials is considered poor when respiratory frequency is greater than 35 breaths/min or has increased by 50% or more; when heart rate is above 140 beats/min or has increased by 20% or more, or arrhythmias have appeared; when systolic blood pressure is lower than 80 mmHg or greater than 160 mmHg; or when patients show agitation, depressed mental status or diaphoresis [26].

A total of 154 patients on weaning trials from mechanical ventilation underwent a test of spontaneous breathing in the intensive care departments of the Santa Creu i Sant Pau Hospital, Barcelona, Spain, and the Getafe Hospital, Getafe, Spain. The patients were disconnected from the ventilator and maintained spontaneous breathing through an endotracheal tube for 30 minutes. Patients who were able to maintain spontaneous breathing were extubated, whereas patients who could not breathe spontaneously were reconnected. When patients were still able to maintain spontaneous

breathing after 48 hours, the weaning trial process was considered successful. If not, patients were reintubated.

The patients in the study were classified into three groups according to the spontaneous breathing test outcome: GS, 94 patients (61 male, 33 female, 65 $\pm$ 17 years) with successful trials who were able to maintain spontaneous breathing after 48 hours; GF, 39 patients (24 male, 15 female, 67 $\pm$ 15 years) who failed to maintain spontaneous breathing and were reconnected after 30 minutes of weaning trials; GR, 21 patients (11 male, 10 female, 68 $\pm$ 14 years) who successfully passed weaning trials, but had to be reintubated in less than 48 hours.

Electrocardiographic (ECG) and respiratory flow signals were measured for each patient. Both signals were recorded synchronously with a sampling frequency of 250 Hz for 30 minutes. Time series of the cardiac interbeat duration $RR(k_1)$ were extracted automatically from the ECG signal using an algorithm based on wavelet analysis [42]. Ectopic beats were determined, removed and interpolated using an algorithm based on local variance estimation. Time series of the breath duration $T_{Tot}(k_2)$ were extracted automatically using an algorithm based on zero-crossing of the respiratory flow signal. Thereafter, they were visually inspected, and edited if necessary.

4.2 Respiratory pattern analysis using SVM

The respiratory pattern describes the mechanical function of the pulmonary system. One way to characterize the respiratory pattern is through the respiratory time series that is extracted from the respiratory flow signal. One approach to finding differences between the GS group, patients who can maintain spontaneous breathing, and the

GF group, those who cannot, is to analyse respiratory pattern variability. An SVM-based feature selection algorithm optimizes the feature subset for better classification.

4.2.1 Methodology

4.2.1.1 Respiratory pattern characterization

Several time series are obtained from the respiratory flow signal: inspiratory time (T_I), expiratory time (T_E), breath duration (T_{Tot}), tidal volume (V_T), fractional inspiratory time (T_I/T_{Tot}), mean inspiratory flow (V_T/T_I) and frequency-tidal volume ratio (f/V_T). These time series characterize the respiratory pattern.

Each one of the seven time series is processed by a running window that consists of several consecutive breath cycles and has a width that ranges from 3 to 100. The mean (m), standard deviation (s), kurtosis (k), skewness (Sk) and interquartile range (I) of the value are calculated for each window. Thus, 35 new time series are obtained for each patient. The optimal width of the running window is selected from between 3 to 100 using a Mann-Whitney test, and the best width result is 15, with $p < 0.001$ in all cases.

Once the window width has been selected, the data for each patient are analysed independently by applying an algorithm based on the k-means method, which automatically determines the best number of clusters for all patients. For the patients in this study, one main cluster contains most of the patterns and has considerable internal cohesion (low intra-cluster variance) that corresponds to more than 96% for each group.

This result is exploited to reduce the data, so that a single pattern of 35 features is associated with each patient. This pattern is computed as the mean value of the data

points in the main (largest) conglomerate of the patient, using the k-means clustering algorithm.

The patients are distributed as follows: 80% for training and 20% for testing. The best classification result is obtained by applying leave-one-out cross-validation with the following 8 features: $s(T_E)$, $m(T_{Tot})$, $m(T_I)$, $m(T_E)$, $s(T_{Tot})$, $I(T_{Tot})$, $m(f/V_T)$, $m(T_I/T_{Tot})$. These features are used for the final SVM-based classification process.

4.2.1.2 Histogram equalization

A reduction in the overlap between successful and unsuccessful patients (GS and GF) may be attained if the variances of the features are similar. However, variances cannot always be expected to be similar. To solve this problem, we propose an equalization of the histograms of the previously selected features, as a nonaffine normalization process [111], [112] and [113].

Histogram equalization or cumulative distribution function (CDF) equalization is a nonparametric method to match the CDF of some given data to a reference distribution. The principle of this method is to find a nonlinear transformation to reduce the mismatch of the two signals. This transformation maps the distribution of a signal back to the distribution of the reference signal, and is defined by means of the CDFs of the signals in the process.

The CDF is estimated by equally spaced intervals to obtain more reliable data. Each interval $x \in [q_i, q_{i+1}[$ is represented by $(x_i,\ F(x_i))$, which corresponds to the average of scores (x_{ij}) and the maximum cumulative distribution value $F(x_i)$, both of which are calculated for each interval of the reference signal, given by

$$x_i = \frac{\sum_{j=1}^{k_i} x_{ij}}{k_i} \quad \text{where} \quad F(x_i) = \frac{K_i}{M} \tag{4.1}$$

where $x_{ij} = x \in [q_i, q_{i+1}[$, k_i is the number of data in the interval $[q_i, q_{i+1}[$, and K_i is the number of data in the interval $[q_0, q_{i+1}[$, and M is the total number of data items.

$F(x_i)$ defines the boundaries of the intervals in the CDF that will be equalized. These boundaries $[q'_i, q'_{i+1}[$ limit the interval of values that fulfil the following expression: $F(q_i) \leq F(y) < F(q_{i+1})$. All values of y that are in the interval $[q'_i, q'_{i+1}[$ will be transformed to their corresponding x_i value.

As a reference, the designed equalization takes the feature whereby the minor classification error is obtained by the leave-one-out cross-validation process, which is the $s(TE)$ feature. Therefore, the CDF of this feature is the reference distribution.

4.2.2 Results

A grid search is performed to find the optimum penalty parameter, C. The minimum C that provides the best classification error accuracy is selected ($C = 15$). Thus, the cost and the generalization error are reduced. An internal n-fold cross-validation shows that the best value of the parameter σ that is used in the kernel function is $\sigma = 0.5$. When all 35 features are used for each patient, the average correct classification rate is 66.67%. A feature selection process is carried out to select the most discriminative feature subset and to remove the remaining noisy features. Both the computational cost and classification error are reduced. The histogram equalization technique is applied to the selected features, to match their CDF to the distribution of the most discriminative feature. This study showed a classification accuracy of 80%, a sensitivity of 86.67%, and a specificity of 73.34%.

Orthogonal projections with principal component analysis are used to visualize the high dimensional input space data on a plane. Fig. 4.1 shows the overlapping position of patients of GS and GF. Figs 4.2 and 4.3 show the final classification of

the training set and test set, respectively.

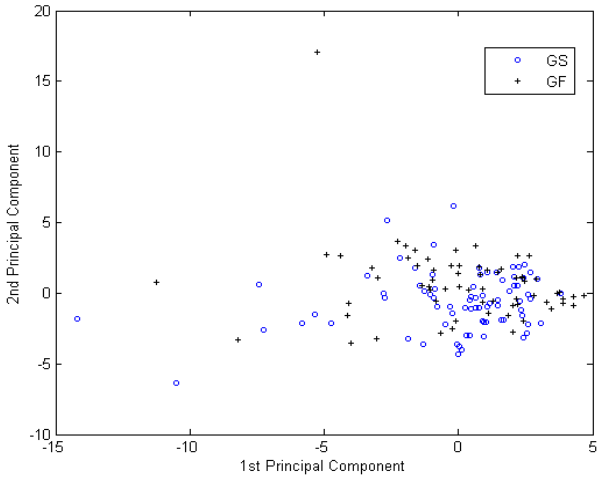

Figure 4.1 Successful (GS) and unsuccessful (GF) patients before the classification. Orthogonal projections with principal component analysis are used to represent the hyperspace data on a plane before the classification.

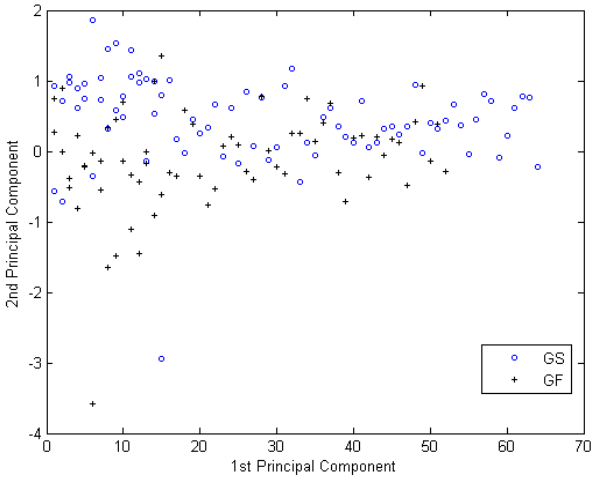

Figure 4.2 Training set of successful (GS) and unsuccessful (GF) patients after the classification. Appropriate feature selection and histogram equalization are obtained with the training set before the final classification.

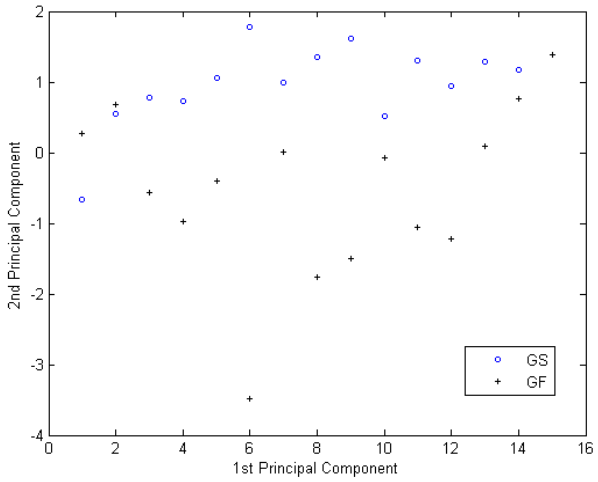

Figure 4.3 Testing set of successful (GS) and unsuccessful (GF) patients after the classification. Appropriate variable selection and histogram equalization are obtained with the training set before the final classification.

4.3 Cardiorespiratory interaction analysis using SVM

The assessment of autonomic control provides information about cardiophysiological imbalances within the cardiorespiratory system. Cardiorespiratory interdependencies during the weaning trials are specific aspects of dynamic autonomic functional coordination. It is still not clear whether there are more stable functional relationships between breaths and heart beats in patients with successful trials. To study cardiorespiratory interactions in patients on weaning trials, we introduce the joint symbolic dynamics of heart rate and respiratory dynamics. This might improve understanding of the physiological processes involved in the weaning procedure. Hence, the study of cardiorespiratory dynamics is simplified to the description of bivariate symbol sequences. Some detailed information is lost, but some of the invariant, robust properties of the dynamics are kept. Univariate symbolic dynamics has been success-

fully applied in heart rate variability analysis and respiratory pattern analysis [114]. Bivariate symbolic dynamics has provided an efficient nonlinear representation of heart rate and systolic blood pressure interactions that offers simple physiological interpretations [15], [115] and [49].

The aim is to use SVM to identify the best joint symbolic dynamic features for the classification of patients with successful trials, GS; patients with unsuccessful trials, GF; and patients who successfully pass the trial but cannot maintain spontaneous breathing and require the reinstitution of mechanical ventilation in less than 48 hours, GR. Joint symbolic dynamic analysis might provide enhanced information about cardiorespiratory interaction in patients on weaning trials.

4.3.1 Methodology

4.3.1.1 Joint symbolic dynamics

To apply joint symbolic dynamics (JSD), the values of the cardiac $RR(k_1)$ and respiratory $T_{Tot}(k_2)$ time series have to be synchronized [116]. The new $RR(n)$ and $T_{Tot}(n)$ time series are obtained by 1-Hz synchronized sampling of the interpolated original $RR(k_1)$ and $T_{Tot}(k_2)$ time series. If x is the bivariate sample vector of the cardiac (c) time series $RR(n)$ and the respiratory (r) time series $T_{Tot}(n)$, as shown in Eq. (4.2), then s represents a bivariate symbol vector, Eq. (4.3). This vector is gained by transforming x using a symbol alphabet according to Eq. (4.4) and Eq. (4.5).

$$x = \left\{ [x_n^c, x_n^r]^T \right\}_{n=0,1,\cdots} x \in \Re \tag{4.2}$$

$$s = \left\{ [s_n^c, s_n^r]^T \right\}_{n=0,1,\cdots} s \in 0, 1 \tag{4.3}$$

$$\begin{aligned} s_n^c = 0 &: (x_{n+1}^c - x_n^c) \leq 0 \\ 1 &: (x_{n+1}^c - x_n^c) > 0 \end{aligned} \tag{4.4}$$

$$\begin{aligned} s_n^r = 0 &: (x_{n+1}^r - x_n^r) \leq 0 \\ 1 &: (x_{n+1}^r - x_n^r) > 0 \end{aligned} \tag{4.5}$$

Thus, the bivariate symbol vector consists of $a = 4$ symbols. Furthermore, this new vector is fractionalized into words w_k of length k. The maximum length of the words is restricted by the occurrence probability $p(w_k)$ of each word type. Therefore, it is indirectly restricted by the number of measured samples. There are two overlapping symbols in consecutive words. Considering the sampling frequency and the 30-minute recordings, the initial series contain 3600 samples and the length of the symbolic series is $N = 3598$. The length of words is limited to $k = 3$, Eq. (4.6). This length spans an 8 x 8 matrix W_{raw} (rows: c - word types of cardiac changes; columns: r - word types of respiratory changes), which range from word type $[000, 000]^T$ to $[111, 111]^T$. Finally, 64 possible word types are obtained [116].

$$p(w_k) = \frac{N}{a^k} = \frac{3598}{4^3} = 56.22 \tag{4.6}$$

Three matrices $W_{raw}(\tau)$ are calculated by shifting the symbol transformed cardiac time series against the symbol-transformed respiratory time series and applying three shift values ($\tau = -2$, 0 and +2 symbols).

The occurrence probability is calculated from the joint matrices $W(\tau)$ for each of the 64 possible word types. To compare the word type distributions between different lengths of datasets, the sum of all counted words is normalized to 1. The normalized

probabilities of the occurrences of all single word types are computed as $p_n(w_{cr})$. The sum of each row in $W_{raw}(\tau)$ is computed as $P_n(w_c)$ and corresponds to the occurrence probability of each word from the cardiac time series, Eq. (4.7). The sum of each column in $W_{raw}(\tau)$ is computed as $P_n(w_r)$ and corresponds to the occurrence probability of each word from the respiratory time series, Eq. (4.8).

$$P_n(w_c) = \sum_r p_n(w_{cr}) \text{ where } r \text{ takes values from "000" to "111"} \tag{4.7}$$

$$P_n(w_r) = \sum_c p_n(w_{cr}) \text{ where } c \text{ takes values from "000" to "111"} \tag{4.8}$$

Therefore 92 features are proposed to discriminate the three groups of patients (GS, GF and GR):

- Features 1 to 64: the occurrence probability of each single word type $p_n(w_{cr})$
- Features 65 to 73: number of words w_{cr} whose occurrence probability $p_n(w_{cr})$ is higher than a probability threshold defined from 1% to 9%
- Features 74 to 81: the occurrence probability of each word from the cardiac series $P_n(w_c)$
- Features 82 to 89: the occurrence probability of each word from the respiratory series $P_n(w_r)$
- Feature 90: the sum of the occurrence probability of the principal diagonal
- Feature 91: the sum of the occurrence probability of the secondary diagonal
- Feature 92: Shannon entropy of the occurrence probability of cardiorespiratory words

4.3.1.2 Optimizing SVM feature selection

It is essential to choose the most robust features from the observed data in terms of empirical accuracy, the general performance of classifiers and the computational efficiency. The optimized feature selection proposed in this study depends directly on the balance index B, which is defined in Chapter 3. This index measures the classification balance at each iteration and permits the extraction of features that maximize the classification accuracy and maintain a low difference between the misclassified data in each group, in turn. The n-fold cross-validation technique is applied to all error measures to avoid the overfitting introduced by the method.

The feature matrix ($W(\tau)$) contains all the features. After optimized feature selection, the most discriminative features are gathered in the optimized feature matrix (W_{SVM}). Both the balance index (B) and any of the performance evaluation measures described in Chapter 3 are assessed for each feature. Only the features that have a maximum performance evaluation and a B that remains below 40% are selected. If the number of selected features is greater than 1, the feature whose B is minimum is added to $W_{SVM}(\tau)$ and removed from the feature matrix ($W(\tau)$). This process is repeated till the most discriminative features have been extracted.

The SVM's accuracy should improve iteratively. However, in practice, beyond a certain point the use of additional features could lead to saturation or even to a worse performance. Therefore, we select the minimum number of features that jointly give the best accuracy by increasing sensitivity (Sn) and specificity (Sp).

To evaluate the accuracy of the proposed balance index, we compare the accuracy of conventional feature selection based only on a single performance evaluation measure, and the accuracy of feature selection based on the same measure combined with

the balance index B. The evaluation measures studied in the forward feature selection include: accuracy (Acc), sensitivity (Sn), specificity (Sp), F-measure, Youden's index (γ) and discriminant power (DP). The whole process is summarized in Fig. 4.4.

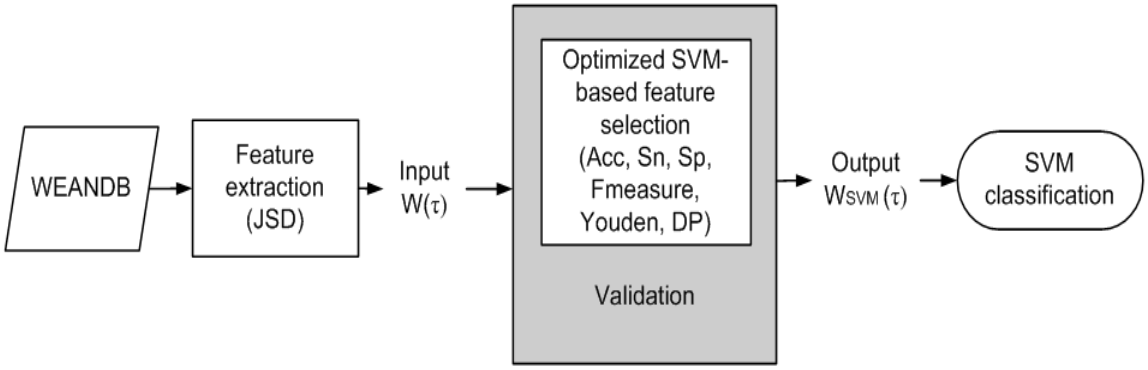

Figure 4.4 Main stages of the feature selection method based on different performance evaluation measures

4.3.2 Data analysis

Four classifications are used to evaluate accuracy in predicting the different groups of patients:

- GS versus GF
- GS versus the rest of the patients (GF and GR)
- GR versus GS
- GR versus the rest of the patients (GS and GF)

A total of 276 features characterize each patient's cardiorespiratory interaction through joint symbolic dynamics, that is, 92 features for each shift value τ (-2, 0, 2). For each classification problem, SVM-based optimized feature selection is applied to the feature matrix $W(\tau)$ and compared with the performance of stepwise linear discriminant analysis (LDA). The most discriminative set of features that determine

patient readiness for extubation and maintain a well-balanced classification outcome are selected by a feature selection process based on SVM or LDA: $W_{SVM}(\tau)$ and $W_{LDA}(\tau)$, respectively (Fig. 4.5).

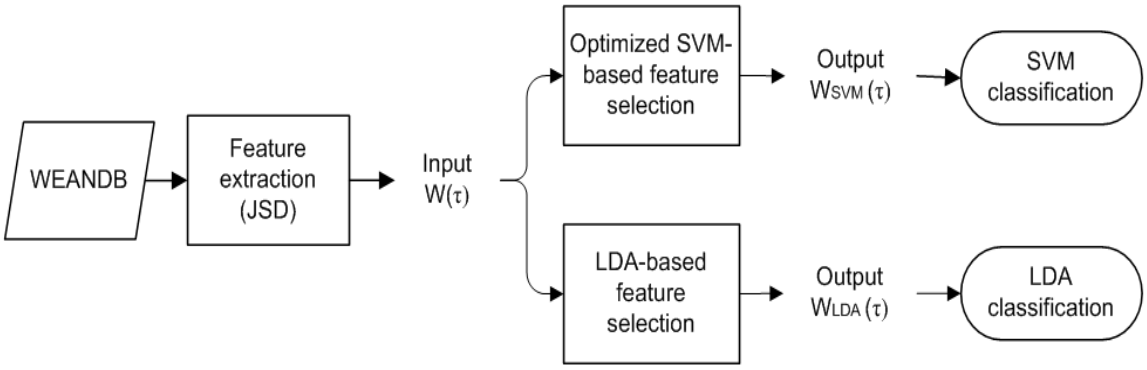

Figure 4.5 Classification process using support vector machines (SVM) and linear discriminant analysis (LDA).

4.3.3 Results

First, we present the statistical analysis of the time series. Then, we discuss the results of the proposed feature selection, which is assessed by different performance evaluation measures. Finally, we describe the results of the optimized feature selection applied to the four classifications.

- Statistical analysis

Table 4.1 shows the mean value $Mean(x)$, standard deviation $SD(x)$ and interquartile range $IQR(x)$ of the $RR(k_1)$ and $T_{Tot}(k_2)$ series that are obtained by comparing the GS patient group with the rest of the patients (GF and GR). The mean values of the cardiac intervals $RR(k_1)$ and breath durations $T_{Tot}(k_2)$ present significant differences in the classification of GS versus the rest of patients (GF and GR), whereas no

significant differences are found in the classification of GS versus GF, GR versus GF or versus the rest of the patients (GS and GF).

Table 4.1 $Mean(x)$, standard deviation $SD(x)$ and interquartile range $IQR(x)$ of the interbeat durations (RR) and breath durations (T_{Tot}), and $p-value$ classifying group GS versus $GF+GR$.

	GS	$GF+GR$	$p-value$
$MeanRR$ $[ms]$	701 ± 122	652 ± 116	0.017
$SD(RR)$ $[ms]$	72 ± 80	62 ± 49	$n.s.$
$IQR(RR)$ $[ms]$	73 ± 78	71 ± 81	$n.s.$
$MeanT_{Tot}$ $[s]$	2.80 ± 0.73	2.4 ± 0.93	0.00013
$SD(T_{Tot})$ $[s]$	0.85 ± 0.96	0.67 ± 0.76	$n.s.$
$IQR(T_{Tot})$ $[s]$	0.50 ± 0.30	0.48 ± 0.48	$n.s.$

- SVM feature selection based on different measures

After the previous grid search the appropriate SVM parameters (C_+ and C_-, and σ) are in the range $[50-100]$ and $[20-100]$, respectively. The n-fold cross-validation technique (N = 10) is applied in all cases to avoid the overfitting introduced by the method. In the optimization process, we use various performance evaluation measures to study the performance of feature selection, either independently or with B. Table 4.2 displays the accuracy of the selected features in predicting GS patients from unsuccessful GF patients.

Thus, when feature selection is applied to unbalanced datasets, the results are unbalanced. The inclusion of the B index in the optimization progress provides a better balance of sensitivity and specificity in all cases. As shown in Table 4.2, optimal

Table 4.2 Accuracy (Acc), balance index (B), sensitivity (Sn), specificity (Sp) and the number of features applied in the SVM classification for every τ value.

SVM based on	$\#features$	B	Acc	Sn	Sp
$Accuracy$	7	66.4%	80.8%	56.4%	91.2%
$Accuracy + B$	6	18.6%	80.0%	74.4%	82.4%
$F\_measure$	10	48.9%	79.2%	61.5%	86.8%
$F\_measure + B$	10	26.3%	76.9%	84.6%	73.6%
DP	8	72.7%	80.0%	51.3%	92.3%
$DP + B$	11	36.4%	76.2%	87.2%	72.5%
$Youden's\ index$	10	48.9%	79.2%	61.5%	86.8%
$Youden's\ index + B$	9	26.3%	76.2%	84.6%	73.7%

feature selection is based on both the accuracy and the balance index. Hence, we focus on optimized feature selection based on the Acc and B index throughout the study.

- B-based SVM feature selection applied to weaning

First, we evaluate accuracy in predicting GS patients and unsuccessful patients (GF). We apply SVM-based optimized feature selection and stepwise LDA with a forward selection algorithm. Figs. 4.6 and 4.7 respectively show the classification accuracy with SVM and LDA, together with their sensitivity and specificity when only the most discriminant features are considered.

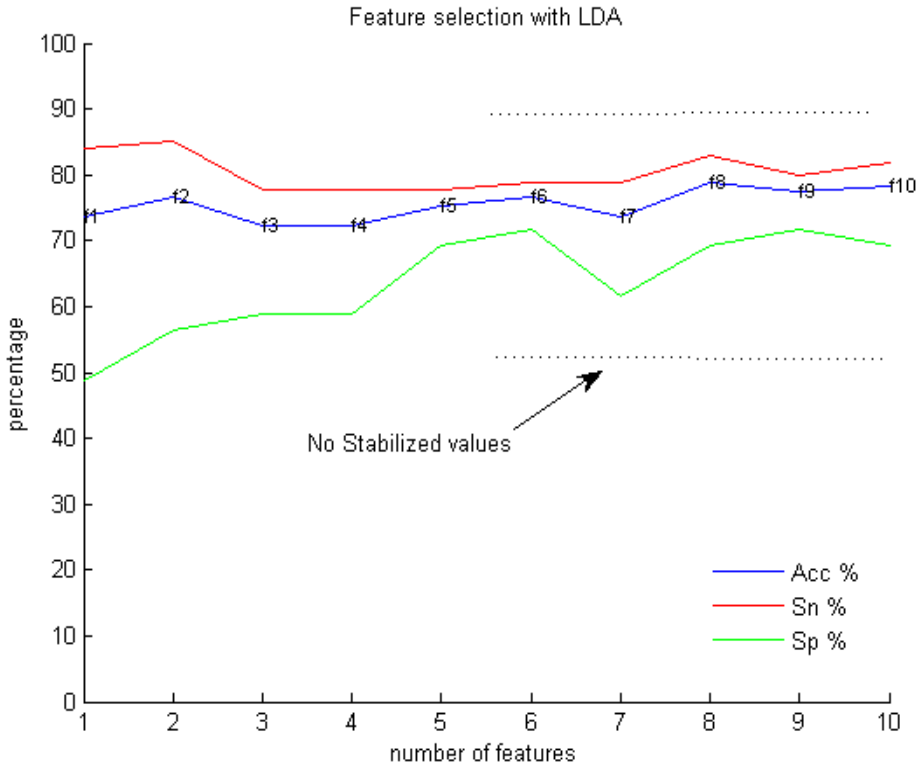

Figure 4.6 Accuracy (Acc), sensitivity (Sn) and specificity (Sp) when a new selected feature is added in the classification of the GS group versus GF, using LDA.

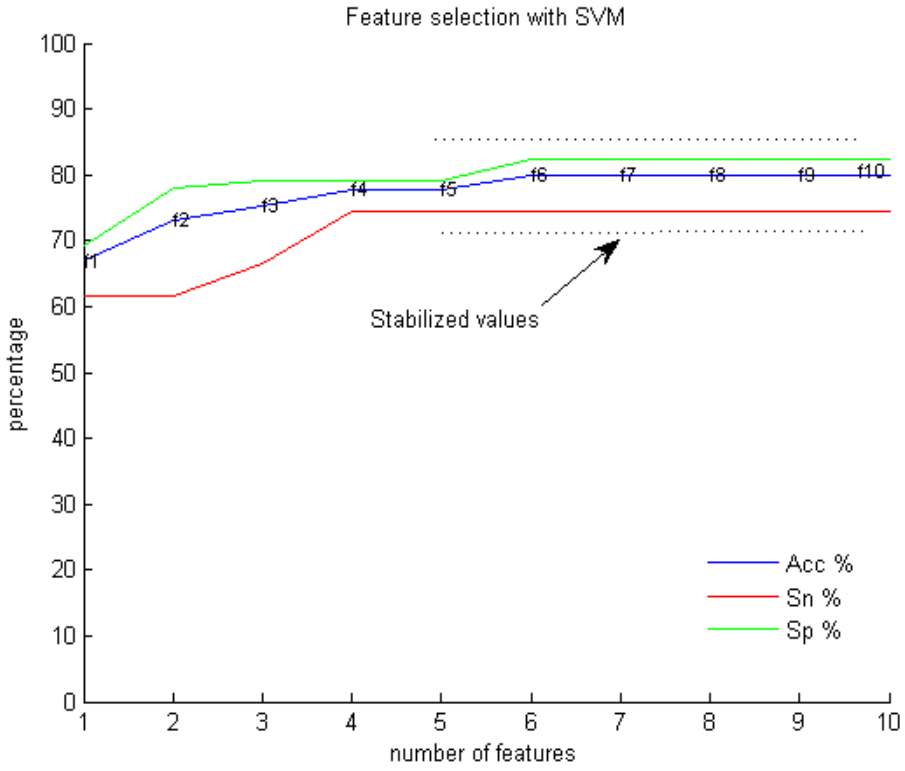

Figure 4.7 Accuracy (Acc), sensitivity (Sn) and specificity (Sp) when a new selected feature is added in the classification of the GS group versus GF, using SVM.

SVM-based feature selection provides the best results, with a global accuracy of 80.0%, sensitivity of 74.4%, and specificity of 82.4% and the use of only 6 features. Only SVM seeks a balanced outcome as well as a good result. The best 6 features selected by both feature selection methods are related to cardiorespiratory interaction (Table 4.3). The most dominant words present alternating patterns in the cardiac rate (101, 110 or 011) and in the respiratory dynamics (001 or 010). There are no monotonous patterns.

Table 4.3 The best feature subset selected by discriminating the group of patients GS from GF with both discriminant methods, using JSD without shifting ($\tau = 0$). *: two symbols shifted to the right ($\tau = 2$), and **: two symbols shifted to the left ($\tau = -2$).

Features	LDA	SVM
$f1$	$p_n(w_{c011\ r010})$	$p_n(w_{c101\ r001})$
$f2$	$p_n(w_{c011\ r001})$	$p_n(w_{c101\ r010})*$
$f3$	$p_n(w_{c101\ r001})$	$p_n(w_{c110\ r100})*$
$f4$	$\sum(p_n(w_{cr})) \geq 8\%$	$p_n(w_{c110\ r001})$
$f5$	$\sum(p_n(w_{cr})) \geq 5\%$	$p_n(w_{c001\ r010})**$
$f6$	$p_n(w_{c110\ r011})$	$p_n(w_{c101\ r001})**$

The proposed B-based SVM feature selection algorithm is applied to predict GS patients from the rest of the patients (GF and GR). The best classification result is obtained with 9 features and has an accuracy of 81.3%, sensitivity of 83.3% and specificity of 78.3%. Fig. 4.8 shows the classification accuracy, the sensitivity and the specificity when the most discriminant features are added (Table 4.4).

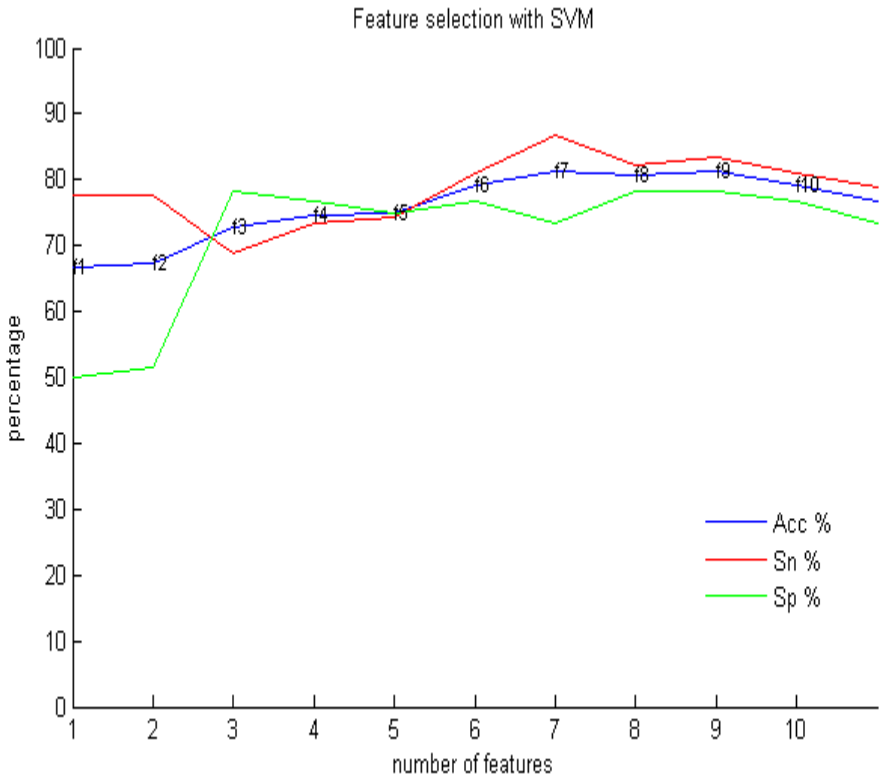

Figure 4.8 Accuracy (Acc), sensitivity (Sn) and specificity (Sp) when a new selected feature is added in the classification of the GS group versus GF and GR, using SVM.

Table 4.4 The best feature subset selected by discriminating the group of patients GS from the rest of the patients ($GR+GF$) by applying SVM and LDA and using JSD with two symbols shifted to the left $\tau = -2$.

Features	SVM
$f1$	$P_n(w_{c101})$
$f2$	$P_n(w_{c100})$
$f3$	$p_n(w_{c101\ r100})$
$f4$	$p_n(w_{c100\ r011})$
$f5$	$p_n(w_{c101\ r101})$
$f6$	$\sum(p_n(w_{cr})) \geq 8\%$
$f7$	$p_n(w_{c010\ r001})$
$f8$	$P_n(w_{c001})$
$f9$	$p_n(w_{c010\ r101})$

The third classification is between patients who successfully passed the trial but had to be reintubated in less than 48 hours (GR), and patients with successful weaning (GS). Clinicians cannot distinguish between those groups, as the test outcome is favourable in both cases. However, in less than 48 hours some patients need to be reintubated. The challenge is to find out which features characterize these patients (GR). The time series analysis (means, standard deviations and interquartile ranges) does not present any significant differences between these two groups. The clinical criteria that are followed to evaluate the readiness of the patients to start the protocol test are the same in both cases.

Fig. 4.9 shows the accuracy, sensitivity and specificity when classifying GR versus GS. Table 4.5 indicates the best 9 features selected through the proposed feature

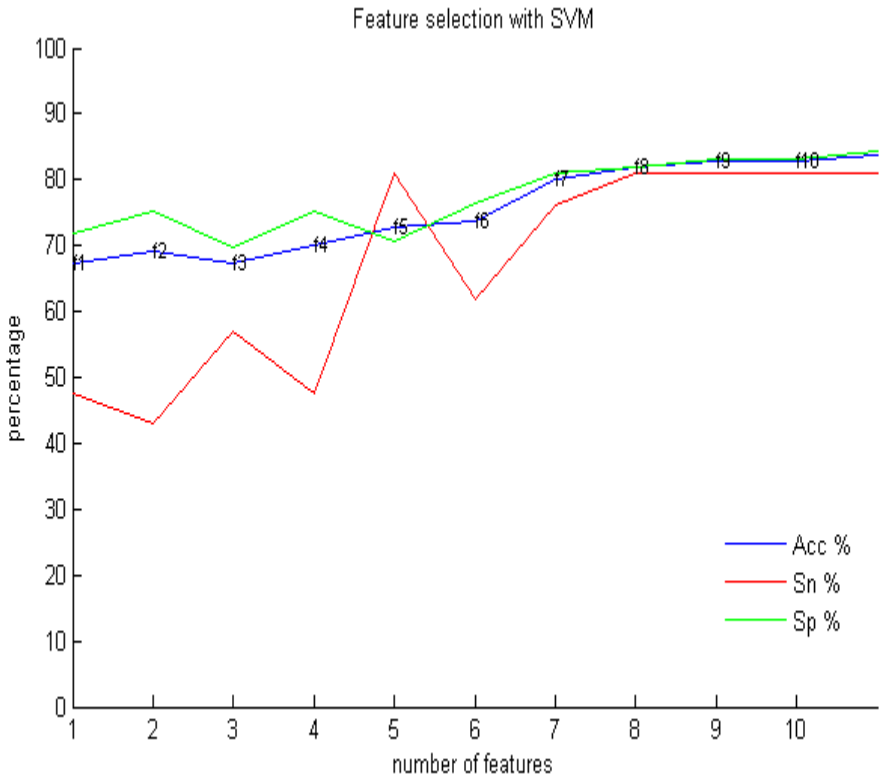

Figure 4.9 Accuracy (Acc), sensitivity (Sn) and specificity (Sp) when a new selected feature is added in the classification of the group of patients GR versus GS, using SVM.

selection. Some of these features present words with monotonous patterns in the cardiac and respiratory dynamics (000 or 111). The percentage of well-classified patients rises to 82.7% with 81.0% of sensitivity and 83.2% of specificity.

Table 4.5 The best feature subset selected by discriminating the group of patients GR from GS using SVM and JSD with two symbols shifted to the left $\tau = -2$.

Features	SVM
$f1$	$p_n(w_{c111\ r101})$
$f2$	$p_n(w_{c011\ r111})$
$f3$	$p_n(w_{c011\ r000})$
$f4$	$p_n(w_{c000\ r101})$
$f5$	$H(W_{\tau=-2})$
$f6$	$p_n(w_{c110\ r010})$
$f7$	$p_n(w_{c000\ r000})$
$f8$	$\sum(p_n(w_{cr})) \geq 5\%$
$f9$	$p_n(w_{c011\ r011})$

In the last classification, we consider reintubated patients (GR) versus the rest of the patients (GS and GF) (Fig. 4.10). The best result is obtained by applying SVM with 10 features (accuracy of 81.0%, sensitivity of 71.4% and specificity of 82.2%). Table 4.6 presents the best 10 features obtained by means of the feature selection, when all the shift values are considered ($\tau = -2, 0, 2$).

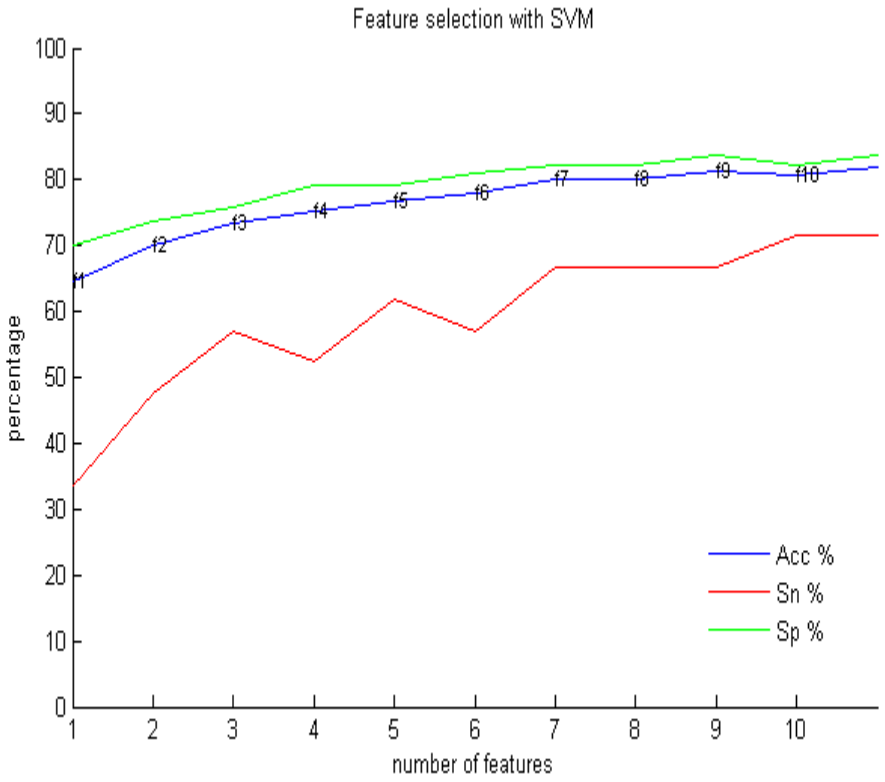

Figure 4.10 Accuracy (Acc), sensitivity (Sn) and specificity (Sp) when a new selected feature is added in the classification of the GR group versus GS and GF, using SVM.

Table 4.6 The best feature subset obtained by discriminating the group of patients GR from the rest ($GS+GF$) by applying SVM and JSD without shifting ($\tau = 0$). *: two symbols shifted to the right ($\tau = 2$), and **: two symbols shifted to the left ($\tau = -2$).

Features	SVM
$f1$	$p_n(w_{c110\ r111})$
$f2$	$\sum(p_n(w_{cr})) \geq 4\%$**
$f3$	$p_n(w_{c011\ r010})$*
$f4$	$p_n(w_{c000\ r100})$
$f5$	$p_n(w_{c001\ r000})$
$f6$	$p_n(w_{c110\ r010})$
$f7$	$p_n(w_{c010\ r101})$*
$f8$	$p_n(w_{c011\ r101})$**
$f9$	$p_n(w_{c011\ r000})$**
$f10$	$p_n(w_{c011\ r100})$

4.4 Conclusion

The spontaneous breathing trial is the main diagnostic test to determine whether patients can be successfully extubated [1]. It has been shown that the rate of successful extubation does not change when the target duration of a spontaneous weaning trial is reduced from 120 minute to 30 minute [15]. Therefore, the electrocardiographic (ECG) and the respiratory flow signal used in this study were acquired during 30 minute spontaneous breathing trials.

In the first study, we used an SVM-based method to analyse respiratory pattern variability in patients during weaning trials, in order to find differences between patients who can maintain spontaneous breathing GS, and patients who fail to maintain

spontaneous breathing GF. Respiratory pattern characterization is developed by a number of respiratory time series. Clustering and validation techniques enable the selection of the best subset of input features, and histogram equalization maps the distribution of the selected features back to the distribution of the most discriminant feature.

Support vector machines trained with the whole set of 35 features achieved a classification accuracy of 66.6%. After a search for the most suitable features and the application of the histogram equalization method, in which the $s(T_E)$ feature is taken as a reference, an accuracy of 80.0%, sensitivity of 86.67% and sensibility of 73.34% is obtained using only 8 of the 35 features. Hence, the SVM analysis can be considered a suitable method for studying respiratory pattern variability in patients on weaning trials.

Numerous clinical indices have been proposed as weaning predictors [18], [117]. Many of these have good sensitivities but most have low specificities, which gives them a poor discrimination result. To achieve more robust and useful automatic indices, we consider the nonlinear joint symbolic dynamic (JSD) procedure to study the cardiac and respiratory signals. The cardiorespiratory dynamics of each patient is therefore characterized by 276 features (92 features, for each $\tau = -2$, 0 and $+2$), which are extracted by applying JSD to the cardiac interbeat and breath duration series. These matrices enable a coarse-grained quantitative assessment of a short-term nonlinear analysis of these interactions.

In spite of having shown remarkable success in many applications, the ability of SVM methods decreases when the datasets are unbalanced. Hence, a new metric called the balance index B is proposed to deal with unbalanced classification problems. Optimized SVM-based feature selection that includes B can overcome this

disadvantage. This method has good predictive performance and a better balance between sensitivity and specificity for an unbalanced dataset. The best result is obtained with optimized feature selection that is based jointly on the accuracy and the balance index, with an accuracy of 80% in the classification of GS and GF, using only 6 features. While the improvement in this study is perhaps not dramatic, it is still of importance as the present classification is based on only 6 features instead of 8. Moreover, good results and a balance between sensitivity and specificity are obtained with 4 features and over.

Once the optimized feature selection method has been established, the prediction of weaning outcome in patients on weaning trials is analysed (GS, GF and GR). The proposed B-based SVM feature selection is compared to LDA. In all cases, SVM feature selection and classification perform better. In the classification of GS patients versus the rest of the patients, the best result is obtained with 9 features, with an accuracy of 81.3% and an acceptable balance between sensitivity and specificity ($83.3\% - 78.3\%$). The features selected by the SVM-based algorithm, unlike the ones selected by LDA, show less presence of respiratory dynamics than cardiac dynamics.

One relevant issue in clinical practice is to distinguish between reintubated and successful patients, since these two groups have the same response to the weaning trial, from a clinical point of view. A good prediction of patients who will require reintubation after having successfully passed the spontaneous breathing test would help in clinical decisions.

The features that are selected in the classification of GR and GS patients are directly related to cardiorespiratory interactions, and provide accurate results in 82.7% of patients. These features present word types with some monotonous patterns in the cardiac and respiratory dynamics, such as 000 or 111 patterns.

Finally, in the classification of GR versus the rest of the patients, the 10 features chosen from SVM are also directly related to cardiorespiratory interactions. In this case, the percentage of well-classified patients is good (81.0%) and there is a balance between sensitivity and specificity.

To sum up, JSD applied to time series of heart rate and respiratory frequency appears to be suitable for the description of cardiorespiratory interactions of patients during weaning trials. The results show good performance of the proposed SVM-based feature selection, since it selects the most relevant features and maintains a balance between sensitivity and specificity for unbalanced groups of data. Therefore, it might be a useful tool for enhancing the analysis of patients on weaning trials, as well as in other clinical studies that involve biomedical time series. This method is versatile, since it could be applied to any classification problem with unbalanced groups.

Nevertheless, additional features and clinical information about the patients before the weaning trial should be considered to increase the discrimination between these three groups, and particularly the reintubated patients.

Chapter 5

Time-frequency analysis of respiratory pattern

Numerous time-frequency techniques have been applied to the respiratory flow signal to characterize the respiratory pattern of patients with chronic heart failure (CHF).

Some artefact reduction techniques are implemented to prepare the respiratory flow signal for further analysis. We compare methods for extracting the envelope of the respiratory flow signal to assess which is most appropriate for this research. Stationary and nonstationary modelling is applied to the signals. The stationarity of the signals is assumed and parametric and nonparametric power spectral density (PSD) are applied to characterize the respiratory pattern in the frequency domain. Finally, a time-varying PSD that is based on a time-varying autoregressive model, is applied to the signals to study respiratory pattern changes over time.

The aim of this chapter is to introduce time-frequency techniques that are applied to the respiratory flow signal to characterize the respiratory pattern in patients with CHF and healthy subjects.

5.1 Respiratory flow signal pre-processing

One key factor in biomedical signal processing is the study of artefacts in the signal, to minimize their influence. A wide variety of artefacts can occur in respiratory flow signals. Some of them are easily identified, such as a missing gap with no respiration activity, but some are exceedingly difficult to distinguish from spontaneous breathing. While the influence of artefacts of technical origin can be reduced by paying more attention to signal acquisition, it is impossible to avoid the artefacts of physiological origin. Consequently, more algorithms are dedicated to physiological artefact removal. We review the most common artefacts in the respiratory flow signals and the techniques designed for their reduction. As normal breathing frequency ranges from 12 to 20 breaths per minute (i.e. 0.20-0.33 Hz), the respiratory flow signals are downsampled to more appropriate sample frequencies (1-2 Hz) in various stages.

5.1.1 Artefact removal

Pre-processing of the respiratory flow signal involves artefact reduction to ensure robust signal analysis. Such processing is essential, as certain artefacts can be difficult to distinguish from a normal breath or normal respiratory events such as a deep breath, cough, sigh or even swallowing. Assuming that these respiratory events take more time than a outlier or spike, we have implemented the following outlier and spike removal algorithms.

- Outlier removal

Samples that exceed a number of standard deviations of data are usually considered outliers. The proposed outlier removal algorithm is based on rejection of the samples

whose amplitude is below the 1^{st} or above the 99^{th} percentile of the entire signal's amplitude histogram. The outliers are replaced with the proper percentile value that corresponds to the 1st or 99th percentile (Fig. 5.1). This artefact rejection is the crudest approach, since it removes less probable data samples, even when they are not artefacts. Thus, it is only appropriate for certain applications.

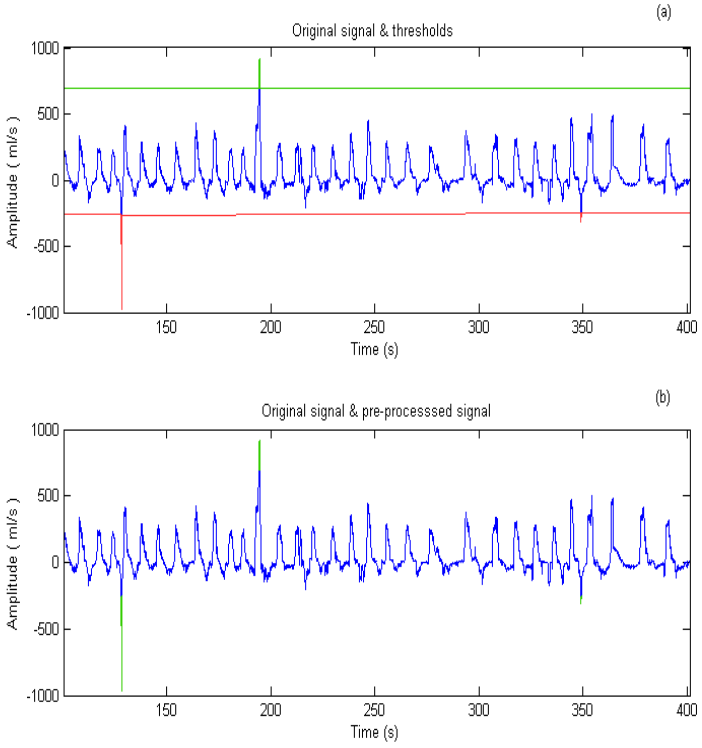

Figure 5.1 Outlier removal: (a) original flow signal with both thresholds (1^{st} and 99^{th} percentile) and (b) overlapped original flow signal and pre-processed flow signal.

- Spike removal

Short duration spike artefacts that are not removed with the percentile test are detected using an auxiliary signal that results from a sampling rate decimation of the

original flow signal to 25 Hz, followed by median filtering. A filter length of 11 is found to be suitable. Whenever the difference between the original and median filtered signals exceeds a certain threshold value, which we set to half the standard deviation of the signal, the original samples are replaced by the median value of the neighbouring samples (Fig. 5.2).

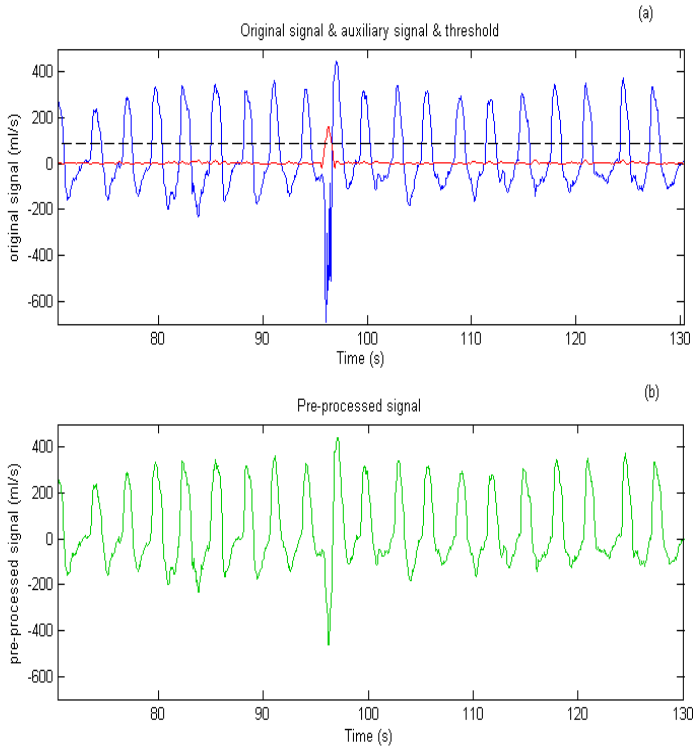

Figure 5.2 Spike reduction: (a) original flow signal, auxiliary signal and the fixed threshold and (b) pre-processed flow signal.

- AR reconstruction

In a few patients, short gaps (< 1 s) with missing samples occurred due to uncontrolled movements of the patients during acquisition. Rather than excluding these recordings from the analysis, interpolation based on AR signal modelling is used to fill in the

gaps [4] and [118]. This interpolation method estimates the AR coefficients from the segment preceding the gap and then uses these coefficients to forward predict the signal across the missing samples. The same process is repeated for the segment after the gap, using backward extrapolation. The gap of missing samples is then replaced by a cross-faded version of the two extrapolated values (Fig. 5.3), using the following window:

$$w(n) = \begin{cases} 1 - \frac{1}{2}(2u(n))^{\alpha}, & u(n) \leq \frac{1}{2} \\ \\ \frac{1}{2}(2 - 2u(n))^{\alpha}, & u(n) > \frac{1}{2} \end{cases} \tag{5.1}$$

where $u(n) = (n - n_s)/(n_e - n_s)$, and n_s and n_e are the indices of the onset and end of the gap, respectively. Cross-fading is carried out by multiplying the forward extrapolated sequence by $w(n)$ and the backward extrapolated sequence by $1 - w(n)$. A linear downslope is attained with $\alpha = 1$, whereas a step-like transition results when $\alpha \to \infty$. The slope of the window is adjusted via the parameter $\alpha = 3$. Finally, as the respiratory frequency does not exceed 0.5 Hz, the respiratory flow signals are decimated to 1 Hz, using appropriate lowpass filtering prior to downsampling.

- Avoiding missing or saturated samples

Another approach to processing signals that contain missing samples or signals that become saturated could be to discard them from subsequent analyses, as they do not reflect respiratory activity. However, the computation of further analyses, such as spectral power, needs to be modified in this case. The first step is to detect the

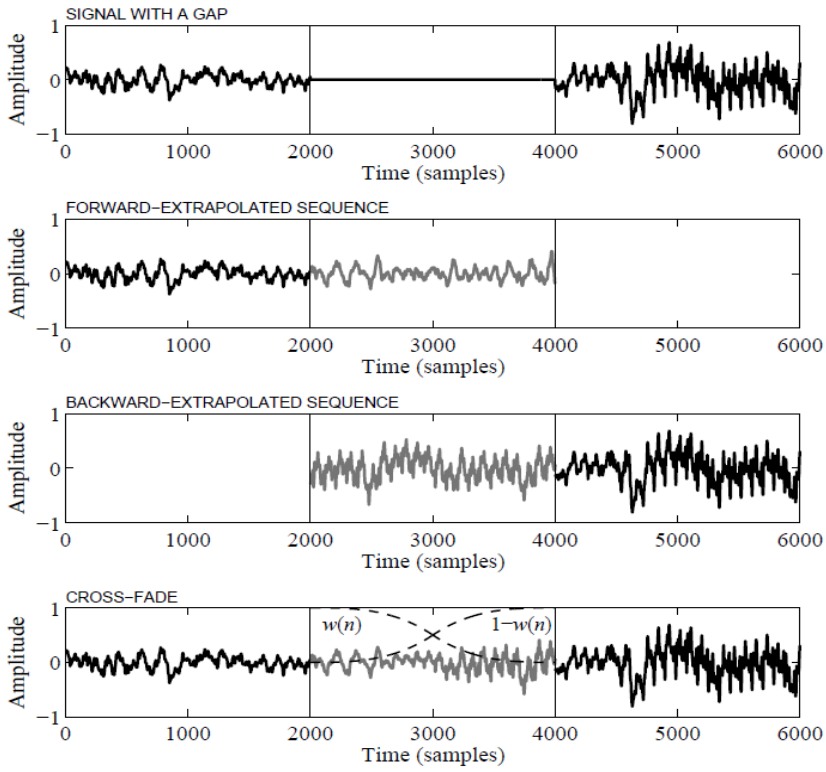

Figure 5.3 AR reconstruction process decomposition taken from [4].

samples to be discarded and represent them by the binary function $g(n)$, defined by

$$g(n) = \begin{cases} 1 & \text{existing,} \\ 0 & \text{discarded.} \end{cases} \tag{5.2}$$

The information on discarded samples is introduced in the correlation function [119], with an indication of whether or not the information given by the sample denoted as $x(n)$ is reliable or not. Hence, the autocorrelation function $r_x(m)$ and the corresponding power spectral density $P_x(e^{j\omega})$ is estimated by

$$r_x(k) = \frac{\sum_{n=1}^{N-k} x(n) \cdot x(n+k) \cdot g(n) \cdot g(n+k)}{\sum_{n=1}^{N-k} g(n) \cdot g(n+k)} \tag{5.3}$$

$$P_x(e^{j\omega}) = \sum_{k=-\infty}^{\infty} r_x(k)e^{-j\omega k}\,. \tag{5.4}$$

5.1.2 Downsampling

The sampling frequency (fs) of the acquired flow signals is 250 Hz, whereas the spectral content of the respiratory flow signals is located in a much lower frequency range (0.20-0.33 Hz) [66]. To condition the respiratory flow signal for a more appropriate analysis, it is downsampled to 1 or 2 Hz, depending on the application.

The Nyquist theorem is accomplished, since the respiratory frequency can range up to 0.5 Hz. However, to ensure that the sampling theorem is satisfied and aliasing is avoided, a low pass filter is applied before the signal is downsampled. The overall process, the filtering and the downsampling is called decimation. A type I eight-order low-pass Chebyshev filter is applied with a cut frequency of $0.8 * (fs/2)/L$, where L is the downsampling factor.

As the downsampling factor is very high (250/1, 250/2), the decimation process is divided into 3 steps. First, we reduce the sampling frequency to 25 Hz, by a downsampling factor of 10. The next decimation stage reduces the sample frequency to 5Hz through a factor of 5. In the last stage, the sample frequency is decreased to 1 or 2 Hz by a resampling factor of 5 of 5/2, respectively.

5.2 Respiratory pattern characterization

Respiratory pattern characterization is based on the envelope of the respiratory flow signal, since this may reflect periodicity in the pattern. The envelope of the respiratory flow signal can be extracted by different methods.

5.2.1 Envelope detection

The envelope of the respiratory flow signal might convey useful information. Specifically, the respiratory modulation frequency appears to be essential in the study of periodic and nonperiodic breathing patterns. Thus, this envelope is studied in depth. Below, we review several envelope extraction methods that have been reported in the literature [120], [121], [122], [123] and [124].

5.2.1.1 Envelope detection in time domain

The most representative time domain envelope extraction techniques are based on calculating the absolute value, the energy, the Shannon energy and Shannon entropy of the signal as a moving average. The respiratory flow signals are decimated to 1 Hz and normalized to between [-1 to 1] by $x_{norm}(n) = x(n)/max(|x|)$, where $x(n)$ is the respiratory flow signal. The computed envelopes are based on the following expressions that are evaluated over the resulting signal $x_{norm}(n)$.

Shannon energy	$E(n) = -x^2_{norm}(n) \cdot log\ x^2_{norm}(n)$
Shannon entropy	$E(n) = -\lvert x_{norm}(n)\rvert \cdot log\ \lvert x_{norm}(n)\rvert$
Absolute value	$E(n) = \lvert x_{norm}(n)\rvert$
Energy	$E(n) = x^2_{norm}(n)$

Normalized average Shannon energy, which is called the Shannon envelope, is a popular technique for the envelope extraction of cardiac sound signals [120] and [121]. The sliding window is defined by fixing the segment and the overlap length. It evaluates the average Shannon energy in continuous signal segments by

$$E(n) = \frac{1}{N} \cdot \sum_{n=1}^{N} -x^2_{norm}(n) \cdot log\ x^2_{norm}(n) \tag{5.5}$$

where $x_{norm}(n)$ is the x decimated and normalized sample signal and N is the signal length in each segment, which corresponds to a frame. The most suitable sliding window for this purpose is a 15-second window with a 5-second overlapping segment.

As illustrated in Fig. 5.4, the absolute value of the flow signal provides all the signal with the same weight, whereas energy attenuates the effect of low value samples and emphasizes the effect of high value samples. In contrast, Shannon entropy emphasizes the effect of low value samples, which makes it more difficult to track the signal outline. Shannon energy emphasizes medium value samples and attenuates the effect of low value samples more than high value samples. It reduces the difference between low and high values, which makes it more appropriate than the absolute value in cardiac sound signal analysis.

5.2.1.2 Envelope detection in the frequency domain

A well-known technique based on the Hilbert transform (a 90-degree phase shifter) extracts the envelope without any previous knowledge of its frequency and phase, and without the need for a sliding window [85]. The respiratory flow signal can be expressed through a deterministic low-pass signal, which is modulated by a cosine with frequency ω_m and phase ϕ by

$$x(n) = a(n)\cos(\omega_m n + \phi) \tag{5.6}$$

where $x(n)$ is the respiratory flow signal and $a(n)$ the envelope of $x(n)$ (the index n represent a discretization of $x(t)$ sampled every $1/fs$ seconds). The signal $x(n)$ can be expressed in the frequency domain as:

$$X(e^{j\omega}) = \frac{1}{2}\left[A(e^{j(\omega-\omega_m-\phi)}) + A(e^{j(\omega+\omega_m+\phi)})\right] \tag{5.7}$$

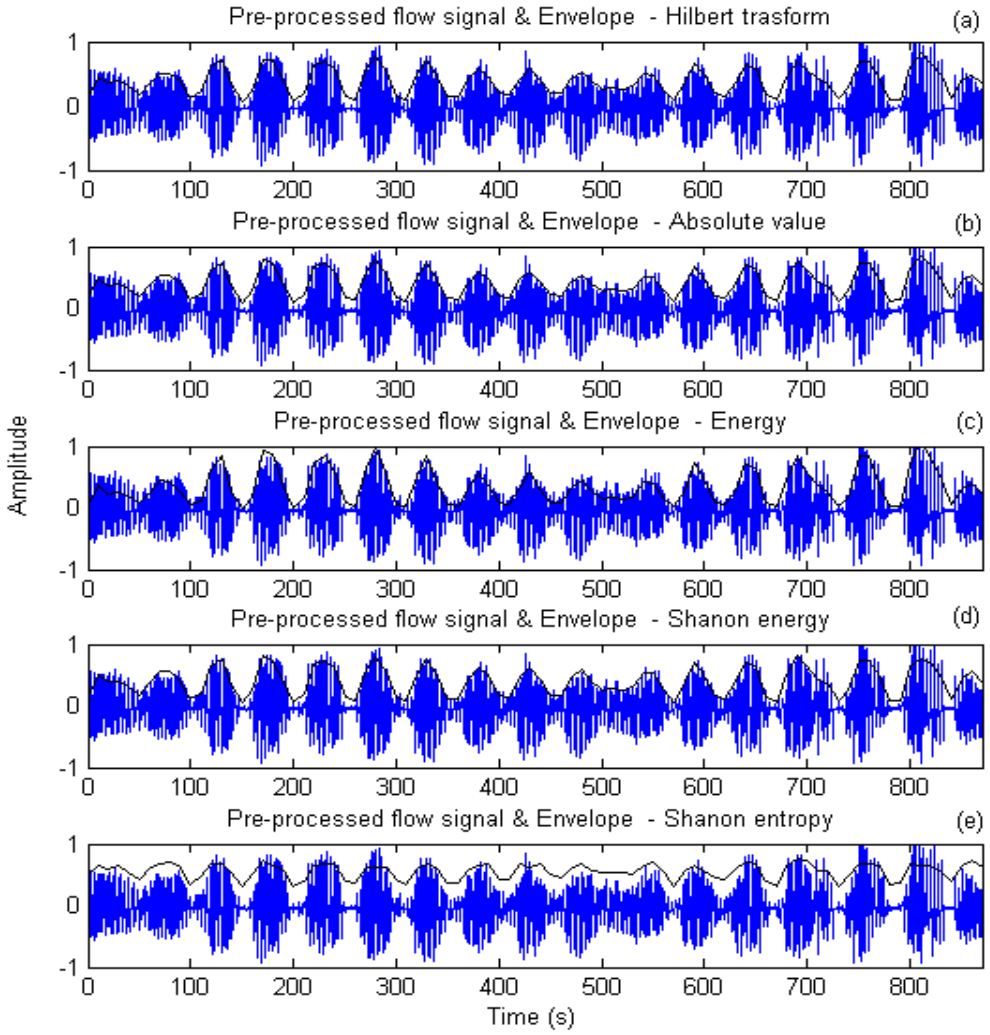

Figure 5.4 Time and frequency domain envelope extraction methods for a real signal.

where $X(e^{j\omega})$ and $A(e^{j\omega})$ are the discrete-time Fourier transform of $x(n)$ and $a(n)$, respectively.

The envelope $a(n)$ is obtained by cancelling out the negative frequencies and shifting the right side spectrum to the origin [125]. The following expression cancels the left side spectrum

$$X_A(e^{j\omega}) = X(e^{j\omega}) + jH(e^{j\omega})X(e^{j\omega}) = X(e^{j\omega}) + j\bar{X}(e^{j\omega}) \tag{5.8}$$

where $H(e^{j\omega})$ is the linear time invariant filter, which is referred to as the Hilbert transform. The output of the Hilbert transform applied to $x(n)$ corresponds to a 90° shifted version of $x(n)$, and is denoted $\overline{x}(n)$. Therefore, $x_A(n)$ represents a frequency-shifted version of the envelope, and the positive-valued envelope is obtained without any knowledge of ω_m or ϕ by

$$x_A(n) = a(n)e^{\ j\omega_m n} \tag{5.9}$$

$$a(n) = |x_A(n)| = \sqrt{x^2(n) + \bar{x}^{\ 2}(n)}. \tag{5.10}$$

Since the frequency bandwidth of the flow envelope signal $a(n)$ is much lower than the original $x(n)$ signal, it is downsampled to 0.1 Hz.

We considered the properties and performance of each envelope detection method and selected the one based on the Hilbert transform to extract the envelope of the respiratory flow signal. This method has high computational efficiency and does not require any previous normalization or subsequent reescalation.

We have observed that the behaviour of the respiratory flow signal in patients with periodic breathing often resembles a signal that is subjected to amplitude modulation (AM). Considering that the respiratory frequency normally ranges from 0.2 Hz to 0.4 Hz and the modulation frequency from 0.01 Hz to 0.04 Hz [66], an AM signal is

simulated. This consists of a 0.3 Hz (f_c) carrier wave modelled by a simple sinusoidal wave of 0.02 Hz (f_m). An example of the simulated signal segment and a real flow signal segment is presented in Fig. 5.5.

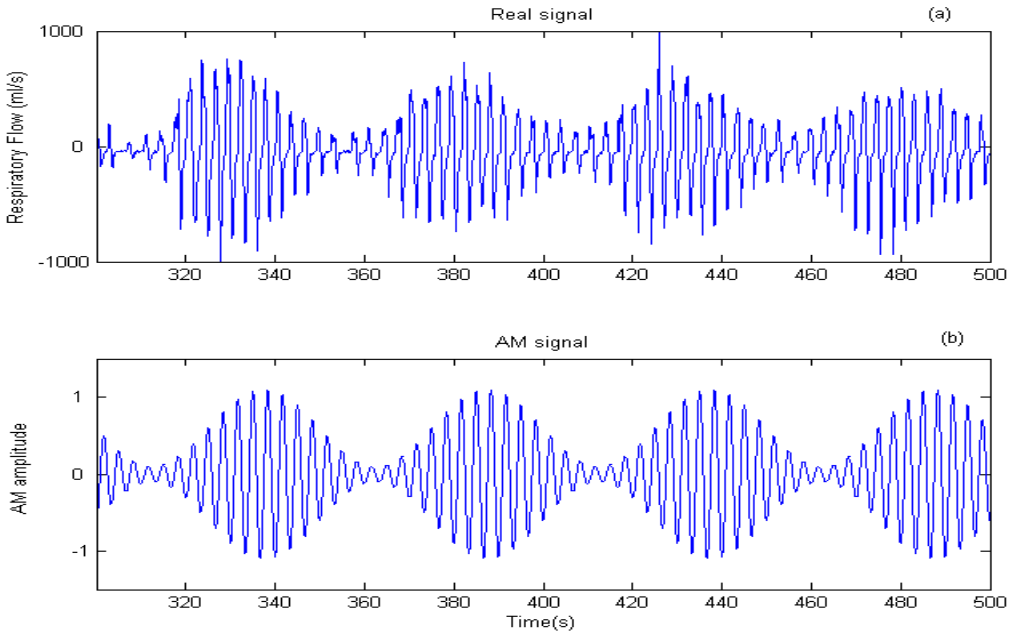

Figure 5.5 (a) Respiratory flow signal segment of a PB patient and (b) the simulated AM signal with a 0.3 Hz carrier and a 0.02 Hz sinusoid as modulation.

The performance of each envelope extraction technique applied to the respiratory flow signal of a patient with periodic breathing and to the simulated AM signal is illustrated in Figs. 5.4 and 5.6, respectively.

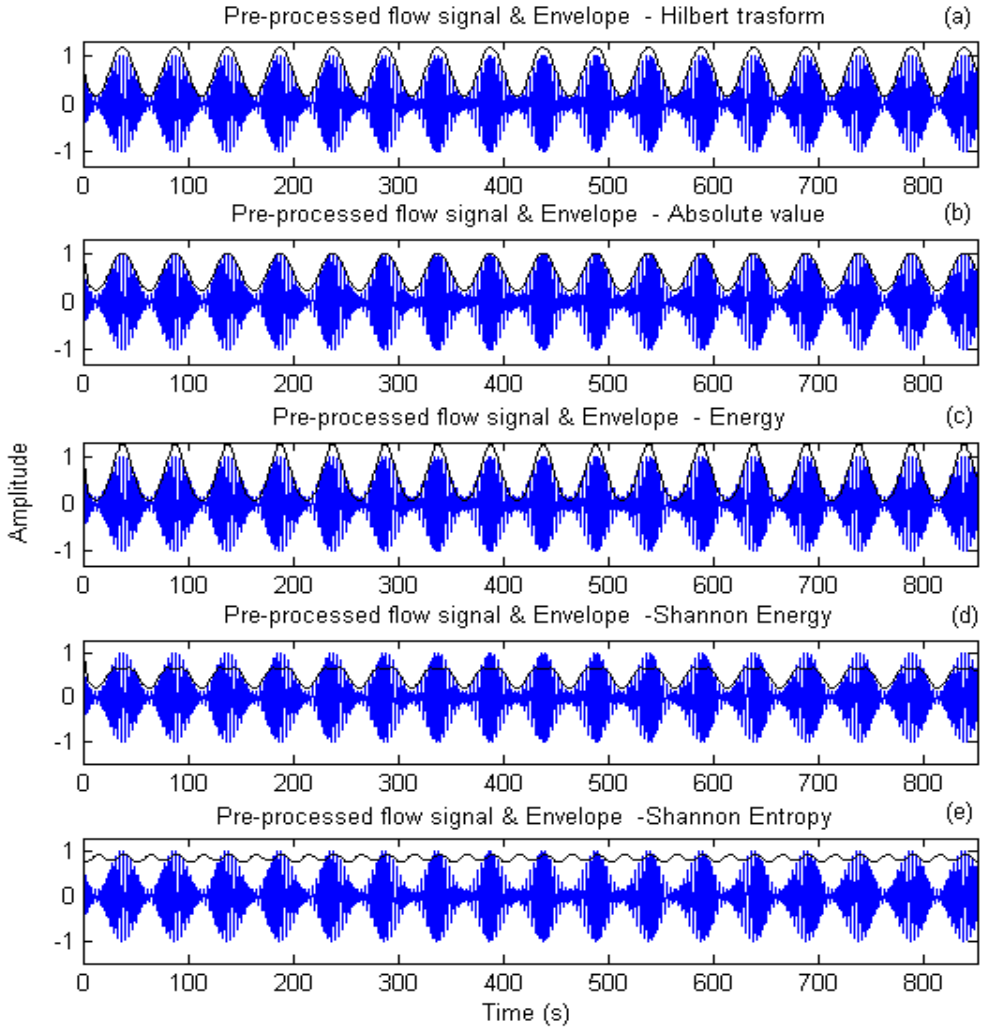

Figure 5.6 Time and frequency domain envelope extraction methods for the AM signal.

5.2.2 Envelope modelling

Autoregressive (AR) and autoregressive moving average (ARMA) models can efficiently present abrupt peaks in their power spectral density, as required for our purpose. Any ARMA model could be represented by an AR model with a sufficiently high model order [126]. When we use an autoregressive AR model, which is also referred to as an all-pole model, the respiratory envelope signal is approximated by the following expression:

$$x[n] = -\sum_{k=1}^{p} a[k] \cdot x[n-k] + u[n] \tag{5.11}$$

where $u[n]$ denotes zero-mean white noise with σ (the estimated error variance), $a[k]$ are the autoregressive coefficients, p is the order of the model and $x[n]$ the respiratory flow signal.

Model coefficients can be estimated directly thought the autocorrelation function by means of the Yule-Walker equations, which describe a nonlinear relation between the AR coefficients and the autocorrelation function of the process. The AR coefficients can therefore be determined by solving a system of linear equations with p unknown variables. The Levinson-Durbin recursion is implemented to resolve this equation system, by exploiting the symmetry and Toeplitz properties of the correlation matrix R_x [127] and [128].

5.2.2.1 Selection of the AR model order

One of the most relevant aspects in power spectral density estimation through AR modelling is the selection of the model order p. This is a trade-off between the fre-

quency resolution and the spurious peaks. If the model order is too low, a highly smoothed spectrum is obtained. If it is too high, spurious low level peaks might be introduced into the spectrum. The accuracy of the AR model is evaluated through the mean square prediction error. Different values are obtained for each power spectral density estimator. The prediction error decreases as the order of the model is increased. To select an appropriate model order, the rate of decrease can be monitored to determine when it becomes slow. However, this method is imprecise in comparison with the best known criteria for selecting the optimum model order, as proposed by Akaike [129], [130], and Risssanen [131]. The first criterion proposed by Akaike is the final prediction error criterion (FPE). The optimum model order minimizes the function

$$FPE(p) = \hat{\sigma}_e^2 \left(\frac{N+p+1}{N-p-1} \right) \tag{5.12}$$

where N is the number of observed data items and $\hat{\sigma_e}$ is the estimated variance of the linear prediction error of a p-order AR model.

The second criterion proposed by Akaike is called the Akaike information criterion (AIC). AIC selects the model order that minimizes

$$AIC(p) = N \cdot ln(\hat{\sigma}_e^2) + 2 \cdot p. \tag{5.13}$$

The criterion proposed by Rissanen is based on selecting the model order that minimizes the description length (MDL), defined as

$$MDL(p) = N \cdot ln(\hat{\sigma}_e^2) + p \cdot ln(N). \tag{5.14}$$

If we consider the results reported in [132], the FPE criterion tends to underestimate the model order. Unlike MDL, AIC is said to be statistically inconsistent

when $N \to \infty$ [133]. We have used the methods described above to study the optimum order for representing the respiratory flow signal and the respiratory envelope signal. Figs. 5.7 and 5.8 illustrate the performance of each criterion using the forward-backward approach, which is applied to the simulated AM signal and its envelope, respectively.

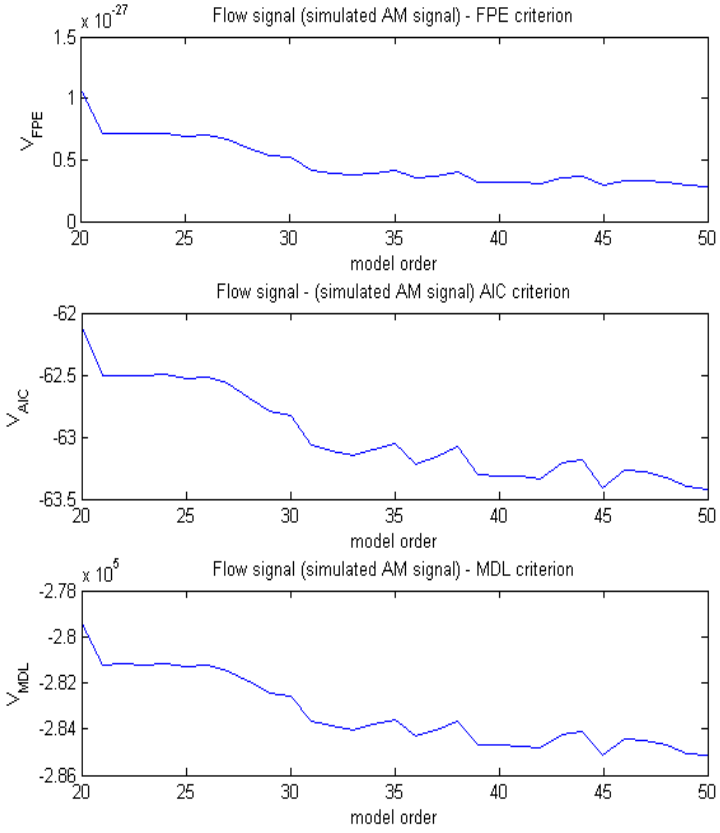

Figure 5.7 (a) *FPE* criterion, (b) *AIC* criterion and (c) *MDL* criterion evaluated by the simulated AM signal.

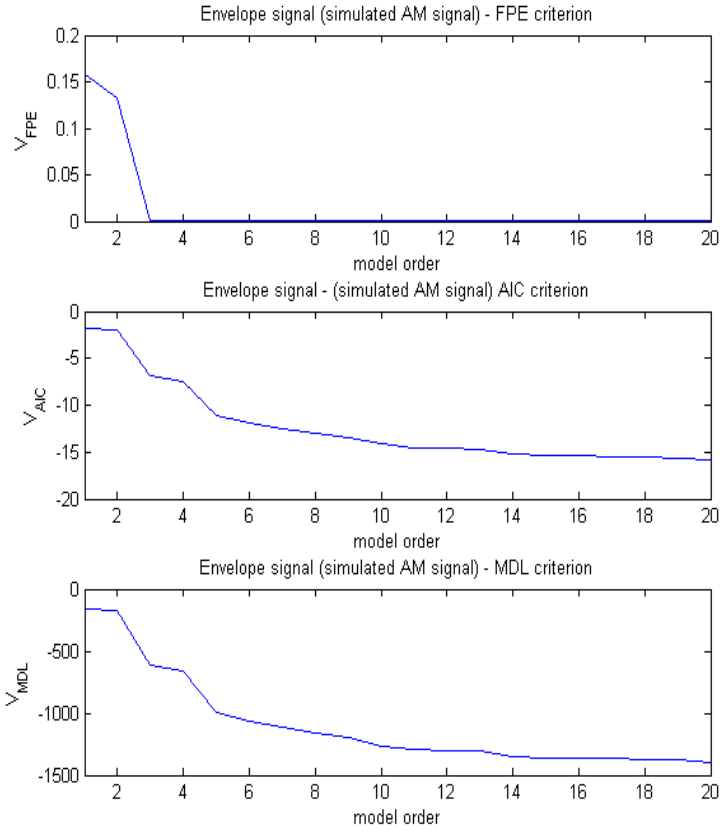

Figure 5.8 (a) FPE criterion, (b) AIC criterion, and (c) MDL criterion evaluated by the simulated AM signal's envelope.

Figs. 5.9 and 5.10 illustrate the performance of each criterion using the forward-backward approach, applied to the respiratory flow signal and the respiratory envelope signal of a CHF patient, respectively.

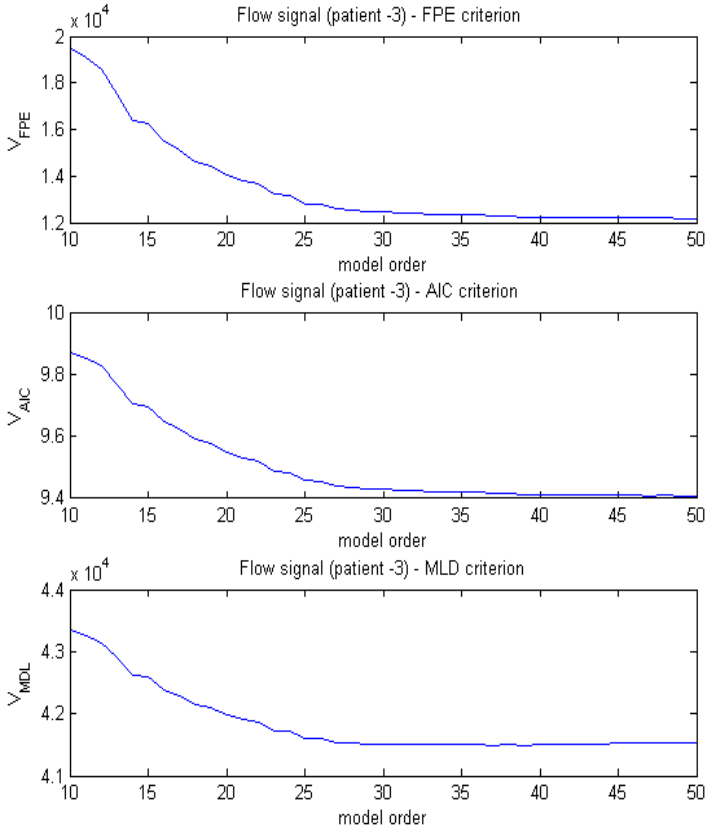

Figure 5.9 (a) FPE criterion, (b) AIC criterion and (c) MDL criterion evaluated for the respiratory flow signal of a CHF patient.

For all the subjects in this study, these methods perform similarly for both the respiratory flow and the envelope signal. However, when the simulated AM signal is studied, FPE and MDL perform similarly but AIC criterion suggests higher order models. Finally, Rissanen's MDL criterion is employed in this research. The mean of the optimum model order that was obtained for each CHF patient and healthy subject is selected as the most appropriate. A 30^{th}-order AR model appropriately represents the respiratory flow signal and a 4^{th}-order AR model represents the respiratory envelope signal.

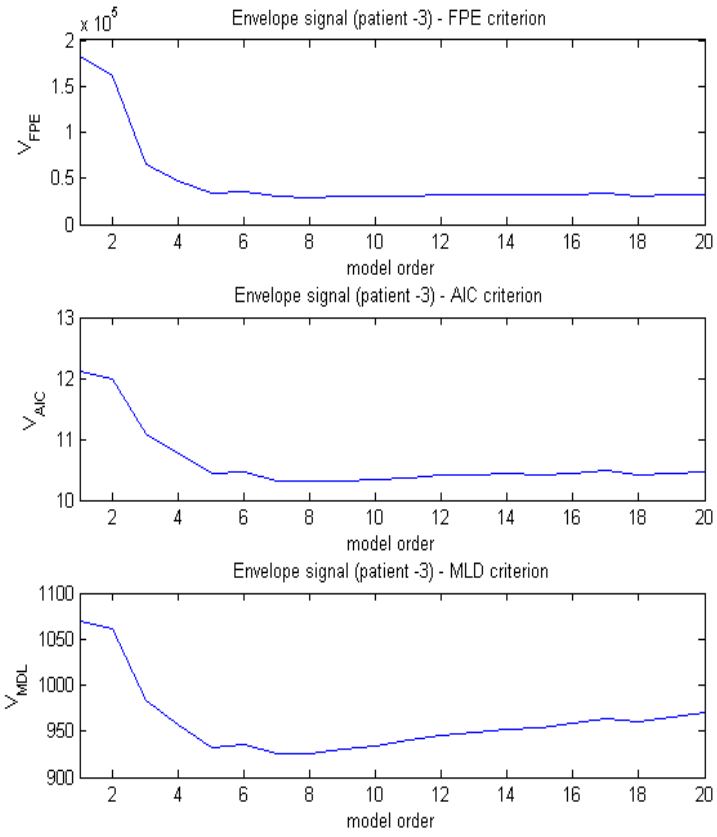

Figure 5.10 (a) FPE criterion, (b) AIC criterion and (c) MDL criterion evaluated for the respiratory flow envelope of a CHF patient.

5.2.2.2 Whiteness test

The model order should ensure that the model correctly represents the data. This is achieved only when the prediction error results in a white noise sequence. Consequently, some of the information is still in the prediction error, when it differs from white noise, which means that the model cannot completely describe the signal. If the prediction error sequence is white noise, the autocorrelation function is theoretically zero. However, the sample autocorrelation is usually different from zero. We have performed a statistical test on the sample autocorrelation of the prediction error. We

have applied the Ljung–Box test $Q(l)$ to prove the whiteness of the prediction error. This tests whether any of a group of autocorrelations of a time series are different from zero. Instead of testing randomness at each distinct lag, this statistical test evaluates the randomness based on a number of lags, by means of

$$Q(l) = N \cdot (N+2) \sum_{i=1}^{l} \frac{r_i^2}{N-i} \tag{5.15}$$

where N is the number of samples, l the number of lags studied, and r_i is the autocorrelation at lag i. We consider the following null hypothesis: $H_0 : r_i = 0$. If the Q value is less than the theoretical value of a significant level of the chi-squared (χ^2) distribution ($p \leq 0.05$), the null hypothesis is rejected. From the prediction error and with $l = 100$, we have $Q(100) = 93$. Since the model order is 30, the degree of freedom of the χ^2 distribution is $100 - 30 = 70$. As $\chi^2_{1-0.05}(70) = 43.22$ and $\chi^2_{0.05}(70) = 104.215$, H_0 is not rejected. The residuals of all 61 signals except two are whitened by the global AR model.

5.2.3 Envelope spectral analysis

Spectral analysis is a powerful technique for characterizing the respiratory flow signal and its envelope, due to its oscillatory behaviour. There are two main classes of spectral analysis: parametric and nonparametric analysis. Fourier-based spectral analysis is referred to as nonparametric spectral estimation, since it does not make any assumptions about how the data were generated. It essentially correlates the data with the sines and cosines of various frequencies to produce a set of coefficients that define the power spectral density (PSD). In contrast to nonparametric methods, parametric methods assume an autoregressive (AR) model as the data generating

process and try to fit the model to the signal by minimizing a given cost function. The most frequently used parametric and nonparametric fundamentals of power spectral estimators are described below.

5.2.3.1 Nonparametric spectral analysis

The power spectral density (PSD) of a stationary random signal $x(n)$ is estimated by

$$P_x(e^{j\omega}) = \sum_{-\infty}^{\infty} r_x(n) \cdot e^{-j\omega n} \tag{5.16}$$

where $r_x(n)$ is the autocorrelation function that characterizes the random process.

In practice, only a single observation of the random process $x(n)$ that consists of a finite sample sequence $x(1), ..., x(N)$ is available for computing the statistical autocorrelation function. It can be approximated by a time average autocorrelation function, if we assume that the process is ergodic in the first and second moments, defined by

$$\hat{r}_x(n) = \sum_{k=0}^{N-1-n} x(n+k) \cdot x(n), \quad n = 0, ..., N-1. \tag{5.17}$$

When the definition of the PSD is combined with the autocorrelation function, the PSD that is commonly known as the periodogram can be computed through

$$\hat{P}_x(e^{j\omega}) = \sum_{-N+1}^{N-1} \hat{r}_x(n) \cdot e^{-j\omega n}, \tag{5.18}$$

where negative lags are obtained by means of the symmetry property $\hat{r}_x(n) = \hat{r}_x(-n)$.

If the autocorrelation function is expressed as a convolution $\hat{r}_x(n) = \frac{1}{N} \cdot x(n) * x(-n)$, a signal-dependent, periodogram expression can easily be derived from

$$\hat{P}_x(e^{j\omega}) = \frac{1}{N} \left| X(e^{j\omega}) \right|^2 = \frac{1}{N} \left| \sum_{0}^{N-1} x(n) \cdot e^{-j\omega n} \right|^2. \tag{5.19}$$

The PSD can be also estimated as the squared magnitude of the signal's Fourier transform $X(e^{j\omega})$. Fourier-based spectral methods are linked to an infinite record of data, therefore the use of a finite data sequence generates some problems. On the one hand, the frequency resolution of these methods is at best equal to the spectral length of the rectangular window, which is approximately $1/N$ at $-3dB$. This cannot be improved by increasing the sample frequency or by zero-padding. On the other hand, the effect of limiting the duration of the signal to N samples is equivalent to multiplying the signal by a rectangular window. This is reflected as the convolution of the respective Fourier transforms in the frequency domain. The Fourier transform of the rectangular window presents a main lobe and several side lobes. In the convolution, the main lobe smears the estimated spectrum and limits the frequency resolution or the degree of detail that can be resolved in the PSD, whereas side lobe convolution introduces side lobe energy that the real spectrum lacks. This undesirable effect is commonly known as spectral leakage [134].

The variance of the estimation $\hat{r}_x(n)$ decays to zero as N tends to ∞, which makes the computed autocorrelation a consistent estimate of the true autocorrelation. In contrast, the variance of the estimation $\hat{P}_x(e^{j\omega})$ does not approach zero as the number of samples increases to ∞ (it does not converge to the true PSD). The periodogram is therefore not consistent enough to compute the PSD. This lack of consistency, together with the problems of smearing, leakage and frequency resolution, provide the motivation for the methods developed by Bartlett in 1948 and Welch in 1967 [134], [128]. The goal of these methods is to reduce the power estimation variance by decreasing the frequency resolution. The use of windowing and averaging techniques diminishes the leakage effect and the periodogram's variance, respectively.

- The Bartlett method

To reduce variance in the periodogram, Bartlett proposed a division of the data sequence into P non-overlapping segments. Each segment has length D ($D \cdot P \leq N$).

$$x_i(n) = x(n+iD) \quad \text{for} \quad \begin{cases} i = 0,1,...,P-1 \\ n = 0,1,...,D-1 \end{cases} \tag{5.20}$$

where $x(n)$ and $x_i(n)$ are the signal and a segment of the signal, respectively. For each segment, the periodogram is calculated by

$$\hat{P}_x^{(i)}(e^{j\omega}) = \frac{1}{D}\left|\sum_{n=0}^{D-1} x_i(n)\cdot e^{-j\omega n}\right|^2, \quad i = 0,1,...,P-1. \tag{5.21}$$

Bartlett's periodogram consists of the average of the P segment periodograms:

$$\hat{P}_{x\ Bartlett}(e^{j\omega}) = \frac{1}{P}\sum_{i=0}^{P-1} \hat{P}_x^{(i)}(e^{j\omega}). \tag{5.22}$$

If the length of the data is reduced from N to D samples, the spectral length of the Bartlett window is increased by a factor of P, which decreases the frequency resolution by the same factor. In exchange, the variance of the PSD estimate is reduced in a way that is inversely proportional to the number of segments P, which increases the stability of the estimator. However, this variance reduction decreases if the segments are statistically dependent. The variance is given by

$$var\left\{\hat{P}_{x\ Bartlett}(e^{j\omega})\right\} \approx \frac{1}{P}\cdot var\left\{\hat{P}_x^{(i)}(e^{j\omega})\right\} \approx \frac{1}{P}P_x^2(e^{j\omega}). \tag{5.23}$$

Therefore, there is a trade-off between the frequency resolution and the variance of the PSD. An increase in the number of samples in each segment D improves the frequency resolution, and an increase in the number of segments P reduces the variance.

- Welch method

Welch modified Bartlett's method by windowing the data segments prior to computing the periodogram and by allowing the data segments to overlap. The purpose of applying the windowing is to reduce the effect of side lobe energy by decreasing the frequency resolution. The aim of permitting overlap is to increase the number of segments that are averaged, so that the variance of the estimate is reduced. If we assume an offset of M samples between successive segments and a segment length of D, the data segments are represented by

$$x_i(n) = x(n+iM) \quad \text{for} \quad \begin{cases} i = 0, 1, ..., L-1 \\ n = 0, 1, ..., D-1 \end{cases} \tag{5.24}$$

where $i \cdot M$ is the starting point for the i_{th} sequence. Note that the amount of overlap between successive sequences is $D - M$. If $M = D$, the segments do not overlap and the number of data segments L is equal to the number of segments in the Bartlett method P. Nevertheless, if $M = D/2$, there is a 50% overlap between successive data segments, and consequently $L = 2 \cdot P$ segments are obtained. The result is a modified periodogram given by

$$\hat{P}_x^{(i)}(e^{j\omega}) = \frac{1}{D \cdot U} \left| \sum_{n=0}^{D-1} x_i(n) \cdot w(n) \cdot e^{-j\omega n} \right|^2, \quad i = 0, 1, ..., L-1 \tag{5.25}$$

where U is the normalization factor for the power in the window function Eq. (5.26). This factor removes the energy bias introduced by the windowing.

$$U = \frac{1}{D} \sum_{n=0}^{D-1} w(n)^2. \tag{5.26}$$

The Welch PSD is estimated by averaging these modified periodograms through

$$\hat{P}_{x\,Welch}(e^{j\omega}) = \frac{1}{L} \sum_{i=0}^{L-1} \hat{P}_x^{(i)}(e^{j\omega}). \tag{5.27}$$

Similar to Bartlett's periodogram, the variance of the PSD is inversely proportional to the number of segments L, and is given by

$$var\left\{\hat{P}_{x\,Welch}(e^{j\omega})\right\} \approx \frac{1}{L}\cdot var\left\{\hat{P}_x^{(i)}(e^{j\omega})\right\} \approx \frac{9}{8L}P_x^2(e^{j\omega}). \tag{5.28}$$

Due to the overlap, the number of segments L in Welch's periodogram is higher than in Bartlett's and consequently the variance is lower. However, this variance reduction decreases if the segments are statistically dependent, so a lot of overlap is not recommended. Hence, there is a trade-off between the number of segments and the overlap to reduce the variance.

Welch proposed the application of a Hanning window with an overlap between segments of 50%. In this way, all the samples except for the $D/2$ samples of the signal edges are used twice, which makes the treatment of each sample equal. The temporal window $w(n)$ controls the leakage effect. The application of a nonrectangular window reduces the distortion introduced by the side lobes, but increases the width of the main lobe. Below, we present the most frequently used window functions in the time and frequency domain.

- Blackman-Tukey method

The Bartlett and Welch methods are both designed to reduce the variance of the periodogram by averaging the periodograms and the modified periodograms, respectively. Blackman-Tukey is another method for reducing the statistical variance of the periodogram by smoothing the periodogram itself [135].

The periodogram is computed by taking the Fourier transform of a consistent estimate of the autocorrelation sequence. However, for any finite data record of length N, the variance of the autocorrelation estimate $\hat{r}_x(n)$ will be large for values

of n that are close to N. Note that the estimate of $\hat{r}_x(n)$ at lag $n = N-1$ is

$$\hat{r}_x(N-1) = \frac{1}{N} x(N-1) \cdot x(0). \tag{5.29}$$

Since little averaging occurs in the formation of the estimates of $\hat{r}_x(n)$ for $n \approx N$, no matter how large N becomes, these estimates will always be unreliable. The variance of the periodogram is decreased by reducing the variance of the autocorrelation estimate. This is achieved by averaging in both the Bartlett and Welch methods. In contrast, in the Blackman-Tukey method the variance of the periodogram is reduced by applying a window to reduce the contribution of unreliable estimates [134]. The Blackman-Tukey PSD ($\hat{P}_{x\ Blackman}$) is given by

$$\hat{P}_{x\ Blackman}(e^{j\omega}) = \sum_{n=-M}^{M} \hat{r}_x(n) \cdot w(n) \cdot e^{-j\omega n}. \tag{5.30}$$

where $w(n)$ is a lag window that is applied to the autocorrelation estimate. For example, if $w(n)$ is a rectangular window that extends from $-M$ to M with $M < N-1$, then the estimates of $\hat{r}_x(n)$ that have the largest variance are set to zero. Consequently, the PSD will have smaller variance. However, this variance reduction leads to a decrease in the frequency resolution, since a smaller number of autocorrelation estimates are used to compute the PSD. In the frequency domain, the Blackman-Tukey method smooths the periodogram by convolving it with the Fourier transform of the autocorrelation window $W(e^{j\omega})$. Consequently, the window that is applied $w(n)$ should be conjugate symmetric so that $W(e^{j\omega})$ is real-valued, and should have a non-negative Fourier transform, so that $\hat{P}_{x\ Blackman}(e^{j\omega})$ is guaranteed to be non-negative.

The variance of the PSD is given by

$$var\left\{\hat{P}_{x\ Blackman}(e^{j\omega})\right\} \approx P_x^2(e^{j\omega}) \cdot \frac{1}{N} \sum_{n=-M}^{M} w^2(n). \tag{5.31}$$

There is a trade-off between bias and variance. For a small bias, M should be large to minimize the width of the main lobe of the $W(e^{j\omega})$, whereas M should be small to minimize the variance. It is suggested that M have a maximum value of $N/5$ [128].

5.2.3.2 Parametric spectral analysis

One of the main problems of the nonparametric methods is the windowing inherent in finite length data sequences. This windowing implies the assumption that the data outside of the observation window are zero. This assumption limits the frequency resolution and the quality of the PSD. Another inherent assumption in the periodogram is that the data are periodic with period N. Neither of these assumptions are realistic, consequently the PSD is biased. Parametric PSD estimation methods aim to estimate a mathematical model that describes the random process. The model can be constructed with a number of parameters that can be estimated from the observed data. The advantage of model-based frequency estimation is its capacity to predict future samples outside of the observation interval, instead of assuming zero. Subsequently, parametric PSD estimation methods avoid the problem of leakage and provide better frequency resolution than the Fourier-based, nonparametric methods described in the preceding section [126], [85].

- Rational transfer function models

The parametric methods considered in this section are based on modelling the data sequence $x(n)$ as the output of a linear time-invariant digital filter driven by a white noise signal. Eq. (5.32) corresponds to the most general linear model, which is referred to as the autoregressive moving average model (ARMA). Without loss of generality,

the transfer function of this filter is given (in $z = e^{j\omega}$ domain) by

$$H(Z) = \frac{B(z)}{A(z)} = \frac{\sum_{k=0}^{q} b_k \cdot z^{-k}}{1 + \sum_{k=1}^{p} a_k \cdot z^{-k}} \tag{5.32}$$

This expression is also called the transfer function of a causal stationary ARMA model of order (p, q). The n_{th} sample of the process that corresponds to this model satisfies the following difference equation:

$$x(n) = -\sum_{k=1}^{p} a_k \cdot x(n-k) + \sum_{k=0}^{q} b_k \cdot u(n-k) \tag{5.33}$$

where $u(n)$ is the input sequence that consists of the samples of a zero-mean white Gaussian noise process with variance σ_u^2, and $x(n)$ is the output sequence whose samples are generated by this expression. When white Gaussian noise is used as input, the goal is to find the filter $H(z)$ that makes its output as close as possible to $x(n)$.

The first term on the right hand side of Eq. (5.33) is a finite order moving average (MA) process, which is an output of a finite impulse response (FIR filter). The second term, in which the value is composed as a weighted combination of past values of $x(n)$, is called an autoregressive (AR) process, which can be seen as the output of an infinite impulse response (IIR filter) [134]. p is the order of the autoregressive part, q is the order of the moving average part and a_k and b_k are the respective AR and MA coefficients of the ARMA model.

If we assume that the input sequence and the observed data are a stationary random process, the power spectral density of the data is

$$P_x(z) = |H(z)|^2 \cdot P_u(z) \tag{5.34}$$

where $P_u(z)$ is the PSD of the input sequence and $H(z)$ is the frequency response

of the model. To estimate the PSD $P_x(z)$, it is convenient to assume that the input $u(n)$ is a zero mean white noise sequence with autocorrelation $P_u(z) = \sigma_u^2$. Then, the PSD of the observed data $x(n)$ is given by

$$P_x(z) = \sigma_u^2 \cdot |H(z)|^2 = \sigma_u^2 \frac{|A(z)|^2}{|B(z)|^2} \tag{5.35}$$

In the model-based approach, the PSD estimation consists of three steps Eq. (5.36). First, the appropriate model that accurately represents the data is selected. Next, the model's coefficients (a_k and b_k) are estimated through the observed data, and finally the model-based power spectral density $P_x(e^{j\omega})$ is computed by replacing the estimated coefficients in the expression Eq. (5.35), evaluated for $z = (e^{j\omega})$, which is defined by [128]

$$P_x(e^{j\omega}) = \sigma_u^2 \cdot \left|H(e^{j\omega})\right|^2 = \sigma_u^2 \frac{\left|A(e^{j\omega})\right|^2}{|B(e^{j\omega})|^2}. \tag{5.36}$$

If $q = 0$ and $b_0 = 1$, the ARMA(p, q) process results in an all-pole filter $H(z) = 1/A(z)$ and its output $x(n)$ is a strictly autoregressive process of order p, which is usually denoted as AR(p). Meanwhile, by setting $A(z) = 1$, so that $H(z) = B(z)$, it becomes an all-zero filter whose output is a a strictly moving average process, referred to as MA(p).

- Autocorrelation-based model's coefficient estimation

There is a basic relationship between the autocorrelation sequence $r_x(n)$ and the coefficients of the model (a_k and b_k) that generates the random process. If we consider an ARMA(p, q) process, the nonlinear relationship between the autocorrelation and model's coefficients is given by

$$r_x(n) = \begin{cases} r_x^*(-n), & n < 0 \\ -\sum_{k=1}^{p} a_k \cdot r_x(n-k) + \sigma_u^2 \cdot \sum_{k=0}^{q-n} b_{k+n} \cdot h^*(k), & 0 \le n \le q \\ -\sum_{k=1}^{p} a_k \cdot r_x(n-k) & n > q \end{cases} \tag{5.37}$$

where $h^*(k)$ is the conjugated linear impulse response to the linear system that transforms the input white Gaussian noise into the random process $x(n)$ and $r_x^*(-n)$ is the conjugated autocorrelation.

For an AR process the relationship is simplified to

$$r_x(n) = \begin{cases} r_x^*(-n), & n < 0 \\ -\sum_{k=1}^{p} a_k \cdot r_x(n-k) + \sigma_u^2 \ , & n = 0 \\ -\sum_{k=1}^{p} a_k \cdot r_x(n-k) & n > 0 \end{cases} \tag{5.38}$$

In this case, we have a linear relationship between $r_x(n)$ and a_k coefficients. These equations are known as the Yule-Walker equations or normal equations for an AR process. The a_k coefficients can therefore be estimated by solving this system of linear equations. The Yule-Walker equations can be expressed in the matrix form

$$R_x \cdot A_p = \sigma_u^2 \cdot I, \tag{5.39}$$

where R_x is the autocorrelation matrix from $A_p^T = \begin{bmatrix} 1, & a_1, & \ldots, & a_p \end{bmatrix}$ (T is the transposed vector), and $I^T = \begin{bmatrix} 1, & 0, & \ldots, 0, \end{bmatrix}$. This is more clearly expressed by

$$\underbrace{\begin{bmatrix} r_x(0) & r_x(-1) & \cdots & r_x(-p) \\ r_x(1) & r_x(0) & \cdots & r_x(-p+1) \\ \vdots & \vdots & \vdots & \vdots \\ r_x(p) & r_x(p-1) & \cdots & r_x(0) \end{bmatrix}}_{R_x} \begin{bmatrix} 1 \\ a_1 \\ \vdots \\ a_p \end{bmatrix} = \begin{bmatrix} \sigma_u^2 \\ 0 \\ \vdots \\ 0 \end{bmatrix}$$

and the variance can be obtained from the equation

$$\sigma_u^2 = r_x(0) + \sum_{k=1}^{p} a_k \cdot r_x(-k). \tag{5.40}$$

For a stationary stochastic process, the autocorrelation matrix R_x is a symmetric and Toeplitz matrix [136]. The solution of the Yule-Walker equations turns out to be very demanding. Levinson-Durbin recursion [127] and [137] is a fast and efficient method that solves these equations by exploiting the symmetry and the Toeplitz properties of the correlation matrix. Not only does it avoid the matrix inversion, but it also provides a new perspective on linear prediction by introducing the lattice filter.

Finally, in an MA model, the autocorrelation sequence is related to the MA coefficients b_k by

$$r_x = \begin{cases} r_x^*(-n), & n < 0 \\ \sigma_u^2 \cdot \sum_{k=0}^{q} b_{k+n} \cdot b_k, & 0 \leq n \leq q \\ 0 & n > q \end{cases} \tag{5.41}$$

- Election of the model

The type of model required and its order have to be specified before the parametric power estimation. Models with poles (AR and ARMA) perform better at representing abrupt peaks in the PSD, whereas models with zeros (MA and ARMA) perform better at representing valleys. ARMA models seem to be the only ones that can represent a PSD with both abrupt peaks and valleys. Kolmogorov's theorem states that any ARMA model can be represented by an AR model with a sufficiently high model order [126]. This, and the fact that the relation between the autoregressive coefficients and the autocorrelation is linear (unlike in ARMA and MA models that are nonlinearly related to $r_x(n)$), has meant that autoregressive modelling has received

more attention than other linear models. AR models provide better spectral resolution in the study of respiratory flow signal patterns, since they are able to efficiently present abrupt peaks in their PSD, as required for our purpose.

- Autoregressive power spectral density estimation

The autoregressive coefficients a_k with $1 \leq k \leq p$ and the variance of the input noise σ_u^2 have to be estimated in Eq. (5.42) before the PSD can be calculated.

$$\begin{aligned} \hat{x}(n) &= -\sum_{k=1}^{p} a_k \cdot x(n-k) + u(n) \\ &= -a_1 \cdot x(n-1) - \cdots - a_p \cdot x(n-p) + u(n). \end{aligned} \tag{5.42}$$

The output signal is obtained by feeding zero-mean white Gaussian noise $u(n)$ to a filter of order p with a transfer function

$$H_{AR}(z) = \frac{1}{A(z)} = \frac{1}{1 + a_1 \cdot z^{-1} + \cdots + a_p \cdot z^{-p}} \tag{5.43}$$

Apart from the zero located at $z = 0$, H(z) is completely defined by its poles, thus the AR model is often called an all-pole model.

Autoregressive modelling is closely related to the linear prediction problem in which the current sample $x(n)$ is predicted from the p previous samples $x(n-1), ..., x(n-p)$ using a FIR filter structure of the predictor. As a result of this relationship, the optimum linear prediction coefficients, which minimize the mean square error, coincide with the AR coefficients as long as the order of the AR model and the linear predictor are identical. This property leads to different spectral estimation techniques based on minimizing the mean squared prediction error [85].

In a linear prediction framework, a new sample $x(n)$ can be predicted from a linear combination of the p preceding samples by

$$\hat{x}(n) = -a_1 \cdot x(n-1) - \cdots - a_p \cdot x(n-p). \tag{5.44}$$

The prediction error $e(n)$ is defined by

$$e(n) = x(n) - \hat{x}(n) = x(n) + \sum_{k=1}^{p} a_k \cdot x(n-k). \tag{5.45}$$

When the prediction error variance defined by $\sigma_e^2 = E[e_p^2(n)]$ is minimized, estimates of the model coefficients can be determined. First, the linear prediction problem is solved. Then, the resulting parameter estimates are substituted into the AR model. In the same way, the variance of the input noise is estimated as the variance of the prediction errors, $\sigma_u^2 = \sigma_e^2$.

Once the AR coefficients and the variance σ_e have been estimated, the PSD of an autoregressive process is computed by means of

$$\hat{P}_{x\ AR}(e^{j\omega}) = \frac{\sigma_e^2}{\left|A_p(e^{j\omega})\right|^2} = \frac{\sigma_e^2}{\left|1 + \sum_{k=0}^{p} a_k \cdot e^{-j\omega k}\right|^2}. \tag{5.46}$$

There are different methods for estimating the AR parameters a_k by means of a finite sequence of observed data. Conceptually, the simplest method involves the use of Yule-Walker equations to solve the system of linear equations. However, much better results are obtained through algorithms that compute the AR coefficients directly from the data, rather than through the autocorrelation sequence, particularly with short data sequences. Three of the most frequently used methods are based on linear prediction by least-squares fitting. The Yule-Walker method and the Covariance method minimize the forward prediction error in a least-square sense, whereas the modified Covariance method minimizes both forward and backward prediction errors. Other spectral estimation techniques such as Burg's method are based on reflection coefficients to minimize the forward and backward prediction error.

Yule-Walker The Yule-Walker or autocorrelation method computes the AR coefficients through a biased autocorrelation estimate to solve Yule-Walker equations by means of the Levinson-Durvin algorithm. A biased estimate of the autocorrelation function should be used to ensure that the autocorrelation matrix is positive semidefinite. Hence, the matrix is invertible and a solution is guaranteed to exist. Although the result is a stable AR model, it performs relatively poorly for short data sequences.

Covariance and Modified Covariance: The only difference between the Covariance method and the autocorrelation method is that, in the latter, all the data that are used are from the observed data sequence, i.e. there is no windowing. The spectral estimates obtained with this method are similar to the ones obtained with the autocorrelation method, particularly when the observed data sequence is much larger than the model order. Modified Covariance provides high resolution for short data sequences, because it minimizes both forward and backward prediction errors. Unlike autocorrelation, covariance methods might produce unstable models. Moreover, the frequency peaks in Modified Covariance might be slightly dependent on the initial phase of the signal.

Burg: Burg's method computes the AR coefficients through an order recursive least squares lattice method, which is based on minimizing the forward-backward error in linear predictors, while the Levinson-Durvin recursion is satisfied. In contrast to other AR methods, it avoids calculations of the autocorrelation form of the data, and instead estimates the reflection coefficients. It is computationally efficient, provide high resolution for short data sequences and assures a stable AR model. However, its accuracy is lower for long data sequences, high order models and high SNR ratios.

Moreover, the power spectral density estimated by Burg's method is susceptible to frequency shifts that result from the initial phase of noisy sinusoidal signals.

5.3 Time-frequency applied to the respiratory flow signal

Fig. 5.11 presents the performance of the spectral techniques applied to the envelope of the simulated AM signal. Figs. 5.12, 5.13, 5.14, and 5.15 show the performance of the aforementioned spectral estimation techniques when they are applied to the envelope signal of CHF patients with different respiratory patterns and to that of a healthy subject.

The Yule-Walker method provides lower resolution when the observed data sequence is too short. Burg and Modified Covariance provide similar frequency resolution that is better than the other two methods. However, the latter method is the most suitable when the objective is to find sinusoid signals, since the power spectral density estimated by Burg's method depends more on the initial phase of the signal than does Modified Covariance. All the techniques for estimating the PSD perform quite similarly. Nevertheless, as this study focuses on the periodicity of the respiratory pattern through the respiratory flow envelope signal, Modified Covariance is the most appropriate method.

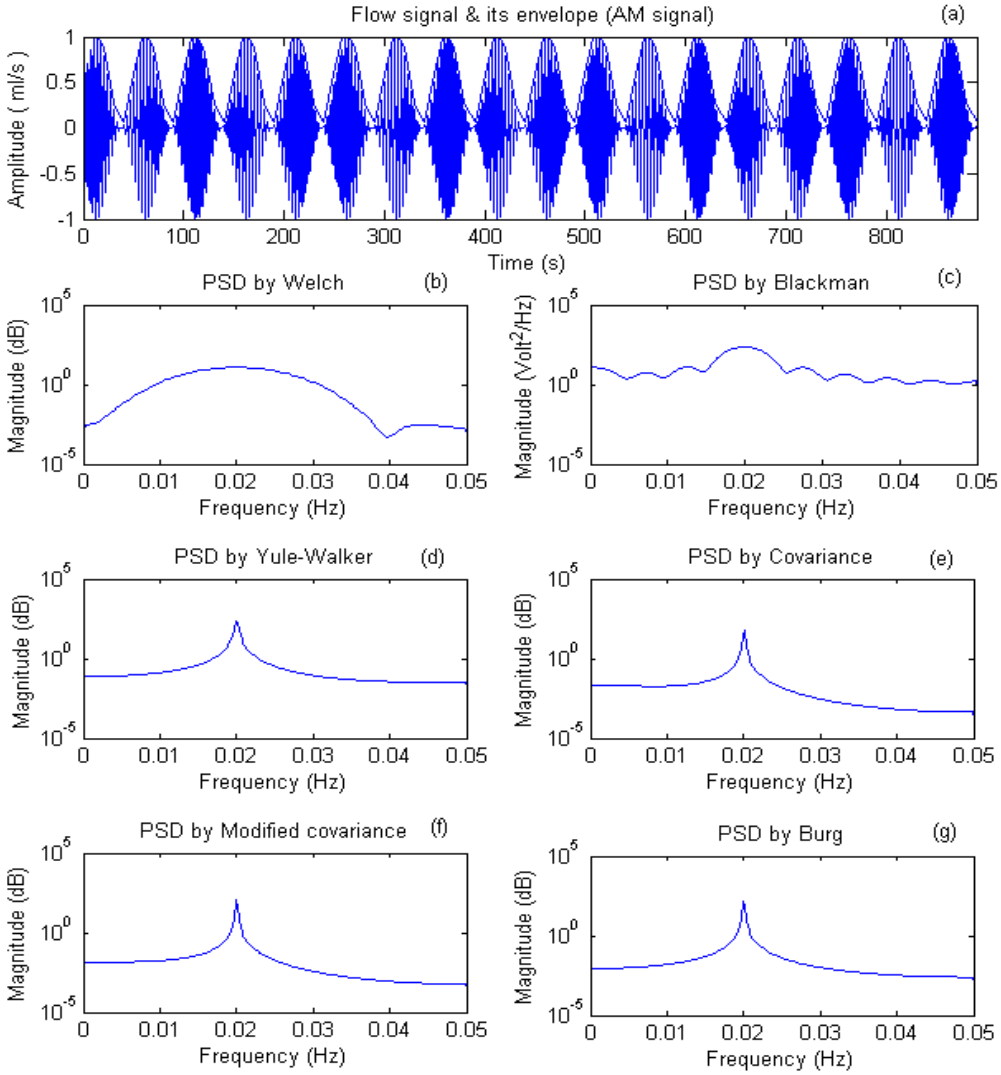

Figure 5.11 (a) Flow signal and its envelope, (b) Welch, (c) Blackman-Tukey, (d) Yule-Walker, (e) Covariance, (f) Modified covariance, and (g) Burg to estimate the PSD of the simulated AM signal envelope.

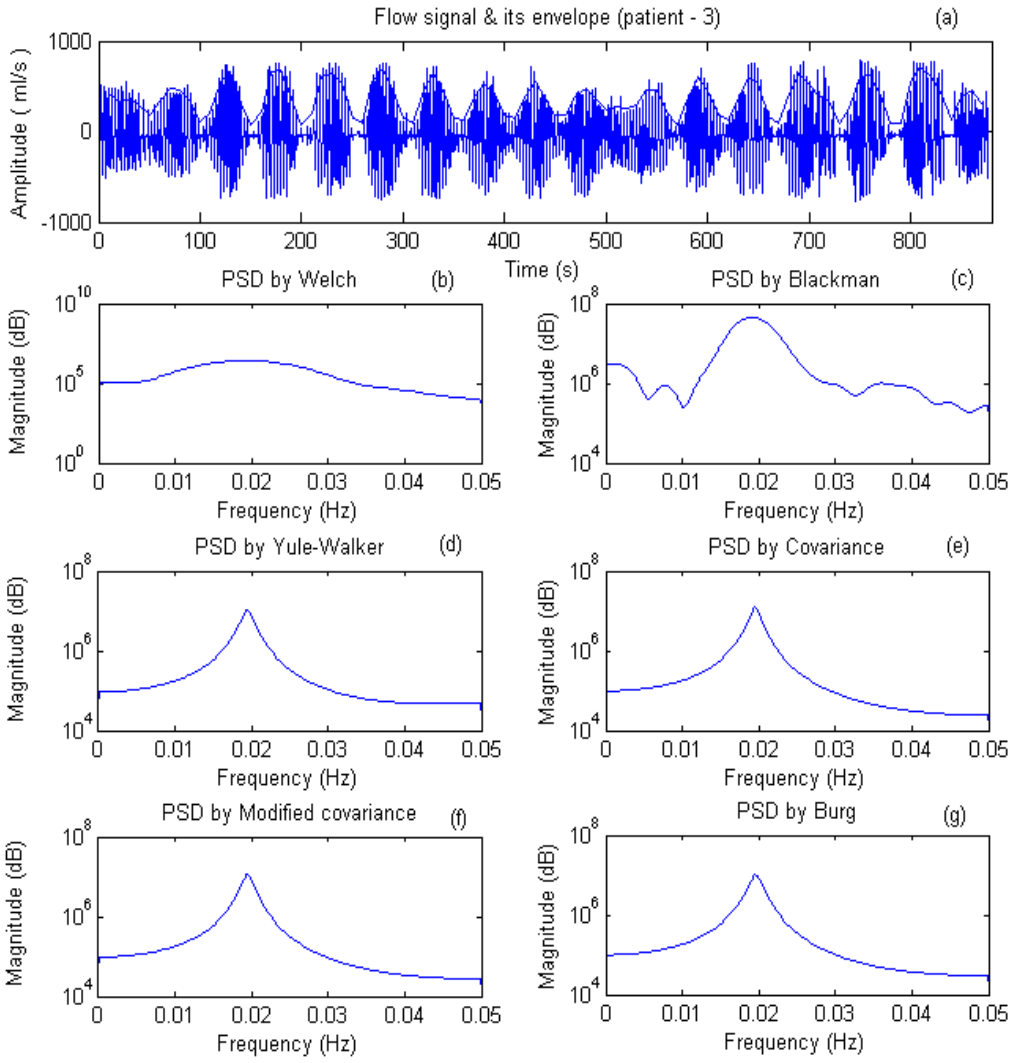

Figure 5.12 (a) Flow signal and its envelope, (b) Welch, (c) Blackman-Tukey, (d) Yule-Walker, (e) Covariance, (f) Modified covariance, and (g) Burg to estimate the PSD of the envelope of a CHF patient with Cheyne-Stokes respiration.

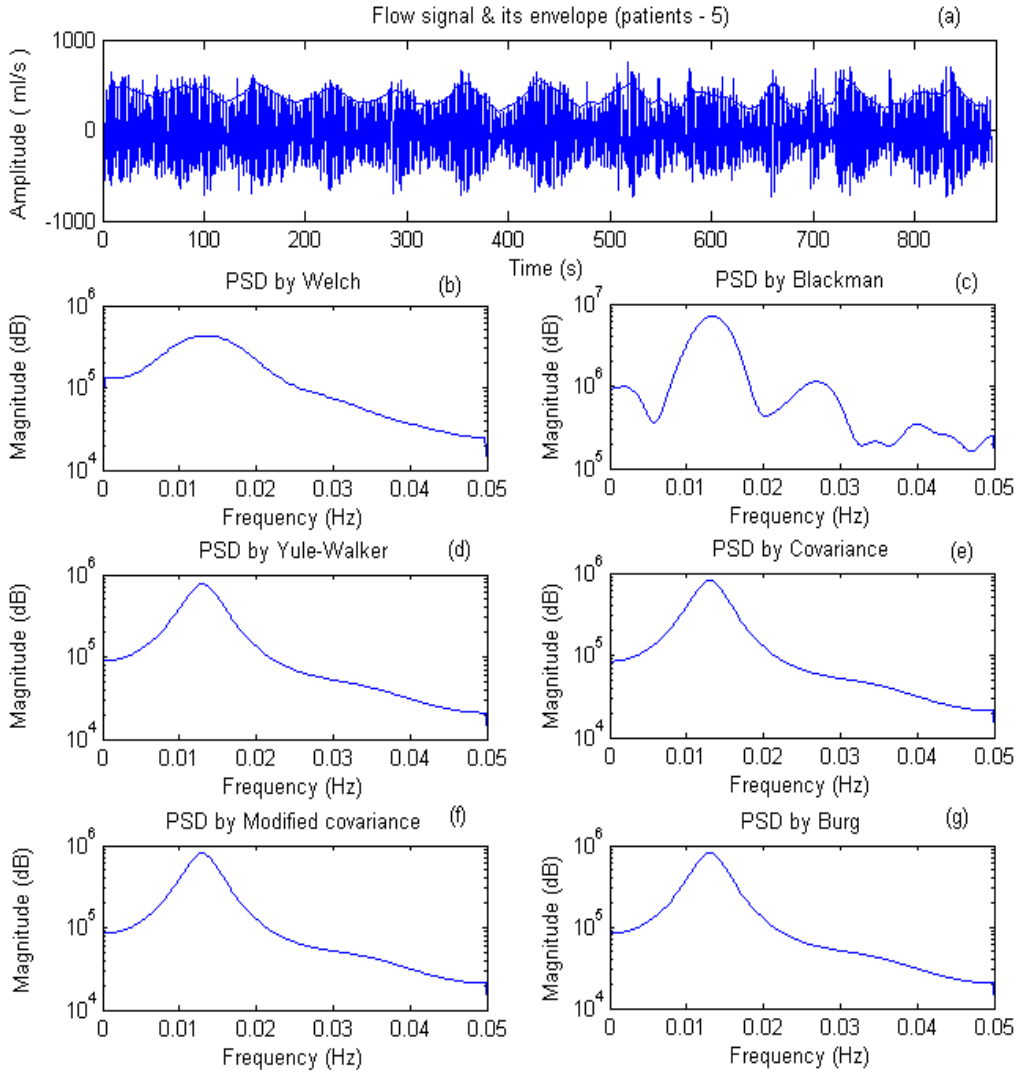

Figure 5.13 (a) Flow signal and its envelope, (b) Welch, (c) Blackman-Tukey, (d) Yule-Walker, (e) Covariance, (f) Modified covariance, and (g) Burg to estimate the PSD of the envelope of a CHF patient with periodic breathing.

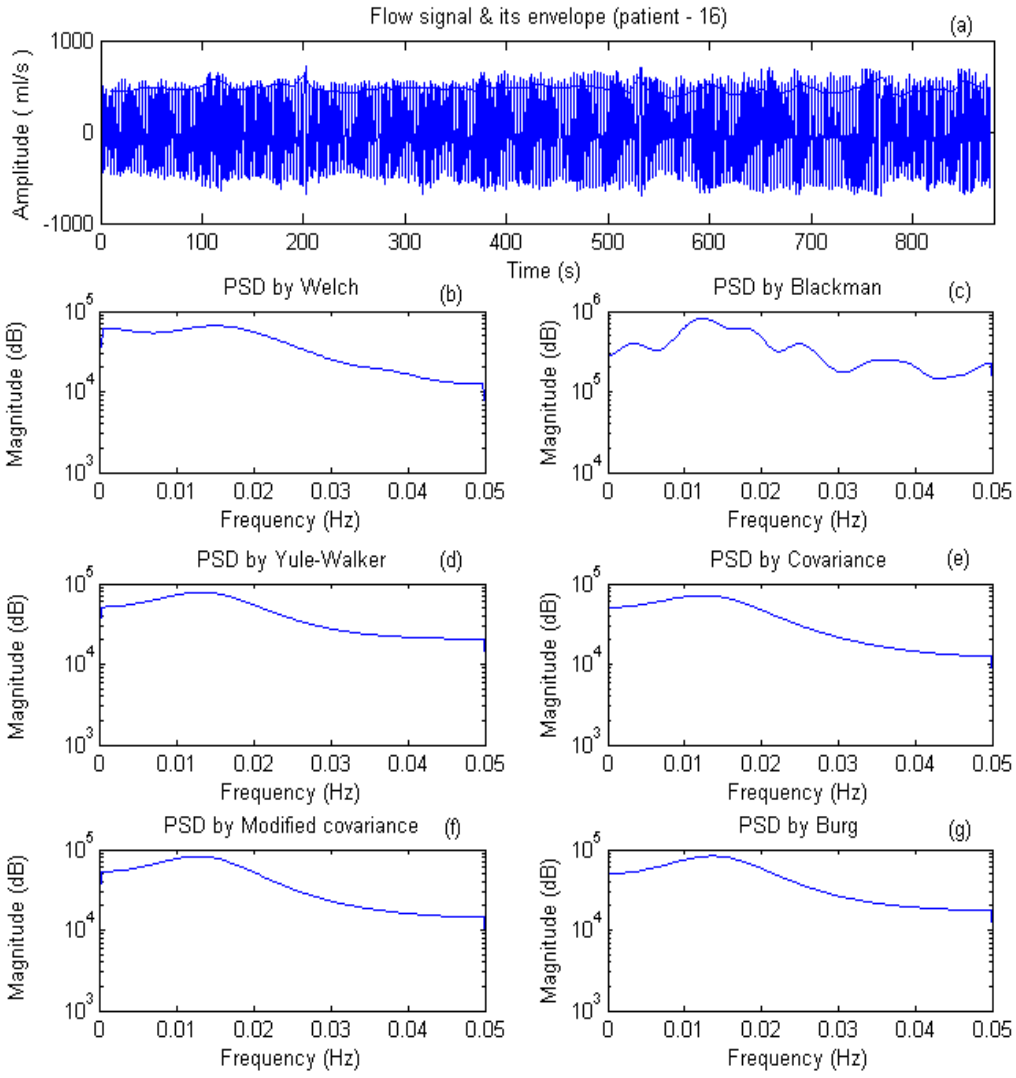

Figure 5.14 (a) Flow signal and its envelope, (b) Welch, (c) Blackman-Tukey, (d) Yule-Walker, (e) Covariance, (f) Modified covariance, and (g) Burg to estimate the PSD of the envelope of a CHF patient with nonperiodic breathing.

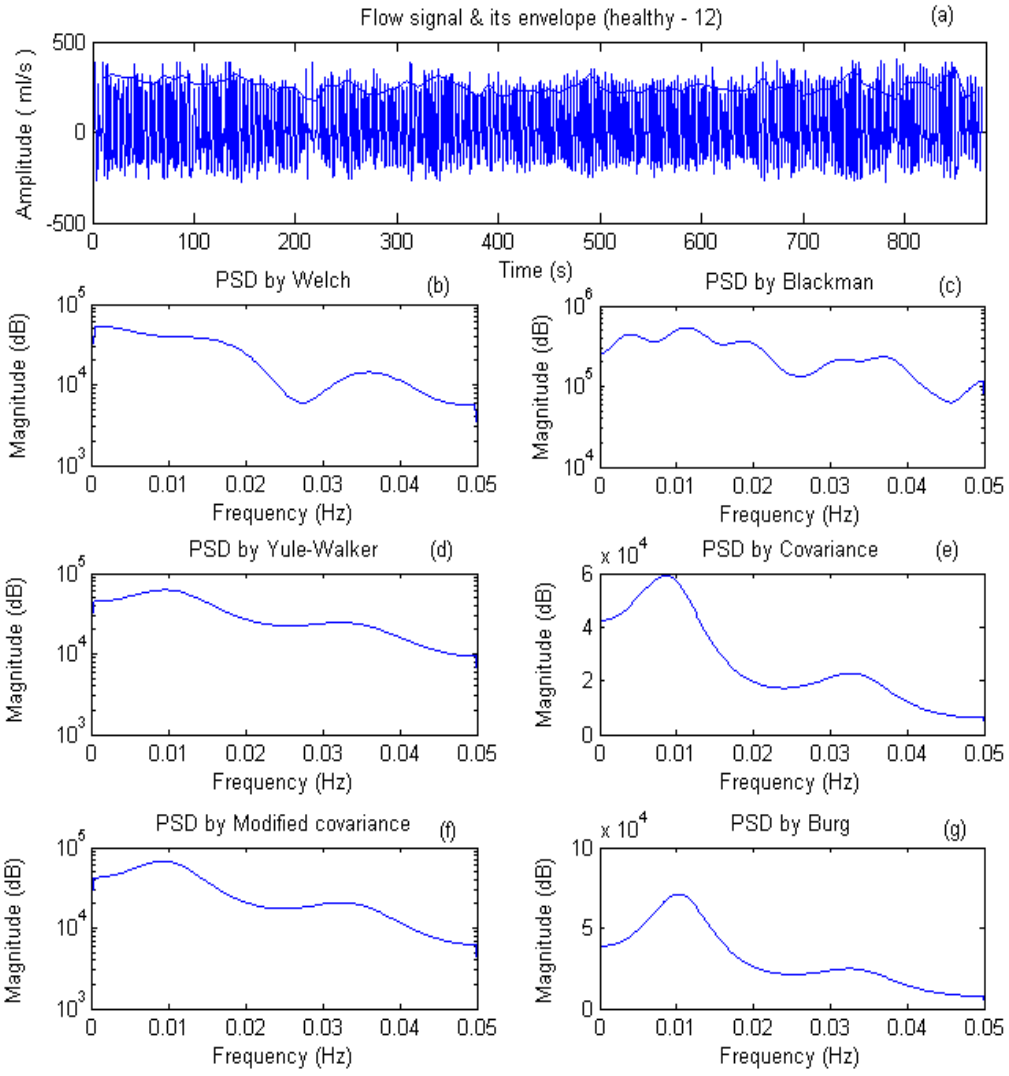

Figure 5.15 (a) Flow signal and its envelope, (b) Welch, (c) Blackman-Tukey, (d) Yule-Walker, (e) Covariance, (f) Modified covariance, and (g) Burg to estimate the PSD of the envelope of a healthy subject.

5.4 Summary

The aim of this chapter is to review the time frequency techniques applied to the study of the respiratory pattern.

A number of artefact removal techniques have been proposed to condition the respiratory flow signal. Both outlier and spike removal stages have prepared the signal for more robust further analyses. A technique based on autoregressive modelling has been implemented to solve short gaps of missing samples. In our case, only two gaps of a few seconds have been observed in the acquired respiratory flow signals. Some applications permit the direct solution of this problem by modifying the computation of further analyses so as to discard them from the processing.

The advantages and disadvantages of most popular methods of envelope detection have been analysed. The method based on the Hilbert transform seemed the most suitable for further spectral analysis. The respiratory pattern has been characterized in the time and frequency domain by a number of parametric and nonparametric techniques. It has been observed by means of different criteria FPE, AIC and MDL and proved statistically by the Ljung–Box test that a 30^{th} order autoregressive model and a 4^{th} order autoregressive model correctly represent the respiratory flow signal and the envelope signal, respectively.

In terms of PSD estimation, it has been observed that the Yule-Walker method provides lower resolution when the observed data sequence is too short. Both the Burg and Modified Covariance methods provide more accurate spectrum estimates than the other techniques. The PSD estimated by Burg's method depends more on the initial phase of the signal than does the Modified Covariance method. Thus, the latter fits better with our objective, which is to analyse the periodicity of the respiratory pattern.

Chapter 6

Respiratory pattern analysis applied to chronic heart failure

6.1 Introduction

Patients with chronic heart failure (CHF) often develop breathing abnormalities, including various forms of oscillatory breathing patterns that are characterized by rises and falls in ventilation [56] and [57]. Previous studies have presented periodic breathing (PB) during sleep or wakefulness as a powerful predictor of poor prognosis in CHF patients [138]. Periodic breathing patterns can be classified into ventilation with apnea, commonly known as Cheyne-Stokes respiration (CSR), or ventilation without apnea [59] and [60]. In this chapter, we investigate the periodicity of the respiratory pattern as an index that is related to the risk level of the CHF patients.

Normal breathing cycle lengths range from 3 to 5 s (i.e., 0.20–0.33 Hz), whereas the PB patterns have cycle lengths from 25 to 100 s (i.e., 0.01–0.04 Hz) [66]. However, the same patient often exhibits a mixture of breathing patterns, including nonperiodic

breathing (with no cyclic modulation of ventilation), mild PB and CSR patterns. The origin of the PB pattern is still a matter of debate among researchers. Respiratory modulation frequency appears to be essential for the understanding of periodic and nonperiodic breathing patterns in CHF patients.

The aim of this chapter is to analyse the breathing pattern in CHF patients and healthy subjects, through the envelope of the respiratory flow signal. Based on autoregressive (AR) power spectral analysis of the envelope, the relevant discriminant band (DB) is determined from the location of the modulation frequency peak, and characterized by a number of spectral parameters.

6.2 Dataset

In this chapter we work with the dataset of CHF patients and the dataset of healthy subjects presented in Chapter 1. These datasets include the respiratory flow signal of 35 healthy volunteers and 26 CHF patients. According to clinical criteria, the CHF patients were classified into two groups: 8 patients with PB patterns (1 female, 71±7 years, 18.4±2.2 breaths/min), and 18 patients with nonperiodic breathing (nPB) pattern (5 female, 62±9 years, 22.5±4.3 breaths/min). Within the PB group, 3 patients were classified as CSR (1 female, 68±6 years, 21.7±4.2 breaths/min) and 5 patients as PB without apnea (no females, 73±8 years, 23.0±4.7 breaths/min). Fig 6.1 illustrates the different flow patterns observed in CSR, PB and nPB patients, and a healthy subject.

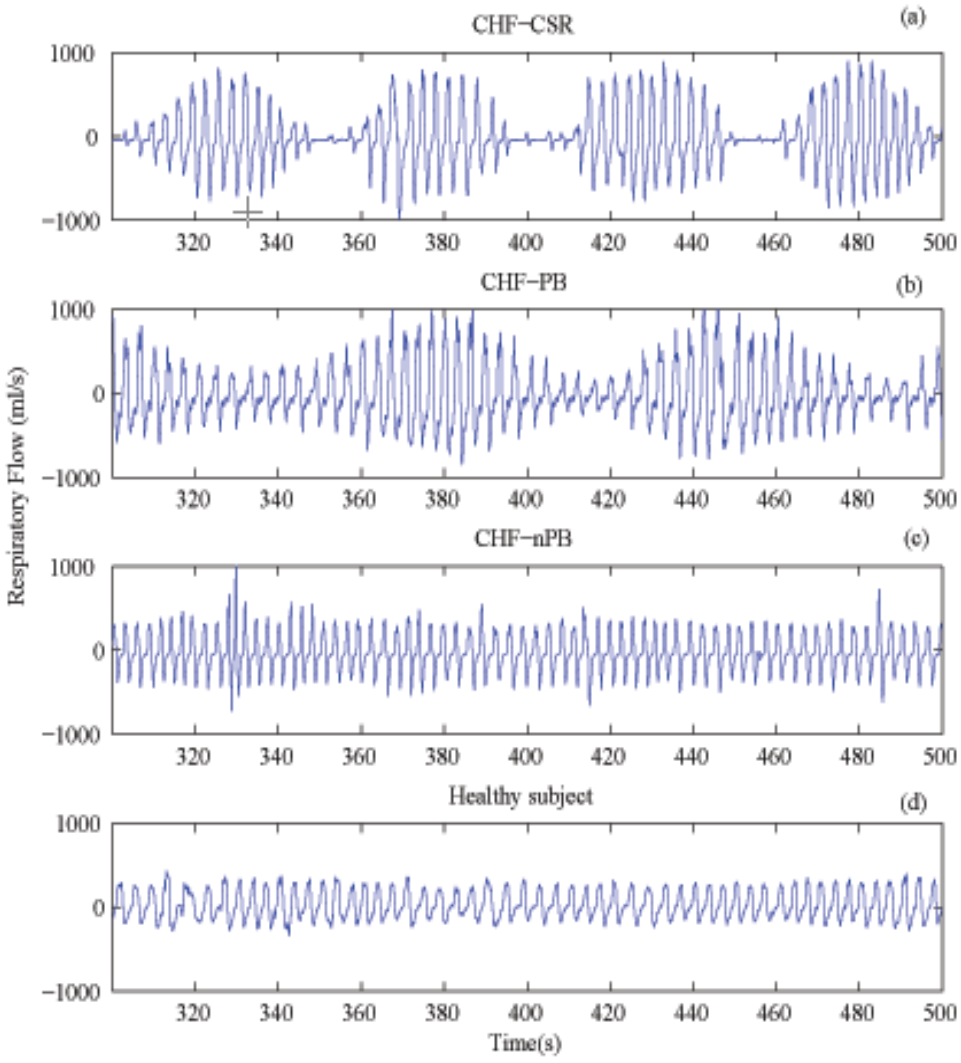

Figure 6.1 The respiratory flow signal exemplified for (a) a Cheyne-Stokes respiration patient, (b) a periodic breathing patient, (c) a nonperiodic breathing patient, and (d) a healthy subject.

6.3 Respiratory pattern in CHF patients and healthy subjects

The respiratory flow signal is pre-processed to reduce artefacts and thus ensure robust signal analysis. Outlier and short-duration spike artefacts are detected and reduced using the techniques described in Chapter 5. In a few patients, short gaps ($< 1\ s$) with missing samples occurred due to uncontrolled movements of the patients during acquisition. To include these recordings in the analysis, interpolation based on AR signal modelling is used to fill in the gaps [4] and [118].

Respiratory pattern characterization is based on the envelope of the respiratory flow signal, which is extracted using the Hilbert transform without any previous knowledge of the frequency and phase [85]. Due to the oscillatory nature of respiratory flow signals, AR modelling is employed for spectral analysis. Therefore, the mean value of the envelope is subtracted and AR modelling is performed on the envelope signal. It is essential to have high spectral resolution in the vicinity of the modulation peak, and therefore the optimum order is determined in each subject using the minimum description length criterion [131]. Then, the maximum of the resulting model order estimates is selected and used as a global model order in the subsequent signal analysis. The Ljung–Box statistical test is applied to prove the whiteness of the prediction error.

6.3.1 Parameter extraction

The most discriminative differences between groups of subjects are observed around the envelope's frequency peak. Thus, we defined the discriminant frequency band (DB) as the frequency interval (Δ_f) centred at the modulation frequency peak (fp).

Various spectral parameters are extracted from the DB, to characterize the respiratory pattern's modulation in the frequency domain. The investigated set of parameters comprise the radius of a complex conjugate pole pair (r) and various spectral parameters, which are listed in Table 6.1 and extracted from the discriminant frequency band (DB). Fig. 6.2 displays the spectral parameters that involve the power (P), right side power (P_R), left side power (P_L), slope (S) and kurtosis measure (K) of the DB.

The respiratory frequency of the 61 subjects in the dataset is found to range from 0.2 to 0.4 Hz, whereas the modulation frequency ranges from 0.01 to 0.04 Hz [66]. Consequently, the modulating frequency peak (fp) is tracked around 0.005 to 0.05 Hz. After a study of the PSD presented by different patients and healthy subjects, the frequency interval is fixed to $\Delta_f = 0.02$ Hz. Fig. 6.3 shows an example of the different discriminant bands presented by CHF patients with different breathing patterns (CSR, PB without apnea, nPB) and a healthy subject. Each subject is characterized by these spectral parameters extracted from the discriminant frequency band (DB), and by the AR coefficients and the two complex conjugate pole radii.

6.3.2 Data analysis

The accuracy of our pattern characterization is evaluated using linear discriminant analysis for the following three classification problems: CHF patients versus healthy subjects, nonperiodic breathing patients versus healthy subjects, and CHF patients with either periodic or nonperiodic breathing.

Firstly, a statistical analysis of the parameters is performed for each classification. Secondly, the p-value of the most statistically significant parameters is estimated for every classification by means of the Mann-Whitney test. Thirdly, a parameter selection process is implemented over the previously evaluated significant parameters

Table 6.1 Parameter description

P	Power in the discriminant band	$[f_p - \Delta_f/2, \quad f_p + \Delta_f/2]$
P_R	Power in the "right band"	$[f_p, \quad f_p + \Delta_f/2]$
P_L	Power in the "left band"	$[f_p - \Delta_f/2, \quad f_p]$
S	Slope from fp to "right band" end	
K	Kurtosis measure	
a_i	AR coefficients	$i = 1$ to 4
r_i	Poles radii	$i = 1, 2$

fp : Frequency peak
Δ_f : Frequency interval

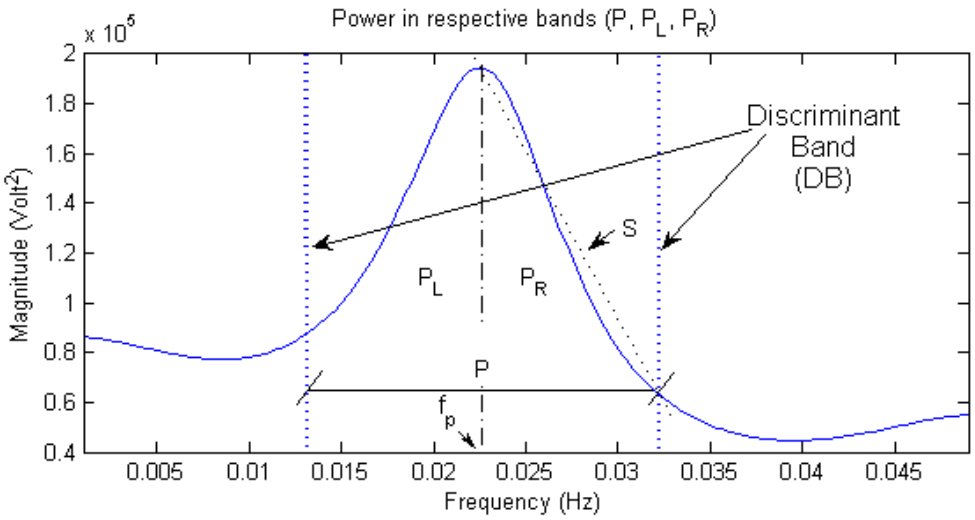

Figure 6.2 Parameters extracted from the discriminant band of the power spectral density.

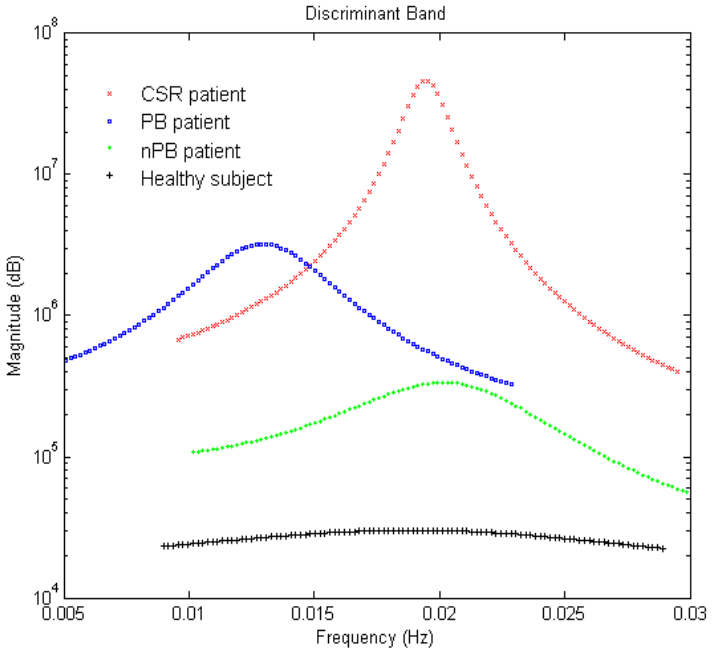

Figure 6.3 Discriminant band (DB) of a CSR patient, a PB patient without apnea, an nPB patient, and a healthy subject.

to select the most relevant subset. The leave-one-out cross-validation technique is applied to the whole optimization process, due to the limited number of CHF patients (26 CHF patients and 35 healthy subjects).

6.3.3 Results

Table 6.2 presents the mean and the standard deviation of the most relevant parameters for each group of patients and the healthy subjects. Table 6.3 shows the p-value of the most statistically significant parameters. Fig. 6.4 illustrates the statistical distribution of the most significant non-correlated parameters (power P, slope S, kurtosis K and main pole radius r_1) in healthy subjects versus CHF patients, in healthy subjects versus nPB patients, and in PB versus nPB patients. The mean of

the P, S, K and r_1 values in CHF patients is higher than in healthy subjects. PB patients show higher P, S, K and r_1 values than nPB patients, since the respiratory peak is much higher and sharper in PB patients and highest in CSR patients.

Table 6.2 Mean and standard deviation of P, P_R, P_L, S, K and r_1 for each group of subjects

	P^*	P_R^*	P_L^*
Healthy	0.91 ± 0.11	0.04 ± 0.06	0.05 ± 0.06
CHF	1.6 ± 2.4	0.7 ± 0.1	0.9 ± 1.4
PB	4.1 ± 3.3	1.8 ± 1.4	2.3 ± 1.9
nPB	0.6 ± 0.5	0.3 ± 0.2	0.3 ± 0.3
	S^*	K	r_1
Healthy	0.06 ± 0.06	2.22 ± 0.79	0.61 ± 0.10
CHF	10 ± 26	3.91 ± 2.85	0.77 ± 0.14
PB	33 ± 41	5.74 ± 3.78	0.89 ± 0.08
nPB	0.85 ± 0.96	3.13 ± 2.01	0.73 ± 0.14

** The values have been divided by* 10^8 *for ease of legibility*

The behaviour of CHF patients with periodic breathing patterns is studied by analysing their envelope's PSD, which is parametrically calculated through AR modelling. We also study the radii of the two complex conjugate poles that define the AR model, and the envelope's autocorrelation.

A clear frequency peak centred between 0.005 and 0.03 Hz can be observed in the PSD of Figs. 6.5 and 6.6. The main pole radius is close to the unit circle that reflects

oscillation, and both show periodicity in their autocorrelation functions.

However, modulation is clearer in CSR patients, since they present a powerful frequency peak and the main pole is next to the unit circle. The power of the frequency peak presented by the nonperiodic breathing patient is considerably lower than the previous PB patterns (Fig. 6.7). The healthy subject presents the least powerful peak (Fig. 6.8), in which the main poles are closer to the origin and the autocorrelation shows no clear periodicity.

Table 6.3 p-value of the most statistically significant parameters for each classification

p-value	CHF vs. Healthy	nPB-CHF vs. Healthy	PB vs. nPB (CHF)
P	$4.3 \cdot 10^{-9}$	$7.3 \cdot 10^{-7}$	$6.8 \cdot 10^{-4}$
P_R	$1.3 \cdot 10^{-8}$	$2.4 \cdot 10^{-6}$	$4.6 \cdot 10^{-4}$
P_L	$3.2 \cdot 10^{-9}$	$5.2 \cdot 10^{-7}$	$1.4 \cdot 10^{-3}$
S	$9.0 \cdot 10^{-10}$	$1.3 \cdot 10^{-7}$	$3.1 \cdot 10^{-4}$
K	$4.7 \cdot 10^{-6}$	$5.2 \cdot 10^{-4}$	$1.3 \cdot 10^{-2}$
r_1	$5.4 \cdot 10^{-6}$	$7.3 \cdot 10^{-4}$	$4.1 \cdot 10^{-3}$

Fig. 6.9 shows the PSD of the groups of patients and healthy subjects. The power of the frequency peak is much higher in CHF patients with PB than in healthy subjects and is highest in CSR patients. Notable differences in the frequency peak position are shown by the patient groups, since the CSR patients' modulation peak is clearly right shifted, which reflects a higher modulation frequency.

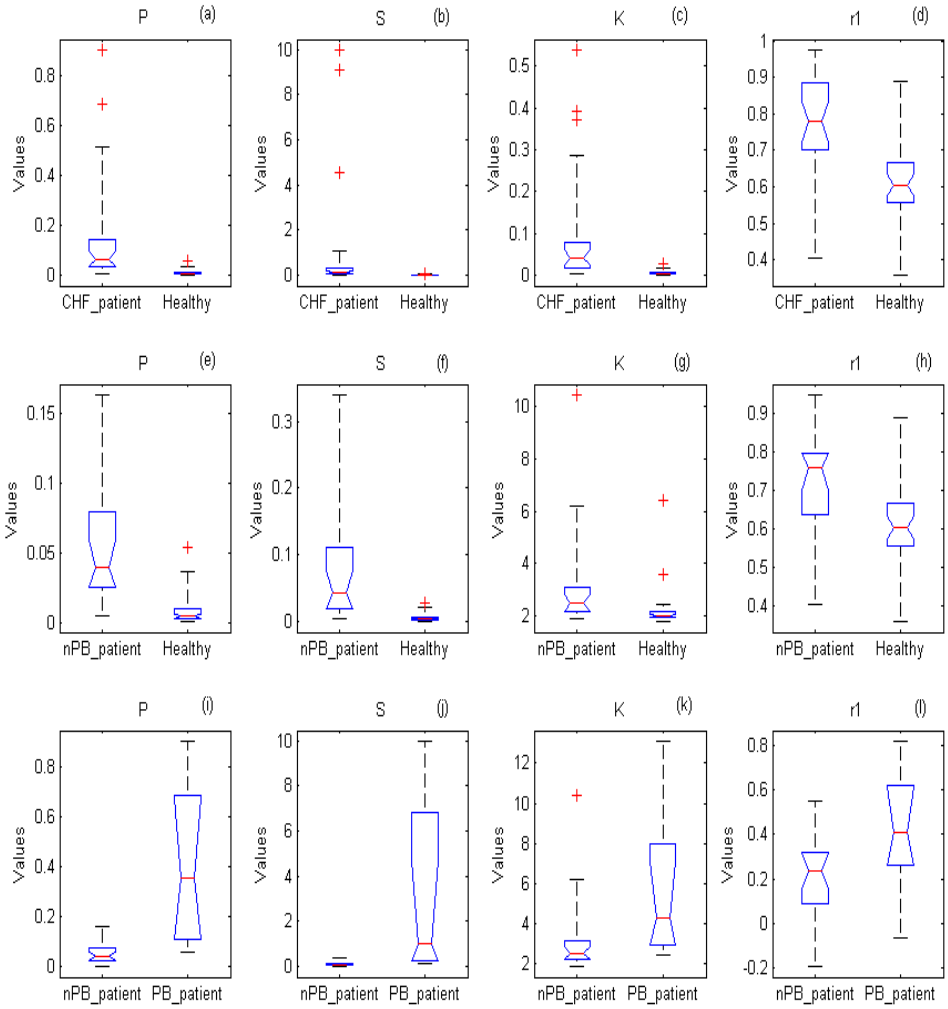

Figure 6.4 Normalized distribution of the most significant non-correlated parameters P, S, K and r_1 selected for each linear classification: (a, b, c, d) CHF patients versus healthy subjects, (e, f, g, h) nPB patients vs. healthy subjects, and (i, j, k, l) PB vs. nPB patients.

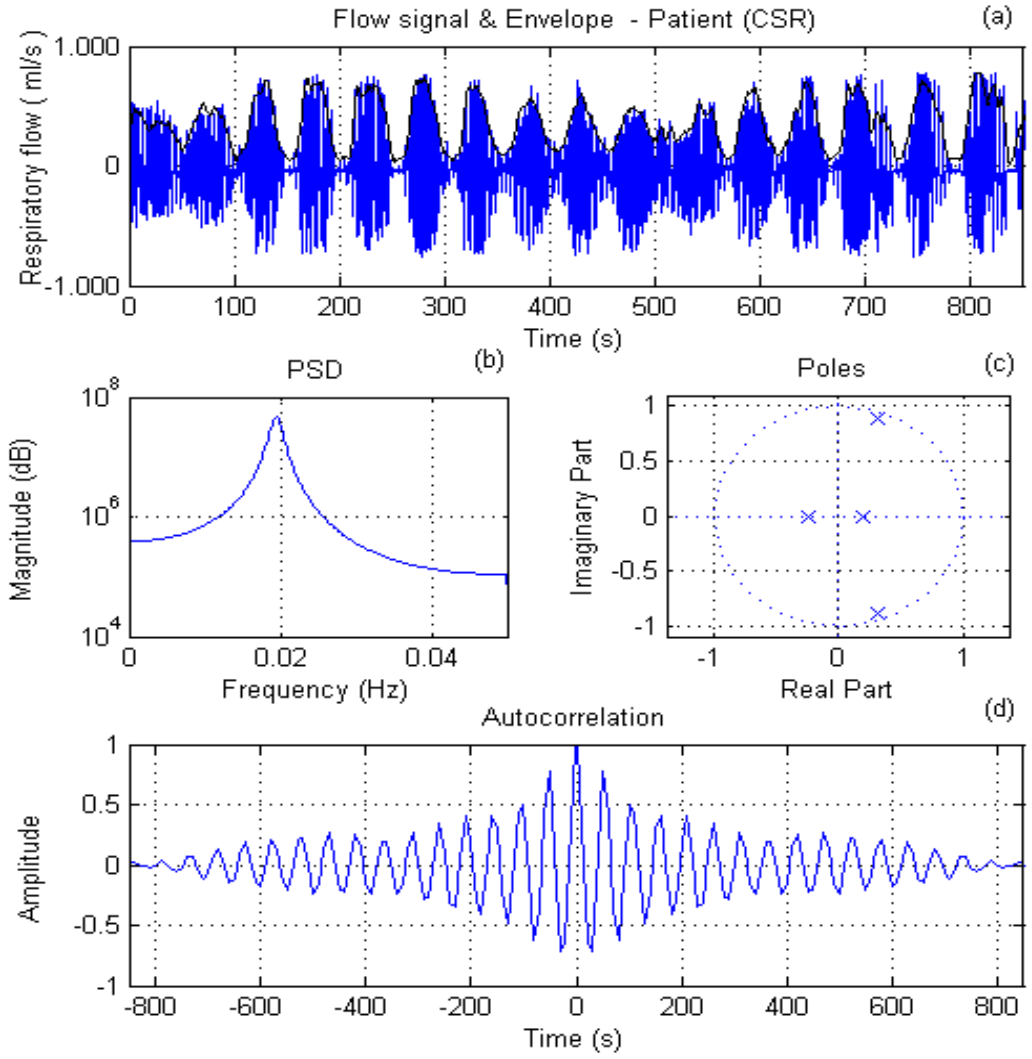

Figure 6.5 (a) The pre-processed flow signal and its envelope, (b) the PSD, (c) the poles of the autoregressive model, and (d) the autocorrelation signal of a patient with Cheyne-Stokes respiration (CSR).

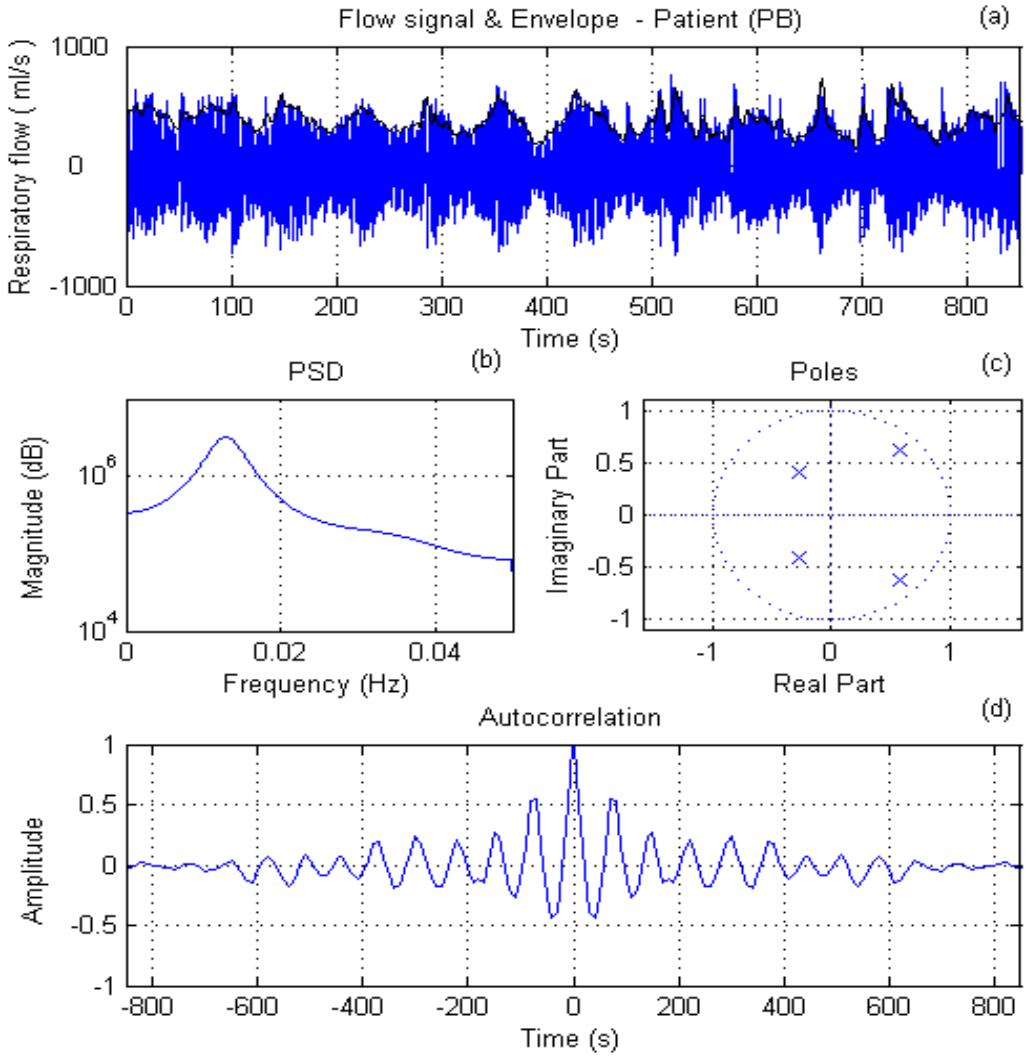

Figure 6.6 (a) The pre-processed flow signal and its envelope, (b) the PSD, (c) the poles of the autoregressive model, and (d) the autocorrelation signal of a patient with periodic breathing without apnea.

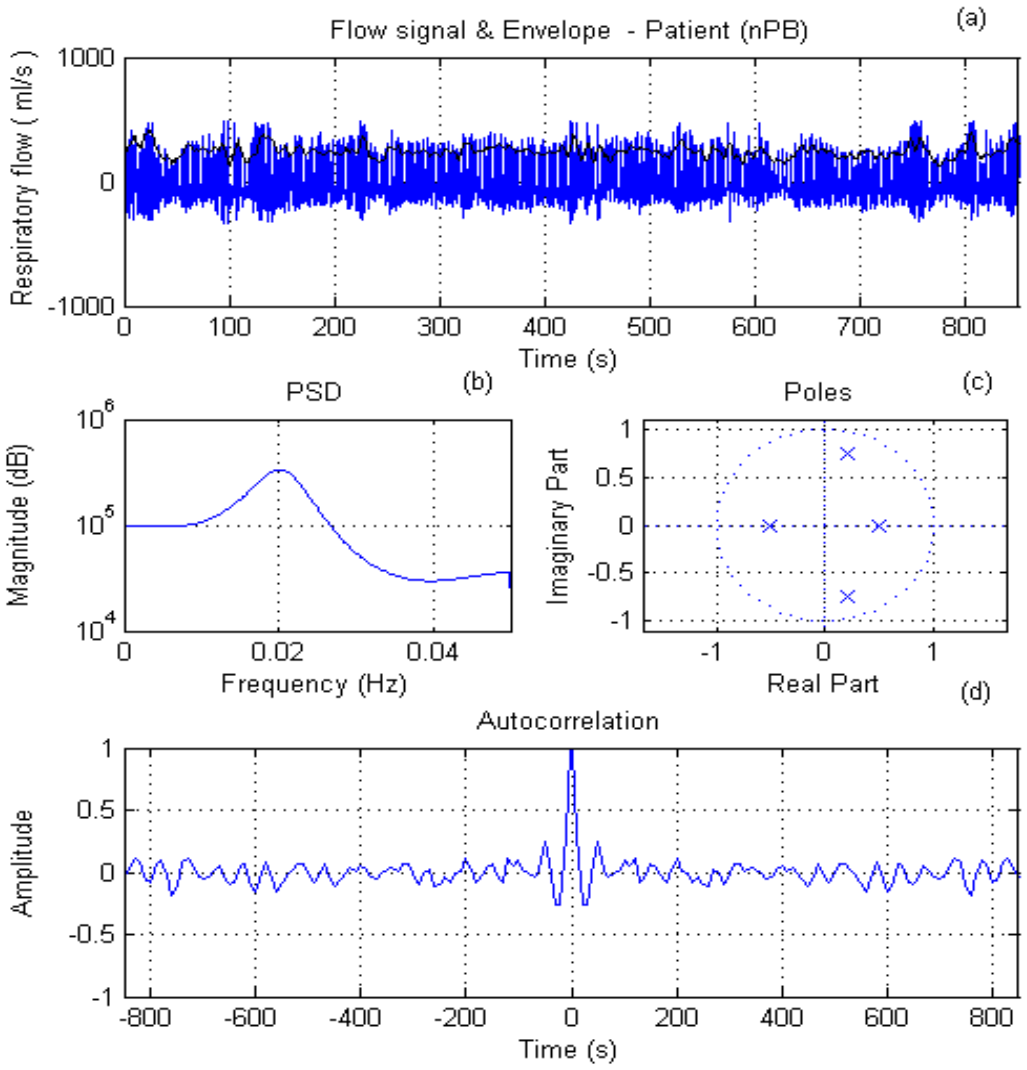

Figure 6.7 (a) The pre-processed flow signal and its envelope, (b) the PSD, (c) the poles of the autoregressive model, and (d) the autocorrelation signal of a patient with nonperiodic breathing (nPB).

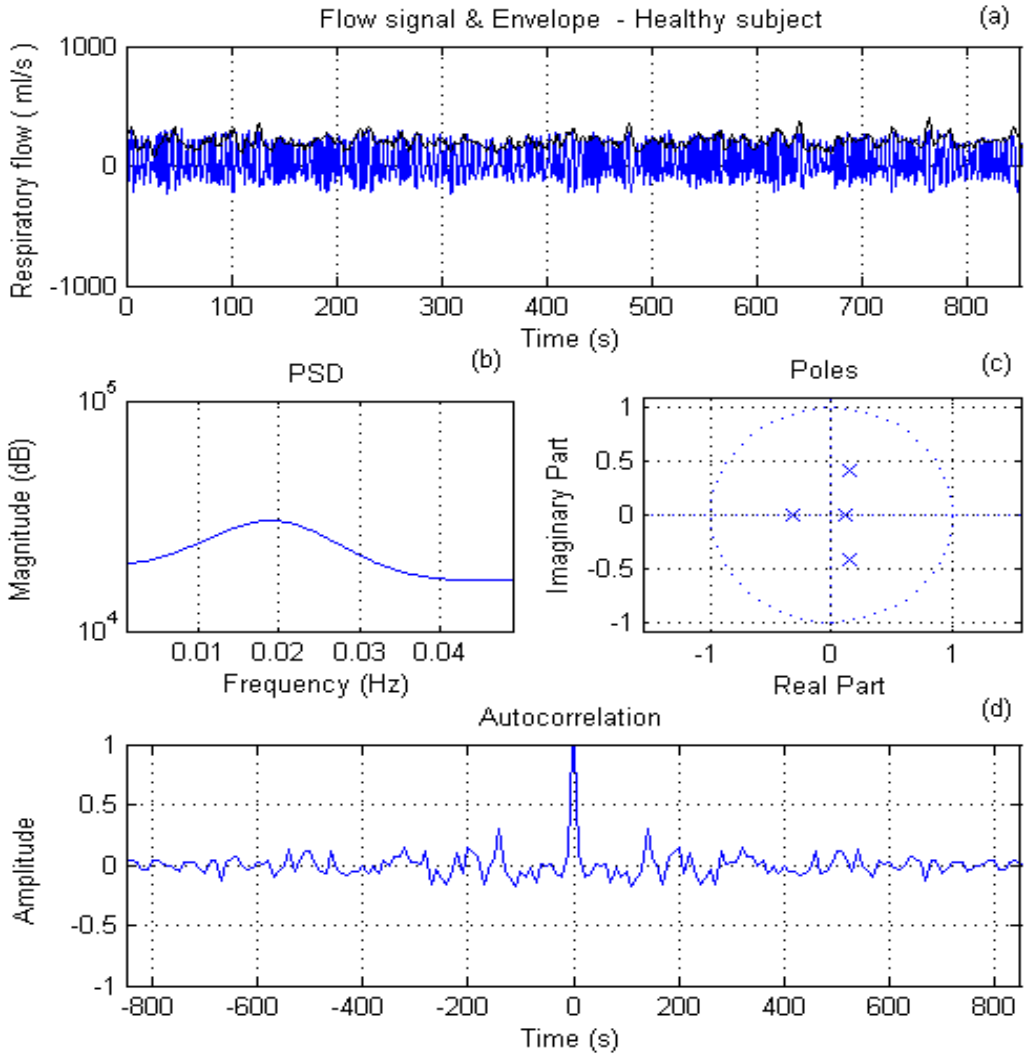

Figure 6.8 (a) The pre-processed flow signal and its envelope, (b) the PSD, (c) the poles of the autoregressive model, and (d) the autocorrelation signal of a healthy subject.

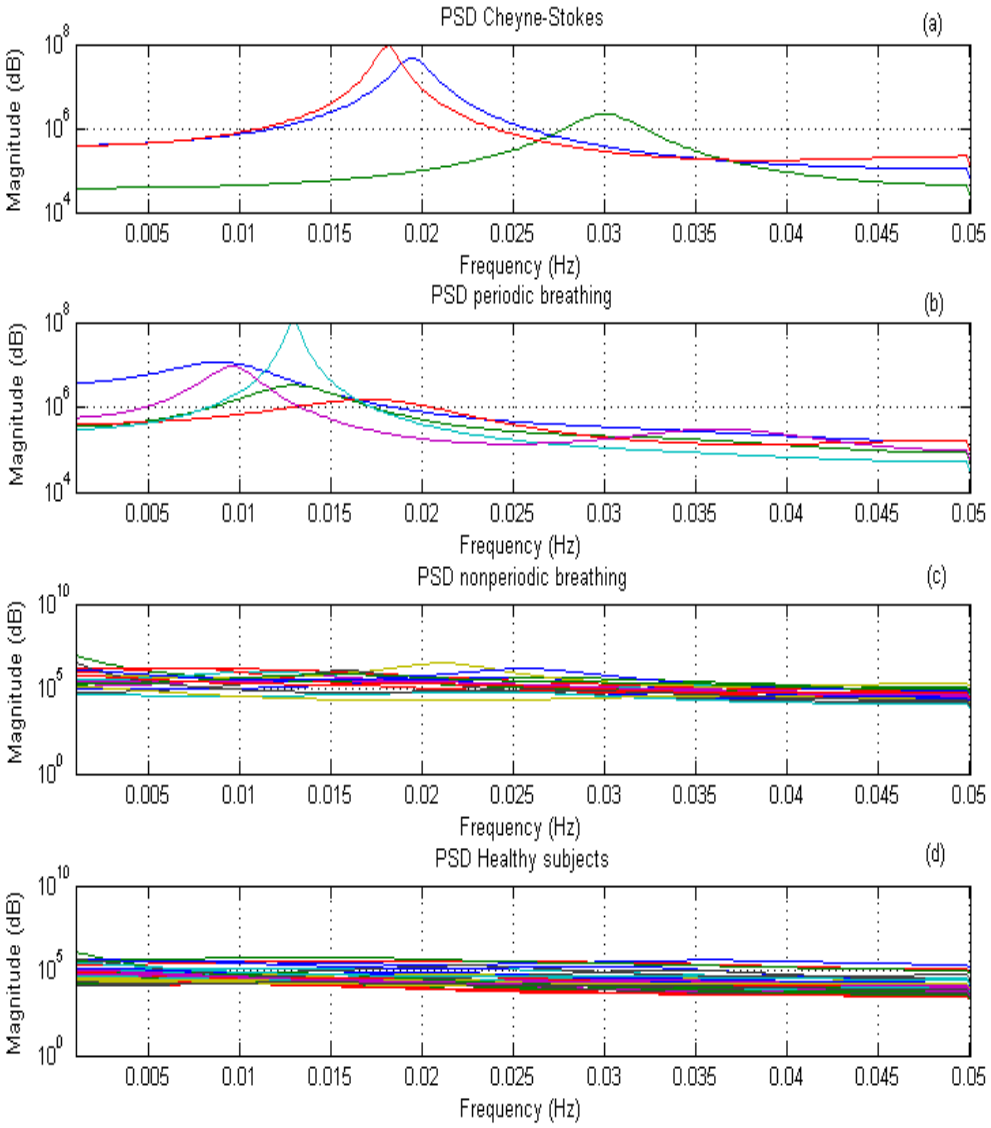

Figure 6.9 PSD of the subjects: (a) CSR patients, (b) PB patients, (c) nPB patients, and (d) healthy subjects.

6.3.4 Performance evaluation

Table 6.4 illustrates the results obtained by applying LDA with the most discriminant parameter for each classification. In general, the best classification results are obtained with parameters related to the spectral power, and with the radius of the main pole. An accuracy of 85.5% and 85.2% is obtained in the classification of CHF patients versus healthy subjects and nPB patients versus healthy subjects, respectively. Similar results have been observed with PL and PR. The ROC curves of the most statistically significant parameters are also studied for each classification. Fig. 6.10 and Table 6.5 present the ROC curve and the area under the curve (AUC), respectively for the three classifications. The AUC values validate the results obtained in all classifications with leave-one-out cross-validation. Similar performance is obtained with power-related parameters. The accuracy slightly decreases with the radius of the main pole.

Table 6.4 Sensitivity (Sn), specificity (Sp), and total accuracy (Acc) obtained with the best parameter for each classification using leave-one-out cross-validation

Classifications	Parameter	Sn	Sp	Acc
CHF vs. Healthy	P	85.2%	85.7%	85.5%
nPB-CHF vs. Healthy	P	84.2%	85.7%	85.2%
PB vs. nPB (CHF)	r_1	87.5%	79.0%	81.5%

Table 6.5 Area under the curve (AUC)

	CHF vs. Healthy	nPB-CHF vs. Healthy	PB vs. nPB (CHF)
P	93.8%	91.1%	92.1%
P_R	92.4%	89.2%	93.4%
P_L	94.1%	91.7%	89.5%
r_1	83.9%	78.0%	85.5%

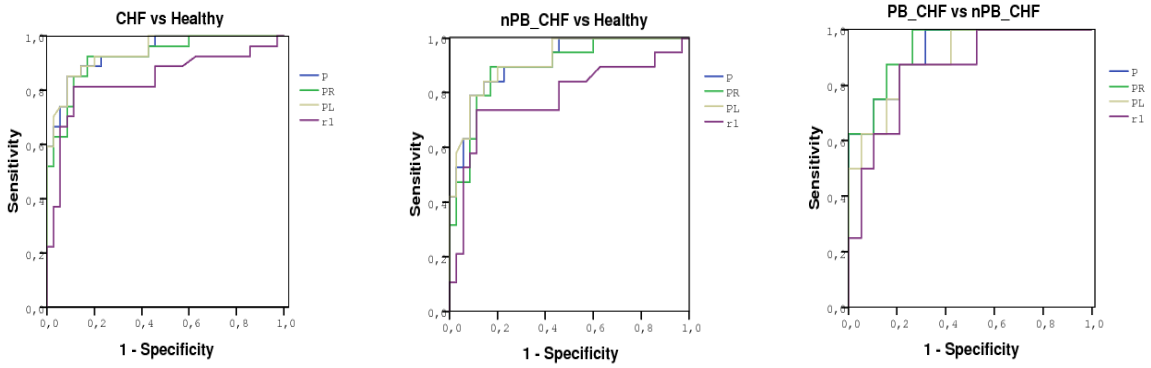

(a) (b) (c)

Figure 6.10 ROC curves of the most significant parameters: power-related parameters (P, P_L, P_R) and main pole radius r_1 in the classification of (a) CHF patients vs. healthy subjects, (b) nPB patients vs. healthy subjects, and (c) PB vs. nPB within the CHF patients.

6.4 Time-varying respiratory pattern in CHF patients and healthy subjects

In our first studies, we assumed stationarity in the respiratory flow signal and characterized the relevant frequency band that was determined by the modulation frequency peak extracted from the respiratory flow envelope signal's power spectrum [38] and [39]. However, it has been reported [66] that the same patient could presents a mixture of breathing patterns, ranging from nonperiodic breathing (with no cyclic modulation of ventilation) through to mild PB and CSR patterns. Conventional spectral analysis assumes stationarity in the signal and is therefore unable to identify pattern changes. One way to overcome this disadvantage could be to permit the AR coefficients to be time-varying. This method is called time-varying autoregressive modelling (TVAR).

We cannot assume that the parameters are arbitrarily time-varying, since the parameter estimation problem would be severely underdetermined, with an infinity of parameter evolutions that yield vanishing prediction errors. Such parameter evolutions are clearly meaningless. One approach to make the estimates meaningful is to assume that the parameter evolution is either slow, smooth or both. There are two approaches to solving the TVAR problem. The stochastic approach, which is based on the recursive estimation of the time-varying coefficient evolution, and the deterministic regression approach, which constrains the temporal evolution of the model coefficients so that it is characterized by a linear combination of a set of basis functions with appropriate properties [139]. The stochastic approach is widely used in biomedical signal processing [80] and [140]. These methods are also called adaptive methods, and the most popular algorithms are the least mean square, the recursive

least square and the Kalman filter.

The respiratory flow pattern might present some slowly changing spectral properties [66]. Thus, one of our main aims is to analyse changes in the respiratory pattern in CHF patients and healthy subjects. For this purpose, we characterize the behaviour of the respiratory envelope signal by means of a TVAR model. The characterization involves both spectral and temporal parameters that are extracted from the power spectrum for each time sample.

6.4.1 Time-varying spectral estimation

A TVAR estimate is used to model the respiratory pattern modulation, assuming that there are slow changes in its spectral properties. Thus, the envelope of the respiratory flow signal is analysed by the following TVAR model

$$\hat{x}(n) = -\sum_{k=1}^{p} a_k(n)x(n-k) + u(n) \tag{6.1}$$

where $u(n)$ denotes zero-mean white noise, $a_k(n)$ for $k = 1, 2, \cdots, p$ are the AR coefficients, p the model order and $\hat{x}(n)$ is the prediction of the envelope signal provided by the AR model. In addition to the AR coefficients, the input noise $u(n)$ is also assumed to be time-varying with variance $\sigma_u(n)^2$. Hence, the PSD of a time-varying process at each time n is given by

$$\hat{P}_{x\ AR}(e^{j\omega}, n) = \frac{\sigma_u(n)^2}{\left|1 + \sum_{k=0}^{p} a_k(n) \cdot e^{-j\omega k}\right|^2} \ . \tag{6.2}$$

Time-varying AR coefficients are determined through an adaptive method that is based on the recursive least squares (RLS) algorithm. The basics of this method are reviewed below.

Recursive least squares

In recursive implementations of the least squares method, the initial conditions are computed and the information contained in the new data is then used to update the old estimates. Thus, the length of the observed data sequence is variable. We introduce the cost function to be minimized as $C(n)$ Eq. (6.3), where n is the variable length of the observed data and $e(i)$ is the prediction error. We introduce a weighting factor ($\beta(n,i)$) in the definition of the cost function.

$$C(n) = \sum_{i=1}^{n} \beta(n,i) \cdot |e(i)|^2. \tag{6.3}$$

The prediction error defined in Eq. (5.45) assumes stationarity, but in this non-stationary scheme the prediction error is described by

$$e(i) = x(i) - \hat{x}(i) = x(i) + \sum_{k=1}^{p} a_k(i) \cdot x(i-k) \tag{6.4}$$

where p is the order of the model, $x(i)$ the desired output, $\hat{x}(i)$ the predicted sequence, and $a_k(i)$ are the time-varying AR coefficients defined at time i as $A_k^T(i) = [a_1(i), a_2(i), \cdots, a_k(i)]$. The weighting factor satisfies $0 < \beta(n,i) \leq 1$, for $i = 1, 2, \cdots, n$. The role of the weighting factor is to ensure that data in the distant past are forgotten, so that the statistical variations of the observed data can be followed when the model operates in a nonstationary environment. A frequent form of weighting is the exponential weighting factor, defined by

$$\beta(n,i) = \lambda^{n-i}, \quad i = 1, 2, \cdots, n \tag{6.5}$$

where λ, commonly known as the forgetting factor, is a constant that is close to, but less than, unity. The inverse of the forgetting factor $1 - \lambda$ is defined as a measure of the memory of the algorithm. When $\lambda = 1$, it corresponds to the ordinary least

square method. According to this forgetting factor, we minimize the following cost function

$$C(n) = \sum_{i=1}^{n} \lambda^{n-i} \cdot |e(i)| \tag{6.6}$$

The optimum value of the time-varying AR coefficient vector $A_p(n)$, for which the cost function reaches its minimum value, is defined by the normal equations. This can be expressed in terms of matrices by $R_x(n) \cdot A_p(n) = r_{\hat{x}x}(n)$, where $r_{\hat{x}x}(n)$ is the cross-correlation between the desired signal and the predicted one. The coefficients that minimize the cost function at the time sample n are found by solving this expression. A recursive solution of the form $A_p(n) = A_p(n-1) + \Delta_{Ap}(n-1)$ is derived, where $\Delta_{Ap}(n-1)$ is a correction factor at time $n-1$. The cross-correlation $r_{\hat{x}x}(n)$ is expressed in terms of $r_{\hat{x}x}(n-1)$ by

$$r_{\hat{x}x}(n) = r_{\hat{x}x}(n-1) + x(n) \cdot \hat{x}^*(n) \tag{6.7}$$

where $\hat{x}^*$ is the conjugate of $\hat{x}$. Similarly, $R_x(n)$ is expressed in terms of $R_x(n-1)$ by

$$R_x(n) = R_x(n-1) + \hat{x}(n)^* \cdot \hat{x}^T(n). \tag{6.8}$$

To generate the AR coefficient's correction factor at time $n-1$ $\Delta_{Ap}(n-1)$, the inverse of the autocorrelation matrix is computed by applying the matrix inversion lemma or Woodbury's identity [141], [142] and [143].

The predicted error (the difference between the observed data sequence $x(n)$ and the predicted sequence $\hat{x}(n)$) is weighted by an exponential window that moves with the data. It provides a better estimate of the model coefficients and better tracking of the time-varying signals. This recursive algorithm updates the AR coefficient vector for each new sample (Fig. 6.11).

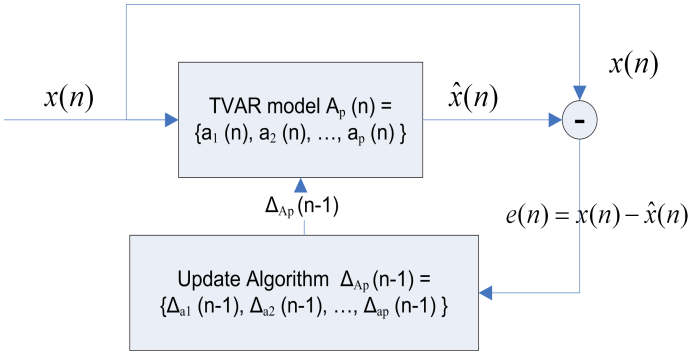

Figure 6.11 Time-varying autoregressive modelling process by means of recursive least squares.

Note that the performance of this algorithm depends on the choice of the forgetting factor $\lambda \in]0,1]$, which controls the length of the prediction error and therefore the amount of memory in the model. Small values of λ imply high potential variability of the AR coefficients, while high values between (0.9 - 0.99) are usually more relevant in practice.

The forgetting factor that minimizes the least square error between the predicted envelope and the real one is selected from the recommended λ range [80].
On average, a value of 0.975 is obtained for CHF patients healthy subjects. According to the results obtained in the stationary case, a 4^{th} order TVAR is optimized for the time-varying characterization of the respiratory pattern. (In the stationary case, the global AR model order is found to be 4. When the Ljung–Box test is applied, the residuals of all 61 signals are found to be whitened by the global AR model.)

The time-varying PSD is estimated by computing the PSD at successive time intervals from the estimated AR coefficients. Fig. 6.12 displays the time-varying power spectrum of each CHF patient group (PB, nPB and CSR patient) and a healthy sub-

ject. The most striking feature of these diagrams is the temporal evolution of the modulation frequency peak.

6.4.2 Time-varying parameter extraction

In addition to the AR coefficients and the two complex conjugate pole radii, the spectral parameters described in Table 6.6 and presented in Fig. 6.13 are extracted from the discriminant frequency band ($DB(n)$), but are know for each time sample n.

Table 6.6 Time-varying parameter description

$fp(n)$	Frequency peak at each time sample
$P(n)$	Power in the DB at each time sample
$P_R(n)$	Power in the "right band' at each time sample
$P_L(n)$	Power in the "right band' at each time sample
$S(n)$	Slope at each time sample
$K(n)$	Kurtosis at each time sample
$a_i(n)$	AR coefficients at each time sample, for $i = 1$ to 4
$r_i(n)$	Poles radii at each time sample, for $i = 1, 2$

The whole parameter set would characterize the behaviour of the respiratory pattern at each time sample. To identify the most frequent pattern presented by each patient and healthy subject, the statistical distribution is evaluated for each time-varying parameter. Table 6.8 summarizes the different parameters and their statistics: mean (m), standard deviation (s), interquartile range (I) and coefficient of variation (c).

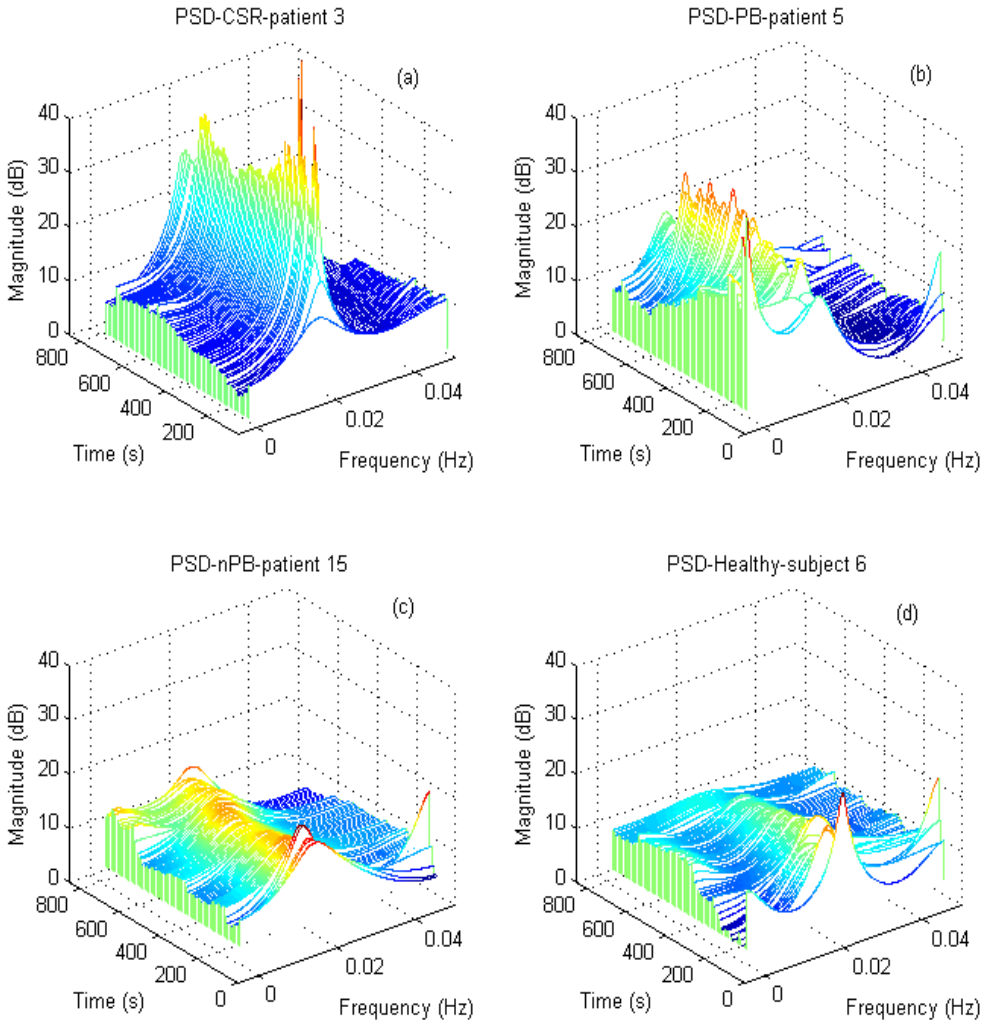

Figure 6.12 Time-varying power spectrum of (a) a CSR patient, (b) a PB patient, (c) an nPB patient, and (d) a healthy subject.

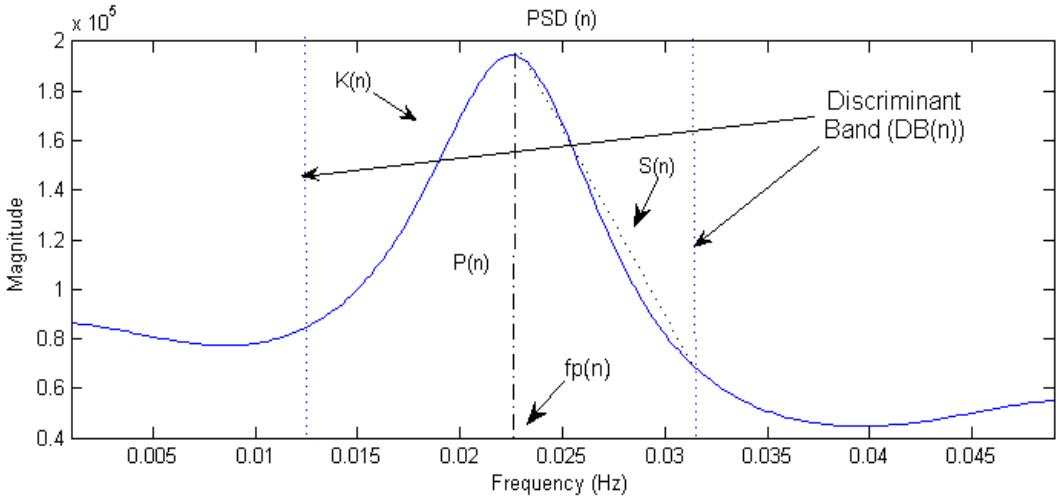

Figure 6.13 Time-varying parameters extracted from the discriminant band.

Table 6.7 Parameter description and statistics

fp; mfp, sfp, Ifp, cfp	Frequency peak
P; mP, sP, IP, cP	Power of DB
S; mS, sS, IS, cS	Slope
K; mK, sK, IK, cK	Kurtosis
$\mathbf{a_i}$; ma_i, sa_i, Ia_i, ca_i	AR coefficients ($i = 1, \ldots, 4$)
$\mathbf{r_i}$; mr_i, sr_i, Ir_i, cr_i	Poles radii ($i = 1, 2$)

6.4.3 Data analysis

Linear discriminant analysis is performed between 26 CHF patients and 35 healthy subjects to study the accuracy of the pattern characterization. The following clas-

sifications are carried out: CHF patients versus healthy subjects, nPB patients versus healthy subjects and an internal CHF patient classification of PB versus nPB. Through the statistics extracted from each parameter distribution, feature selection is applied to the statistically significant parameters, to select the most discriminant subset using leave-one-out cross-validation.

6.4.4 Results

Table 6.8 presents the mean and the standard deviation of statistically significant parameters for each group of patients and healthy subjects. Table 6.9 shows the p-value of these parameters using the Mann-Whitney test.

Table 6.8 Mean and standard deviation of mP, mK, mS, mr_1, ca_1, cK, cP and cS for each group of subjects

	mP^*	mK	mS^*	mr_1
Healthy	1.24 ± 4.82	3.65 ± 6.26	4.0 ± 16.7	0.62 ± 0.08
CHF	1.30 ± 1.79	5.40 ± 6.25	22.0 ± 6.1	0.77 ± 0.11
PB	2.80 ± 2.74	10.36 ± 9.91	72.2 ± 97.6	0.85 ± 0.11
nPB	0.64 ± 0.37	3.31 ± 1.67	0.88 ± 1.38	0.73 ± 0.09
	ca_1	cK	cP^*	cS^*
Healthy	0.11 ± 0.07	0.34 ± 0.71	0.08 ± 0.11	0.10 ± 0.14
CHF	0.19 ± 0.14	1.62 ± 2.59	0.58 ± 0.99	5.93 ± 20.32
PB	0.32 ± 0.17	3.41 ± 4.15	1.39 ± 1.54	19.0 ± 35.8
nPB	0.13 ± 0.09	0.86 ± 0.96	0.24 ± 0.27	0.42 ± 0.83

**The values have been divided by* 10^4 *for ease of legibility*

Table 6.10 presents the classification results with the most discriminative parameters. High accuracy is obtained with a single parameter in all classifications. These results improve slightly when a second parameter is added. Similar results have been observed with the statistics of the other parameters: mK, cK, cS, mS, and cP. Fig. 6.14 presents the ROC curve and the AUC for the three classifications.

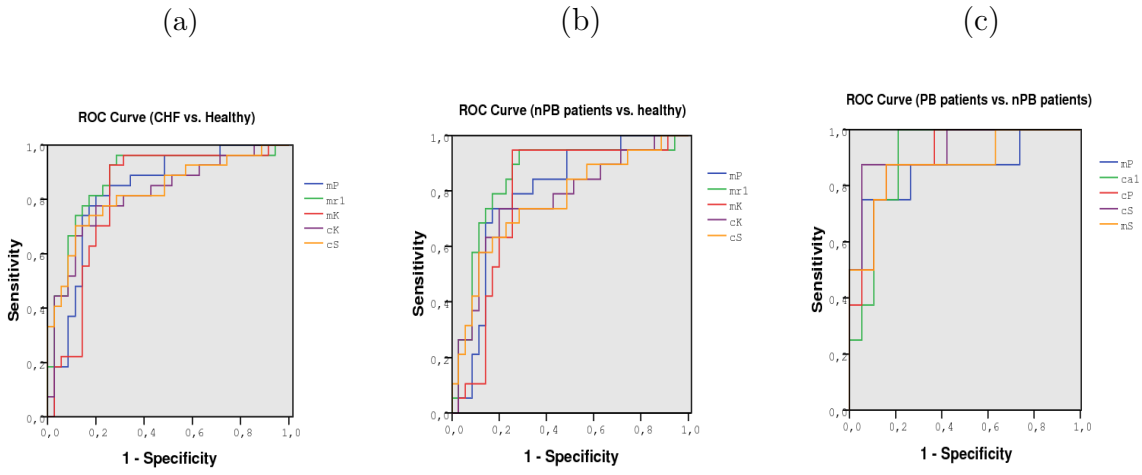

(a)	(b)	(c)
mP: 83.1%	mP: 83.1%	mP: 83.1%
mr_1: 88.0%	mr_1: 88.0%	mr_1: 88.0%
mK: 81.5%	mK: 78.2%	cP: 90.1%
cK: 81.8%	cK: 76.5%	cS: 92.8%
cS: 82.9%	cS: 76.1%	mS: 87.5%

Figure 6.14 ROC curves of the most significant parameters: (a) CHF patients vs. healthy subjects, (b) nPB patients vs. healthy subjects, and (c) PB vs. nPB within the CHF patients.

Table 6.9 p-value of the classifications: CHF patients versus healthy subjects, nPB patients versus healthy subjects, and within the CHF patients, PB versus nPB

	mP	mK	mS	mr_1
CHF vs. Healthy	$9.1 \cdot 10^{-6}$	$2.4 \cdot 10^{-5}$	$6.8 \cdot 10^{-5}$	$3.3 \cdot 10^{-7}$
nPB(CHF) vs. Healthy	$4.5 \cdot 10^{-4}$	0.01	0.03	$2.7 \cdot 10^{-5}$
nPB vs. PB (CHF)	0.03	0.02	0.002	0.013
	ca_1	cK	cP	cS
CHF vs. Healthy	0.02	$1.9 \cdot 10^{-5}$	$1.44 \cdot 10^{-5}$	$1.04 \cdot 10^{-5}$
nPB(CHF) vs. Healthy	$n.s.$	0.01	0.02	0.02
nPB vs. PB (CHF)	0.001	0.03	0.001	0.001

Table 6.10 Sensitivity (Sn), specificity (Sp), and total accuracy (Acc) obtained with the best parameters for each classification using leave-one-out cross-validation

Classifications	**Best Features**	**Sn**	**Sp**	**Acc**
CHF vs.	mr_1	74.1%	88.6%	82.3%
Healthy	$mr_1 + mP$	74.1%	91.4%	83.9%
nPB-CHF vs.	mr_1	73.7%	82.9%	79.6%
Healthy	$mr_1 + mP$	79.0%	85.7%	83.3%
PB vs.	ca_1	75.0%	89.5%	85.2%
nPB (CHF)	$ca_1 + mP$	75.0%	94.7%	88.9%

6.5 Conclusion

This chapter introduces envelope-based respiratory pattern characterization of CHF patients and healthy subjects. We study respiratory pattern periodicity as a risk index by means of characterization of the respiratory flow signal envelope. Our previous studies [38] and [39] introduced the fact that respiratory periodicity could be detected from the envelope of the flow signal using time-frequency analysis. This method could be used to discriminate respiratory patterns in CHF patients. To extend this work, which only studied CHF patients, in this study we derive various parameters from the time-frequency characterization of the envelope and use these parameters to identify different respiratory patterns in CHF patients and healthy subjects.

One advantage of this study is that an outlier removal pre-processing stage prepares the respiratory flow signals for robust envelope extraction. Although different methods have been tried to extract the respiratory flow envelope, the one based on the Hilbert transform performed best in our study.

The main goal of this study is to identify and characterize respiratory patterns derived from subjects with periodic or nonperiodic breathing. Although statistically significant differences are found for a variety of parameters, the best cross-validated discrimination between them was in general achieved with the power evaluated over the discriminant band.

Power-related parameters achieve the best results in all the classifications performed with healthy subjects and CHF patients, which includes patients with periodic breathing patterns with and without apnea, and patients with nonperiodic breathing patterns. However, the main pole radius produces good results when periodic and nonperiodic breathing patterns are classified in CHF patients. The ROC curves

validate the results for the identification of different respiratory patterns.

In addition, time-varying AR modelling is proposed to characterize the temporal evolution of respiratory flow signal patterns. The time-variant AR coefficients, pole radius, and various spectral parameters can be used to study changes in patterns and to classify CHF patients and healthy subjects. The statistical distribution is evaluated for each parameter, to identify the predominant respiratory pattern. After feature selection, the percentage of subjects who are correctly classified with the mr_1 (mean of the main pole radius) and the mP (mean of the DB power) is 83.9%, with 74.1% of sensitivity and 91.7% of specificity when CHF patients are classified versus healthy subjects, and 83.3%, with 79.0% of sensitivity and 85.7% of specificity when nPB patients are classified versus healthy subjects. The parameters mP and the ca_1 (coefficient of variation of the first AR coefficient), which are selected as the most discriminant in the classification of PB and nPB within CHF patients, result in 88.9% of patients who are well-classified with 75.0% of sensitivity and 94.7% of specificity. The ROCs validate the results obtained in all classifications with leave-one-out cross-validation.

These results indicate that power-related parameters and the main pole position of the respiratory envelope signal are powerful indices for the identification of periodic breathing. Additionally, time-varying modulation of the flow envelope signal can be used to accurately characterize the temporal evolution of respiratory patterns. The significance of our results needs to be further established using a larger dataset.

Chapter 7

Correntropy-based respiratory pattern analysis

Natural processes that are of interest for engineering have two basic characteristics: a statistical distribution of data and a time structure. Time itself is fundamental to many real-world problems and random variables are hardly ever independently distributed. A number of methods are based on studying the statistical distribution, and ignore the time structure. Other methods only focus on quantifying the time structure. An accurate description of a stochastic process requires information about its distribution and its time structure. A single measure that includes both characteristics would greatly enhance the theory of stochastic random processes. Thus, Santamaria et al. [81] recently introduced a generalization of the correlation function for stochastic processes, called correntropy. The advantage of this new measure is that it contains information on both the statistical distribution and the time structure of the underlying dataset, simultaneously.

Second-order statistics in the form of correlation and the mean square error (MSE)

are probably the most widely utilized methods for quantifying the similarity between two random variables [82]. However, the optimality of these methods is limited by the Gaussianity and linearity of the data. Therefore, autocorrelation and power spectrum algorithms only characterize second-order statistics. In many applications where non-Gaussianity and nonlinearities are present, these second-order statistical methods might fail to provide all the relevant information about the signals under study.

In the literature, kernel-based techniques, such as support vector machines [144], kernel principal component analysis [145], kernel Fisher discriminant analysis [146], and kernel canonical correlation analysis [147] and [148], represent a major development in machine learning. This is mainly because kernel methods exploit information about the inner products between data items. The use of kernel methods makes correntropy computationally efficient, since it can be computed directly from the data. Another property of the correntropy function is its robustness against impulsive noise.

Correntropy has been successfully applied to signal processing and machine learning problems, such as blind equalization [81], minimum average correlation energy filter [149], principal component analysis [150] and others.

This chapter introduces the correntropy measure and a number of functions that are derived from it, such as centred correntropy and correntropy spectral density. Correntropy involves information on higher-order statistics that can be expected to facilitate the detection of respiratory nonlinearities. These nonlinearities cannot be identified by conventional techniques based on second-order statistics. The aim of this chapter is apply centred correntropy to the study of the respiratory flow signal in chronic heart failure (CHF) patients with periodic breathing (PB) and nonperiodic breathing (nPB) patterns. Thus, we define parameters that can improve prognosis

and serve as indicators of patient condition. For this purpose, we work with the datasets of CHF patients and healthy subjects that were presented in Chapter 1.

7.1 Correntropy: definition

The correlation function is probably the most widely utilized similarity measure. However, as it only considers second-order statistics, its success depends on the assumption of the Gaussianity of the variables. Inspired by information theoretical learning (ITL), a new localized similarity measure has recently been defined called the generalized correlation function (GCF) or correntropy.

Correntropy is a localized similarity measure that is defined in terms of inner products of vectors in a kernel feature space. It involves a positive definite kernel function which implicitly transforms the original signal into a high dimensional reproducing kernel Hilbert space (RKHS) [151] in a nonlinear way, and then efficiently calculates the generalized correlation in that RKHS. The inner product, as a natural way of norm or similarity measure, reflects the interaction between vectors in the feature space. These vectors are separated by a time delay in the input space. As correntropy is directly related to Renyi's quadratic entropy calculated through Parzen windowing [152], it provides information about statistical distribution in the input space. The ability to reflect nonlinear characteristics of the signal makes correntropy a well-qualified candidate for the characterization of nonlinear dynamics.

Correntropy is a positive definite kernel function that implicitly transforms the original signal into a high dimensional space in a nonlinear way, and efficiently calculates the generalized correlation in that space.

In addition to the time structure, it adds statistical distribution information that

consists of information about higher order moments of the probability density function. As it is not restricted to second-order statistics, correntropy is very useful in non-Gaussian signal processing.

Correntropy transforms component-wise data to the feature space by $\phi(\cdot)$ and then calculates the correlation. Therefore, it can be presented as an inner product in the feature space as $V(x,y) = E[\phi(x)\phi(y)]$. This inner product permits generalization of the correlation to the nonlinear case by means of different kernel functions. The kernel function κ, maps the data of the input space into the feature space. If the kernel is positive definite and satisfies Mercer's conditions [97] and [153], the inner product in the feature space satisfies $\kappa(x,y) = \phi(x)\phi(y)$. This idea enables us to obtain nonlinear versions of any linear algorithm expressed in terms of inner product. There is no need to know the mapping function $\phi(\cdot)$ explicitly, as only the kernel function $\kappa(\cdot,\cdot)$ is required. This makes it easier to calculate the correntropy directly from the data.

7.2 Correntropy: estimation

For a discrete-time, strictly stationary stochastic process $x(n)$, $n = 0,\ldots,N-1$, in which N is the number of samples, the correntropy function $V(m)$ is defined as [81] and [154]

$$V(m) = E[\kappa(x(n), x(n-m))], \tag{7.1}$$

where $E[\cdot]$ is the statistical expectation operator, $\kappa(\cdot)$ is a symmetric, positive definite kernel function, and N is the number of samples.

In the literature, sigmoidal, Gaussian, polynomial, and spline kernels are among the most commonly used symmetric positive definite kernel functions. They are

applied in diverse areas such as machine learning, function approximation, density estimation, and support vector machine classification [144] and [155]. The Gaussian kernel function that is applied in the present study is given by

$$\kappa(x(n), x(n-m)) = \frac{1}{\sqrt{2\pi}\sigma} \exp\left[-\frac{(x(n)-x(n-m))^2}{2\sigma^2}\right], \tag{7.2}$$

where σ is referred to as the kernel size ("standard deviation").

When the Taylor series expansion is applied to the Gaussian kernel, we can rewrite the correntropy function as

$$V(m) = \frac{1}{\sqrt{2\pi}\sigma} \sum_{k=0}^{\infty} \frac{(-1)^k}{2\sigma^{2k}k!} E\left[(x(n)-x(n-m))^{2k}\right], \tag{7.3}$$

which contains all even-order moments of the random variable $(x(n)-x(n-m))$.

Different kernel functions would yield different expansions, but all the aforementioned kernel functions are nonlinear and therefore include higher-order statistical information about the stochastic process.

The emphasis given to higher-order moments is controlled by σ. In this study, σ is determined by Silverman's rule of density estimation [156]:

$$\sigma = 0.9AN^{-1/5}, \tag{7.4}$$

where A is the smaller value of the standard deviation of data samples and the data interquartile range scaled by 1.34, and N is the number of samples. This rule is simple to apply and is known to produce reasonable values with scalar signals, such as flow signals. As σ increases, the high-order moments decay and the second-order moments tend to dominate. In fact, for kernel size values that are 10 times higher than the size suggested by Silverman, correntropy starts to approach correlation [149].

7.3 Centred correntropy

The mean of the transformed data is subtracted in the centred correntropy function $V_c(m)$, to reduce the effect of output DC bias [154] and [149]. This function is defined by

$$V_c(m) = E_{x(n)x(n-m)}[\kappa(x(n), x(n-m))] - E_{x(n)}E_{x(n-m)}[\kappa(x(n), x(n-m))] \quad (7.5)$$

where $E_{x(n)}E_{x(n-m)}[\kappa(x(n), x(n-m)]$ is the square mean of the transformed data and corresponds to the correntropy mean value ($\overline{V}$), which can be estimated through the kernel function from the original data as

$$\overline{V} = \frac{1}{N^2}\sum_{n=1}^{N}\sum_{m=n+1}^{N}\kappa(x(n), x(n-m)) \quad (7.6)$$

Note that correntropy is the joint expectation of $\kappa(x(n), x(n-m))$, while centred correntropy is the difference between the joint expectation and the product of marginal expectations of $\kappa(x(n), x(n-m))$. The results are therefore based on centred correntropy, which is estimated by $\hat{V}_c(m) = \hat{V}(m) - \overline{V}$.

Correntropy modification

The flow signals sometimes contain missing samples or become saturated. Such samples must be discarded from subsequent analyses, as they do not reflect respiratory activity (as described in Chapter 5). However, samples that are to be discarded are easily detected, and are here represented by the binary function $g(n)$, defined by

$$g(n) = \begin{cases} 1 & \text{existing,} \\ 0 & \text{discarded.} \end{cases} \quad (7.7)$$

Information on discarded samples is introduced in the correntropy estimator in a way similar to that of the sample estimator of the correlation function [119]. Hence, the sample estimator of $V(m)$ in (7.1) is given by

$$\hat{V}(m) = \frac{1}{U(m)} \sum_{n=m}^{N} \kappa(x(n), x(n-m)) g(n) g(n-m), \tag{7.8}$$

where

$$U(m) = \sum_{n=m}^{N} g(n) g(n-m). \tag{7.9}$$

In addition to the aforementioned signal problems, a variety of other artefacts are observed in flow signals. In general, these problems call for various pre-processing algorithms that condition the acquired signal (see Chapter 5). One great advantage of correntropy is its robustness against impulsive noise, as the Gaussian kernel makes $\kappa(x(n), x(n-m)) \approx 0$ when either $x(n)$ or $x(n-m)$ is an outlier. Due to this property, the results of this research are obtained without any kind of pre-processing.

7.4 Correntropy: properties

Some important properties of correntropy are presented below [82]. These properties consider a discrete-time, strictly stationary stochastic process $x(n)$. Note that the properties are also satisfied for continuous-time processes.

- Property 1: considering $x(n) \in \Re$ and $n \in T$ where T is an index set, for any symmetric positive definite kernel (i.e. the Mercer kernel) $\kappa(x(n), x(n-m))$ defined on $\Re$ x $\Re$, the correntropy defined as $V(m) = E[\kappa(x(n), x(n-m))]$ is a reproducing kernel, RKHS.

- Property 2: $V(m)$ is a symmetric function $V(m) = V(-m)$.

- Property 3: $V(m)$ reaches its maximum at the origin, with a maximum value of $V(m) \leq V(0),\ \forall m$.

- Property 4: $V(m) \geq 0$ and $V(0) = 1/\sqrt{2\pi}\sigma$.

- Property 5: if the samples $x(n),\ n = 0,\ldots,N-1$ are drawn independently and identically distributed according to some unknown (but fixed) probability distribution of the samples in the process, then the mean value of the correntropy converges asymptotically to the estimate of information potential obtained through Parzen windowing with Gaussian kernels.

- Property 6: given $V(m)$ for $m = 0,\cdots,p-1$, then the correntropy matrix of dimensions $p \times p$ is Toeplitz and positive definite [136], [128].

$$\mathbf{V}= \begin{bmatrix} V(0) & V(-1) & \cdots & V(-p) \\ V(1) & V(0) & \cdots & V(-p+1) \\ \vdots & \vdots & \vdots & \vdots \\ V(p) & V(p-1) & \cdots & V(0) \end{bmatrix}$$

  This property opens up the possibility of applying the new function to all the signal processing methods that use conventional correlation matrices: signal and noise subspace decompositions, projections, etc. In particular, we defined a generalized power spectral density.

- Property 7: If we consider $x(n) \in \Re,\ n \in T$, then we have a discrete-time, wide-sense stationary zero-mean Gaussian process with autocorrelation function $r(m) = E(x(n) - x(n-m))$. The correntropy function for this process is given

by

$$V(m) = \begin{cases} \frac{1}{\sqrt{2\pi}\sigma} & m = 0 \\ \frac{1}{\sqrt{2\pi(\sigma^2+\sigma^2(m)}} & m \neq 0 \end{cases} \tag{7.10}$$

where σ is the kernel size and $\sigma^2(m) = 2(r(0) - r(m))$.

7.5 Correntropy spectral density

Similar to the conventional correlation function, the correntropy function is positive definite and therefore lends itself to use in many signal processing techniques. Since we are particularly interested in exploring the spectral properties of respiratory flow signals, correntropy spectral density (CSD) is introduced, which is a generalization of the conventional PSD [81]. The CSD is based on the Fourier transform of the correntropy function, i.e.

$$\hat{P}(e^{j\omega}) = \sum_{m=-(N-1)}^{N-1} \hat{V}_c(m) e^{-j\omega m}. \tag{7.11}$$

As the flow signal is oscillatory in nature, with a spectrum that exhibits pronounced peaks, nonparametric and parametric spectral analysis is applied. Periodogram-based spectral analysis, such as the Welch and Blackman-Tukey methods described in Chapter 5 are used. The autoregressive (AR) coefficients can be estimated from the correntropy function using the Yule–Walker equations, or any other of the many well-known estimation techniques [157]. This can be achieved because the correntropy matrix, whose elements are defined by $\hat{V}_c(m)$, is Toeplitz and positive definite, as is the conventional correlation matrix [81]. Autoregressive spectral analysis offers

better spectral resolution than periodogram-based spectral analysis.

In this research, it is essential to have high spectral resolution in the vicinity of the respiratory and modulation peaks. Consequently, the following procedure is adopted. First, the optimum order is determined for each subject using the minimum description length criterion [131]. Then, the maximum of the resulting model order estimates is selected and used as a global model order in the subsequent signal analysis. This model order ensures that the data is represented correctly when the prediction error is a white sequence. We apply a statistical test (Ljung–Box) to prove the whiteness of the prediction error.

7.6 Parameter extraction

In the time domain, the respiratory pattern is characterized by the correntropy mean $\overline{V}$, i.e. Renyi's entropy. In the frequency domain, the correntropy spectral density mean and three parameters are derived from the two CSD frequency bands that are centred either around the respiratory frequency (Δf_r: the respiratory frequency bandwidth) or the modulation frequency (Δf_m: the modulation frequency bandwidth).

The modulation frequency of PB patterns typically ranges from 0.005 to 0.05 Hz. Therefore, the modulation frequency peak (fp_m) is located in this band with $\Delta f_m =$ 0.02 Hz. The respiratory frequency peak (fp_r) is tracked in the band from 0.2 to 0.4 Hz with $\Delta f_r = 0.2$ Hz. The individual powers of the two frequency bands, P_m and P_r, their ratio $R = P_m/P_r$, and the correntropy spectral density mean $\overline{P}$ constitute the four spectral parameters that were investigated (Table 7.1). These parameters are derived from parametric and nonparametric CSD.

Table 7.1 Parameter description

Parameter	Description
P_m	Power of the modulation frequency band
P_r	Power of the respiratory frequency band
R	P_m/P_r
$\overline{V}$	Correntropy mean or information potential
$\overline{P}$	Correntropy spectral density mean

7.6.1 Simulated data

The behaviour of the respiratory flow signal in PB patients often resembles that of a signal subjected to amplitude modulation (AM). To illustrate certain properties of the method's performance, the following AM signal is studied

$$x(n) = (1 + \mu \cos(\omega_m n)) \cos(\omega_c n), \tag{7.12}$$

where $f_c = \omega_c/2\pi$ is the carrier frequency, $f_m = \omega_m/2\pi$ is the modulation frequency, and $\mu \in [0, 1]$ is the modulation index. Fig. 7.1 shows an example in which the characteristics of the respiratory flow signal and the AM signal are quite similar.

7.6.2 Data analysis

The pattern characterization accuracy of the proposed parameters is evaluated in terms of the following three classification problems: CHF patients with either PB or nPB, CHF patients versus healthy subjects, and nPB patients versus healthy subjects. Linear discriminant analysis is used to implement a parameter selection process

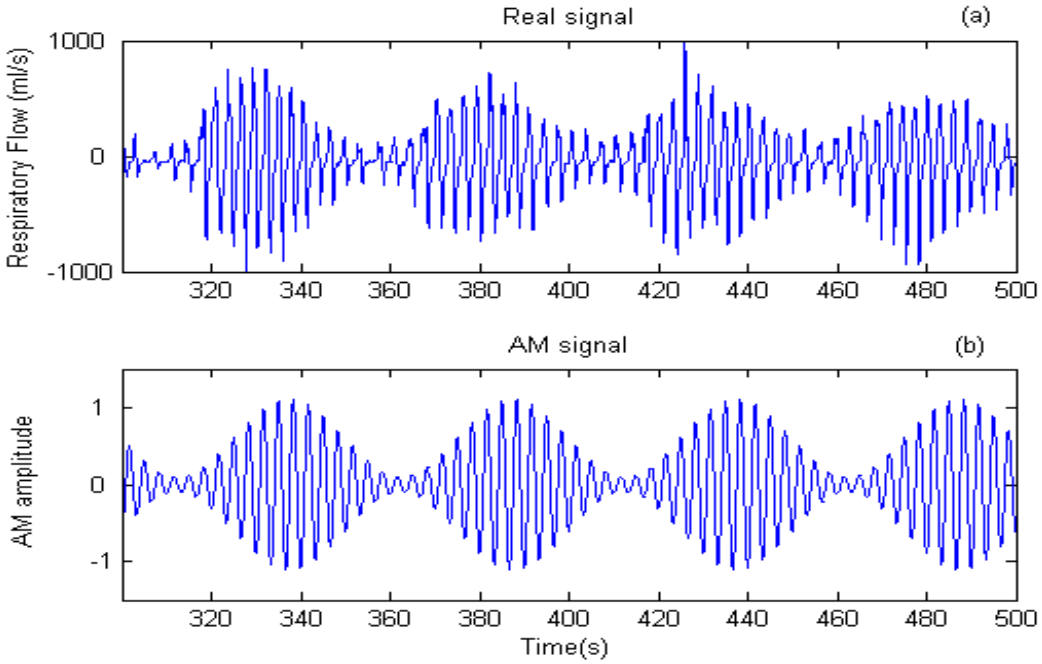

Figure 7.1 (a) A respiratory flow signal acquired from a PB patient, and (b) a simulated AM signal with 0.3 Hz carrier ("respiratory") frequency, 0.02 Hz modulation frequency, and $\mu = 0.8$.

that is based on leave-one-out cross-validation. Only the single most discriminative parameter is considered for each classification.

7.7 Results

For the 61 subjects, the respiratory frequency is found to range from 0.2 to 0.4 Hz, and the modulation frequency from 0.01 to 0.04 Hz. These frequency ranges are in good agreement with those reported by Pinna et al. [66]. The flow signals are decimated from 250 to 2 Hz, using null-phase antialiasing filtering, to account for the fact that the frequencies of interest only range up to about 0.5 Hz. It is particularly important to avoid oversampling when the AR spectral analysis is undertaken [85].

In the AR approach, the global AR model order is found to be 30 when the optimum order selection procedure is applied. When the Ljung–Box test is applied, the residuals of all 61 signals except two are found to be whitened by the global AR model. Within periodogram-based spectral analysis, Blackman-Tukey have provided good spectral resolution using a Hamming window and 200 lags. The sole design parameter of the method σ is determined by Silverman's rule in (7.4) (referred to as σ_{opt}), and is investigated for some deviating values ($0.1 * \sigma_{opt}$ and $10 * \sigma_{opt}$). To make the figures comparable, the scales have been normalized to unity.

7.7.1 Simulated signals

Fig. 7.2 illustrates the performance of the aforementioned methods in terms of the power spectrum of the AM signal. This figure shows that spectra based on correntropy and correlation have very different characteristics. The main difference is the location of f_m. For correntropy-based spectra, f_m is found in the baseband and f_c is accompanied by a number of harmonics. For correlation-based spectra, the peaks are located at $f_m - f_c$, f_c and $f_m + f_c$, respectively, as suggested by classical AM analysis. Note that Blackman-Tukey's method is unable to resolve the two peaks at $f_m - f_c$ and $f_m + f_c$ (Fig. 7.2(e)); no harmonic pattern is present in the correlation-based spectra. Thus, correntropy-based spectra has the advantage of exhibiting peaks at the positions of f_m and f_c, which are easy to detect. The sideband peaks of the correlation-based spectra can be difficult to detect as they tend to smear with the respiratory peak at f_c.

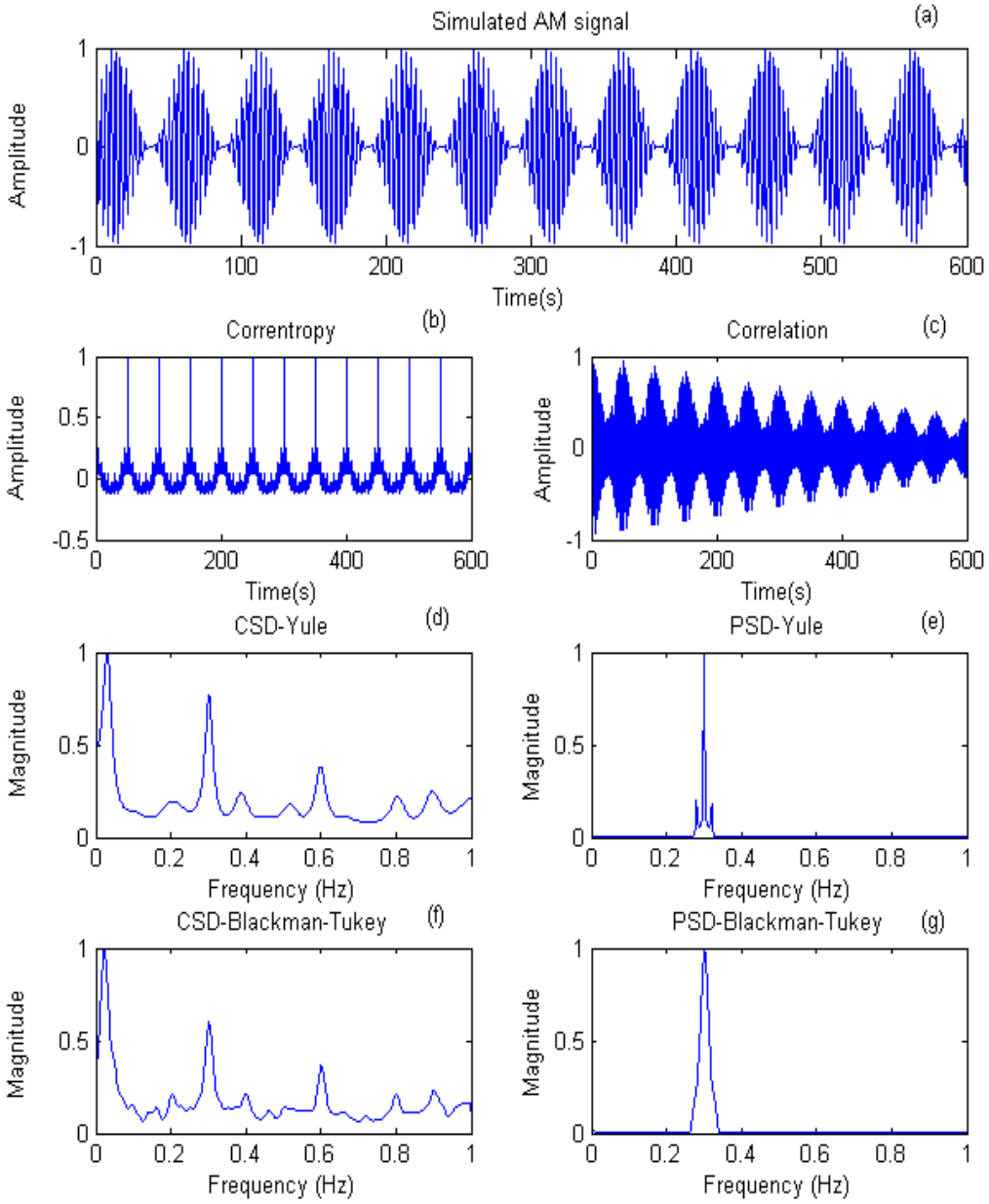

Figure 7.2 (a) A simulated AM signal with 0.3 Hz carrier frequency, 0.02 Hz modulation frequency, and $\mu = 1$, (b) its correntropy function and (c) its correlation function. The CSD obtained with (d) Yule–Walker's method and (f) Blackman-Tukey's method. The PSD obtained with (e) Yule–Walker's method and (g) Blackman-Tukey's method.

Fig. 7.3 illustrates the robustness of the correntropy technique by adding randomly occurring impulsive noise to the AM signal analysed in Fig. 7.2. The modulation peaks present in Fig. 7.2(e) can no longer be discerned in Fig. 7.3(e).

Figs. 7.4 and 7.5 show the performance of the centred correntropy by analysing the same AM signal distorted by impulsive noise, with different kernel sizes ($0.1\sigma_{opt}$ and $10\sigma_{opt}$, respectively). In both cases, the performance of the correntropy becomes significantly worse. As σ increases, the higher-order moments influence decay and the correntropy becomes more similar to the correlation signal. However, as σ decreases, the higher-order moments become more relevant in the correntropy and more peaks appear in the CSD, which makes it difficult to detect the respiratory and modulation peak.

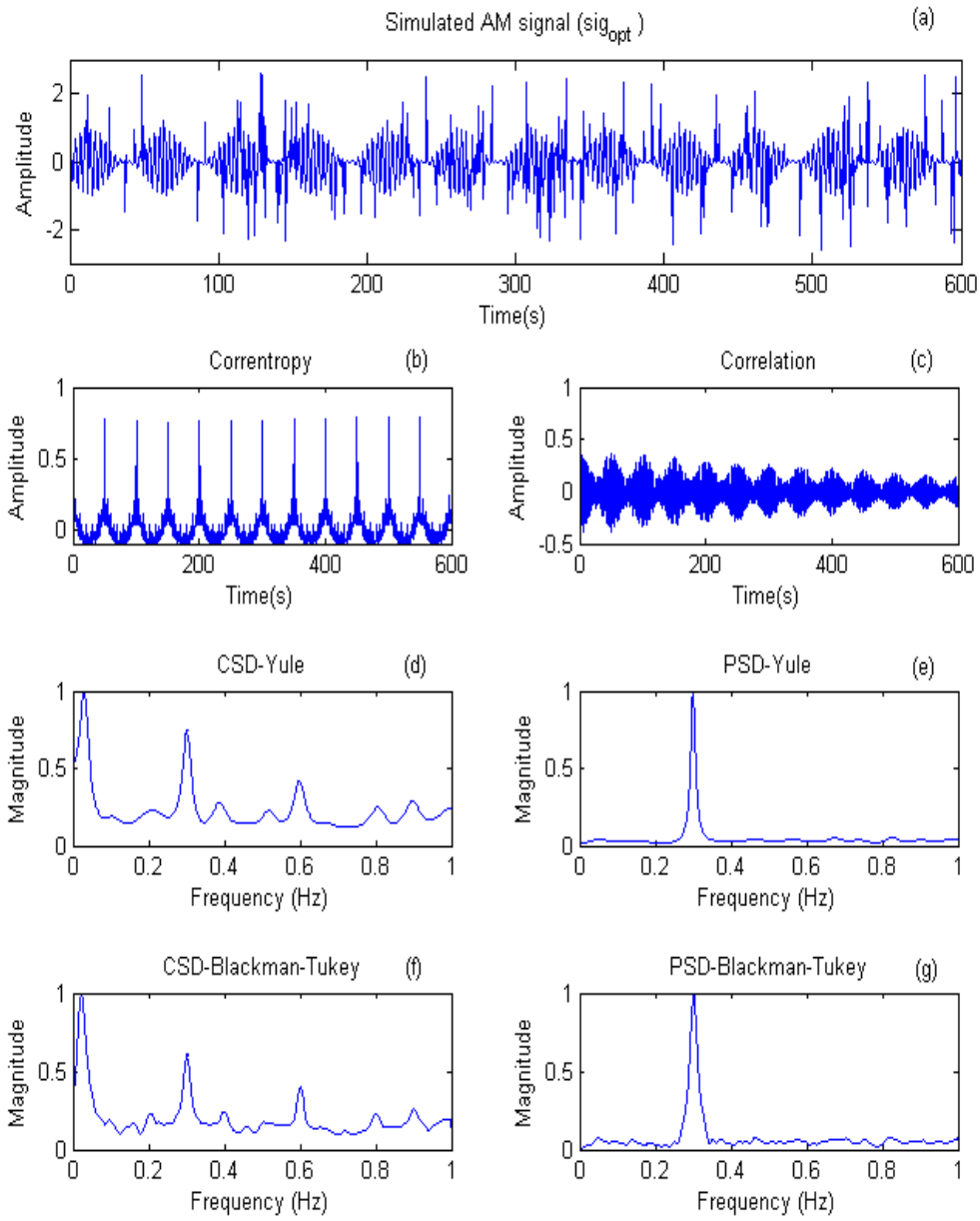

Figure 7.3 (a) The simulated AM signal (0.3 Hz carrier frequency, 0.02 Hz modulation frequency and $\mu = 1$) with some outliers randomly added, (b) its correntropy function computed with σ_{opt} and (c) its correlation function. The CSD obtained with (d) Yule–Walker's method and (f) Blackman-Tukey's method. The PSD obtained with (e) Yule–Walker's method and (g) Blackman-Tukey's method.

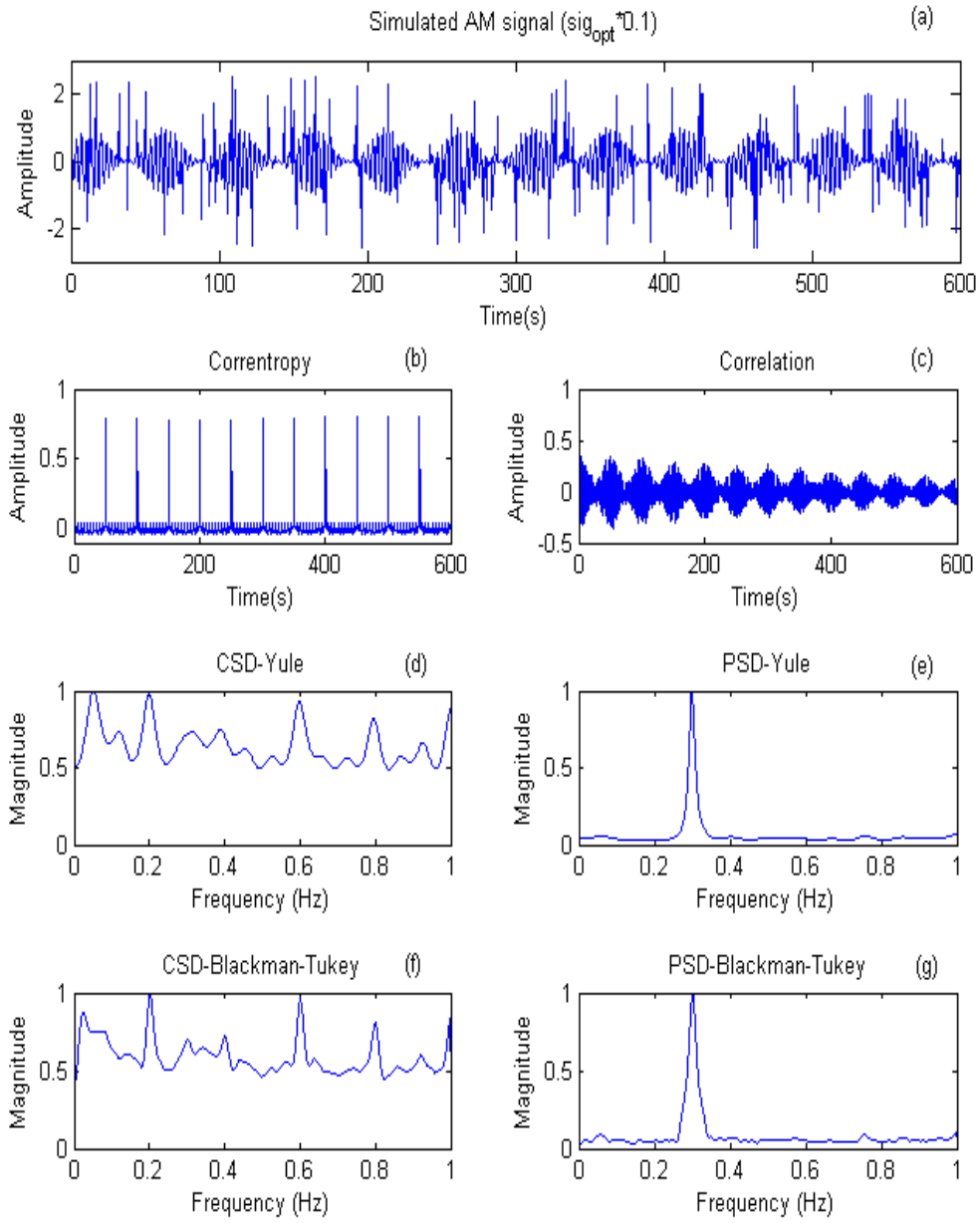

Figure 7.4 (a) The simulated AM signal (0.3 Hz carrier frequency, 0.02 Hz modulation frequency and $\mu = 1$) with some outliers randomly added, (b) its correntropy function computed with $0.1\sigma_{opt}$ and (c) its correlation function. The CSD obtained with (d) Yule–Walker's method and (f) Blackman-Tukey's method. The PSD obtained with (e) Yule–Walker's method and (g) Blackman-Tukey's method.

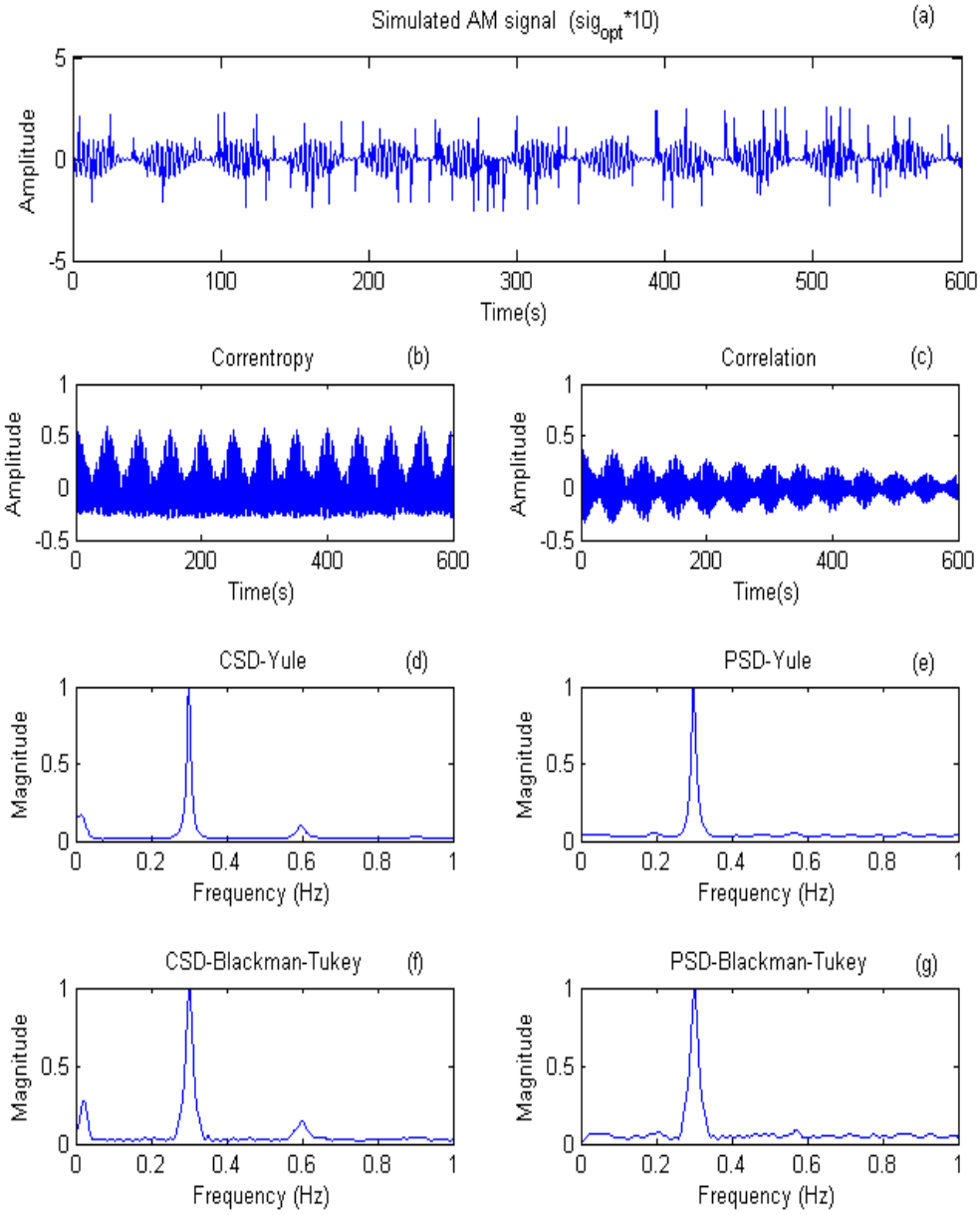

Figure 7.5 (a) The simulated AM signal (0.3 Hz carrier frequency, 0.02 Hz modulation frequency and $\mu = 1$) with some outliers randomly added, (b) its correntropy function computed with $10\sigma_{opt}$ and (c) its correlation function. The CSD obtained with (d) Yule–Walker's method and (f) Blackman-Tukey's method. The PSD obtained with (e) Yule–Walker's method and (g) Blackman-Tukey's method.

As shown in these figures, the selection of the kernel size has considerable influence on the correntropy performance when the signal is contaminated with impulsive noise. Since the respiratory flow signals contain a smaller amount of impulsive noise than in the above simulation, the selection of kernel size is less critical.

7.7.2 Real Signals

Spectral analysis is also performed on signals from CHF patients (Figs. 7.6–7.8) and a healthy subject (Fig. 7.9), to illustrate differences in respiratory patterns. The respiratory peak is clearly visible in both types of spectra. The correntropy-based spectra of the healthy subject (Fig. 7.9(d)) lacks a peak that corresponds to the modulation frequency, unlike the spectra of CHF patients. The PB patients present much more prominent modulation peaks (Figs. 7.6(d) and 7.7(d)) than the nPB patients (Fig. 7.8(d)). It is clear from these examples that the modulation frequency peak is easily detected in correntropy-based spectra, but not in correlation-based spectra. In fact, the latter type of spectrum does not even lend itself to sideband peak detection.

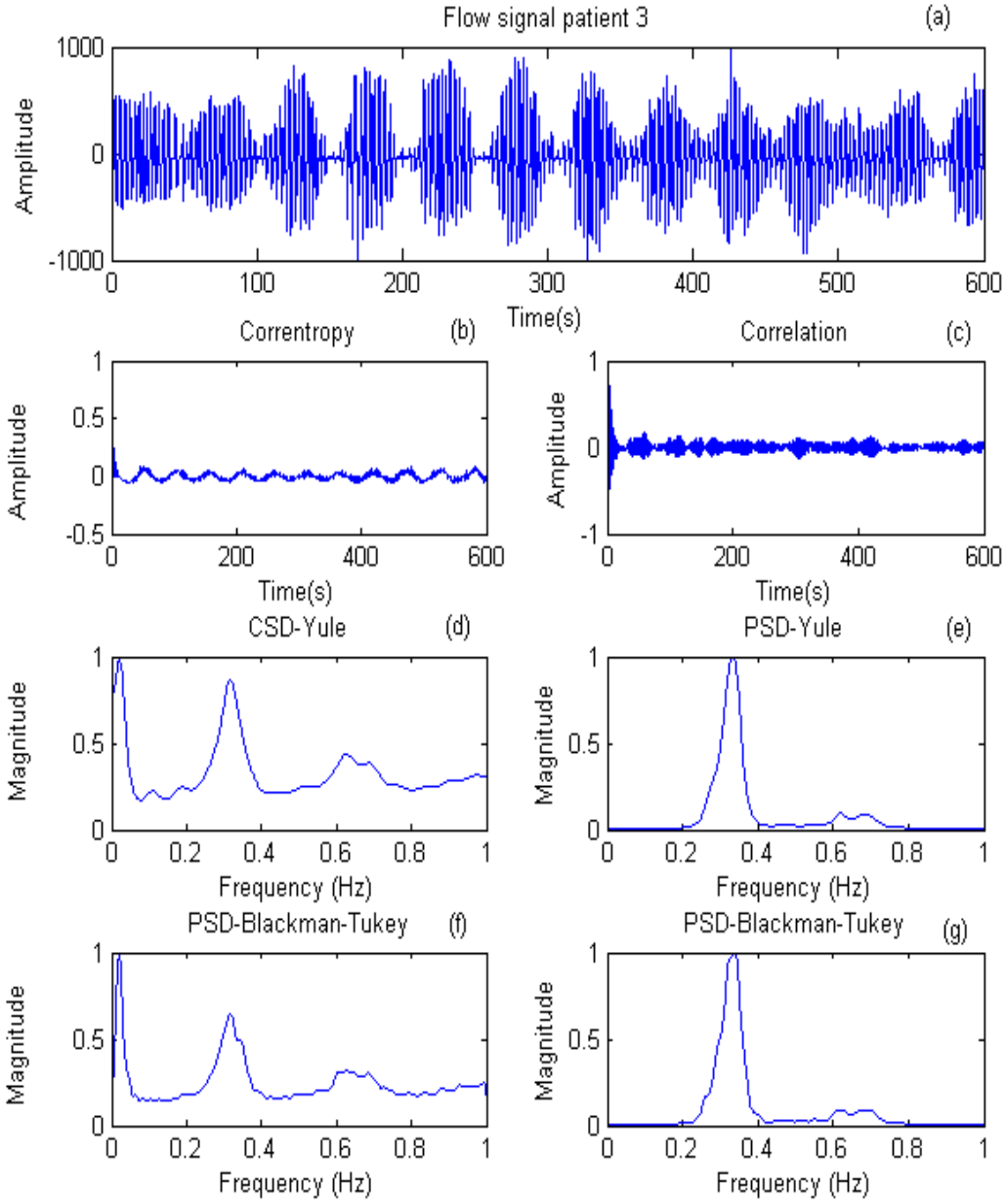

Figure 7.6 (a) The respiratory flow signal of a CSR patient, (b) its correntropy function, and (c) its correlation function. The CSD obtained with (d) Yule–Walker's method and (f) Blackman-Tukey's method. The PSD obtained with (e) Yule–Walker's method and (g) Blackman-Tukey's method.

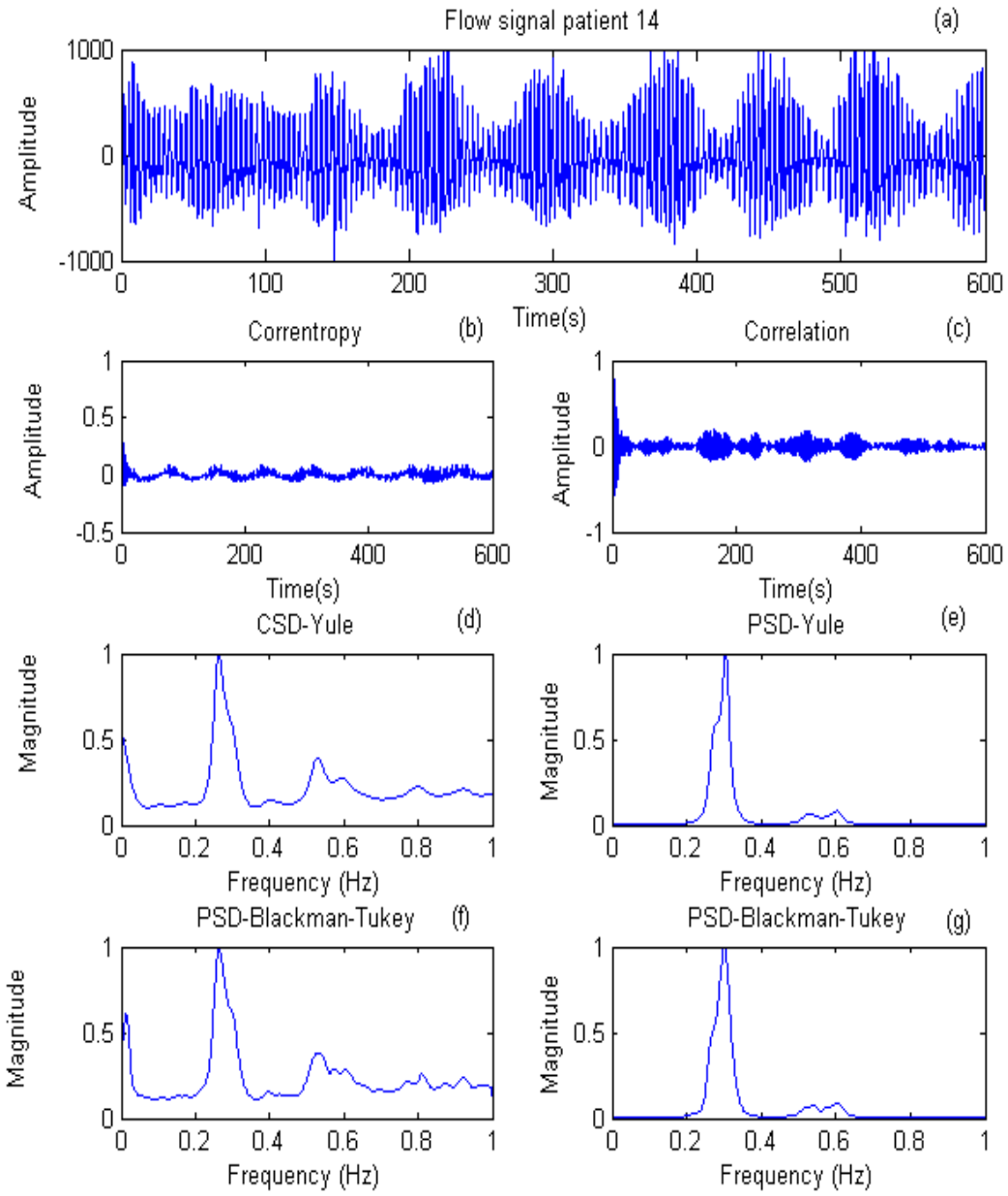

Figure 7.7 (a) The respiratory flow signal of a CHF patient with PB, (b) its correntropy function, and (c) its correlation function. The CSD obtained with (d) Yule–Walker's method and (f) Blackman-Tukey's method. The PSD obtained with (e) Yule–Walker's method and (g) Blackman-Tukey's method.

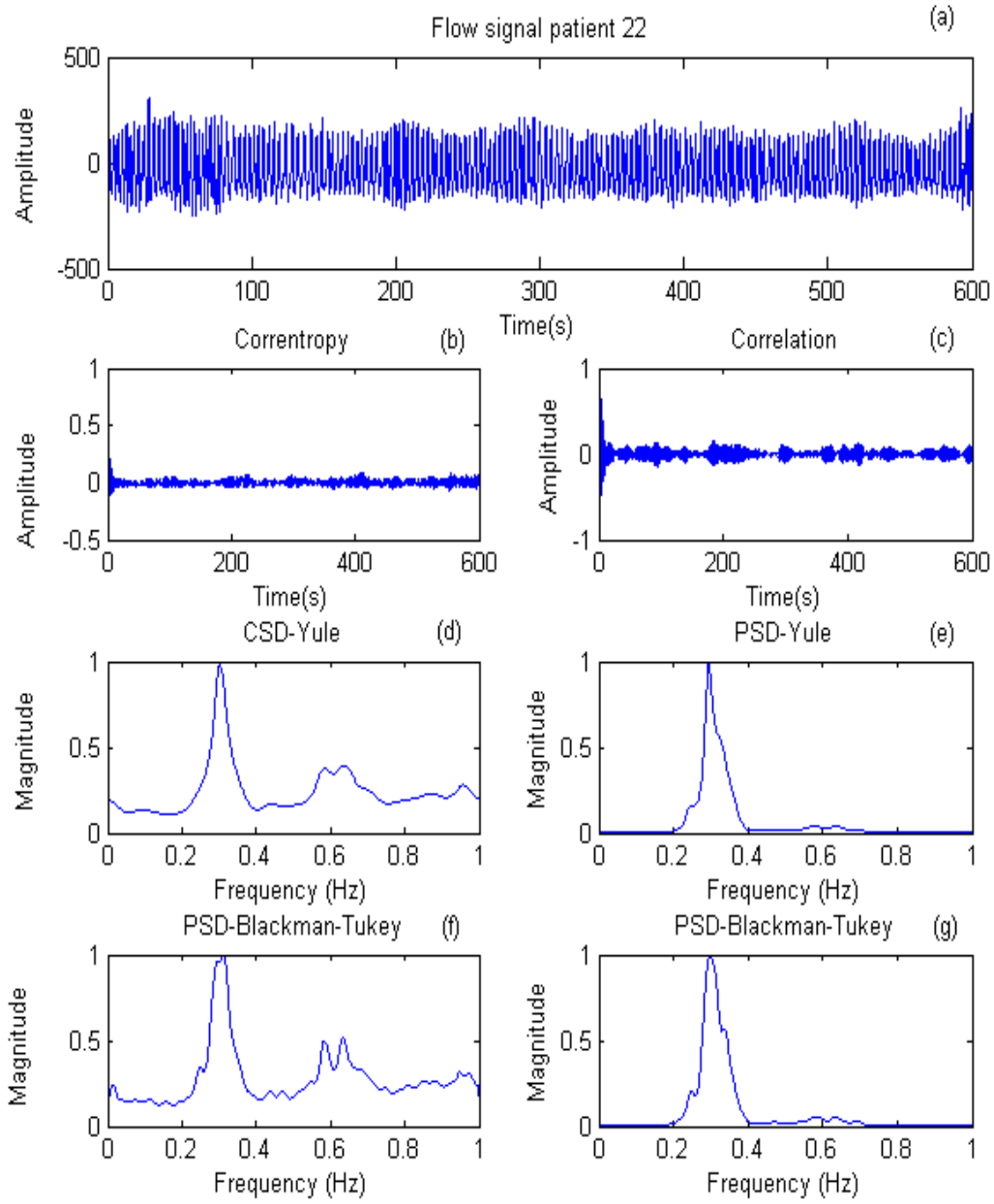

Figure 7.8 (a) The respiratory flow signal of a CHF patient with nPB, (b) its correntropy function, and (c) its correlation function. The CSD obtained with (d) Yule–Walker's method and (f) Blackman-Tukey's method. The PSD obtained with (e) Yule–Walker's method and (g) Blackman-Tukey's method.

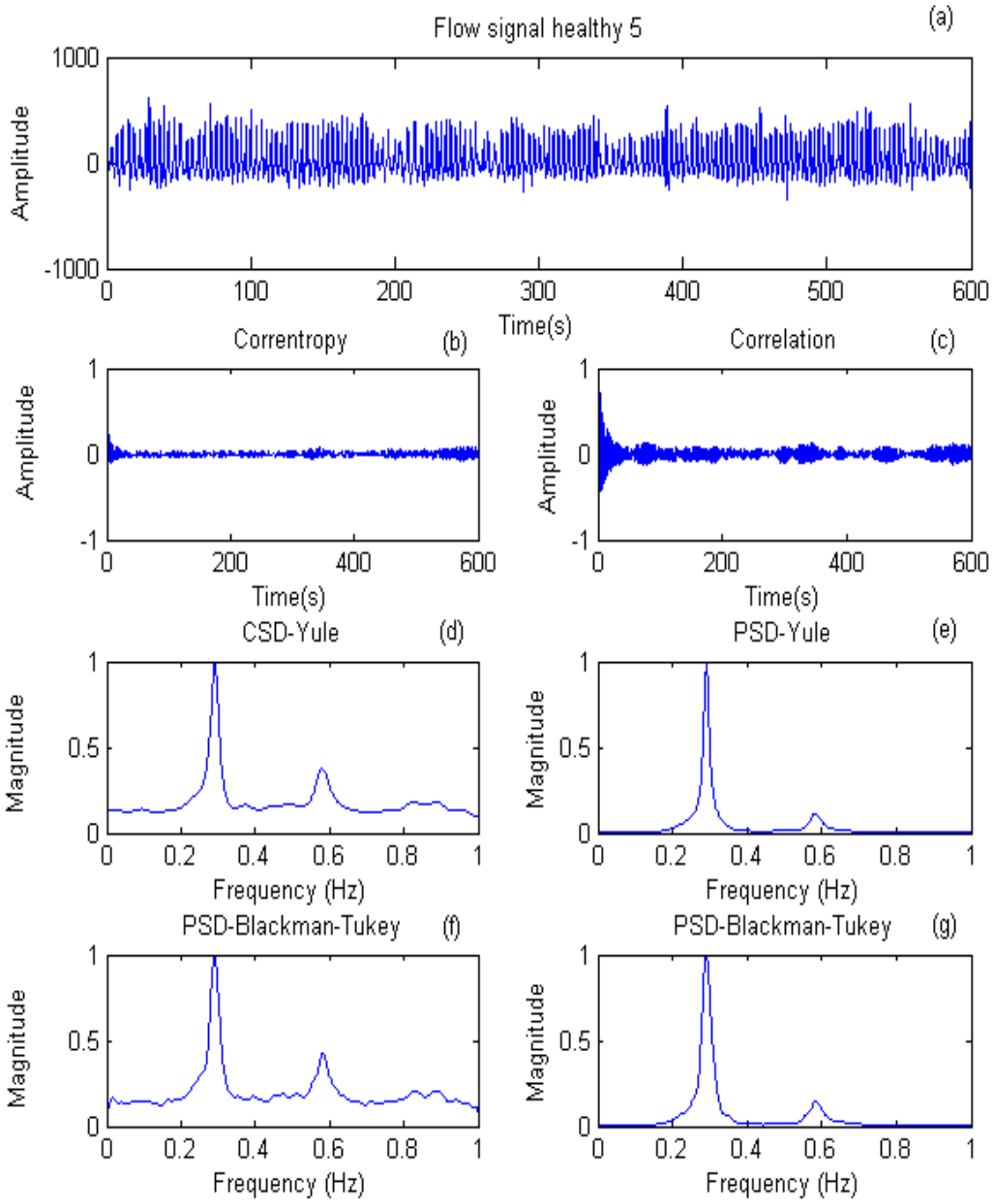

Figure 7.9 (a) The respiratory flow signal of a healthy subject, (b) its correntropy function, and (c) its correlation function. The CSD obtained with (d) Yule–Walker's method and (f) Blackman-Tukey's method. The PSD obtained with (e) Yule–Walker's method and (g) Blackman-Tukey's method.

7.7.3 Sensitivity to σ

The choice of σ is illustrated for an AM signal and a flow signal using the CSD, Fig. 7.10. The σ-value was chosen with reference to the optimal value σ_{opt} given by Silverman's rule. For the AM signal, it is obvious that the power of the modulation peak decreases as σ increases, i.e. $10\sigma_{opt}$, whereas the power of the spurious harmonics increases as σ decreases, i.e. $0.1\sigma_{opt}$. When these three σ-values are considered, the two peaks of interest are most easily detected for σ_{opt}. For the flow signal, similar behaviour is observed, although the changes in spectral shape are less pronounced for different values of σ than for the AM signal.

7.7.4 Performance evaluation

Table 7.2 presents the mean and the standard deviation of the most relevant parameters for each group of patients and healthy subjects, and Table 7.3 shows the p-value of each parameter for every classification.

Table 7.2 Mean and standard deviation of $\overline{V}$ and R for each group of subjects *

	$\overline{V}$	R_{Yule}	$\overline{P}_{Yule}$	$R_{Blackman}$	$\overline{P}_{Blackman}$
Healthy	0.12 ± 0.05	8.4 ± 8.4	0.61 ± 0.24	6.9 ± 2.0	2.39 ± 0.89
CHF	0.04 ± 0.02	9.2 ± 4.9	0.21 ± 0.08	9.3 ± 5.7	0.85 ± 0.30
PB	0.03 ± 0.01	14.2 ± 5.8	0.18 ± 0.06	15.6 ± 7.0	0.74 ± 0.24
nPB	0.04 ± 0.02	7.1 ± 2.4	0.22 ± 0.08	6.6 ± 1.8	0.89 ± 0.32

** The values have been multiplied by 100 for ease of legibility*

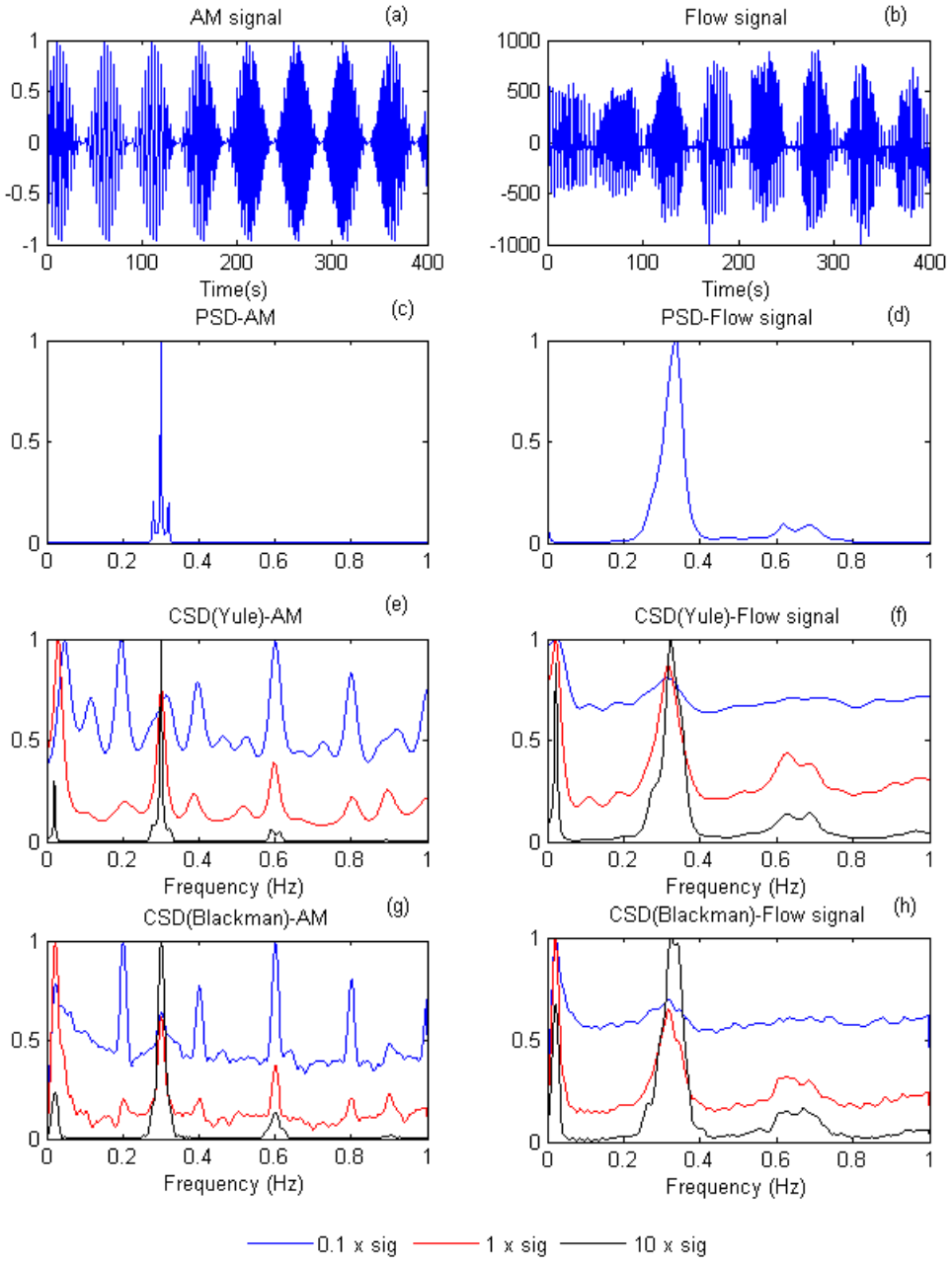

Figure 7.10 (a) A simulated AM signal and (b) a respiratory flow signal of a PB patient. Their respective (c), (d) PSDs, (e), (f) parametric CSDs and (g), (h) nonparametric CSDs evaluated all for the kernel values $0.1\sigma_{opt}$, σ_{opt}, and $10\sigma_{opt}$.

Table 7.3 p-value of the classifications: CHF patients versus healthy subjects, nPB patients versus healthy subjects, and PB versus nPB within the CHF patients

	$\overline{V}$	R_{Yule}	$\overline{P}_{Yule}$	$R_{Blackman}$	$\overline{P}_{Blackman}$
CHF vs. Healthy	$1.1 \cdot 10^{-10}$	$n.s.$	$1.0 \cdot 10^{-10}$	$n.s.$	$1.1 \cdot 10^{-10}$
nPB(CHF) vs. Healthy	$1.1 \cdot 10^{-8}$	$n.s.$	$8.9 \cdot 10^{-9}$	$n.s.$	$1.1 \cdot 10^{-8}$
nPB vs. PB (CHF)	$n.s.$	$2.1 \cdot 10^{-3}$	$n.s.$	$2.0 \cdot 10^{-4}$	$n.s.$

Table 7.4 Sensitivity (Sn), specificity (Sp) and accuracy (Acc) obtained with the best parameter for each classification using leave-one-out cross-validation

Classification	**Parameter**	**Sn**	**Sp**	**Acc**
CHF vs. Healthy	$\overline{V}$	96.3%	94.3%	95.2%
	$\overline{P}$	96.3%	94.3%	95.2%
nPB-CHF vs. Healthy	$\overline{V}$	94.7%	94.3%	94.4%
	$\overline{P}$	94.7%	94.3%	94.4%
PB vs. nPB (CHF)	R	75.0%	94.7%	88.9%

Table 7.4 shows the classification results obtained when only the most discriminative parameter is applied. The parameters derived from Blackman-Tukey and AR modelling provide very similar classification results. The accuracy obtained with the ratio (R) derived from the Blackman method $R_{Blackman}$ is slightly lower than that obtained with the ratio derived from the AR modelling R_{Yule}, (85.2% versus 88.9%). In general, the best classification results have been obtained with power-related spectral

parameters. However, the correntropy mean $\overline{V}$ and the correntropy spectral density mean $\overline{P}$ provide similar results when they are used to classify patients versus healthy subjects, and nPB patients versus healthy subjects (95.2% and 94.4%, respectively). When PB and nPB patients are classified within the CHF group, only the power-related spectral parameters are found to produce good results, with an accuracy of 88.9%.

Sensitivity to different values of σ is evaluated as described before for $0.1\sigma_{opt}, \sigma_{opt}$, and $10\sigma_{opt}$, with respect to the three classification tasks and involving only the most discriminative parameter. Fig. 7.11 and Table 7.5 present the ROC curve for the three classifications. The choice of σ is not critical for the classification, as the area under the ROC is essentially unchanged for the different values of σ. As shown in Figs. 7.4 and 7.5, the selection of kernel size has considerable influence on correntropy performance when the signal is contaminated with impulsive noise. Since the respiratory flow signal does not contain as large an amount of impulsive noise as in the above simulation, the selection of kernel size is less critical.

Table 7.5 Sensitivity of the kernel parameter σ in terms of the area under the ROC obtained for the best parameter for each classification

Area under the ROC	**Parameter**	$0.1\sigma_{opt}$	σ_{opt}	$10\sigma_{opt}$
CHF vs. Healthy	$\overline{V}$	0.98	0.98	0.98
	$\overline{P}$	0.98	0.98	0.96
nPB-CHF vs. Healthy	$\overline{V}$	0.97	0.97	0.98
	$\overline{P}$	0.98	0.98	0.96
PB vs. nPB (CHF)	R	0.70	0.88	0.90

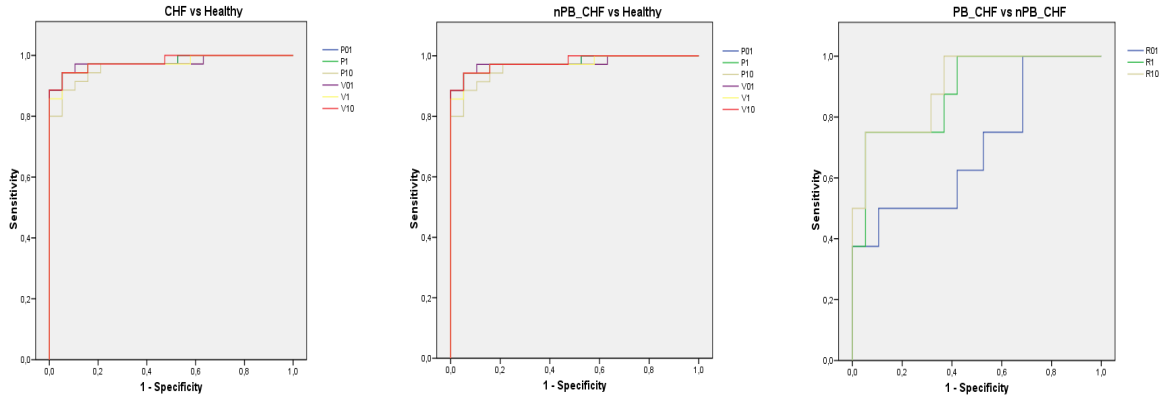

(a) (b) (c)

Figure 7.11 Sensitivity of the kernel parameter σ in terms of the area under the ROC obtained for the best parameters in the classification of (a) CHF patients vs. healthy subjects, (b) nPB patients vs. healthy subjects, and (c) PB vs. nPB within the CHF patients.

7.8 Conclusion

This chapter investigates the use of correntropy for the spectral characterization of respiratory patterns in CHF patients. In contrast to the conventional second-order correlation function, the correntropy function accounts for higher-order moments and is robust to outliers. As a result of the former property, respiratory and modulation frequencies appear at their actual locations along the frequency axis in the CSD (see Appendix A for an explanation of this property). Hence, correntropy circumvents problems that may arise when the modulation frequency peak is identified directly from the conventional PSD, due to insufficient spectral resolution. This problem is illustrated for the simulated AM signal. In addition, the use of correntropy eliminates the demodulation step, which was an integral part of our previous studies [38] and [39], as described in Chapter 6. In those studies, respiratory periodicity was detected from the envelope of the flow signal and various parameters were derived

from its time–frequency representation and used in the classification of respiratory patterns in CHF patients. Using a three-parameter procedure which involved the AR coefficients, an accuracy of 84.6% was achieved in classifying PB and nPB patients. Obviously, this result is inferior to the one achieved here, which had an accuracy of 88.9%. While this improvement is perhaps not dramatic, it is still of importance as the present classification is based on only one parameter instead of three. The inferior result of the previous study was primarily due to difficulties in identifying the modulation frequency.

Another attractive property of the correntropy function is its robustness against outliers, which is explained by the fact that the inner product is computed via the Gaussian kernel in the parameter space that tends to zero when outliers occur. Such robustness is essential in the analysis of respiratory signals, since they are frequently corrupted with noise and spike artefacts. In the present research, this property has meant that the pre-processing required for outlier rejection in our previous studies [38] and [39] could be completely eliminated without impairing the classification performance. Accordingly, the present method is considerably more efficient than our previous methods, from a computational perspective.

The choice of σ is found to be uncritical, as rather large changes in value do not greatly alter performance. Using Silverman's rule, the performance in terms of sensitivity and specificity remained essentially the same, even when the value was 10 times larger or 10 times smaller than the value given by the rule. However, a further increase of σ causes the importance of higher-order moments to decay much faster, so that correntropy approaches the second-order correlation, whereas a further decrease in σ leads to meaningless spectral estimation.

The proposed method is very simple in structure, as σ constitutes the only design

parameter. The model order, which would be treated as a design parameter by some [158] and [85], was fixed for all subjects once it had been estimated from the dataset. The chosen model order of 30 is, in fact, less critical as the classification performance was virtually identical when orders between 25 and 35 were used.

The main goal of this research has been to identify CHF patients' condition noninvasively by characterizing and classifying respiratory flow patterns from patients with PB and nPB. In general, the best results were achieved with CSD-related parameters that characterize the power in Δf_m and Δf_r, i.e., P_m and R. These parameters achieved the best results in all the classifications performed with CHF patients, including CSR patients, PB patients without apnea, and nPB patients. It should be noted that all patients, i.e. both PB and nPB, exhibit various degrees of periodicity depending on their condition, whereas healthy subjects have no pronounced periodicity.

Since patients with PB patterns exhibit a larger modulation peak in proportion to the respiratory peak than nPB patients, the ratio between the power in the modulation band and the respiration band is a suitable parameter for classifying PB and nPB patients. The promising classification results are explained by the fact that the CSD provides a clearer-cut representation of the modulation peak than the PSD. In general, CHF patients present an increased amplitude on ventilation, which is reflected in their respiratory flow signal. Since correntropy is based on the distance between samples, the correntropy mean is higher in healthy subjects than in CHF patients. Consequently, the mean of the spectral power that is based on correntropy is higher in healthy subjects. Therefore, the correntropy mean and the correntropy spectral density mean both provide excellent results in the classification of CHF and healthy subjects, as well as of nPB patients and healthy subjects (CHF vs. healthy

95.2%, and nPB vs. healthy 94.4%).

The main goal of most studies of breathing patterns in CHF patients differs from the present one, as other studies have focused on the prediction of mortality, e.g. by exploring the properties of heart rate variability with linear [159] and [160] and nonlinear techniques [161]. Consequently, it is difficult to compare the present results with those obtained in other studies.

The small size of the dataset is a limitation of the present study. Hence, although the results are promising, their significance needs to be further established using a larger set. As a consequence of the small size, we decided to investigate the performance of single-parameter linear classification only.

Chapter 8

Conclusions

This thesis research has mainly focused on the study and characterization of breathing patterns through the respiratory flow signal of patients on weaning trials from mechanical ventilation, and patients with chronic heart failure (CHF). Different studies have been developed to extract enhanced information about the respiratory pattern and cardiorespiratory interactions, to improve the weaning outcome in patients with mechanical ventilation and to help in the diagnosis of patients with CHF.

To study these two challenging problems, we have proposed a proper description of the breathing pattern by means of various classical signal processing techniques including time-frequency analysis, linear and nonlinear analysis, time-varying analysis, as well as innovative techniques that have not yet been used in the study of the respiratory signal, such as correntropy.

The first part of this research is related to the study of patients on weaning trials. We compare patients with successful trials, patients with unsuccessful trials and patients who successfully pass the trials but cannot maintain spontaneous breathing and require the reinstitution of mechanical ventilation in less than 48 hours.

New indices have been proposed that are based on the variability of breathing pattern and/or cardiorespiratory interactions to characterize these groups of patients and predict the weaning outcome. Pattern recognition algorithms and new support vector machine-based (SVM-based) feature selection have been implemented to extract the most robust indices for these patients, and to help in the assessment of the best time to extubate the patient. A reduction in weaning failure will decrease the distress suffered by reintubated patients and the mortality rate of patients on weaning trials.

The second part of this research is related to patients with CHF. A number of different techniques have been applied to recognize periodic breathing patterns, non-periodic breathing patterns and Cheyne-Stokes respiration. As reported in clinical practice, these patterns are related to the condition of CHF patients. Therefore, respiratory pattern characterization could help in the diagnosis and stratification of the CHF patients.

Different classification techniques have been evaluated and compared to estimate the best characterization of breathing pattern for each case. A multivariable statistical analysis has been developed to determine the most significant indices in the study of patients undergoing extubation and those with heart failure.

This dissertation contributes to the analysis of biomedical signals, specifically in these two challenging problems of clinical practice. The original contributions of this thesis focuses on the identification and automatic classification of respiratory patterns.

The small size of the datasets is a limitation of the present research. Therefore, the cross-validation technique is used throughout. Although the results are promising, their significance needs to be further established on a larger set.

8.1 Weaning readiness assessment

The study of respiratory pattern variability and cardiorespiratory interactions provided enhanced information about the weaning procedure. The use of signal processing techniques and pattern recognition enabled us to obtain new indices for the characterization of different respiratory patterns. Below, we summarize our contribution to the study of weaning procedure. In our first study [36] we proposed a method based on support vector machines to analyse respiratory pattern variability in patients during weaning trials. The respiratory pattern characterization was developed by means of a number of respiratory time series. Clustering and validation techniques enabled us to select the best subset of input features. Histogram equalization mapped the distribution of the selected features back to the distribution of the feature that gave the best classification result. Significant differences were found between patients who were capable of maintaining spontaneous breathing and those who failed to maintain spontaneous breathing. The results enabled us to consider SVM analysis as a missing method to study respiratory pattern variability in patients on weaning trials.

Numerous clinical indices have been proposed in the literature as weaning predictors [18] and [117]. Many of them are sufficiently sensitive, but most have low specificity, which leads to poor discrimination results. Thus, our second study [162] and [163] proposed a nonlinear procedure for studying cardiac and respiratory flow signals, to provide more robust and useful indices. The results showed that joint symbolic dynamics applied to time series of heart rate and respiratory frequency was suitable for the description of cardiorespiratory interactions of patients during the weaning trial process. An optimized SVM-based feature selection was implemented for unbalanced datasets, based on a new metric called the balance index B. This

procedure provided accurate results in the classification of different groups of patients, and maintained a good balance between sensitivity and specificity, even for unbalanced datasets.

Therefore, these methods could be suitable for reducing the number of patients who successfully pass the trial, but cannot maintain spontaneous breathing and need to be reintubated in less than 48 hours.

8.2 Chronic heart failure

The study and characterization of periodic breathing patterns, nonperiodic breathing patterns and Cheyne-Stokes respiration provide enhanced information for the prognosis of CHF patients. These patterns have been compared with the breathing pattern of healthy subjects. Periodic breathing could be used as a risk index and enable the automatic classification of CHF patients with different conditions and healthy subjects. Below we summarize our contribution to the study of periodic breathing in CHF patients.

Our first research [38] and [39] was based on the study of the envelope of the respiratory flow signal through a time-frequency analysis to characterize and discriminate respiratory patterns in these patients. As an extension of previous studies [79], various parameters were derived from the time-frequency characterization of the envelope and used to identify different respiratory patterns in CHF patients and healthy subjects. The temporal evolution of the respiratory flow patterns was studied through a time-varying AR modelling [41]. The statistical distribution is evaluated for each parameter derived from the time-varying respiratory pattern characterization, to identify the predominant pattern. The results enable us to consider power

related parameters of the respiratory envelope signal as powerful indices to identify periodic breathing. Additionally, time-varying modulation of the flow envelope signal provides accurate results in the characterization of the temporal evolution of these respiratory patterns.

The use of correntropy provides better classification results with only one parameter and eliminates the demodulation step, which was an integral part of our previous studies. The promising classification results are explained by the fact that the correntropy spectral density provides a more clear-cut representation of the modulation peak than the power spectral density. In general, CHF patients present an increased amplitude on ventilation, which is reflected in their respiratory flow signal. Since correntropy is based on the distance between samples, the correntropy mean is higher in healthy subjects than in CHF patients. Consequently, the mean of the correntropy-based spectral power is also higher in healthy subjects. Therefore, both the correntropy mean and the correntropy spectral density mean provide excellent results in the classification of CHF patients and healthy subjects, as well as that of nonperiodic breathing patients and healthy subjects.

8.3 Future extension

Future research could focus on implementing a continuous periodicity risk index for patients with CHF. The purpose of this index is to provide a percentage of periodicity for each subject, which might reflect the patient's condition. Moreover, as we have developed a time-varying method to characterize the signal, we could implement this index so that it is time-varying. By means of the time-varying periodicity index, we might be able to control the condition of the patient at each moment.

One limitation of the research is the small number of patients in the dataset. Therefore, one of the main objectives for the future is new database acquisition that includes not only the respiratory flow and ECG signals, but also the blood pressure signal. This database would enable the validation of all the studies developed in this thesis.

Since correntropy involves information on higher-order statistics and enables the detection of respiratory nonlinearities that conventional techniques based on second-order statistics cannot identify, another future goal is to exploit the nonlinear information provided by correntropy in CHF patients and healthy subjects, and compare the performance of this method with that of other nonlinear techniques.

The respiratory pattern of CHF patients has been characterized, but we have not studied cardiorespiratory interactions to date. A number of techniques could be used to characterize cardiorespiratory dynamics, such as joint symbolic dynamics and innovative cross-correntropy.

A final study should be carried out that includes all the relevant clinical information and all the significant indices. This would increase our knowledge of these patients and contribute to clinical practice.

Bibliography

[1] J.-M. Boles *et al.*, "Weaning from mechanical ventilation," Eur. Respir. J. **29,** 1033–1056 (2007).

[2] A. C. Guyton and J. E. Hall, *Textbook of Medical Physiology, 11th Edition*, 11 ed. (Elsevier Saunders, 2006).

[3] A. K. Jain, R. P. Duin, and J. Mao, "Statistical Pattern Recognition: A Review," IEEE Trans. Pattern Anal. Mach. Intell. **22,** 4–37 (2000).

[4] I. Kauppinen, J. Kauppinen, and P. Saarinen, "A method for long extrapolation of audio signals," J. Audio Eng. Soc. **49,** 1167–1180 (2001).

[5] A. Kulkarni and V. Agarwal, "Extubation failure in intensive care unit: Predictors and management," Indian J. Crit. Care. Med. **12,** 1–9 (2008).

[6] A. M. H. Valdivieso, Ph.D. thesis, Technical University of Catalonia (UPC), Barcelona, Spain, 2007.

[7] M. R. Miller *et al.*, "Standardisation of spirometry," Eur. Respir. J. **26,** 319–338 (2005).

[8] J. L. Hankinson, J. R. Odencrantz, and K. B. Fedan, "Spirometric Reference Values from a Sample of the General U.S. Population," Am. J. Resp. Critical Care Medicine **159,** 179–187 (1999).

[9] J. S. Aldás, P. C. Clará, J. C. Gómez, N. G. Mangado, L. P. Ballesteros, and J. R. Torrent, "Recomendaciones SEPAR: Espirometría forzada," Technical report, Sociedad Española de Neumología y Cirugía Torácica: SEPAR, Barcelona, Spain (2006) .

[10] P. Neumann, J. Zinserling, C. Haase, M. Sydow, and H. Burchardi, "Evaluation of Respiratory Inductive Plethysmography in Controlled Ventilation," Chest **113,** 443–451 (1998).

[11] N. O. Stromberg, G. O. Dahlback, and P. M. Gustafsson, "Evaluation of various models for respiratory inductance plethysmography calibration," J. Appl. Physiol. **74,** 1206–1211 (1993).

[12] P.-Y. Carry, P. Baconnier, A. Eberhard, P. Cotte, and G. Benchetrit, "Evaluation of Respiratory Inductive Plethysmography," Chest **111,** 910–915 (1997).

[13] G. C. White, *Basic Clinical Lab Competencies for Respiratory Care*, 4 ed. (Cengage Learning, 2002).

[14] L. Brochard, A. Rauss, S. Benito, G. Conti, J. Mancebo, N. Rekik, A. Gasparetto, and F. Lemaire, "Comparison of three methods of gradual withdrawal from ventilatory support during weaning from mechanical ventilation," Am. J. Resp. Critical Care Medicine **150,** 896–903 (1994).

[15] A. Esteban *et al.*, "A Comparison of Four Methods of Weaning Patients from Mechanical Ventilation," N. Engl. J. Med. **332,** 345–350 (1995).

[16] S. P. Stawicki, "Mechanical ventilation: Weaning and extubation," Opus 12 Scientist **1,** 13–16 (2007).

[17] N. R. MacIntyre, "Evidence-Based Guidelines for Weaning and Discontinuing Ventilatory Support*," Chest **120,** 375–396 (2001).

[18] M. Meade, G. Guyatt, D. Cook, L. Griffith, T. Sinuff, C. Kergl, J. Mancebo, A. Esteban, and S. Epstein, "Predicting Success in Weaning From Mechanical Ventilation*," Chest **120,** 400S–424S (2001).

[19] S. K. Epstein and R. L. Ciubotaru, "Independent Effects of Etiology of Failure and Time to Reintubation on Outcome for Patients Failing Extubation," Am. J. Resp. Critical Care Medicine **158,** 489–493 (1998).

[20] C. Seymour, A. Martinez, J. Christie, and B. Fuchs, "The outcome of extubation failure in a community hospital intensive care unit: a cohort study," Critical Care **8,** R322–R327 (2004).

[21] S. K. Epstein, R. L. Ciubotaru, and J. B. Wong, "Effect of Failed Extubation on the Outcome of Mechanical Ventilation," Chest **112,** 186–192 (1997).

[22] A. Esteban *et al.*, "Extubation Outcome after Spontaneous Breathing Trials with T-Tube or Pressure Support Ventilation," Am. J. Resp. Critical Care Medicine **156,** 459–465 (1997).

[23] M. J. Tobin, "Role and interpretation of weaning predictors," In *5th International Consensus Conference in Intensive Care Medicine: Weaning from Mechanical Ventilation*, (Budapest, 2006).

[24] A. Esteban *et al.*, "Effect of Spontaneous Breathing Trial Duration on Outcome of Attempts to Discontinue Mechanical Ventilation," Am. J. Resp. Critical Care Medicine **159,** 512–518 (1999).

[25] E. W. Ely, A. M. Baker, D. P. Dunagan, H. L. Burke, A. C. Smith, P. T. Kelly, M. M. Johnson, R. W. Browder, D. L. Bowton, and E. F. Haponik, "Effect on the Duration of Mechanical Ventilation of Identifying Patients Capable of Breathing Spontaneously," N. Engl. J. Med. **335,** 1864–1869 (1996).

[26] I. Vallverdu, N. Calaf, M. Subirana, A. Net, S. Benito, and J. Mancebo, "Clinical Characteristics, Respiratory Functional Parameters, and Outcome of a Two-Hour T-Piece Trial in Patients Weaning from Mechanical Ventilation," Am. J. Resp. Critical Care Medicine **158,** 1855–1862 (1998).

[27] J. A. Farias *et al.*, "A comparison of two methods to perform a breathing trial before extubation in pediatric intensive care patients," Intensive Care Med. **27,** 1649–1654 (2001).

[28] M. J. Tobin, "Of Principles and Protocols and Weaning," Am. J. Resp. Critical Care Medicine **169,** 661–662 (2004).

[29] J. P. Casaseca, M. Martin-Fernandez, and C. Alberola-Lopez, "Weaning from Mechanical Ventilation: a Multimodal Signal Analysis," IEEE Trans. Biomed. Eng. **53,** 1330–1345 (2006).

[30] A. Jubran, B. J. B. Grant, F. Laghi, S. Parthasarathy, and M. J. Tobin, "Weaning Prediction: Esophageal Pressure Monitoring Complements Readiness Testing," Am. J. Resp. Critical Care Medicine **171,** 1252–1259 (2005).

[31] C. S. Sassoon and C. K. Mahutte, "Airway occlusion pressure and breathing pattern as predictors of weaning outcome," Am. Rev. Respir. Dis. p. 148:860 (1993).

[32] B. Mauo-Ying, H. Shu-Shya, Y. Huey-Wen, K. Benjamin Ing-Tiau, L. Yu-Ting, W. Jia-Horng, and K. Yu Ru, "Breathing pattern variability: a weaning predictor in postoperative patients recovering from systemic inflammatory response syndrome," Intensive Care Med. **30,** 241–248 (2004).

[33] M. Engoren, "Approximate entropy of respiratory rate and tidal volume during weaning from mechanical ventilation.," Crit. Care Med. **26,** 1817–1840 (1998).

[34] L. H. I. Preas, A. Jubran, R. W. Vandivier, D. Reda, P. J. Godin, S. M. Banks, M. J. Tobin, and A. F. Suffredini, "Effect of Endotoxin on Ventilation and Breath Variability . Role of Cyclooxygenase Pathway," Am. J. Resp. Critical Care Medicine **164,** 620–626 (2001).

[35] M. J. Tobin, "Breathing pattern analysis," Intensive Care Med. **18,** 193–201 (1992).

[36] B. Giraldo, A. Garde, C. Arizmendi, R. Jané, S. Benito, I. Diaz, and D. Ballesteros, "Support Vector Machine Classification Applied on Weaning Trials Patients," In *Engineering in Medicine and Biology Society, 2006. EMBS '06. 28th Annual International Conference of the IEEE*, pp. 5587–5590 (2006).

[37] B. F. Giraldo, C. Arizmendi, E. Romero, R. Alquezar, P. Caminal, S. Benito, and D. Ballesteros, "Patients on Weaning Trials from Mechanical Ventilation Classified with Neural Networks and Feature Selection," In *Engineering in Medicine and Biology Society, 2006. EMBS'06. 28th Annual International Conference of the IEEE*, pp. 2195–2198 (2006).

[38] A. Garde, B. Giraldo, R. Jané, I. Diaz, S. Herrera, S. Benito, M. Domingo, and A. Bayes-Genis, "Analysis of respiratory flow signals in chronic heart failure patients with periodic breathing," In *Proc. IEEE Conf. Eng. Med. Biol.*, pp. 307–310 (2007).

[39] A. Garde, B. F. Giraldo, R. Jané, I. Diaz, S. Herrera, S. Benito, M. Domingo, and A. Bayes-Genis, "Characterization of periodic and non-periodic breathing pattern in chronic heart failure patients," In *Proc. IEEE Conf. Eng. Med. Biol.*, pp. 3227–3230 (2008).

[40] J. G. Van den Aardweg and J. M. Karemaker, "Influence of Chemoreflexes on Respiratory Variability in Healthy Subjects," Am. J. Resp. Critical Care Medicine **165,** 1041–1047 (2002).

[41] A. Garde, B. F. Giraldo, R. Jané, and L. Sörnmo, "Time-varying respiratory pattern characterization in chronic heart failure patients and healthy subjects," In *Engineering in Medicine and Biology Society, 2009. EMBC'09. Annual International Conference of the IEEE*, pp. 4007–4010 (Minneapolis, Minnesota, USA, 2009).

[42] J. P. Martinez, R. Almeida, S. Olmos, A. P. Rocha, and P. Laguna, "A wavelet-based ECG delineator: evaluation on standard databases," IEEE Trans. Biomed. Eng. **51,** 570–581 (2004).

[43] B. P. Marchant, "Time-frequency Analysis for Biosystems Engineering," Biosystems Engineering **85,** 261–281 (2003).

[44] E. N. Bruce, "Temporal variations in the pattern of breathing," J. Appl. Physiol **80,** 1079–1087 (1996).

[45] T. Brack, A. Jubran, and M. J. Tobin, "Dyspnea and Decreased Variability of Breathing in Patients with Restrictive Lung Disease," Am. J. Resp. Critical Care Medicine **165,** 1260–1264 (2002).

[46] J. S. Richmann and J. R. Moorman, "Physiological time-series analysis using approximate entropy and sample entropy," Am. J. Physiol- Heart Circ Physiol **278,** 2039–2049 (2000).

[47] D. E. Lake, J. S. Richman, M. P. Griffin, and J. R. Moorman, "Sample entropy analysis of neonatal heart rate variability," Am. J. Physiol. Regul. Integr. Comp. Physiol. **283,** 789–797 (2002).

[48] M. El-Khatib, G. Jamaleddine, R. Soubra, and M. Muallem, "Pattern of spontaneous breathing: potential marker for weaning outcome," Intensive Care Med. **27,** 52–58 (2001).

[49] P. Caminal, M. Vallverdu, B. Giraldo, S. Benito, G. Vazquez, and A. Voss, "Optimized symbolic dynamics approach for the analysis of the respiratory pattern," IEEE Trans. Biomed. Eng. **52,** 1832–1839 (2005).

[50] P. Casaseca-de-la Higuera, F. Simmross-Wattenberg, M. Martin-Fernandez, and C. Alberola-Lopez, "A Multichannel Model-Based Methodology for Extubation Readiness Decision of Patients on Weaning Trials," IEEE Trans. Biomed. Eng. **56,** 1849–1863 (2009).

[51] J.-C. Hsu, Y.-F. Chen, H.-H. Lin, C.-H. Li, and X. Jiang, "Construction of Prediction Module for Successful Ventilator Weaning," Lecture Notes in Computer Science pp. 766–775 (2007).

[52] P. C. de la Higuera, R. de Luis-García, F. S. Wattenberg, and C. A. López, "Weaning from mechanical ventilation: Feature extraction from a statistical signal processing viewpoint," In *Eur. Signal Process. Conf. (EUSIPCO)*, (Antalya, Turkey, 2005).

[53] I. Cygankiewicz, W. Zareba, and A. B. de Luna, "Prognostic value of Holter monitoring in congestive heart failure," Cardiol. J. **15,** 313–23 (2008).

[54] S. Neubauer, "The failing heart–an engine out of fuel," N. Engl. J. Med. **356,** 1140–1151 (2007).

[55] M. Dayer and M. R. Cowie, "Heart failure: diagnosis and healthcare burden," Clin. Med. **4,** 13–18 (2004).

[56] N. Cherniack and G. Longobardo, "Abnormalities in respiratory rhythm," Handbook of Physiology. The Respiratory System. Control of breathing **2,** 729–749 (1986).

[57] T. Yajima, A. Koike, K. Sugimoto, Y. Miyahara, F. Marumo, and M. Hiroe, "Mechanism of periodic breathing in patients with cardiovascular disease," Chest **106,** 142–146 (1994).

[58] P. Agostoni, A. Apostolo, and R. K. Albert, "Mechanisms of Periodic Breathing During Exercise in Patients With Chronic Heart Failure*," Chest **133,** 197–203 (2008).

[59] G. Lorenzi-Filho, P. R. Genta, A. C. Figueiredo, and D. Inoue, "Cheyne-Stokes respiration in patients with congestive heart failure: causes and consequences," Clinics **60,** 333–344 (2005).

[60] D. P. Francis, K. Willson, L. C. Davies, A. J. Coats, and M. Piepoli, "Quantitative general theory for periodic breathing in chronic heart failure and its clinical implications," Circulation **102,** 2214–2221 (2000).

[61] G. D. Pinna, R. Maestri, A. Mortara, P. Johnson, T. Witkowski, P. Ponikowski, D. Andrews, S. Capomolla, M. T. La Rovere, and P. Sleight, "Nocturnal periodic breathing is an independent predictor of cardiac death and multiple hospital admissions in Heart failure," In *Proc. Computers in Cardiology*, **33,** 837–840 (2006).

[62] M. Guazzi, M. Samaja, R. Arena, M. Vicenzi, and M. D. Guazzi, "Long-Term Use of Sildenafil in the Therapeutic Management of Heart Failure," J. Am. Coll. Cardiol. **50,** 2136–2144 (2007).

[63] R. Poletti, C. Passino, L. Zyw, A. Giannoni, C. Prontera, F. Bramanti, A. Clerico, M. Piepoli, and M. Emdin, "Risk factors and prognostic value of daytime Cheyne-Stokes respiration in chronic heart failure patients," Int. J. Cardiol. **137,** 47–53 (2009).

[64] U. Corra, M. Pistono, A. Mezzani, A. Braghiroli, A. Giordano, P. Lanfranchi, E. Bosimini, M. Gnemmi, and P. Giannuzzi, "Sleep and Exertional Periodic Breathing in Chronic Heart Failure: Prognostic Importance and Interdependence," Circulation **113,** 44–50 (2006).

[65] S. Chakko and M. Gheorghiade, "Estimating severity of chronic heart failure: a clinical challenge for the 1990s," Am. Heart. J. **124,** 260–264 (1992).

[66] G. D. Pinna, R. Maestri, A. Mortara, M. T. La Rovere, F. Fanfulla, and P. Sleight, "Periodic breathing in heart failure patients: testing the hypothesis of instability of the chemoreflex loop," J. Appl. Physiol. **89,** 2147–2157 (2000).

[67] P. Ponikowski, S. D. Anker, T. P. Chua, D. Francis, W. Banasiak, P. A. Poole-Wilson, A. J. Coats, and M. Piepoli, "Oscillatory breathing patterns during wakefulness in patients with chronic heart failure: clinical implications and role of augmented peripheral chemosensitivity," Circulation **100,** 2418–2424 (1999).

[68] J. P. Ribeiro, "Periodic breathing in heart failure: bridging the gap between the sleep laboratory and the exercise laboratory," Circulation **113,** 9–10 (2006).

[69] G. R. H. Sandercock and D. A. Brodie, "The Role of Heart Rate Variability in Prognosis for Different Modes of Death in Chronic Heart Failure," Pacing Clin. Electrophysiol. **29,** 892–904 (2006).

[70] A. Vazir, M. Dayer, P. C. Hastings, H. F. McIntyre, M. Y. Henein, P. A. Poole-Wilson, M. R. Cowie, M. J. Morrell, and A. K. Simonds, "Can heart rate variation rule out sleep-disordered breathing in heart failure?," Eur. Resp. J. **27,** 571–577 (2006).

[71] P. J. Hanly and N. S. Zuberi-Khokhar, "Increased mortality associated with Cheyne-Stokes respiration in patients with congestive heart failure," Am. J. Resp. Critical Care Medicine **153,** 272–276 (1996).

[72] S. Javaheri, T. J. Parker, J. D. Liming, W. S. Corbett, H. Nishiyama, L. Wexler, and G. A. Roselle, "Sleep apnea in 81 ambulatory male patients with stable heart failure. Types and their prevalences, consequences, and presentations," Circulation **97,** 2154–2159 (1998).

[73] Y. Kaneko, J. S. Floras, K. Usui, J. Plante, R. Tkacova, T. Kubo, S. Ando, and T. D. Bradley, "Cardiovascular effects of continuous positive airway pressure in patients with heart failure and obstructive sleep apnea," N. Engl. J. Med. **348,** 1233–1241 (2003).

[74] D. R. Mansfield, N. C. Gollogly, D. M. Kaye, M. Richardson, P. Bergin, and M. T. Naughton, "Controlled trial of continuous positive airway pressure in obstructive sleep apnea and heart failure," Am. J. Resp. Critical Care Medicine **169,** 361–366 (2004).

[75] A. Mortara, P. Sleight, G. D. Pinna, R. Maestri, A. Prpa, M. T. La Rovere, F. Cobelli, and L. Tavazzi, "Abnormal awake respiratory patterns are common in chronic heart failure and may prevent evaluation of autonomic tone by measures of heart rate variability," Circulation **96,** 246–252 (1997).

[76] U. Corra, A. Giordano, E. Bosimini, A. Mezzani, M. Piepoli, A. J. Coats, and P. Giannuzzi, "Oscillatory ventilation during exercise in patients with chronic heart failure: clinical correlates and prognostic implications," Chest **121,** 1572–1580 (2002).

[77] T. Brack, I. Th uer, C. F. Clarenbach, O. Senn, G. Noll, E. W. Russi, and K. E. Bloch, "Daytime Cheyne-Stokes Respiration in Ambulatory Patients With Severe Congestive Heart Failure Is Associated With Increased Mortality*," Chest **132,** 1463–1471 (2007).

[78] R. Maestri *et al.*, "Nonlinear indices of heart rate variability in chronic heart failure patients: redundancy and comparative clinical value," J. Cardiovasc. Electrophysiol. **18,** 425–33 (2007).

[79] A. Garde, L. Sörnmo, R. Jané, and B. F. Giraldo, "Breathing Pattern Characterization in Chronic Heart Failure Patients using Respiratory Flow Signal," Ann. Biomed. Eng (2010).

[80] A. M. Bianchi, L. Mainardi, E. Petrucci, M. G. Signorini, M. Mainardi, and S. Cerutti, "Time-variant power spectrum analysis for the detection of transient episodes in HRV signal," IEEE Trans. Biomed. Eng. **40,** 136–144 (1993).

[81] I. Santamaria, P. P. Pokharel, and J. C. Principe, "Generalized correlation function: definition, properties, and application to blind equalization," IEEE Trans. Sig. Proc. **54,** 2187–2197 (2006).

[82] W. Liu, P. P. Pokharel, and J. C. Principe, "Correntropy: properties and applications in non-Gaussian signal processing," IEEE Trans. Sig. Proc. **55,** 5286–5298 (2007).

[83] A. Garde, L. Sörnmo, R. Jané, and B. F. Giraldo, "Correntropy-based analysis of respiratory patterns in patients with chronic heart failure," In *Engineering in Medicine and Biology Society, 2009. EMBC'09. Annual International Conference of the IEEE*, pp. 4687–4690 (Minneapolis, Minnesota, USA, 2009).

[84] A. Garde, L. Sörnmo, R. Jané, and B. F. Giraldo, "Correntropy-based Spectral Characterization of Respiratory Patterns in Patients with Chronic Heart Failure," IEEE Trans. Biomed. Eng. pp. 1–9 (2010).

[85] L. Sörnmo and P. Laguna, *Bioelectrical Signal Processing in Cardiac and Neurological Applications* (Elsevier/Academic Press, Amsterdam, 2005).

[86] R. O. Duda, P. E. Hart, and D. G. Stork, *Pattern Classification (2nd Edition)*, 2 ed. (Wiley-Interscience, 2000).

[87] B. D. Ripley and N. L. Hjort, *Pattern Recognition and Neural Networks* (Cambridge University Press, New York, NY, USA, 1995).

[88] R. J. Schalkoff, *Pattern Recognition: Statistical, Structural and Neural Approaches* (Wiley, 1991).

[89] J. Luque, R. Morros, A. Garde, J. Anguita, M. Farrús, D. Macho, F. Marqués, C. Martínez, V. Vilaplana, and J. Hernando, "Audio, video and multimodal person identification in a smart room," Lecture Notes in Computer Science **4122,** 258–269 (2007).

[90] V. N. Vapnik, "Pattern recognition using generalized portrait method," Automation and Remote Control **24,** 774–780 (1963).

[91] B. Scholkopf and A. J. Smola, *Learning with Kernels: Support Vector Machines, Regularization, Optimization, and Beyond* (MIT Press, Cambridge, MA, USA, 2002).

[92] G. Georgoulas, D. Stylios, and P. Groumpos, "Predicting the risk of metabolic acidosis for newborns based on fetal heart rate signal classification using support vector machines," IEEE Trans. Biomed. Eng. **53,** 875–884 (2006).

[93] C. J. C. Burges, "A Tutorial on Support Vector Machines for Pattern Recognition," Data Min. Knowl. Discov. **2,** 121–167 (1998).

[94] N. Cristianini and J. Shawe-Taylor, *An introduction to support vector machines: and other kernel based learning methods* (Cambridge University Press, Amsterdam, 2000).

[95] E. Osuna, R. Freund, and F. Girosi, "Support Vector Machines: Training and Applications," Technical report, Cambridge, MA, USA (1997) .

[96] C. Cortes and V. Vapnik, "Support-Vector Networks," In *Machine Learning*, pp. 273–297 (1995).

[97] J. Mercer, "Functions of Positive and Negative Type, and their Connection with the Theory of Integral Equations," Philosophical Transactions of the Royal Society of London. Series A, Containing Papers of a Mathematical or Physical Character **209,** 415–446 (1909).

[98] A. Temko, Ph.D. thesis, Technical University of Catalonia (UPC), Barcelona, Spain, 2008.

[99] M. Sokolova, N. Japkowicz, and S. Szpakowicz, "Beyond Accuracy, F-Score and ROC: A Family of Discriminant Measures for Performance Evaluation," Advances in Artificial Intelligence pp. 1015–1021 (2006).

[100] A. Jain and D. Zongker, "Feature Selection: Evaluation, Application, and Small Sample Performance," IEEE Trans. Pattern Anal. Mach. Intell. **19,** 153–158 (1997).

[101] X. Qiao and Y. Liu, "Adaptive Weighted Learning for Unbalanced Multicategory Classification," Biometrics **65,** 159–168 (2008).

[102] A. B. Owen, "Infinitely Imbalanced Logistic Regression," J. Mach. Learn. Res. **8,** 761–773 (2007).

[103] N. V. Chawla and N. Japkowicz, "Editorial: Special Issue on Learning from Imbalanced Data Sets," SIGKDD Explorations 6 (2004).

[104] N. Japkowicz and S. Stephen, "The class imbalance problem: A systematic study," Intell. Data Anal. **6,** 429–449 (2002).

[105] M. A. Maloof, "Learning when data sets are imbalanced and when costs are unequal and unknown," In *ICML-2003 Workshop on Learning from Imbalanced Data Sets II*, (2003).

[106] Y. Zhao and Q. He, "An unbalanced dataset classification approach based on v-Support Vector Machine," In *WCICA-2006, Proc. of the Sixth World Congress on Intelligent Control and Automation*, pp. 10496–10501 (2006).

[107] T. Eitrich and B. Lang, "Parallel tuning of support vector machine learning parameters for large and unbalanced data sets," Lecture Notes in Computer Science **3695/2005,** 253–264 (2005).

[108] T. Eitrich and B. Lang, "Efficient optimization of support vector machine learning parameters for unbalanced datasets," J. Comput. Appl. Math. **196,** 425–436 (2006).

[109] A. Esteban *et al.*, "Noninvasive Positive-Pressure Ventilation for Respiratory Failure after Extubation," N. Engl. J. Med. **350,** 2452–2460 (2004).

[110] M. J. Tobin, "Advances in mechanical ventilation.," N. Engl. J. Med. **344,** 1986–1996 (2001).

[111] F. Hilger, Ph.D. thesis, RWTH Aachen University, Aachen, Germany, 2004.

[112] P. Ejarque, A. Garde, J. Anguita, and J. Hernando, "On the use of genuine-impostor statistical information for score fusion in multimodal biometrics," Annals of Telecommunications, Special Issue on Multimodal Biometrics **62,** 109–129 (2006).

[113] M. Farrus, A. Garde, P. Ejarque, J. Luque, and J. Hernando, "On the Fusion of Prosody, Voice Spectrum and Face Features for Multimodal Person Verification," In *Proceedings of the 9th International Conference on Spoken Language Processing ICSLP 2006*, (Pittsburgh, PA, USA, 2006).

[114] A. Voss, S. Schulz, R. Schroeder, M. Baumert, and P. Caminal, "Methods derived from nonlinear dynamics for analysing heart rate variability," Philosophical Transactions of the Royal Society, A: Mathematical, Physical and Engineering Sciences **367,** 277–296 (2008).

[115] A. Voss, V. Baier, S. Schulz, and K. J. Bar, "Linear and nonlinear methods for analyses of cardiovascular variability in bipolar disorders," Bipolar Disorders **8,** 441–452 (2006).

[116] M. Baumert, T. Walther, J. Hopfe, R. Stepan, R. Faber, and A. Voss, "Joint symbolic dynamic analysis of beat to beat interactions of heart rate and systolic blood pressure in normal pregnancy," Med. Biol. Eng. Comput. **10,** 241–245 (2002).

[117] G. Conti, M. Luca, M. A. Pennisi, F. Cavaliere, A. Arcangeli, M. G. Bocci, R. Proietti, and M. Antonelli, "A prospective, blinded evaluation of indexes proposed to predict weaning from mechanical ventilation," Intensive Care Med. **30,** 830–836 (2004).

[118] K. Roth, I. Kauppinen, P. A. A. Esquef, and V. Valimaki, "Frequency warped Burg's method for AR-modeling," In *Applications of Signal Processing to Audio and Acoustics, 2003 IEEE Workshop on.*, pp. 5–8 (2003).

[119] Y. Rosen and B. Porat, "The second-order moments of sample covariances for time series with missing observations," IEEE Trans. Info. Theory. **35,** 334–341 (1989).

[120] H. Liang, S. Lukkarinen, and I. Hartimo, "Heart sound segmentation algorithm based on heart sound envelogram," In *Proc. Computers in Cardiology*, pp. 105–108 (1997).

[121] J. Martínez-Alajarín and R. Ruiz-Merino, "Efficient method for events detection in phonocardiographic signals," In *Proceedings-SPIE the international society for optical engineering*, **5839,** 398–409 (International Society for Optical Engineering, USA, 2005).

[122] Z. Jiang and S. Choi, "A cardiac sound characteristic waveform method for in-home heart disorder monitoring with electric stethoscope," Expert Systems with Applications **31,** 286–298 (2006).

[123] C. N. Gupta, R. Palaniappan, S. Swaminathan, and S. M. Krishnan, "Neural network classification of homomorphic segmented heart sounds," Applied Soft Computing **7,** 286–297 (2007).

[124] S. Choi and Z. Jiang, "Comparison of envelope extraction algorithms for cardiac sound signal segmentation," Expert Systems with Applications **34,** 1056–1069 (2008).

[125] J. G. Proakis, *Digital Communications*, 4th ed. (Prentice-Hall, New Jersey, 2001).

[126] A. Kolmogorov, "Interpolation and extrapolation of random stationary sequences," Izv. Akad. Nauk SSSR Ser. Mat. **5,** 3–14 (1941).

[127] N. Levinson, "The Wiener RMS error criterion in filter design and prediction," J. Math. Phys. **25,** 261–278 (1947).

[128] M. H. Hayes, *Statistical Digital Signal Processing and Modeling* (Wiley, 1996).

[129] H. Akaike, "Fitting autoregressive models for prediction," Annals of the Institute of Statistical Mathematics **21,** 243–247 (1969).

[130] H. Akaike, "A new look at the statistical model identification," IEEE Trans. Automat. Control **19,** 716–723 (1974).

[131] J. Rissanen, "Modeling By Shortest Data Description," Automatica **14,** 465–471 (1978).

[132] J. G. Berryman, "Choice of operator length for maximum entropy spectral analysis," Geophysics p. 1383Ű1391 (1978).

[133] R. Kashyap, "Inconsistency of the AIC rule for estimating the order of autoregressive models," IEEE Trans. Automat. Control **25,** 996–998 (1980).

[134] J. G. Proakis and D. K. Manolakis, *Digital Signal Processing (4th Edition)* (Prentice Hall, 2006).

[135] R. B. Blackman and J. W. Tukey, *The Measurement of Power Spectra, From the Point of View of Communications Engineering* (Dover Publications, New York, 1959).

[136] R. Gray, "Toeplitz and circulant matrices: A review,", 1977.

[137] J. Durbin, "The fitting of time-series models," Rev. Inst. Int. Stat. **3,** 233–244 (1960).

[138] P. A. Lanfranchi, A. Braghiroli, E. Bosimini, G. Mazzuero, R. Colombo, C. F. Donner, and P. Giannuzzi, "Prognostic value of nocturnal Cheyne–Stokes respiration in chronic heart failure," Circulation **99,** 1435–1440 (1999).

[139] J. P. Kaipio and P. A. Karjalainen, "Estimation of event-related synchronization changes by a new TVAR method," IEEE Trans. Biomed. Eng. **44,** 649–656 (1997).

[140] Y. I. Abramovich, N. K. Spencer, and M. D. E. Turley, "Time-Varying Autoregressive (TVAR) Models for Multiple Radar Observations.," IEEE Trans. Sig. Proc. **55,** 1298–1311 (2007).

[141] S. Haykin, *Adaptive Filter Theory (4th Edition)* (Prentice Hall, 2001).

[142] B. Widrow and S. Stearns, *Adaptive Signal Processing* (Prentice Hall, NJ, 1985).

[143] L. Ljung and T. Soderstrom, *Theory and Practice of Recursive Identification (Signal Processing, Optimization, and Control)* (The MIT Press, 1983).

[144] V. N. Vapnik, *Statistical Learning Theory* (Wiley, New York, 1998).

[145] B. Schölkopf, A. Smola, and K.-R. Müller, "Nonlinear Component Analysis as a Kernel Eigenvalue Problem," Neural Comput. **10,** 1299–1319 (1998).

[146] S. Mika, G. Ratsch, J. Weston, B. Scholkopf, and K. R. Mullers, "Fisher discriminant analysis with kernels," In , pp. 41–48 (1999).

[147] F. R. Bach and M. I. Jordan, "Kernel independent component analysis," J. Mach. Learn. Res. **3,** 1–48 (2003).

[148] D. R. Hardoon, S. R. Szedmak, and J. R. Shawe-taylor, "Canonical Correlation Analysis: An Overview with Application to Learning Methods," Neural Comput. **16,** 2639–2664 (2004).

[149] K.-H. Jeong, W. Liu, S. Han, E. Hasanbelliu, and J. C. Principe, "The correntropy MACE filter," Pattern Recogn. **42,** 871–885 (2009).

[150] A. R. C. P. Xu Jian-Wu, P. P. Pokharel and J. C. Principe, "Nonlinear Component Analysis Based on Correntropy," In *International Joint Conference on Neural Networks, IJCNN 06*, pp. 1851–1855 (2006).

[151] N. Aronszajn, "Theory of Reproducing Kernels," Trans. Amer. Math. Soc. **68,** 337–404 (1950).

[152] E. Parzen, "On Estimation of a Probability Density Function and Mode," Ann. Math. Stat. **33,** 1065–1076 (1962).

[153] V. N. Vapnik, *The Nature of Statistical Learning Theory (Information Science and Statistics)* (Springer, 1999).

[154] J. Wu Xu and J. C. Principe, "A Pitch Detector Based on a Generalized Correlation Function," IEEE Trans. Audio, Speech, Language Proc. **16,** 1420–1432 (2008).

[155] M. G. Genton, "Classes of kernels for machine learning: a statistics perspective," J. Mach. Learn. Res. **2,** 299–312 (2002).

[156] B. W. Silverman, *Density Estimation for Statistics and Data Analysis* (Chapman & Hall/CRC, 1986).

[157] C. W. Therrien, *Discrete Random Signals and Statistical Signal Processing* (Prentice-Hall, New Jersey, 1992).

[158] G. E. Birch, P. D. Lawrence, J. C. Lind, and R. D. Hare, "Application of prewhitening to AR spectral estimation of EEG," IEEE Trans. Biomed. Eng. **35,** 640–645 (1988).

[159] M. Galinier *et al.*, "Depressed low frequency power of heart rate variability as an independent predictor of sudden death in chronic heart failure," Eur. Heart J. **21,** 475–482 (2000).

[160] M. T. La Rovere *et al.*, "Short-term heart rate variability strongly predicts sudden cardiac death in chronic heart failure patients," Circulation **107,** 565–570 (2003).

[161] N. M. Arzeno, M. T. Kearney, D. L. Eckberg, J. Nolan, and C. S. Poon, *Proc. IEEE Conf. Eng. Med. Biol.* (2007), pp. 5051–5054.

[162] A. Garde, R. Schroeder, A. Voss, P. Caminal, S. Benito, and B. F. Giraldo, "Patients on Weaning Trials Classified with Support Vector Machines," Physiol. Meas. (2010).

[163] A. Garde, A. Voss, P. Caminal, S. Benito, and B. F. Giraldo, "SVM Feature Selection for Unbalanced Classification Applied to Weaning," Artif. Intell. Med. (2010).

Publications derived from this thesis

[Giraldo 2006a] B. Giraldo, A. Garde, C. Arizmendi, R. Jané, S. Benito, I. Diaz, and D. Ballesteros, "Support Vector Machine Classification Applied on Weaning Trials Patients," In *Engineering in Medicine and Biology Society, 2006. EMBC'06. Annual International Conference of the IEEE*, pp. 5587–5590 (2006).

[Giraldo 2006b] B. Giraldo, A. Garde, C. Arizmendi, R. Jané, S. Benito, I. Diaz, D. Ballesteros (2006) "Clasificación de pacientes en proceso de extubación mediante Máquinas de Soporte Vectorial" XXIV Congreso Anual de la Sociedad Española de Ingeniería Biomédica, Pamplona, Noviembre 6-8, 2006., pp. 173-176.

[Garde 2007a] A. Garde, B. Giraldo, R. Jané, I. Diaz, S. Herrera, S. Benito, M. Domingo, and A. Bayes-Genis, "Analysis of respiratory flow signals in chronic heart failure patients with periodic breathing," In *Engineering in Medicine and Biology Society, 2007. EMBC'07. Annual International Conference of the IEEE*, pp. 307–310, 2007.

[Garde 2007b] A. Garde, Giraldo B.F., R. Jané, I. Diaz, S. Herrera, S. Benito, M. Domingo, A. Bayés-Genís, (2007). "Caracterización de la respiración periódica en pacientes con insuficiencia cardiaca crónica". XXV Congreso Anual de la Sociedad Española de Ingeniería Biomédica, Cartagena, Noviembre 14-16, 2007., pp. 20-23.

[Garde 2008a] A. Garde, B. F. Giraldo, R. Jané, I. Diaz, S. Herrera, S. Benito, M. Domingo, and A. Bayes-Genis, "Characterization of periodic and non-periodic breathing pattern in chronic heart failure patients," In *Engineering in Medicine and Biology Society, 2008. EMBC'08. Annual International Conference of the IEEE*, pp. 3227–3230, 2008.

[Seeck 2008] A. Seeck, A. Garde, M. Schuepbach, B. Giraldo, E. Sanz, T. Huebner, P.

Caminal, A. Voss "Diagnosis of Ischemic Heart Disease with Cardiogoniometry - Linear discriminant analysis versus Support Vector Machines" 4th European Conference of the International Federation for Medical and Biological Engineering, ECIFMBE 2008 23-27 November 2008 Antwerp, Belgium, pp. 389-392, ISBN: 978-3-540-89207-6.

[Garde 2008b] A. Garde, Giraldo B.F., R. Jané, I. Diaz, S. Herrera, S. Benito, M. Domingo, A. Bayés-Genís, (2008). "Caracterización de Patrones de Respiración Periódicos y no Periódicos en Pacientes con Insuficiencia Cardiaca Crónica". XXVI Congreso Anual de la Sociedad Española de Ingeniería Biomédica, Valladolid, Octubre 15-17, 2008, pp 387 - 390.

[Garde 2009a] A. Garde, L. Sörnmo, R. Jané, and B. F. Giraldo, "Correntropy-based analysis of respiratory patterns in patients with chronic heart failure," In *Engineering in Medicine and Biology Society, 2009. EMBC'09. Annual International Conference of the IEEE*, pp. 4687–4690 (Minneapolis, Minnesota, USA, 2009).

[Garde 2009b] A. Garde, B. F. Giraldo, R. Jané, and L. Sörnmo, "Time-varying respiratory pattern characterization in chronic heart failure patients and healthy subjects," In *Engineering in Medicine and Biology Society, 2009. EMBC'09. Annual International Conference of the IEEE*, pp. 4007–4010 (Minneapolis, Minnesota, USA, 2009).

[Garde 2009c] A. Garde, B. Giraldo, R. Jané, L. Sörnmo, (2009). "Caracterización tiempo-variante del patrón respiratorio en pacientes con insuficiencia cardiaca crónica y sujetos sanos" XXVII Congreso Anual de la Sociedad Española de Ingeniería Biomédica, Cadiz, 2009.

[Garde 2009d] A. Garde, B. Giraldo, R. Jané, L. Sörnmo, (2009). "Análisis del patrón respiratorio en pacientes con insuficiencia cardiaca criónica aplicando correntropy" XXVII Congreso Anual de la Sociedad Española de Ingeniería Biomédica, Cadiz, 2009.

[Garde 2010a] A. Garde, L. Sörnmo, R. Jané, and B. F. Giraldo, "Correntropy-based Spectral Characterization of Respiratory Patterns in Patients with Chronic Heart Failure," IEEE Trans. Biomed. Eng, 2010, DOI 10.1109/TBME.2010.2044176 (in press).

[Garde 2010b] A. Garde, L. Sörnmo, R. Jané, and B. F. Giraldo, "Breathing Pattern Characterization in Chronic Heart Failure Patients using Respiratory Flow Signal," Ann. Biomed. Eng, 2010, ABME2497 (mayor revision).

[Garde 2010c] A. Garde, R. Schroeder, A. Voss, P. Caminal, S. Benito, and B. F. Gi-

raldo, “Patients on Weaning Trials Classified with Support Vector Machines,” Physiol. Meas, 2010, PMEA/343694/PAP (in press).

[Garde 2010d] A. Garde, A. Voss, P. Caminal, S. Benito, and B. F. Giraldo, “SVM Feature Selection for Unbalanced Classification Applied to Weaning,” Phys. Med. and Biol., 2010 (submitted).

Appendix A

Correntropy in detail

This appendix explains why correntropy makes the respiratory and modulation frequency peaks more discernible without requiring demodulation. The starting point is the AM signal,

$$x(n) = (1 + \mu M(n))C(n), \tag{A.1}$$

being $M(n) = \cos(\omega_m n)$ and $C(n) = \cos(\omega_c n)$. The corresponding correlation function is given by

$$R_x(n) = (1 + \mu^2 R_M(n)) \cos(\omega_c n), \tag{A.2}$$

where $R_M(n)$ denotes the correlation function of $M(n)$. Thus, $R_x(n)$ is proportional to $R_M(n)$, and is modulated by ω_c.

It can be shown that the correntropy function of $x(n)$ is proportional to both $V_M(n)$ and $V_C(n)$. For a Gaussian kernel, $V_M(n)$ reaches its maximum only when $M(n) = M(n+m)$. When this occurs, we have $\kappa(x_n - x_{n-m}) = 1/\sqrt{2\pi}\sigma$, and
$M(n) = M(n+m) \rightarrow \cos(\omega_m n) = \cos(\omega_m(n+m)), \Leftrightarrow m\omega_m n = 2\pi k,\ k = 1, 2, \ldots$.

The maximum values are obtained when $m = m_m = 2\pi k/\omega_m = T_m F_s k$, where F_s is the sampling rate and T_m is the modulation period. The correntropy $V_M(n)$ reaches its maximum for each m_m and decreases rapidly when the difference $M(n) - M(n+m)$ increases. For $V_C(n)$, the maximum values are reached when $m = m_c = 2\pi k/\omega_c = T_c F_s k$, where T_c is the carrier period.

The correntropy function $V_x(n)$ reaches its maximum when m is a multiple of both T_m and T_c, whereas the relative maximum values are reached when $m = m_c$, as $\omega_m \leq \omega_c \rightarrow T_m \geq T_c \rightarrow m_m \geq m_c$. Thus, the maximum value is given by the modulation signal (m_m).

The maximum value $1/\sqrt{2\pi}\sigma$ is only reached when both periods are multiples, i.e. $T_m = kT_c$, otherwise the value is lower. The maximum value appears in each modulation period, which explains why the modulation frequency peak is sometimes higher than the respiratory frequency peak. Thus, it can be stated that correntropy enhances the modulation peak. Figure A.1 demonstrates the property that $R_x(n) \propto R_M(n)$ is modulated by $C(n)$, whereas $V_x(n) \propto \gamma V_M(n) + \beta V_C(n)$, where γ and β are positive constants.

Renyi's entropy is estimated as:

$$H_a(X) = \frac{1}{1-\alpha} \log \sum p_X^a(x) \tag{A.3}$$

where

$$H_a(X) = \frac{1}{1-\alpha} \log \int f_X^a(x) dx \tag{A.4}$$

Information Potential IP (as an estimator of quadratic entropy). A nonparametric estimate of quadratic entropy is obtained directly from the data, through IP.

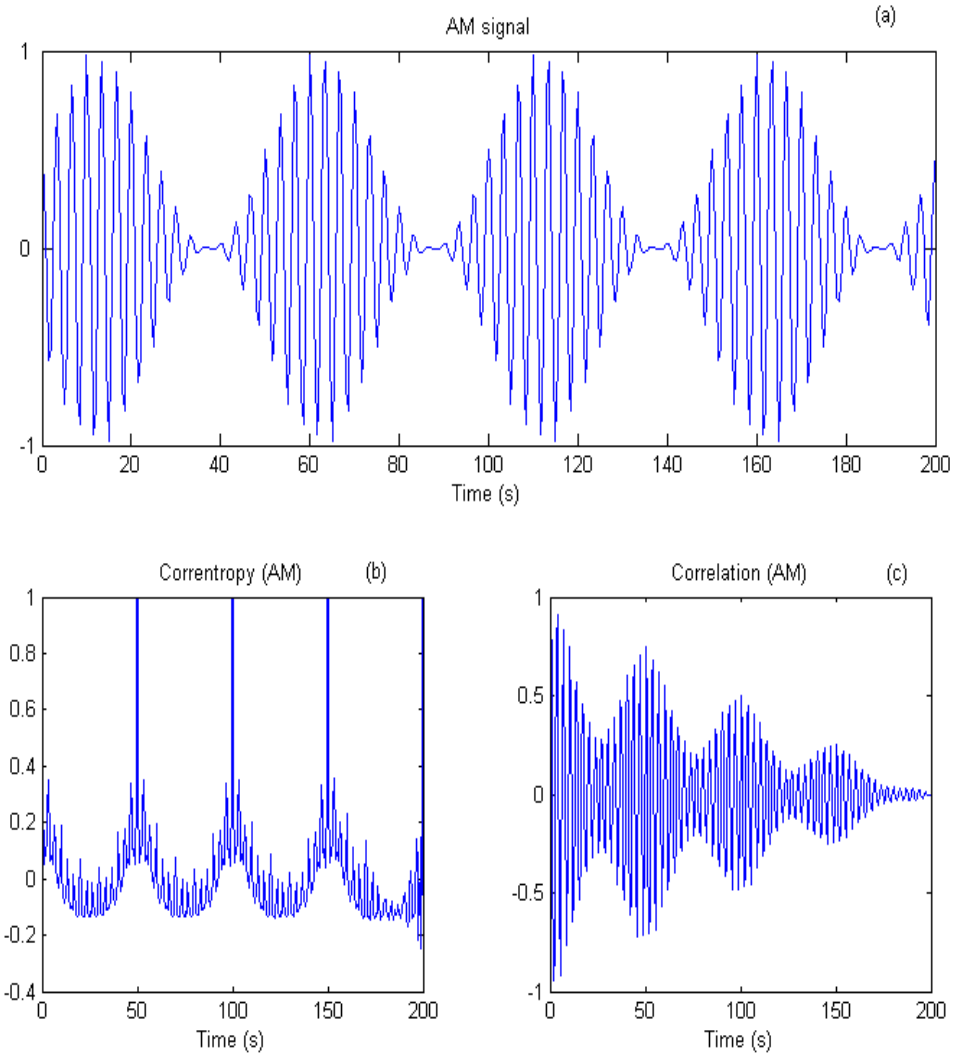

Figure A.1 (a) An AM signal, (b) its correntropy function, using σ given by Silverman's rule, and (c) its correlation function.

$$H^2(X) = -\log IP(x) \tag{A.5}$$

where

$$IP(X) = \frac{1}{N^2}\sum_{j=1}^{N}\sum_{i=1}^{N}\kappa_{\sqrt{2}\sigma}(x_j - x_i) \tag{A.6}$$

The probability density that is estimated with Parzen kernels can be considered to define an information potential field over the space of the samples. The entropy is now expressed in terms of potential energy. Entropy maximization becomes equivalent to the minimization of information potential. As this is similar to the kernel trick used in support vector machines, and due to the Mercer conditions, we never have to explicitly estimate the probability density function (PDF), which greatly increases the applicability of the method.

Parzen window method , also called the kernel estimation method, this is one of the most popular nonparametric methods used to estimate the PDF of a random variable. First, the kernel function has to be determined. In this study, we use a Gaussian kernel:

$$G\left(x, \sigma^2\right) = \frac{1}{\sqrt{2\pi}\sigma}\exp\left[-\frac{x^T x}{2\sigma^2}\right] \tag{A.7}$$

where σ is a kernel size and x is an n dimensional variable. Therefore, the whole density ($f(x)$) is the average of all the kernel functions obtained by applying the kernel to all samples.

$$f(x) = \frac{1}{N}\sum_{i=1}^{N} G(x - a(i), \sigma^2) \tag{A.8}$$

being, the data set $= \{a(i) | i = 1, \ldots, N\}$.